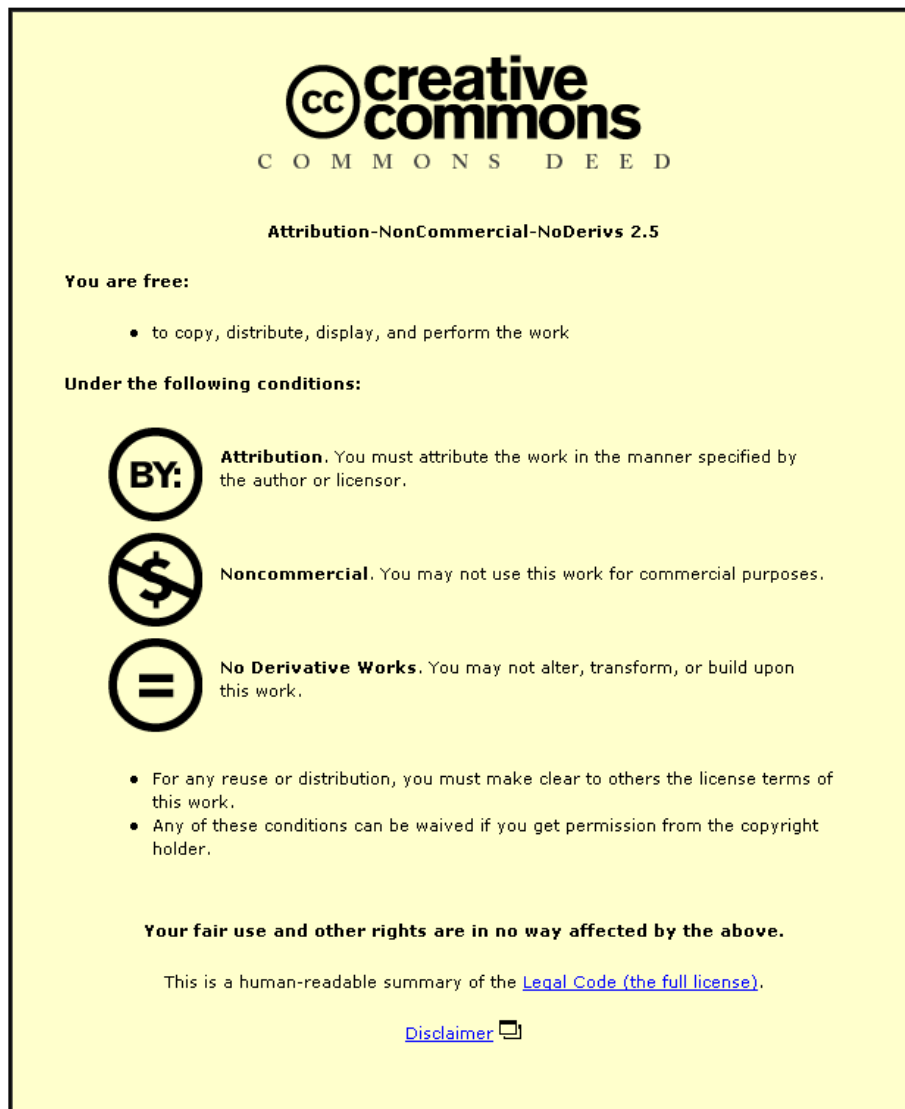


This item was submitted to Loughborough's Institutional Repository (<https://dspace.lboro.ac.uk/>) by the author and is made available under the following Creative Commons Licence conditions.



For the full text of this licence, please go to:
<http://creativecommons.org/licenses/by-nc-nd/2.5/>

**ADVANCED CONTROL STRATEGIES FOR
TILTING TRAINS**

by

Argyrios Christou Zolotas

**A DOCTORAL THESIS SUBMITTED IN PARTIAL FULFILLMENT
OF THE REQUIREMENTS FOR THE AWARD OF**

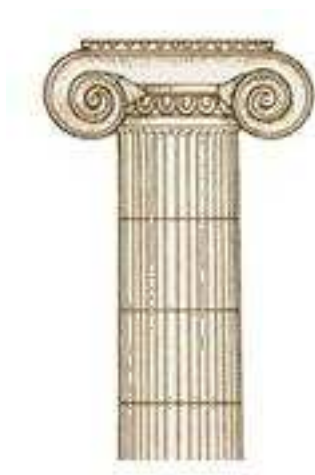
DOCTOR OF PHILOSOPHY

OF LOUGHBOROUGH UNIVERSITY

September 2002

© Copyright by Argyrios C. Zolotas, 2002-2003

Αφιερωμένο στον πολυαγαπημένο μου νονό, στην οικογένεια μου και σε όλους όσοι βοήθησαν ώστε να γίνει εφικτή αυτή η διδακτορική διατριβή.



Dedicated to my beloved (late) godfather, my family and all the people that made this thesis possible.

*This Thesis was typeset in 11pt Roman fonts using L^AT_EX₂ ϵ , L^AT_EX-CAD,
WinEdt 5 and Mayura Draw.*

Contents

Synopsis	ix
List of Publications	x
Acknowledgements	xi
List of Tables	xii
List of Figures	xiv
Glossary and Acronyms	xviii
1 Introduction	1
1.1 Problems Running at High Speed on Existing Tracks	2
1.2 Active Suspensions	3
1.2.1 Main active suspension areas	4
1.3 Tilting Train Technology	4
1.3.1 The concept of tilting trains	5
1.3.2 Tilt angle effects	7
1.3.3 Tilting system mechanical configurations	8
1.3.4 Problem definition of tilting	8
1.4 Motivation for this Thesis	12
1.5 Work Addressed in this Thesis	12
1.5.1 Thesis structure	12
1.6 Published Work	14
1.7 Thesis Contributions	14
2 Literature Survey	15
2.1 Active suspensions	15
2.2 Tilting trains	16

2.2.1	Work on Control studies	17
2.2.2	Work on Application of Tilt	18
2.3	Summary	18
3	Track Geometry and Tilt System Assessment methods	20
3.1	Deterministic Inputs	20
3.2	Random (Stochastic) Inputs	22
3.2.1	Representation of lateral track irregularities	23
3.3	Tilt System Performance Assessment Methods	24
3.3.1	Curve Transition Performance (Deterministic criterion)	24
•	Example of deterministic tilt performance	26
3.3.2	Straight Track Performance (Stochastic criterion)	29
3.4	Ride Quality Calculation Methods (Random Inputs)	29
3.4.1	Frequency response analysis	30
3.4.2	Time based Covariance analysis	31
3.4.3	Time history analysis	33
3.5	Summary	34
4	Tilt Control Prerequisites	35
4.1	System Requirements	35
4.2	Full vs Partial Tilt	35
4.3	Tilt Control Objectives	36
4.4	Tilting Vehicle Configuration Cases	37
I	Active Anti-Roll Bar (ARB) Studies	39
5	Modelling of Vehicle Dynamics using Active ARB	40
5.1	Linear Two Degree-of-Freedom Endview Model	41
5.2	Identification of Vehicle Sway Modes	45
5.3	Non-linear Three Degree-of-Freedom Endview Model	49
5.3.1	Comparison between the 2 D-o-F linear and 3 D-o-F non-linear models	52
5.4	Linear Four Degree-of-Freedom Endview Model	56
5.5	Summary	62
6	Basic Tilt Control Strategies for Active ARB	63
6.1	Basic Nulling Tilt Control	64
6.1.1	PI-control of the basic nulling tilt process	67

6.1.2	Complementary filter approach of the basic nulling tilt process . . .	70
6.2	Basic Command-driven schemes	72
6.2.1	Local vehicle Command-driven	72
6.2.2	Command-driven with precedence	77
6.3	Summary	80
7	Advanced Control Studies for Active ARB	81
7.1	Linear-Quadratic Regulator (LQR) optimal control	82
7.1.1	LQR Preliminaries - Full State Feedback	82
7.1.2	Partial-nulling Optimal P+I control with output regulation	83
7.2	Model Based Estimation ‘Nulling’ Control Incorporating a Kalman Filter	90
7.2.1	Kalman Filter Preliminaries	90
7.3	‘Nulling’ Control based upon the ‘True’ Cant Deficiency	91
7.3.1	Tilt Controller Design upon Model Based Estimator	98
7.4	Robust \mathcal{H}_∞ -based Control Schemes	103
7.4.1	Preliminaries	103
7.4.2	Basic Notation	104
•	Frequency Domain Spaces and Norms	104
•	Linear Fractional Transformations	105
7.4.3	\mathcal{H}_∞ Mixed Sensitivity Design	107
•	Mixed sensitivity for tilt control	108
7.4.4	Multi-objective $\mathcal{H}_\infty/\mathcal{H}_2$ Robust Control via LMI approach	116
7.5	Concluding remarks	125
II	Tilt Mechanism Studies below Secondary Suspensions	128
8	Modelling of Vehicle Dynamics using tilting bolster	129
8.1	Tilt Mechanism Preliminaries	129
8.2	Vehicle Modelling	130
8.3	Summary	137
9	Control Studies for the Tilt Mechanism Application	138
9.1	Basic control approaches	138
9.1.1	Basic Partial-nulling control	138
9.1.2	Basic Command-Driven with Precedence Control	141
9.2	Advanced Control I (Modern Control)	145
9.2.1	LQR (Optimal P+I) Nulling Tilt Strategy for Tilt Mechanism Model	145

9.2.2	Extension of Model-Based Estimation Control for Tilt Mechanism Model	151
•	Estimator Design	151
•	Tilt Controller Design based upon Model Based Estimator	153
9.3	Advanced Control II (Post-Modern Control)	157
9.3.1	\mathcal{H}_∞ Loop Shaping Robust-Control Design via the Co-Prime Factorization Method	157
•	\mathcal{H}_∞ coprime factorisation for tilt control	159
9.4	Concluding remarks	166
10	Conclusions and Future Work	167
10.1	Conclusions	167
10.2	Suggestions for Future Work	174
III	Bibliography/References	176
	Bibliography	177
IV	Appendices	184
A	Summary of Track Profiles and Vehicle Parameter Values	185
A.1	Track Profiles	186
A.1.1	Anti-Roll Bar studies	186
A.1.2	Tilt Mechanism Studies	187
A.2	Vehicle Parameter Values	188
A.2.1	Vehicle with Active Anti-Roll Bar	188
A.2.2	Vehicle with Tilting Mechanism below Secondary Suspension	189
B	Theory Supplement	190
B.1	Covariance analysis of systems excited by white noise inputs	190
B.2	Basic Control Theory	195
B.2.1	Feedback Control Systems	195
B.3	Non-Minimum Phase System Symbolic Analysis	196
B.3.1	Calculation of Time Delay Introduced by Low-Pass Filters	198
C	Evaluation for curve transition passenger comfort	200
C.1	P_{CT} Factor Calculation	200

D	Suspension Components Modelling	202
D.1	Airspring Modelling	202
D.1.1	Model One	202
D.1.2	Model Two	203
D.1.3	Model Three	205
D.2	Suspension having Dampers with End-Stiffness	206
E	Model State Space Matrices	208
E.1	Anti-Roll Bar Model (4 DoF Linear) A, B	209
E.2	Tilt Mechanism Model A	210
F	\mathcal{H}_∞-based Controller Structures	213
F.1	Mixed Sensitivity for ARB model	213
F.1.1	$K(s)$ for weightings set 1	213
F.1.2	$K(s)$ for weightings set 2	214
F.2	Multi-Objective $\mathcal{H}_\infty/\mathcal{H}_2$ for ARB Model	216
F.3	\mathcal{H}_∞ Coprime Factorisation for Tilt Mechanism Model	219
G	Publications of Research Work	222
H	Software files (Matlab & Vampire)	255
H.1	MATLAB FILES	256
H.1.1	Related to Active Anti Roll Bar studies	256
H.1.2	Related to Tilt Mechanism Bar studies	275
H.1.3	Related to Assessment	291
H.2	VAMPIRE FILES	292

EMAIL AUTHOR REGARDING ANY QUERIES: A.ZOLOTAS@IEEE.ORG

Synopsis

The use of tilting bodies on railway vehicles is becoming increasingly widespread: a number of well-established services using tilt technology already exist around the world, and will appear again in the UK over the next year or so. The motivation for tilting railway vehicles is that they give a cost-effective means of achieving a substantial reduction in journey time by increasing the vehicle speed during curves.

Early tilt controller designs were based upon local vehicle measurements, however at that time this approach did not prove very successful. Nowadays most European manufacturers use the so called ‘precedence’ control scheme, utilising measurements from precedent vehicles to achieve ‘precedence’ information. However, achieving a satisfactory local tilt control strategy is still an important research target because of the system simplifications and more straightforward failure detection.

The thesis describes a comprehensive study of tilt control, and its aim is to employ advanced control techniques - based upon practical sensors - with the particular objective of identifying effective strategies which can be applied to each vehicle independently, i.e. without using precedence control. The sensors employed for control design are in particular mounted on the vehicle passenger coach. Most of the work has been undertaken using **MATLAB**, and this has included a proper assessment of the ride quality issues.

List of Publications

- (i). Zolotas, A. C., Goodall, R. M., *Advanced Control Strategies for tilting railway vehicles*, UKACC, Control 2000, Cambridge, UK, Sep. 2000
- (ii). Zolotas, A. C., Halikias, G. D., Goodall, R. M., *A Comparison of Tilt Control approaches for high speed railway vehicles*, Proceedings ICSE 2000, Coventry, UK, Vol. 2, pp. 632-636, Sep. 2000
- (iii). Goodall, R. M., Zolotas, A. C., Evans, J., *Assessment of the Performance of Tilt System Controllers*, The Railway Conference at Railtex 2000, NEC Birmingham, UK, Nov. 21-23, 2000
- (iv). Zolotas, A. C., Goodall, R. M., Halikias, G. D., *New control strategies for tilting trains*, IAVSD Symposium 2001, Lyngby-Copenhagen, DK, Aug. 20-24, 2001

Acknowledgements

I would like to express my gratitude to my supervisor, Professor Roger Goodall for introducing me to tilting train technology and giving me the opportunity to work on such an interesting problem. His support, guidance and continuous encouragement during all this years of my research study were invaluable.

Dr George Halikias expressed his interest in my work and shared with me his knowledge of robust and optimal control and provided many useful references and friendly encouragement. He also introduced me in the ‘art’ of \LaTeX [pronounced La-Tech (gr. $\Lambda\alpha\text{-}T\epsilon\chi$), from the greek word $\tau\epsilon\chi$ abbrev. for *technology* (gr. $TE\chi\nu\omicron\lambda\omicron\gamma\iota\alpha$)] with which this thesis was produced.

I would also like to acknowledge my fellow colleagues, Dr Edwin Foo, Javier Perez and Dr Hong Li, in the Systems and Control Group of Loughborough University for been very supportive on a number of technical issues related to my research work. Many thanks to Dr John Pearson for his valuable help on Kalman filter issues and **VAMPIRE** implementation, and Dr Zoltan Nagy for the enlightening conversations. Also Dr Steve Rothberg (Dept. of Mechanical Engineering) for his support on vehicle systems modelling. Not to forget Jerry Evans and Alan Minnis, both from AEAT Derby UK, for providing support on **VAMPIRE**[®] package. My kindest regards to Dr Imad Jaimoukha (Dept. of Electrical and Electronic Eng., Imperial College) who provided invaluable help during the final stage of the thesis production.

I am very grateful to all my family for their patience, trust, support (both mental and financial) and more importantly their *love*.

I should also mention that my graduate studies in Loughborough were supported by the Department of Electronic and Electrical Engineering together with the Faculty of Engineering.

Not to forget all my friends, especially Dr Alexandros Feresidis (for being an interesting person to meet and also my flatmate for the past three years, ...indeed it seems a long time, in Loughborough).

Last but not least, a very big *thank you* to Matoula (for changing my life in general...) for her love, patience, support and encouragement particularly during the last phase of the thesis.

London, England
September 2002

Argyrios Zolotas

London, England
September 2002

Argyrios Zolotas

List of Tables

1.1	Tilt angle effects	7
3.1	Sample of Comparison of RMS deviations	29
4.1	Tilt application test cases	38
5.1	System modes of the two degree-of-freedom model	43
5.2	Linear and Non-linear System modes	52
5.3	Four D-o-F ARB vehicle model dynamic modes	60
5.4	Track profiles for the 4 D-o-F ARB linear model	60
5.5	Assessment of non-tilting vehicle @ 45(m/s)	62
6.1	Open-loop poles and zeros of $G_{y_1u}(j\omega)$	66
6.2	PI-control basic nulling approach assessment @ 58(m/s) - ($k_g = .225$, $\tau_m = 0.4$ s)	68
6.3	Basic nulling complementary filter approach - assessment @ 58(m/s) . .	74
6.4	Effect of low-pass filtering on command-driven control ($v = 58(m/s)$) . .	75
6.5	Basic command-driven with precedence approach - assessment @ 58(m/s)	79
7.1	LQ output regulation controller performance, $v = 58(\frac{m}{s})$	85
7.2	(LQR) optimal P+I control assessment @ 58(m/s)	89
7.3	Model-based estimation scheme assessment @ 58(m/s) - (PID approach) .	99
7.4	Mixed Sensitivity \mathcal{H}_∞ approach, weightings set 1, @ 58(m/s)	113
7.5	Mixed Sensitivity \mathcal{H}_∞ approach, weightings set 2, @ 58(m/s)	115
7.6	α - β combinations for the $\mathcal{H}_\infty/\mathcal{H}_2$ problem	121
7.7	$\mathcal{H}_\infty/\mathcal{H}_2$ multi-objective LMI approach @ 58(m/s)	124
8.1	Tilt mechanism vehicle model dynamic modes	134
8.2	Track profiles for the tilting mechanism linear model	134
8.3	Assessment of passive (tilt mechanism) vehicle @ 45(m/s)	134

9.1	Mechanism basic nulling scheme assessment @ 58(m/s) - (PI approach)	140
9.2	Mechanism basic precedence scheme assessment @ 58(m/s)	145
9.3	Mechanism LQR+I advanced control scheme assessment @ 58(m/s)	149
9.4	MBE-based advanced control scheme assessment @ 58(m/s)	156
9.5	Trade-off of coprime factorisation with variable k_1 (@ 58m/s)	161
9.6	\mathcal{H}_∞ coprime approach controller assessment “best” design @ 58(m/s)	162
10.1	Overall research classification of proposed tilt control strategies	173
A.1	Parameters based upon the Bombardier Pro Rail current best configuration	188
A.2	Parameters based loosely based on post-apt test coach 48204 (seats full) with slightly increased lateral stiffness	189
F.1	Controller TF coefficients for mixed sensitivity set 1	214
F.2	Controller TF coefficients for mixed sensitivity set 2	215

List of Figures

1.1	Sample of high speed train mechanical arrangement	2
1.2	Suspension configuration	3
1.3	General active suspension scheme	3
1.4	Curving forces applied on a railway vehicle	5
1.5	Curved track profile	6
1.6	Passenger perceived curving acceleration	6
1.7	Tilt mechanisms (across and above secondary suspensions)	9
1.8	Examples of tilt mechanism configurations below secondary suspensions	10
1.9	Nulling and command-driven control configurations	11
1.10	Command driven with precedence control scheme	11
3.1	Deterministic track curvature	21
3.2	Deterministic track cant	21
3.3	Curved track section	22
3.4	Lateral Track misalignments	23
3.5	Calculation of deviation of actual from ideal responses for acceleration and roll velocity	26
3.6	Acceleration, jerk and roll rate time history	27
3.7	P_{CT} factors: (a)seated, (b)standing and (c)max tilt angle	27
3.8	Vehicle responses	28
4.1	Full vs Partial Tilt Compensation	36
5.1	Two degree-of-freedom model	41
5.2	Block diagram of the two degree of model	44
5.3	(a) Body cog displacement on curved track (2-DoF model). (b) Sway mode analysis model	45
5.4	Location of nodes for the sway motions	47
5.5	Sway mode centres	48
5.6	3 D-o-F ARB model setup	49

5.7	Body c.o.g. displacement on curved track (3 D-o-F model)	51
5.8	Time history results for deterministic track	53
5.9	Time history results for stochastic track	53
5.10	Non linear model Simulink	55
5.11	Four degree-of-freedom model	56
5.12	End-moment effect for the four degree-of-freedom model	59
5.13	Vehicle body/bogie time histories @ 45(m/s)	61
6.1	Loading gauge and basic nulling tilt	64
6.2	Nominal open-loop frequency responses	66
6.3	Non-minimum phase limitations	67
6.4	PI Block	67
6.5	Basic nulling scheme with $P + I$ time history results for design track . .	69
6.6	Basic nulling, designed system frequency responses	70
6.7	Complementary filter control approach	71
6.8	CF approach, designed system frequency responses	72
6.9	CF approach, simulation results on curved track	73
6.10	Local command-driven scheme	74
6.11	Command-driven tilt performance on design track	76
6.12	Command-driven with precedence approach	77
6.13	Basic nulling, designed system frequency responses	79
6.14	Command-driven with precedence basic approach, demonstration on curved track	80
7.1	Optimal P+I output regulation	85
7.2	LQR with integral action transition performance, set 1	87
7.3	LQR with integral action transition performance, set 2	88
7.4	Plant with Estimator (Kalman filter)	89
7.5	Plant with Estimator (Kalman filter)	91
7.6	Model-based estimation control scheme	92
7.7	LQR with integral action transition performance	94
7.8	‘True’ cant deficiency estimates, estimate (dark), error (grey)	95
7.9	Stochastic-Deterministic weighting curves for KBF	97
7.10	P+I+D with approximate derivative plus series LPF	98
7.11	Frequency response analysis of MBE control designed system for partial ‘true’ cant deficiency	100
7.12	MBE ‘nulling’ approach, curved track simulation results, set 1	101
7.13	MBE ‘nulling’ approach, curved track simulation results, set 2	102

7.14	The Generalised Regulator Configuration	106
7.15	A general regulation control problem	107
7.16	$S/KS/T$ mixed-sensitivity General Control problem formulation for tilt control	109
7.17	Mixed sensitivity design set 1	113
7.18	Design track time history results for mixed sensitivity weightings set 1 .	114
7.19	Mixed sensitivity design set 2	115
7.20	Design track time history results for mixed sensitivity weightings set 2 .	117
7.21	The Generalised Regulator Configuration for multi-objective control . .	118
7.22	Multi-objective $\mathcal{H}_\infty/\mathcal{H}_2$ LMI approach scheme	120
7.23	Design track time history results for $\mathcal{H}_\infty/\mathcal{H}_2$ “best” design	125
7.24	Controller performance with parametric change	126
8.1	Vampire model of the tilting train (single vehicle)	130
8.2	Vehicle with tilt mechanism below secondary	131
8.3	Actuator configuration	132
8.4	Simulations results for the passive (tilt mechanism) vehicle	135
8.5	Comparison of Vampire (dash-dotted) and Matlab (solid) generated models for the deterministic case based upon the vehicle body	136
9.1	Basic partial-nulling scheme for vehicle with tilting bolster	139
9.2	Uncompensated OL frequency response from u to effective cant deficiency	140
9.3	Basic nulling for mechanism, designed system frequency responses . . .	141
9.4	Mechanism basic nulling scheme with $P + I$ time history results (design track), set 1	142
9.5	Mechanism basic nulling scheme with $P + I$ time history results (design track), set 2	143
9.6	Mechanism Basic Precedence Tilt	144
9.7	Mechanism basic precedence scheme time history results (design track), set 1	146
9.8	Mechanism basic precedence scheme time history results (design track), set 2	147
9.9	Mechanism advanced LQR+Integral scheme results (design track) . . .	150
9.10	‘True’ cant deficiency estimate	152
9.11	MBE-based control approach for tilt mechanism model	153
9.12	MBE control design - Open loop	154
9.13	Main Closed Loop designed system	155
9.14	Mechanism advanced MBE scheme results (design track)	156

9.15	Coprime factor robust stabilisation problem	158
9.16	Coprime factors loop shaping design process	159
9.17	Best design for coprime factorisation \mathcal{H}_∞ method frequency responses	161
9.18	Design track time history results for \mathcal{H}_∞ coprime “best” design	163
9.19	Robust performance test for coprime \mathcal{H}_∞ design	165
A.1	Track features for anti-roll bar studies	186
A.2	Track features for tilt-mechanism studies	187
B.1	General linear system	190
B.2	One-degree of freedom feedback control system	195
B.3	Open-loop system including original and LP delayed signals for comparison	199
C.1	Calculation of quantities \ddot{y} , \ddot{y} and $\dot{\theta}$ for P_{CT} factor evaluation	201
D.1	Airspring Model 1	202
D.2	Airspring Model 2	204
D.3	Airspring Model 3	205
D.4	Damper with end-stiffness	206

Glossary and Acronyms

δ_a	ARB Actuator roll angle
$\Phi(t, \tau)$	State Transition Matrix
$\theta_b, \dot{\theta}_b, \ddot{\theta}_b$	Bogie roll angle, rate, acceleration
$\theta_o, \dot{\theta}_o, \ddot{\theta}_o$	Track cant angle, rate, acceleration
$\theta_v, \dot{\theta}_v, \ddot{\theta}_v$	Body roll angle, rate, acceleration
τ_m	P+I compensator time constant
θ'_{dmm}	Measured effective body cant deficiency for partial tilt (Mechanism model)
θ'_{dm}	Measured effective body cant deficiency for partial tilt (ARB model)
θ'_{tdm}	True effective body cant deficiency for partial tilt (Mechanism model)
θ'_{td}	True effective cant deficiency (ARB)
θ_{2sr}	Secondary suspension roll angle (between body-bogie)
θ_{dmm}	Measured body cant deficiency for partial tilt (Mechanism model)
θ_{dm}	Measured body cant deficiency for partial tilt (ARB model)
θ_{m_i}	Ideal mechanism roll input
$\theta_m, \dot{\theta}_m$	Actual mechanism roll position, rate
θ_{tdm}	True body cant deficiency (Mechanism model)
θ_{td}	True cant deficiency (ARB)

$\ \cdot\ _2$	$\mathcal{L}_2/\mathcal{H}_2$ norm
$\ \cdot\ _\infty$	$\mathcal{L}_\infty/\mathcal{H}_\infty$ norm
$\bar{\sigma}[\cdot]$	maximum singular value
$\underline{\sigma}[\cdot]$	minimum singular value
A^T	Transpose of a matrix/vector
A^*	Complex conjugate transpose
$E\{\cdot\}, E[\cdot]$	Expected value of a given quantity
$tr(\cdot)$	Trace of a given expression
i_{vr}, i_{br}	Roll inertias of vehicle body, bogie
$\mathcal{F}_L(P, K)$	(Lower) Linear Fractional Transformation
m_v, m_b	Masses of vehicle body, bogie
\Re	field of real numbers
$y_b, \dot{y}_b, \ddot{y}_b$	Bogie lateral displacement, velocity, acceleration
$y_o, \dot{y}_o, \ddot{y}_o$	Track lateral irregularities displacement, rate, acceleration
$y_v, \dot{y}_v, \ddot{y}_v$	Body lateral displacement, rate, acceleration
A, B, C, D	State space realisation of a system
c_{vr}	Anti-roll bar damping per bogie
c_{py}	Primary lateral damping
c_{pz}	Primary vertical damping
c_{rz}	Airspring reservoir damping
c_{sy}	Secondary lateral damping
d_1	Airspring semi-spacing
d_2	Primary vertical suspension semi-spacing
h_1	Secondary lateral suspension spacing (bogie cog)
h_2	Secondary lateral suspension spacing (bogie cog)

h_3	Primary lateral suspension spacing (bogie cog)
h_{g1}	Height ARL of body cog
h_{g2}	Height ARL of bogie cog
h_{mt}	Mechanism c.o.g. vertical separation from effective tilt centre
$j\Re$	Imaginary field of the complex plane
K_f	Optimal estimator (Kalman) gain matrix
k_p	Proportional gain
K_r	Optimal regulator (LQR) gain matrix
k_{vr}	Anti-roll bar stiffness
k_{az}	Airspring area stiffness
k_{csy}	Secondary lateral damper end-stiffness
k_g	P+I compensator gain
k_{py}	Primary lateral stiffness
k_{pz}	Primary vertical stiffness
k_{rz}	Airspring reservoir stiffness
k_{sy}	Secondary lateral stiffness
k_{sz}	Airspring series stiffness
L	Loop Transfer Function
Q	State weighting matrix (LQR)
Q_o	Output measurements weighting matrix (LQR)
Q_{kf}	Process noise weighting matrix (KBF)
R_k	Control weighting matrix (LQR)
R_{kf}	Sensor noise weighting matrix (KBF)
S, T, KS	Sensitivity, Complementary Sensitivity, Control Sensitivity
v	vehicle forward speed

z_v, z_o	Body vertical displacement, Track vertical displacement
ARB, A.R.B.	Anti-Roll Bar
BIBO.....	Bounded Input Bounded Output
c.o.g, C.O.G.	Centre of Gravity
CF	Complementary Filter
D-o-F, DoF	Degree-of-Freedom
e.c.d.	Effective Cant deficiency for partial tilt
KBF.....	Kalman Bucy Filter
LCF.....	Left Coprime Factorisation
LFT.....	Linear Fractional Transformations
LMI,LMIs	Linear Matrix Inequalities
LQG.....	Linear Quadratic Gaussian
LQR.....	Linear Quadratic Regulator
LTI.....	Linear Time Invariant
LTR.....	Loop Transfer Recovery
MBE	Model Based Estimation
MIMO.....	Multi-Input Multi-Output
MISO.....	Multi-Input Single-Output
P+I, PI.....	Proportional-plus-Integral
RHP, LHP.....	Right and Left Half Plane
SISO	Single Input Single Output

Other symbols and acronyms are defined as they appear

Chapter 1

Introduction

When trains were first introduced as a means of mass transportation they were successful due to the fast and reliable services they offered. Since then, the advanced automobile technology caused the car to become a popular way of transport for short distances. Nowadays cars on good quality high speed motorways can achieve speeds of up to $150 - 200(km/h)$ (depending on law constraints). Similarly, the rapid progress in the area of aerospace engineering enhanced the use of airplanes for long distances. The consequence of these developments was that trains were losing their value as a form of transport. Trains operating on conventional (or existing) tracks were becoming relatively slower and less flexible than other means of transport while the price remained high, causing uncompetitive services. Building new modern infrastructures or alternatively improving the existing routes was difficult due to the high cost and also there was no guarantee of overall profit. The alternative would be the introduction of trains capable of operating at high speed on the existing tracks, *high speed* trains.

A high speed train is a dynamically complex system, and Figure 1.1 illustrates the complex dynamic nature which has evolved over a period of two centuries of railway development. The ‘passive’ suspension arrangement shown is separated into two parts:

1. the *primary suspension* between the wheelsets and the vehicle bogies
2. the *secondary suspension* between the vehicle bogies and the vehicle body.

The former helps with the guidance (running stability) of the vehicle, while the latter is used to provide passenger ride comfort (high frequency isolation).

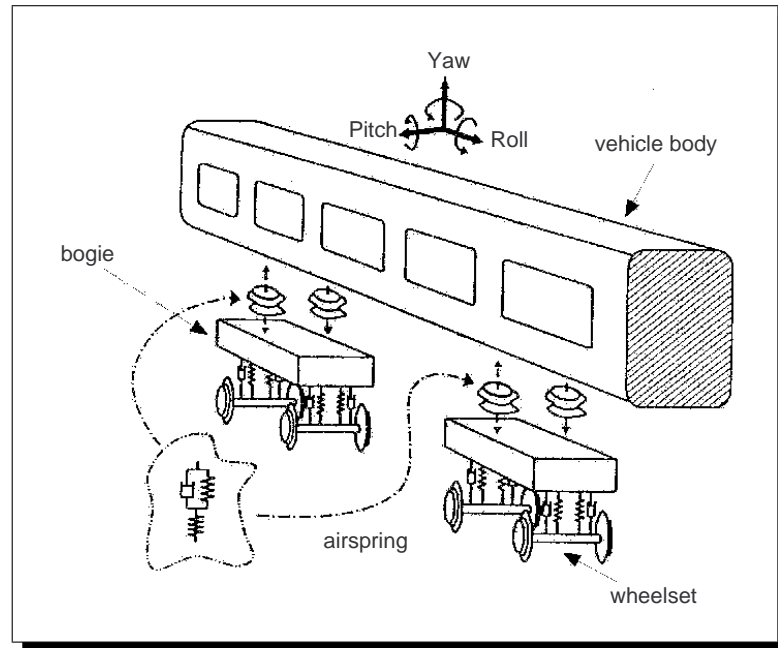


Figure 1.1: Sample of high speed train mechanical arrangement

1.1 Problems Running at High Speed on Existing Tracks

Improved vehicle speeds and reducing journey times also have drawbacks, the primary problem being that high speed operation affects the performance on both straight and curved track.

The effect of straight track irregularities perceived by the passengers increases as speed increases. Likewise, when the vehicle traverses a curve, passengers feel a centrifugal force which is proportional to the square of the velocity. Softer passive suspensions will improve the straight track ride quality while stiffer suspensions will guarantee small suspension deflection on curved paths. This results in a difficult trade-off between straight track and curving performance.

Traction (the capability of achieving high speed) and braking power (faster trains need to slow down) can be addressed as associative problems. Safety is not a crucial issue since the speed at which a train becomes unstable can be very high. However, passengers object to the increase of train speed especially round corners because it can make passengers nervous, feeling uncomfortable or nauseated. To accommodate all the above, a solution is the use of *active suspensions* which is discussed in the next section.

1.2 Active Suspensions

Active suspension technology is an expansion of the existing mechanical systems to include active elements. Figure 1.2 illustrates the difference between passive and active suspensions. The advances in active suspensions enhance the use of high speed trains. The use of appropriately arranged active elements affects positively the dynamic properties of the basic passive configuration, improving the ride quality and keeping the track maintenance cost low.

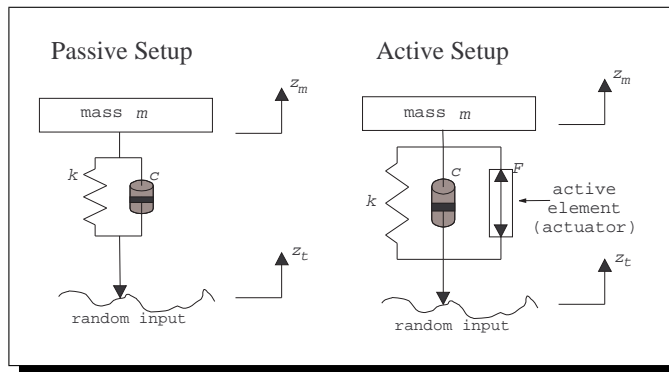


Figure 1.2: Suspension configuration

A block diagram representation of a railway vehicle dynamic system is shown in Figure 1.3. The response of the vehicle to the inputs (track inputs, load changes, etc.) is governed by the control law. Hence the overall performance depends on the sensors and the actuators used as well as on the software of the controller. The feedback action is used to modify accordingly the response of the mechanical system [Goo97].

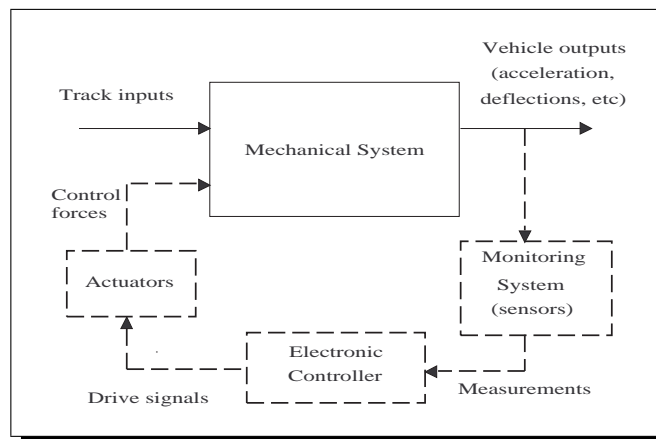


Figure 1.3: General active suspension scheme

1.2.1 Main active suspension areas

Three principal areas of active suspensions used in high speed trains are: *active primary*, *active secondary* and *tilting*.

1. *Active primary* suspension define active control applied onto the vehicle's primary suspensions (i.e. vertical, lateral or longitudinal). The important consideration is to guarantee running stability and curving performance.
2. *Active secondary* concerns the use of active control to improve the behaviour of vertical and lateral secondary suspension systems. The importance is to provide ride comfort.
3. *Tilting*, which is a particular form of active secondary suspension, uses full-active control of the secondary *roll* suspensions, and is the main focus of this thesis.

1.3 Tilting Train Technology

When a train traverses a curve at high speed the passengers experience a centrifugal force, and similar forces act on the body and the bogies. The suspension geometry and the forward speed of the vehicle determine the amount of roll into or out of the curve by the vehicle. The centrifugal force is a function of $\frac{v^2}{R}$. In order to maintain the level of centrifugal force while increasing the vehicle forward velocity, the curve radius must also increase by a certain factor which often for practical reasons is impossible (i.e. triple the velocity and the curve radius must increase by a factor of nine). This is why even apparently gentle curves can be much more of a problem while running in high speed than one might think, due to the fact that the force rises with the square of velocity.

Often railway operators face a decision for building a high speed railway transport system. On the one hand is the option to invest money into building new tracks with larger curve radii dedicated for modern high speed trains without tilt, i.e. TGV (France) or ICE (Germany). On the other is to use the existing rail infrastructure and invest money into the trains. However for high speed vehicles to negotiate curves safely at higher speeds, on existing tracks, while maintaining passenger comfort at acceptable levels, it is necessary to use *tilting technology*.

1.3.1 The concept of tilting trains

The amount of lateral force experienced by the passengers can be reduced by *tilting* (leaning inwards) the vehicle body. Figure 1.4(a) illustrates the forces acting on a non-tilting vehicle traversing a curve, while Figure 1.4(b) presents the situation for a tilting vehicle on the same curve (θ_v is the body roll, θ_o is the track cant angle, R the curve radius and v the forward speed).

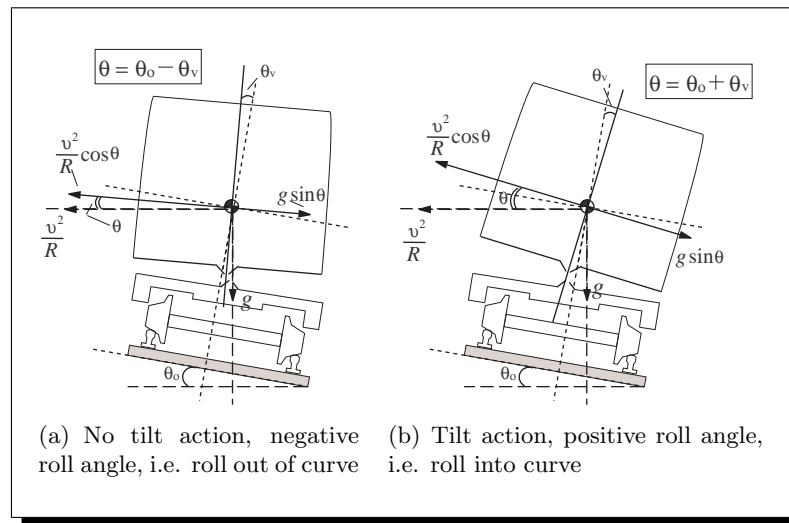


Figure 1.4: Curving forces applied on a railway vehicle

Figure 1.5 presents a diagram of a curved track. The ‘curve transition’ segment provides the smooth transition from straight track to steady-state curve (i.e. the section having a measurable curvature). The cant and curvature change (magnitudes increasing or decreasing linearly) during the curve transition while reaching the steady-state values on steady-state curve. This of course has an impact on the forces acting on the train and thus on the levels of lateral acceleration perceived by the passengers. Note that the duration of curve transitions depends upon the operating vehicle speed. The curved track is normally canted or banked and designed with a specific speed in mind (design speed), to compensate for the curving acceleration perceived by the passengers.

Figure 1.6(a) illustrates the passenger acceleration for a non-tilting (conventional) vehicle running at nominal speed for a given track. At higher speeds, and for the same track, the transition becomes more severe (slope on transition is sharper) due to the smaller duration time, and also the level of steady-state lateral acceleration felt by the passengers increase (Figure 1.6(b)). At this point the introduction of tilt action will allow the vehicle operation at speeds higher than those acceptable to passengers in a

non-tilting vehicle, Figure 1.6(b). Note that some modern high speed lines (i.e. in France and Germany) are designed to have curved tracks with longer transitions and larger curvatures to allow for the operation of non-tilting high speed trains.

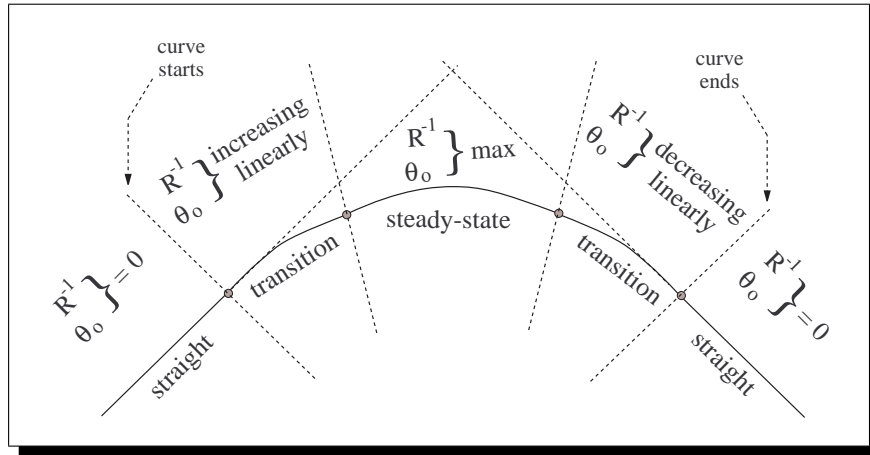


Figure 1.5: Curved track profile

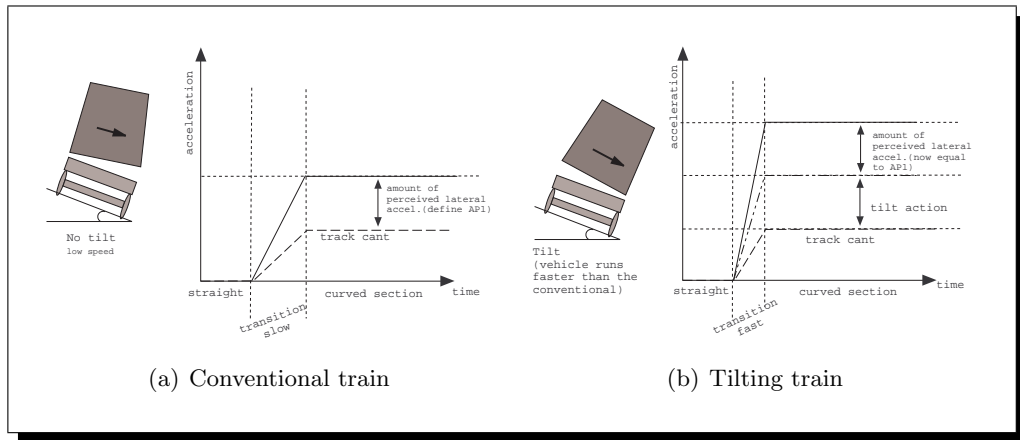


Figure 1.6: Passenger perceived curving acceleration

Although tilt action can provide an increase in passenger comfort at conventional vehicle speeds, the main commercial benefit from the use of tilting vehicles is the reduction of journey times without degrading passenger comfort levels on conventional railtracks. A deciding factor for the reduction in journey time is the frequency of curves appearing in the particular route, i.e. the more curvaceous the route, the greater is the benefit of tilt.

1.3.2 Tilt angle effects

The benefit of introducing tilt angle on the lateral acceleration perceived by passengers during curves is given in Table 1.1. The curving acceleration (m/s^2) is calculated using the following (small angle approximation) expression:

$$\ddot{y}_i = \frac{v^2}{R} - g(\theta_o + \theta_{t_i}), \quad i = 1, 2, 3, \dots, n \quad (1.1)$$

where, v is the vehicle forward speed (m/s), θ_t is the tilt angle (deg), R the curve radius (m), θ_o the track cant angle (deg).

The calculations were based on a curved track profile having a radius of 1200(m) and 6° of track cant angle. The nominal vehicle curving speed was assumed to be 50(m/s).

Table 1.1: Tilt angle effects

Vehicle	(i)	Vehicle body tilt angle θ_v (deg)	Lateral acceleration \ddot{y} (m/s^2)	Reduction in acceleration $\mu_{\ddot{y}}$ (%)	Increase in curving speed α_v (%)
without tilt	(1)	0	1.06	0	0
with tilt	(2)	1	0.88	16.20	4.03
	(3)	2	0.71	32.43	7.91
	(4)	3	0.54	48.64	11.65
	(5)	4	0.37	64.85	15.27
	(6)	5	0.20	81.10	18.78
	(7)	6	0.03	97.28	22.19

Table 1.1 illustrates the benefits of incorporating tilt action on a vehicle. The second column lists the passenger lateral acceleration for the nominal speed, while the third column presents the reduction in lateral acceleration for the corresponding tilt angles based upon the nominal speed. The percentage in operational speed increase for a given tilt angle is shown in the fourth column, as this is particularly important. This is based upon the lateral acceleration experienced by the passengers being equal to that of a non-tilting train running at a slower speed. The calculation of the quantities presented in the table are based on the following

- Nominal passenger acceleration for $i = 1$, $\ddot{y}_o = \frac{v_o^2}{R} - g\theta_o$, $v_o = 50(\frac{m}{s})$
- Reduction in passenger acceleration $\mu_{\ddot{y}} = \left| \frac{\ddot{y}_o - \ddot{y}_i}{\ddot{y}_o} \times 100 \right|$ where \ddot{y}_i is given in (1.1) with $i = 2, 3, \dots, 7$
- Speed increase $\alpha_v = \left| \frac{v_o - v_i}{v_o} \times 100 \right|$ where $v_i = \sqrt{\ddot{y}_i R + g(\theta_o + \theta_{t_i})}$, $i = 2, 3, \dots, 7$

1.3.3 Tilting system mechanical configurations

The early tilt experiments on trains involved vehicle bodies with a low centre of gravity to allow for the centrifugal forces acting on the carriage to cause a passive vehicle tilt action. This approach of using *inertial forces* to let the train tilt was not proven to be very successful. However, passive tilting technology is undoubtedly cheaper compared to active tilting and is still used in the case of small tilt angle applications.

Nowadays, there are three basic mechanical configurations for tilt:

1. *through* (or *across*) the secondary suspension, (Figure 1.7(a))
2. *above* the secondary suspension, (Figure 1.7(b))
3. *below* the secondary suspension, (Figure 1.8(a),1.8(b),1.8(c))

The first option involves control of the airsprings or more recently active anti-roll bars (or stabilisers) to apply tilt directly through the secondary suspension [PGP98]. Although simple to implement, it tends to restrict the amount of tilt due to limitation factors from the suspension and the actuators used (in some cases a single central airspring can be used to allow further tilt action). As a result, most tilt systems use separate mechanisms which have inclined swing links in order to provide a tilting bolster which offers tilt action either above (suspension below mechanism) or below (suspension above mechanism) the secondary suspension. The lateral track forces are inevitably increased as a consequence, but careful bogie design can mitigate this and in general railways have found that there is sufficient margin not to compromise safety.

1.3.4 Problem definition of tilting

The requirements for an active tilting system implementation are: *sensors* to provide measurements for the control strategy, a *controller* to provide the tilt signal, and *active elements* to rotate the vehicle body. The tilt control system performance is very important and its aim is to respond fast to changes in track cant and curvature without significantly degrading the ride quality during straight-track running.

A number of approaches have been used for controlling the tilt systems. These approaches in general can be divided into three sections: *nulling*, *command-driven* and *command-driven with precedence* control.

Nulling control, which was the early control approach, attempts to drive the measured lateral body acceleration to zero on a steady curve, Figure 1.9(a). The feedback

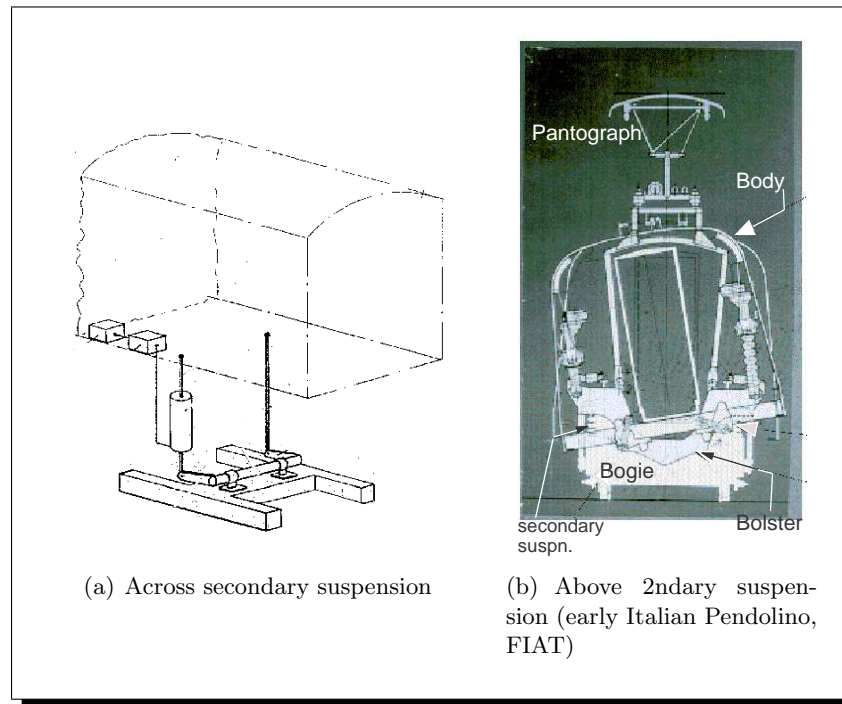


Figure 1.7: Tilt mechanisms (across and above secondary suspensions)

signal is provided from a body-mounted accelerometer. The clear advantage is that the body-mounted sensor does not encounter the large effects of track irregularities due to the action of the secondary suspension as a mechanical filter. The primary drawback with this strategy is that the sensor, mounted on the tilting vehicle body, is within the control loop. This causes interactions between suspension and controller dynamics, which can lead to stability problems.

A further problem is that full compensation of the lateral acceleration does not provide optimum ride quality when curve transitions are taken into account. Trying to reduce the lateral acceleration to zero can result in high roll rates which can be uncomfortable to passengers. Empirical studies during the 1980s [Har86] assessed the passenger comfort on curve transitions and enabled the vehicle curving response to be properly determined.

Command-driven control was the next development, as a result of the ‘nulling’ control strategy limitations. This approach uses both the cant deficiency, obtained from an accelerometer mounted on the bogie, and an additional feedback of tilt angle, to drive the tilt actuators Figure 1.9(b). Full and partial tilt compensation depends on

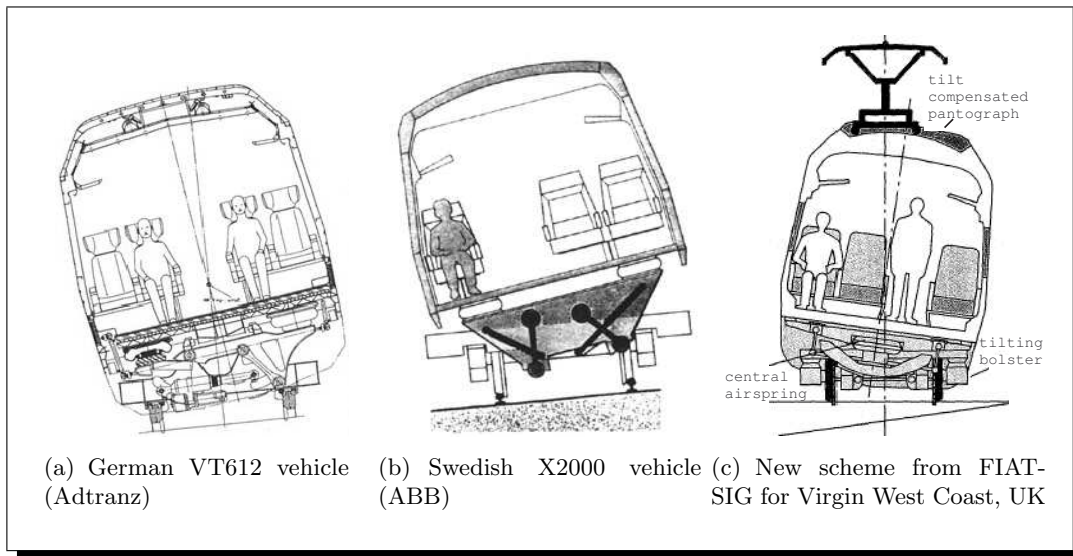


Figure 1.8: Examples of tilt mechanism configurations below secondary suspensions

gain factor K . Making K equal to unity provides full tilt compensation. However, setting K less than unity provides partial compensation which proved the essential point to getting the right transition response. Note that partial compensation can also be achieved with the *nulling* controller by adding a tilt angle feedback, shown in the dotted box of Figure 1.9(a).

In the case of command-driven tilt control the sensor is not affected by the suspension response (it is now situated outside the control loop). However, there are two main problems associated with this control approach. Firstly, due to the harsh environment of the bogie, the accelerometer measures not only the curving acceleration but also acceleration components due to track irregularities. The tilt system responds to the effects of the track misalignments and leads to worsening of the straight track performance. Moreover, the addition of a filter to reduce the effects of high frequency components and the required level of filtering for getting a satisfactory straight track performance introduces a significant time delay on curve transitions. This led to the development of the command-driven with *precedence* control approach.

Precedence control is a *command-driven* strategy which derives the tilt command signal from the preceding vehicle with a filter designed in such a way that the delay introduced will be compensated by the precedence effect, Figure 1.3.4. There has been some development of the concept, including the use of additional sensors (i.e. roll gyroscopes) to further optimise the system response, but the overall principles remain

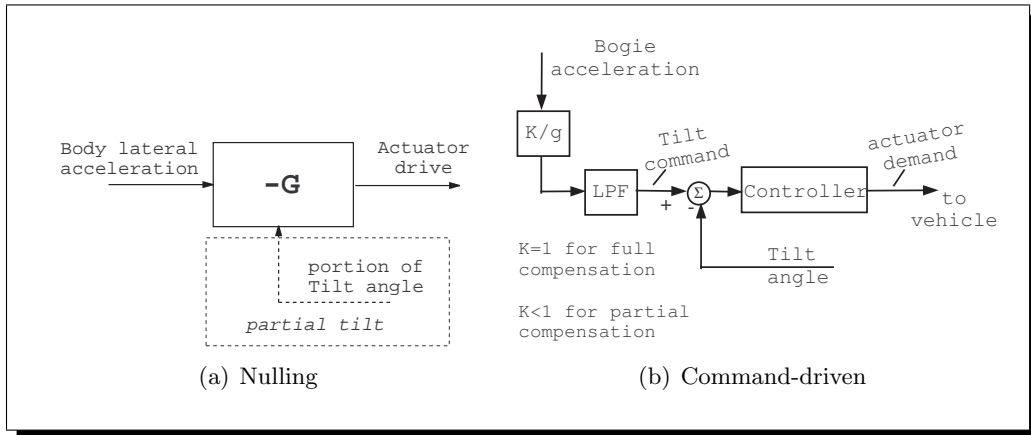


Figure 1.9: Nulling and command-driven control configurations

the same. Normally a single command signal would be generated from the first vehicle and transmitted *digitally* with appropriate time delays down the train. Consequently the *velocity* and the *direction of travel* are important factors for the correct operation of the tilt system. This strategy proved to be successful and it is nowadays used by most tilting train manufacturers. However it is a complex scheme, direction-sensitive, signal connections between trains are required, while the tilt system performance can be *optimised* for a specific route operation. Moreover, leading vehicles have inferior performance due to lack of *precedence*.

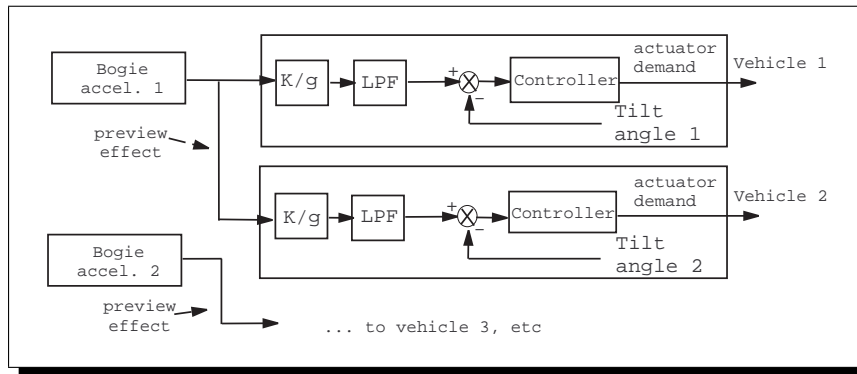


Figure 1.10: Command driven with precedence control scheme

A recent development uses a track database to provide the tilt command signal instead of the sensors used in the previous strategies. The accuracy of the track information provided from the database is a vital factor for this approach to produce effective results.

1.4 Motivation for this Thesis

That tilting trains have been successful is not in doubt. However, the tilt control system design involved mainly *intuitive* or *classical* control methods. As a matter of fact, the published material on tilt system design is primarily based on experimental work. Still, it may be possible to derive a simpler control approach which provides effective tilt action based on individual vehicles using a form of advanced signal processing. Clearly the need of studying ‘in-depth’ the tilt system design from a theoretical point of view is of great importance.

The motivation of this research is to undertake the first rigorous theoretical study of tilt control. Tilt controller settings have been mainly derived from experimental work due to the complex nature of passenger reactions. After the introduction of a comfort index during the 1980s [Har86], the need for more demanding design approaches became essential. Moreover, the mechanical systems which provide the tilt action are continually being developed.

Hence the objectives and their priority in this thesis are: (i) to investigate the dynamic behaviour of tilting trains, (ii) examine various tilt mechanisms and (iii) to develop advanced *local*, based upon single vehicle, tilt control strategies taking ride quality properly into account.

1.5 Work Addressed in this Thesis

The body of work described in this thesis takes the proven concept of tilting trains and enhances it through the use of newer so called ‘modern’ control concepts. The principal area of investigation is that of control strategies for local, i.e. based on single vehicles, tilt control. At present tilt control is based on precedence schemes which can be complex, direction-sensitive and front vehicles have inferior performance due to lack of precedence.

Applying ‘modern’ control techniques, local vehicle tilt control can be utilised by using more sophisticated controller structures to provide results comparable to the precedence schemes.

1.5.1 Thesis structure

The thesis is laid out as follows:

- Chapter 2 is a detailed survey of work involving tilting trains and their applications. It also includes a review on the general area of active suspensions.
- Chapter 3 discusses on track geometry and the methods used for assessing the control strategies developed.
- Chapter 4 presents the prerequisites on designing tilt controllers.
- PART I contains the study of tilting based upon active anti-roll bars (tilt across secondary suspensions).
 - Chapter 5 provide a detailed modelling of a tilting train involving an active anti-roll bar and investigates the dynamic behaviour of the vehicle.
 - Chapter 6 discusses on the limitations of the early ‘nulling’ classical control strategy, investigates its limitations and illustrates the approach currently used by tilt manufacturers.
 - Chapter 7 proposes alternative control designs based upon advanced concepts for designing local/vehicle tilt controllers for the active ARB; with improved performance mainly based upon body-mounted sensors.
- PART II presents the study of a tilting mechanism for providing tilt below the secondary suspension.
 - Chapter 8 discusses the modelling of the vehicle using the tilting mechanism structure. It also reveals the differences relative to the anti-roll bar system.
 - Chapter 9 is an adaptation of the control schemes designed for an anti-roll bar, to the case of the tilting mechanism. It also extends the advanced control concepts with respect to overall system performance, based upon the tilting bolster.
- Chapter 10 contains a conclusion and discussion on the overall thesis results, while suggests possible further work.
- The following information is included in the Appendix: (A) Track Profiles and Vehicle Parameter Values, (B) Supplement on Theoretical Concepts, (C) P_{CT} Factor Evaluation, (D) Modelling of Suspension Elements, (E) List of State Space Model Matrices, (F) Controller Structures for \mathcal{H}_∞ Schemes, (G) Research Work Publications, (H) List of Software sample files.

1.6 Published Work

An amount of work included in this thesis has been published in the following papers:

1. Zolotas, A. C., Goodall, R. M., *Advanced Control Strategies for tilting railway vehicles*, UKACC, Control 2000, Cambridge, UK, Sep. 2000
2. Zolotas, A. C., Halikias, G. D., Goodall, R. M., *A Comparison of Tilt Control approaches for high speed railway vehicles*, Proceedings ICSE 2000, Coventry, UK, Vol. 2, pp. 632-636, Sep. 2000
3. Goodall, R. M., Zolotas, A. C., Evans, J., *Assessment of the Performance of Tilt System Controllers*, The Railway Conference at Railtex 2000, NEC Birmingham, UK, Nov. 21-23, 2000
4. Zolotas, A. C., Goodall, R. M., Halikias, G. D., *New control strategies for tilting trains*, IAVSD Symposium 2001, Lyngby-Copenhagen, DK, Aug. 20-24, 2001

1.7 Thesis Contributions

This thesis addresses a number of issues concerning tilt controllers and makes contributions in the following areas:

- (a). Fundamental study of the tilt control concept;
- (b). Development of detailed vehicle models of tilting trains for control design;
- (c). Theoretical investigation of the ‘nulling’ tilt control problem;
- (d). Assessment approach of dynamic tilt controllers performance;
- (e). The novel idea of employing modern control concepts for tilt control for efficient local tilt control design, especially in the area of estimation and robust \mathcal{H}_∞ control.

Chapter 2

Literature Survey

The purpose of this review is not to provide an extensive coverage of all the literature available but to highlight the relevant studies to this research. The first section presents a brief coverage on literature related to active suspensions, the second part is a survey on the work done specifically on tilting train.

2.1 Active suspensions

The idea of active suspensions was introduced during the late 1960s. From this a large number of studies continued particularly in the field of automotive and railway vehicle suspensions. The basis of most active suspensions was *skyhook damping* - connecting the vehicle via a damper to the 'sky' - which was introduced by Karnopp et al in 1974 [KCH74]. Since then it has been used as the basic introduction to active suspensions by many researchers. Of course the implementation of skyhook damping is impossible using passive components, instead an arrangement of actuators is used to produce the same effect.

The need for active suspensions is well discussed by both Karnopp [Kar78] and Goodall and Kortüm [GK90]. There are review papers presenting the benefits of using active suspension technology in the area of railway vehicles [GK83], [Her81]. General discussion papers also exist [KH91], [Wic92], [AW95], introducing to the basic concepts of active suspension technology. Williams [Wil86] compares classical and optimal control approaches for active suspensions, while Pratt [Pra96] is concerned with applying active suspension specifically to high-speed trains. Both of the above researchers include a comprehensive description of the skyhook damping. Other technical papers emphasise the limitations related to the use of active suspension technology [Goo93], which are mainly connected to interactions due to vehicle geometry, the complex nature of

the active suspension systems and the high power consumption. In search of a more detailed list of references the reader is referred to Elbeheiry et al [E⁺95].

2.2 Tilting trains

The theory behind tilting has been understood for many decades but little work had been done until the 1960s. Certain experiments were carried out both in United States and Europe [Ano70] involving pendular-suspension coaches. The idea of powered tilt was introduced by British Railways in 1968. From this point tilting trains start gaining ground as manufacturers realised that it was one of the cheapest ways to raise the average speeds (simply run faster through curves!) [Kof70]. Much development work was undertaken during the 1970s in UK, Sweden, Italy and North America [San74], [Eli97]. Most of the experiments succeeded and the experimental trains continued into commercial operation, apart from UK's Advanced Passenger Train (APT) [BK82]. From 1982 after the ECE (European Commission for Europe) received a resolution to take the appropriate steps for improving railway links [Bin87], the situation has changed much and it is clear that tilting trains 'are here to stay'. As a matter of fact, UK's Virgin Rail will introduce tilting train technology in the West Coast Line [Ano98b] and its franchise commitments also include the scope for infrastructure upgrade [Wat99].

Articles [Aut99] presenting the commercial benefits offered by using tilting technology in railway vehicles, e.g. reduced journey time and passenger comfort, may be found. Other review papers describe the concept of tilting and its application to railway vehicles. For example, Goodall R.M. in two of his papers, [Goo97], [Goo99], gives a comprehensive study on the concept of tilt and the tilt system configuration and he also emphasises the role of active suspensions for future development. A detailed review on current tilting train implementation is included in the former of his papers. Harris et al [HSS98] present the concept of tilting and the performance advantage of tilting systems while introducing the limits to tilt applications and tilt second order effects such as increased track forces and fuel savings. Also Schmid [Sch97] presents a review on the tilt debate from an operations angle and focuses on developments in the UK.

A number of studies concentrate on specific issues in relation to tilting vehicle technology. Gawthorpe and Johnson [GJ] address the importance of the aerodynamic effects for tilting trains. They also stress that the aerodynamic implications for tilting trains originate from the higher speeds allowed for tilting trains rather than from the tilting

action itself. The extent and severity of each effect is described, such as pressure waves when travelling in tunnels, interaction with other traffic and cross-wind effects. In the offered solutions the benefits from the use of *pressure sealed* rolling stock is largely emphasised.

The use of the bogie in a tilting train structure is also very important. Kayserling [Kay74] presents a technical description of the work done during the 1970s on power bogies incorporating body-tilt via secondary air-suspensions for the ET 403 tilting train. Huber [Hub97] presents the development of a bogie-based tilt option, in which he emphasises the simplicity and flexibility with such a configuration. Andersson [And94] discusses the improvements in tilt and bogie dynamics based on the X2000 high speed train. The author introduces the X2000 tilting train technology which comprises *self-steering bogies* and presents the possibilities and limitations for future developments. Limitations such as the delay in tilt systems, tilt performance in the presence of straight track misalignments and infrastructure implementation are presented based on results from the X2000 experience. He also discusses the safety criteria relevant to the bogie dynamics and suspensions. A recent paper [AH99] reviews the principal designs of bogies for tilting trains, the main issues being radial steering and active lateral suspensions.

2.2.1 Work on Control studies

Published papers on tilt control studies may be found, though only few exist on detailed theoretical control studies of tilt system design. One study presented the use of inverse dynamics to define a tilt control strategy in order to determine the optimum command signals used in a tilting train through curves [S⁺96], [G⁺98]. The *inverse dynamics* method is introduced via a simple example and simulation using real track data demonstrated the effectiveness of the method in the design of the tilt control system. Pearson et al [PGP98] presented the design of an active anti-roll bar tilt system, although for limited tilt action, emphasising the simplicity of the implementation and the limitation factors introduced, and compared classical and optimal control methods. The simulation results based on both the single-end and full vehicle models showed good tilting performance for both methods, the optimal approach being marginally better. A number of control studies in Japan presented the control of tilting trains via the airsprings [H⁺91],[N⁺97], [N⁺72]. A recent study in China [Shu99] demonstrated the control of tilting vehicles using *adaptive* control based on a new multi-body system dynamics model, while another in Germany presented a control design using *predictive*

[Bär99] control. A \mathcal{H}_∞ robust approach, although based upon experimental data was presented in [MH99]. Moreover, a recent paper by Kent and Evans [KE00] discusses on the analysis and control of a tilting train using ‘hardware-in-loop’ simulation based upon a demonstration tilting vehicle. Such a technique is an effective tool for testing before the introduction of real vehicles in passenger service.

2.2.2 Work on Application of Tilt

A number of well-established tilting train services exist in Europe, Japan and North America, while new project work is undertaken [Goo97]. In Europe tilting trains operate successfully in Italy, Sweden, Spain and Germany and newer development work is on-going in Switzerland, Austria and Spain. The Italian tilting train *Pendolino*, operating since 1988 [CPM96], uses hydraulic actuation and tilts above the secondary suspension offering a maximum tilt angle of 8° . Sweden developed its own tilting train the *X2000* which started operating in 1990. The system uses hydraulic actuation and tilts below the secondary suspension [A⁺95]. In the UK, Virgin will have its first tilting train in operation. FIAT-SIG developed a tilt system which is based on Pendolino tilt control but uses electro-mechanical actuation [For95]. In Germany, Adtranz (formerly AEG) work involved a tilting system using electro-mechanical actuators [Sau96], a concept initially investigated in the UK [PP83]. An experimental work from Siemens SGP (Austria) is also based on electro-mechanical actuators [Str97], notably the control strategy is not based on precedence control. Hydraulic actuation was used in experiments undertaken by CAF in Spain on applying inverse dynamics to design the active tilting system [S⁺96].

North American tilting train services use vehicles designed by Bombardier, with a tilt configuration similar to the X2000 Swedish tilting train [Goo97]. On the other hand, Japanese research work is mainly based on applying active tilting through the airsprings, due to the narrow gauge of their conventional railway structure [H⁺91], [N⁺72], [N⁺97]. Most of the Japanese systems use stored track data and train position information [K⁺93], [H⁺91]. There are also new experimental work under way but no details are given by the manufacturers. A more detailed survey on tilting train applications can be found in Goodall [Goo97].

2.3 Summary

This review covers aspects on active suspensions and in particular tilting systems: history, implementation, control studies, applications. The evolution of tilting control

systems was mainly based on industrial studies, however a number of academic studies is also referenced.

Chapter 3

Track Geometry and Tilt System Assessment methods

Track geometry refers to the variety of parameters that describe both the layout and path of a railway track. Railway vehicles are dynamically-complex systems which are subject to such a variety of inputs from the track. Broadly these can be categorised into the following two categories:

- (a). Stochastic inputs (or Track irregularities), i.e. random changes in the track vertical, lateral, and cross-level position,
- (b). Deterministic (or Design track) inputs, such as curves and gradients.

This thesis deals with two specific forms of *track geometry*: (a) lateral track irregularities (random changes in the lateral track position) and (b) deterministic curved sections.

3.1 Deterministic Inputs

Deterministic inputs arise from the intended geometrical layout of the track, which are designed by civil engineers to ensure that the effect upon the passengers meets defined comfort requirements. For tilting trains this relates to curved sections, i.e. track segments with measurable curvature (R^{-1}) as shown in Figure 3.1.

To minimise the effect of the centrifugal forces experienced by the vehicle on the curve, the track is leaned inwards or “canted” in order to rotate the vehicle inwards (Figure 3.1).

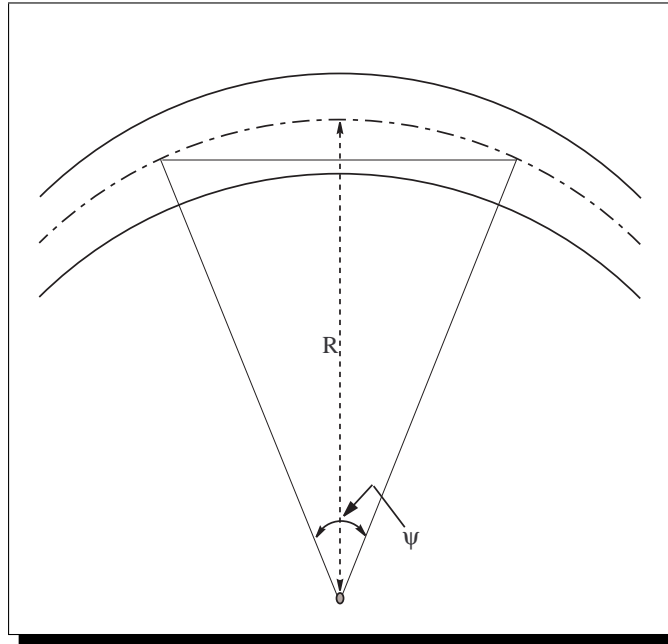


Figure 3.1: Deterministic track curvature

The rates of cant and curvature are changing linearly during the curve transitions, while settling on their steady-state values on steady-state curve, see Figure 3.3.

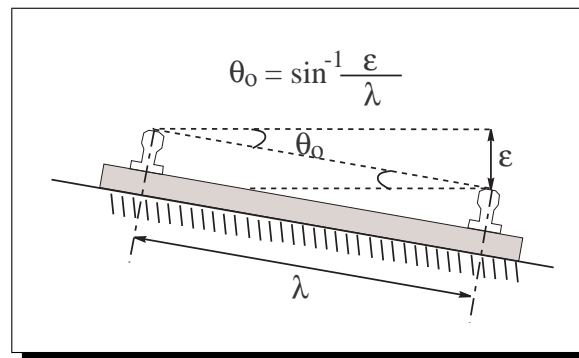


Figure 3.2: Deterministic track cant

The resultant lateral acceleration is known as *cant deficiency*, which defines the difference between the existing degree of cant and the degree required to fully eliminate the effect of centrifugal force at maximum allowable speed [För00]. Note that the amount of cant angle is limited due to safety and technical reasons (i.e. slow freight trains on curves, switching).

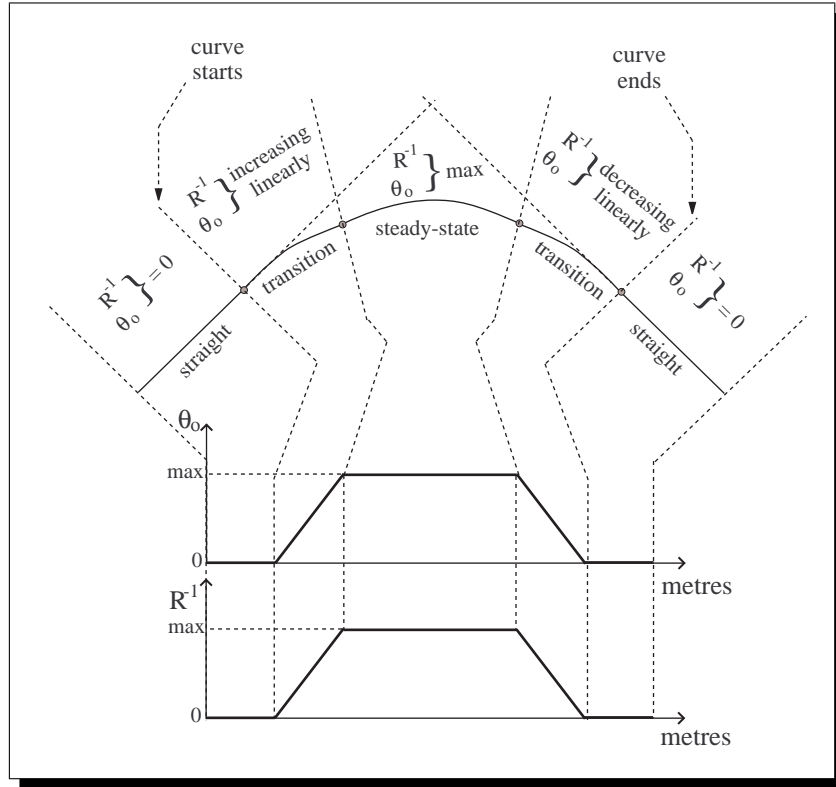


Figure 3.3: Curved track section

The expression for cant deficiency is

$$\mathcal{D} = \frac{v^2}{gR} - \theta_o \quad (3.1)$$

and depends upon vehicle speed v , track curvature R^{-1} and cant angle θ_o . Typically curved tracks in the UK are designed to provide a cant deficiency of around 5.83° ($1 \frac{m}{s^2}$). In addition, the transitions are carefully designed for appropriate cant and curvature rates over a period of approximately 2-3 seconds. A summary of the deterministic track profiles used in this thesis can be found in Appendix A.1.

3.2 Random (Stochastic) Inputs

No railway track is laid perfectly, as a consequence there will always be small deviations from the ideal path or nominal centerline. Stochastic track inputs represent the deviations of the actual track from the intended alignment, these could involve lateral alignment and/or gauge, and vertical alignment and/or cross-level (cant deviations). A sample of lateral track misalignments can be seen in Figure 3.4.

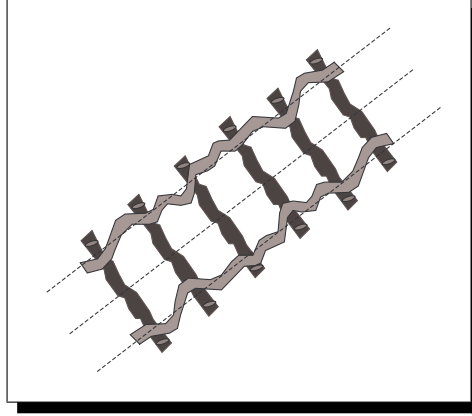


Figure 3.4: Lateral Track misalignments

3.2.1 Representation of lateral track irregularities

This thesis involved the use of lateral track irregularities for the purposes of vehicle response studies. However, accurately representing the lateral track irregularities is difficult [Pra96]. An approximate expression for the lateral track measured spatial spectra is:

$$S_S(f_s) = \frac{\Omega_1}{f_s^3} \quad m^2(\text{cycle}/m)^{-1} \quad (3.2)$$

The above information need to be converted into a temporal form in order to be used in dynamic analysis. The relationship between the spatial wavelengths of expression (3.2) and the temporal excitation, is velocity dependent (3.3). That means a given wavelength would excite the vehicle with a different frequency at a different speed.

$$f_s(\text{cycles}/m) = \frac{f_t(\text{cycles}/s)}{v(\text{m}/s)} \quad (3.3)$$

Substituting (3.3) into (3.2), the track wavelengths in terms of the temporal frequency f_t is given by:

$$S_S(f_t) = \frac{\Omega_1 v^3}{f_t^3} \quad m^2(\text{cycle}/m)^{-1} \quad (3.4)$$

Expression (3.4) can be converted to a spectrum with a temporal base by performing the following division:

$$S_T(f_t) \quad m^2(\text{cycle}/s)^{-1} = \frac{S_S(f_t)}{v} \frac{m^2(\text{cycle}/m)^{-1}}{(m/s)} \quad (3.5)$$

Usually the track input is in terms of the velocity rather than the displacement. Hence, the first step is to express spectrum $S_T(f_t)$ in terms of radians rather than cycles:

$$S_T(f_t) = \frac{\Omega_1 v^2}{2\pi f_t^3} \quad m^2(\text{rad}/s)^{-1} \quad (3.6)$$

Then the derivative of the above spectrum is derived by simply multiplying the spectrum by $(2\pi f_t)^2$. Thus,

$$\dot{S}_T(f_t) \quad (m/s)^2(rad/s)^{-1} = S_T(f_t) \quad m^2(rad/s)^{-1} \times (2\pi f_t)^2 \quad (3.7)$$

which implies

$$\dot{S}_T(\omega_t) = \frac{2\pi\Omega_l v^2}{f_t} \quad (m/s)^2(rad/s)^{-1} \quad (3.8)$$

The final expression comes in terms of cycles rather than radians, and is given by:

$$\dot{S}_T(f_t) = \frac{(2\pi)^2\Omega_l v^2}{f_t} \quad (m/s)^2(Hz)^{-1} \quad (3.9)$$

It can be easily seen that the lateral track velocity represents a *coloured noise* and has a steady roll-off as frequency increases. The result of (3.9) is widely used in this thesis, characterised by a lateral track roughness of $\{\Omega_l\}$ of $0.33 \cdot 10^{-8}m$. An appropriately defined shaping filter was used to shape the noise spectrum. More details can be found in Appendix A.1.

3.3 Tilt System Performance Assessment Methods

Although active tilting has become a standard technology incorporated into the railway industry, a number of issues remain which need to be resolved for determining the performance of tilting trains. Qualitatively, a good tilt control system will respond principally to the deterministic track inputs, while ignoring as much as possible any random track irregularities. In order to assess different tilt control approaches in an objective manner, it is essential to define appropriate criteria and conditions.

3.3.1 Curve Transition Performance (Deterministic criterion)

The assessment of tilt controllers used in this thesis, is based upon work presented in [GZE00] which proposes a more rigorous overall approach for accessing the deterministic performance of tilt control systems. The procedure is as follows:

The curve transition response is separated into two aspects

1. Investigation of the fundamental tilting response based upon the P_{CT} factor (see Appendix C)
2. Investigation of the transitional dynamic suspension effects based upon the “*ideal tilting*” approach

The assessment of tilting train curve transition performance based upon the P_{CT} factors arose from the difficulties with tilting trains, and relies upon a comprehensive experimental/empirical study undertaken in the 1980s [Har86]. This approach is now accepted as European Standard [Ano98a] and details on the equations which provide the values are given in Appendix C, from which it can be seen that the passenger comfort is affected by three variables: *lateral acceleration*, *lateral jerk* and *roll velocity*. The expressions are derived empirically and provide the percentage of passengers who feel uncomfortable during the curve transition, both standing and seated, hence providing a realistic and objective measure. The P_{CT} evaluation formula applies for the transition entry on curves and reverse transitions, having a time duration of at least 2 seconds.

The fundamental tilting response, provided by the P_{CT} factors, must be as good as a passive vehicle at lower (non-tilting) speed, otherwise the passenger comfort will inevitably be diminished, regardless to the effectiveness of the tilt control system. It is possible therefore to introduce the idea of “ideal tilting”, i.e. where the tilt action follows the specified tilt compensation in an ideal manner, defined on the basis of the maximum tilt angle and cant deficiency compensation factor. This combination of parameters can be optimised using the P_{CT} factor approach for deterministic inputs in order to choose a basic operating condition, and this will give “ideal” P_{CT} values (one for standing, one for sitting).

Moreover, it is necessary to quantify the *additional* dynamic effects which are caused by the suspension/controller dynamics as the transitions to and from the curves are encountered, essentially the deviations from the “ideal” response mentioned in the previous paragraph. These deviations relate to both the lateral acceleration and roll velocity, although the former is the main consideration. The aim is to *minimise* the *resultant deviations*, and the values derived for a normal passive suspension can be used as a guide for their acceptable size. The calculation for the deviations is defined as follows:

- $|\ddot{y}_m - \ddot{y}_{m_i}|$, the deviation of the actual lateral acceleration \ddot{y}_m from the ideal lateral acceleration \ddot{y}_{m_i} , in the time interval between 1s before the start of the curve transition and 3.6s after the end of the transition (Figure 3.5)
- $|\dot{\theta}_m - \dot{\theta}_{m_i}|$, the deviation of the actual absolute roll velocity $\dot{\theta}_m$ from the ideal absolute roll velocity $\dot{\theta}_{m_i}$, in the time interval between 1s before the start of the curve transition and 3.6s after the end of the transition (Figure 3.5)

The analysis is based upon a perfectly-aligned track in which the cant and curvature

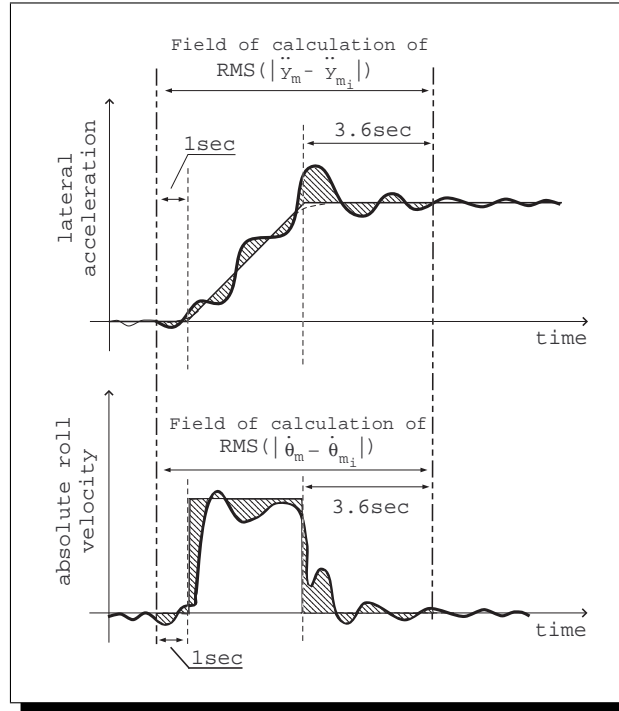


Figure 3.5: Calculation of deviation of actual from ideal responses for acceleration and roll velocity

rise linearly with time/distance, while the tilting action is applied in a similarly synchronised manner.

- **Example of deterministic tilt performance**

Consider the following curved track input:

Curve radius $R=1000\text{m}$; track cant $\theta_{cant} = 6^\circ$; transition length = 145m

Cant deficiency = 6° ; passive vehicle speed $v_o = 159 \frac{\text{km}}{\text{h}}$

Passive roll-out (assumed) = 0.6° ; $P_{CT}^{(\text{standing})} = 29.0\%$; $P_{CT}^{(\text{seated})} = 7.9\%$

For the tilting case two things need to be specified, the cant deficiency compensation factor and the “speed-up” factor, i.e. the ratio of tilting to non-tilting speeds. The right hand diagram of Figure 3.6 shows the ideal values for a typical tilting condition - 30% increase in speed and 60% cant deficiency compensation. Comparing the two diagrams shows that, although the lateral acceleration is reduced, the jerk and roll rates are increased compared to the passive case.

The P_{CT} factors for the tilting train can then be evaluated, and compared with those for the non-tilting vehicle; the required tilt angle also emerges from the calculation process. Figure 3.7 shows respectively the two P_{CT} factors and the maximum tilt angle for speed-up factors of 15-35% with compensation factors varying from 40-80%.

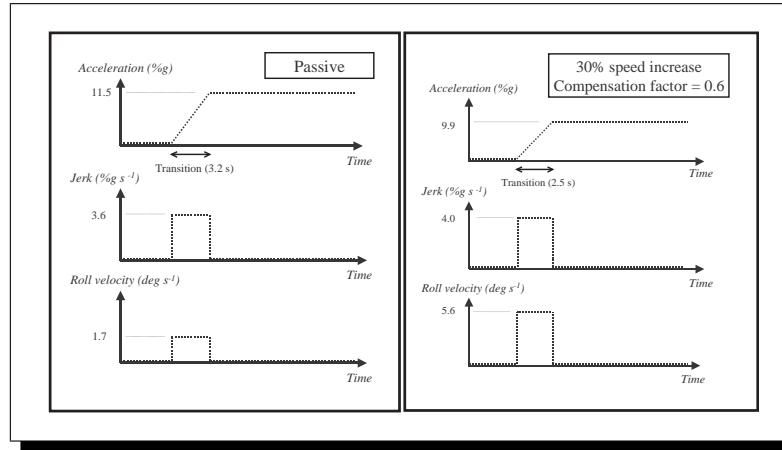


Figure 3.6: Acceleration, jerk and roll rate time history

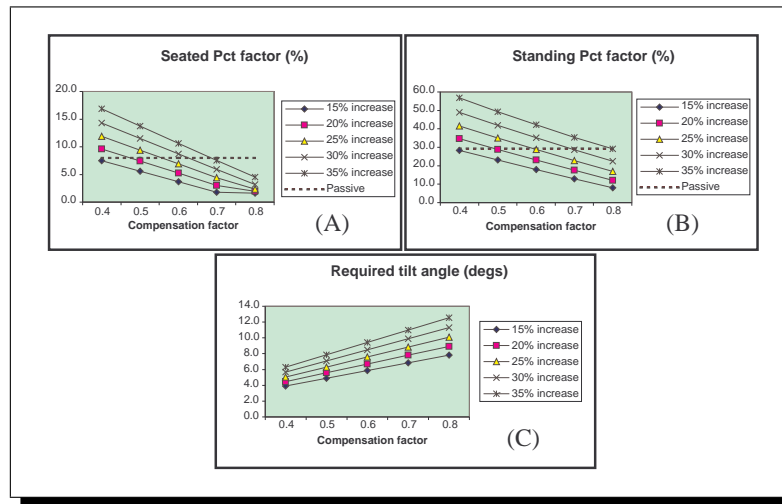


Figure 3.7: P_{CT} factors: (a)seated, (b)standing and (c)max tilt angle

From these it can be seen that to satisfy the requirement for seated passengers a 30% increase in speed is possible with a compensation factor of 0.63 and a tilt angle of 9 degrees; for standing passengers the corresponding values are 0.69 and 10 degrees. It is clear therefore that, given the industry maximum of around 8-9 degrees, 30% speed-up cannot be achieved without

deteriorating the passengers' comfort during curve transitions. For a 25% increase in speed the values are: for seated 0.57 and 6.6 degrees; for standing 0.61 and 7.8 degrees.

Note that the transition length used is relatively long (more than 3sec at non-tilting speed). Use of a shorter transition would increase the tilting P_{CT} , effectively reducing the speed-up potential.

Two sample control strategies were used for comparison based upon the proposed method: a command-driven with precedence type and a recently suggested model-based estimation scheme used for local/vehicle control (details can be found in [GZE00] and in Chapters 7, 9). The assessment involves 30% speed increase and 60% tilt compensation. Since the passive (non-tilting) case obviously provides a useful baseline for the size of the deviations, this has been included, and Figures 3.8(a) and 3.8 show the time histories. The "ideal" acceleration and roll rates are also shown on the graphs so that the dynamic deviations caused by the suspension and/or controller dynamics can be clearly seen. Table 3.1 provides a qualitative comparison, presenting the r.m.s. values of deviations during the curve transition.

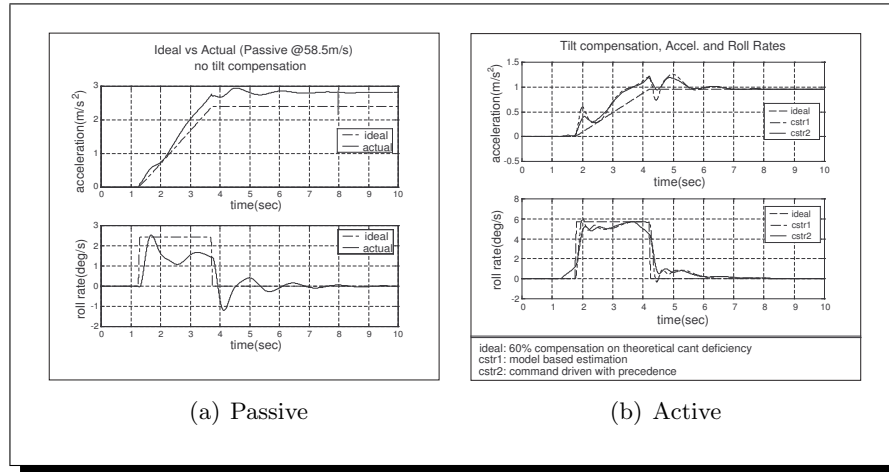


Figure 3.8: Vehicle responses

Table 3.1: Sample of Comparison of RMS deviations

	Passive @45 $\frac{m}{s}$	Passive @58.5 $\frac{m}{s}$	Precedence @58.5 $\frac{m}{s}$	Model-based Estim. @58.5 $\frac{m}{s}$
Deviations Roll rate ($\frac{deg}{s}$)	0.009	0.012	0.017	0.016
Deviations Acceleration (%g)	0.90	1.775	1.05	1.40

3.3.2 Straight Track Performance (Stochastic criterion)

The analysis of the performance of the tilting suspension in the stochastic case relies upon the calculation of precise values for the ride quality in response to the effects of the track misalignments.

The criterion for straight track performance is to allow the degradation of the lateral ride quality by no more than a specified margin compared with the non-tilting vehicle, a typical value being 7.5% which is used throughout in this thesis. It is required for the assessment of the tilt controller performance this comparison to be made at the higher speed (note however that the passive vehicle is used only for comparison, and in reality it will not run at excess speeds). Naturally a comparison of ride quality with a lower speed vehicle would be also needed, although achieving a acceptable ride quality at elevated speeds will involve either improved overall suspensions or better quality railtrack, i.e. not a function of the tilt controller [GZE00].

It is worth mentioning that a number of tilt control approaches include a facility where the tilt action is disabled on straight track, for example with a roll gyroscope on the bogie provided to indicate the start of the curve. Nonetheless these are generally effective only on long sections of straight track. Still, interactions between the lateral suspensions and the tilt controller will occur both on steady curves and immediately following a curve, thus the proposed criterion is a sensible target, even with these enhanced schemes.

3.4 Ride Quality Calculation Methods (Random Inputs)

Ride quality is generally characterised by the Root Mean Square (R.M.S.) acceleration perceived by the passengers when the vehicle is excited by the roughness of the track irregularities.

There are three methods of calculating the R.M.S. acceleration values for ride quality used in this thesis. The first method is the well known *frequency response* analysis, the second is the time based *covariance* analysis, while the final one is the *time history*

analysis.

Ride quality is closely connected to human evaluation of comfort, and its assessment is based upon given statistics and weighting factors [För00]. However, there is much argument concerning the appearance of such relations, i.e. choice of weights, statistical approaches or evaluation formulae. In the author's opinion the raw accelerations provide an effective comparative measure of ride quality without the need of additional weighting functions. Thus, the approach for ride quality assessment described in this thesis is based upon the use of raw accelerations.

3.4.1 Frequency response analysis

The output power spectrum $S_y(\omega)$ is equal to the square of the system transfer function $H(j\omega)$ multiplied by the input power spectrum $S_w(\omega)$ [Tho93]

$$S_y(\omega) = |H(j\omega)|^2 S_w(\omega) \quad (3.10)$$

In the case where w_i , $i = 1, 2, \dots, N$ uncorrelated inputs exist for which the cross-spectral density terms are zero, expression (3.10) can be generalised to define the total output power spectrum $S_{y_{tot}}(\omega)$

$$S_{y_{tot}}(\omega) = \sum_{i=1}^N |H_m(j\omega)|^2 S_{w_i}(\omega) \quad (3.11)$$

$H_m(j\omega)$ represents the transfer functions between the output quantity and the various input signals. Usually this can be multivariable, i.e. when R.M.S. values for more than one output signals are required relative to a number of inputs, and can be represented as

$$H_m(j\omega) = C(j\omega I - A)^{-1} W + D_w \quad (3.12)$$

where A is the state matrix, W the disturbance matrix, C the output state matrix and D_w the output distribution disturbance matrix.

The mean square value of the response can be now calculated, for a SISO system, using the following expression

$$\overline{y^2} = \int_{-\infty}^{\infty} |H(j\omega)|^2 S_w(\omega) d\omega \quad (3.13)$$

Note that care should be taken when defining the Fourier Transform for the calculation of the mean square value. Both the definition of the Fourier Transform and the input power spectrum should be subject to the same function (either with respect to *rads/s* or w.r.t. *Hz*). Otherwise, the integration will undoubtedly cause confusion regarding the

frequency and the result will not be as expected. For example an alternative definition for the mean square value is

$$\overline{y^2} = \frac{1}{2\pi} \int_{-\infty}^{\infty} |H(jf)|^2 S_w(f) df \quad (3.14)$$

where $S_w(\omega)$ was replaced by $\frac{S_w(f)}{2\pi}$ so as to integrate w.r.t. Hz .

In practice it is preferable to work with spectral densities over only the positive range of frequencies, thus (3.13) changes into

$$\overline{y^2} = 2 \int_0^{\infty} |H(j\omega)|^2 S_w(\omega) d\omega \quad (3.15)$$

Finally, the root mean square value of the response is given by

$$y_{rms} = \sqrt{\overline{y^2}} = \sqrt{2 \int_0^{\infty} |H(j\omega)|^2 S_w(\omega) d\omega} \quad (3.16)$$

When $S_w(\omega)$ is not flat spectrum (i.e. input noise is not white), it is a matter of re-arranging the system response to also include the shaping filter function $H_f(j\omega)$ of the noise spectrum, i.e. $\tilde{H}(j\omega) = H(j\omega)H_f(j\omega)$.

Lateral ride quality is a very important quantity in this thesis, and its R.M.S. can be evaluated with respect to the track velocity input spectrum from

$$\ddot{y}_{m_{rms}} = \sqrt{2 \int_0^{\infty} |H_{rq}(j\omega)|^2 \dot{S}_T(\omega) d\omega} \quad (3.17)$$

where $H_{rq}(j\omega)$ is the transfer function between the measured lateral acceleration and the lateral track velocity input, \dot{S}_T is given in (3.8). Sufficient results can be obtained, from expression (3.16), to indicate as to whether the tilt system provides the required ride quality. This procedure can be extended for systems with time delays [Pad95] if required.

3.4.2 Time based Covariance analysis

The frequency-domain analysis can sometimes be computationally intensive, especially in the case of large scale systems, the reason being the requirement of a complete numerical integration. An alternative technique is the *time-based covariance analysis*, which utilises the solution of the *Lyapunov* matrix stability equation.

In this method two stages are required: (i) the calculation of the state transition matrix for a stable dynamic system, and (ii) the solution of the Lyapunov equation (the theory behind this concept is included in Appendix B.1). The vehicle model can be represented using the following linear state-space formulation:

$$\dot{x} = Ax + \Gamma w \quad (3.18)$$

$$y = Cx + Hw \quad (3.19)$$

where A is the state matrix, Γ the disturbance input matrix and w the disturbance input (note that when the model is strictly proper $H = 0$). The system is driven by one random input which is a Gaussian white noise process and can be used in Lyapunov equation (3.20) to provide the stationary state covariance matrix P_x ($\dot{P}_x = 0$) of the system.

$$AP_x + P_x A^T + \Gamma Q_w \Gamma^T = 0 \quad (3.20)$$

where Q_w is the covariance of the (white) noise input $w(t)$. Matrices $A, \Gamma Q_w \Gamma^T$ are square matrices of identical sizes, while P_x is a positive definite square matrix, and also symmetric if $\Gamma Q_w \Gamma^T$ is symmetric. It should be noted that the positive definite solution of the Lyapunov equation exists only for *stable* systems and P_x is finite only when the system is *strictly proper*.

The covariance of the output vector can be derived by

$$P_y = CP_x C^T \quad (3.21)$$

while the R.M.S. for the individual output quantities is given by

$$y_{rms} = \sqrt{|P_{y_{ij}}|}, \quad \text{for } i = j = 1, 2, \dots, n \quad (3.22)$$

Sometimes the model might include pure integrators which is unacceptable with the covariance analysis, these need to be modified using appropriate low pass filters to make the technique workable.

In practice there is no white noise excitation process with infinite bandwidth. In such cases it is viable to develop a shaping filter to modify the white noise input to represent the characteristics of the actual physical process (i.e. coloured noise processes). The next step is to incorporate the shaping filter into the dynamics of the system and follow the same procedure as before [Pad95].

3.4.3 Time history analysis

A different approach to find the R.M.S. of a signal is to investigate the vehicle model output responses with respect to the track data recordings. This technique is particularly useful in the case of non-linear systems. Note that both the *Frequency domain* and *Time-based covariance* analysis previously described, require the system to be represented in a *linear* state-space form. Thus in the case of non-linear systems or in systems incorporating active non-linear suspensions, *time history analysis* may be preferable.

The simplest way of analysing the system is to obtain the track data and simulate the response of the railway vehicle model on a computer. The outputs from the simulation will be time histories and either can be used to provide the R.M.S. values directly, or a ‘Fast Fourier Transform’ can be performed to analyse the frequency information of the signals (system resonances).

The model can be arranged in a state-space form, i.e. $\left\{ \begin{array}{l} \dot{x} = Ax + \Gamma\dot{w} \\ y = Cx + H\dot{w} \end{array} \right\}$ which can represent either the passive vehicle model or any additional active suspensions. The model can be also arranged to include non-linearities if necessary. An appropriate ride index can be then formed by selecting the different variables of interest via matrix C .

The root mean square value for a given output can be found using

$$y_{rms} = \sqrt{E[y^2(t)]} = \sqrt{\overline{y^2}} = \sqrt{\lim_{T \rightarrow \infty} \frac{1}{T} \int_0^T y^2 dt} \quad (3.23)$$

or similarly

$$y_{rms} \approx \sqrt{\frac{1}{n} \sum_{i=1}^n y_i^2} \quad (3.24)$$

where n is the number of elements in the data sample. From the above expressions it can be easily seen that the accuracy of the R.M.S. value depends upon the available duration of track data (i.e. $T \rightarrow \infty$) and also the number of sample points n . Therefore for accurate results a sufficiently long track should be selected together with an adequate number of sample points. The same applies if an FFT is to be employed, a sufficient number of points should be used to reveal accurate information of the signal frequency content (i.e. improve the resolution).

There may be some minor differences in the stochastic assessment of the control strategies from case to case. This is not a problem due to the fact that some cases incorporate the time history analysis, while other use the covariance approach.

3.5 Summary

This chapter has introduced the area of track geometry for railway applications related to both deterministic and stochastic cases. It also presented a way to correctly represent the characteristics of the lateral track misalignments for the stochastic approach.

The tilt performance assessment is separated into two aspects: (i) the deterministic criterion based upon the \mathbf{P}_{CT} factor and the deviations from the ‘ideal’ tilting responses, and (ii) the stochastic criterion based upon the evaluation of ride quality (rms acceleration levels). Three methods were presented for the purposes of calculating rms values: (i) Frequency response analysis, (ii) time-based covariance, and (iii) time history. Examples of the assessment approaches can be found throughout this thesis.

Chapter 4

Tilt Control Prerequisites

4.1 System Requirements

In order to apply active tilt control on railway vehicles, the following hardware and software specifications are necessary:

1. sensors to provide continuous measurements of the required signals for the control scheme (typically body lateral acceleration, secondary suspension angle, body absolute roll velocity)
2. a controller structure to determine the tilt demand necessary to compensate for the perceived lateral forces during the curved track duration and
3. an active means to rotate the vehicle body, this may involve hydraulic, pneumatic or electro-mechanical actuators

As discussed earlier in the thesis, types of tilt currently used by manufacturers are: *tilt across*, *below* or *above* the secondary suspensions.

4.2 Full vs Partial Tilt

In the early days of tilt, it was normal to reduce the lateral acceleration on steady-state curve to zero. However this approach was quickly abandoned because it was found that the high roll rates of the body during the curve transition caused a significant proportion of the passengers to experience motion sickness, a phenomenon which previously had been extremely rare in trains. As a result tilt control strategies have been adapted to utilise partial tilt compensation, i.e. compensate only for a portion of steady-state curving acceleration. This approach not only reduces roll rates but also minimizes the conflict in human perception which is believed to play an important role

in motion sickness, see Figure 4.1. Therefore, *partial tilt* control is employed in the studies throughout this thesis.

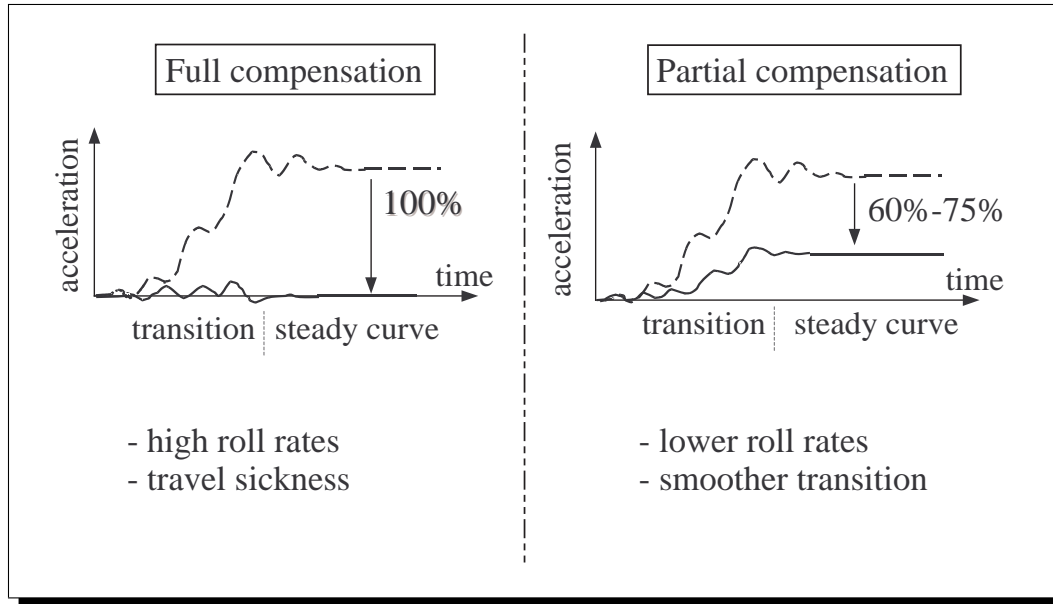


Figure 4.1: Full vs Partial Tilt Compensation

4.3 Tilt Control Objectives

The performance of the tilt control system on the curve transitions is critical. Primarily the passenger ride comfort provided by the tilting vehicle should not be degraded compared to the non-tilting vehicle speeds. The main objective of a tilt control system is to provide an acceptably fast response to changes in track cant and curvature (deterministic features) while not reacting significantly to track irregularities (stochastic features). However, in any tilt control system there is a fundamental trade-off between the vehicle curve transition response and straight track performance. It should be noted at this point that any tilt control system directly controls the secondary suspension roll angle and not the vehicle lateral acceleration.

Incorporating an excessively fast controller may provide high roll rates and also jerk levels which are unacceptable. On the other hand, a slow controller will provide low roll rates and probably jerk levels, thus giving an unacceptable increase of the lateral acceleration during the curve transition before compensating by tilting the vehicle body.

The lateral acceleration experienced on the vehicle body during a curved track consists of

- a. a component due to the deterministic track features (cant and curvature) combined with the body tilt angle and
- b. a component due to the suspension dynamic response (lower sway oscillations) to both deterministic and stochastic track features.

In summary, the main performance requirements for the tilt control system are:

1. to reduce the lateral acceleration perceived by the passengers on curves,
2. to provide a comfortable response during curve transitions (tilting trains are designed to operate at higher speeds and the curve transition time therefore decreases) based upon the P_{CT} and “ideal tilting” criterion and
3. to maintain the straight track performance within acceptable limits (specified as not more than 7.5% deterioration compared to the passive suspension system at the same speed).

From a control point of view the objectives of the tilt control system can be translated as: increasing the response of the system at low frequencies (deterministic track features) while reducing the high frequency system response (stochastic track features) and maintaining stability.

4.4 Tilting Vehicle Configuration Cases

Two tilting vehicle configurations are employed in this thesis for the purposes of tilt control applications. The first case, which forms the main part of this research work, involves a vehicle model with an *active anti-roll bar*, which is a tilt across the secondary suspension application. The parameters shown in the ‘ARB’ column of Table 4.1 were arbitrarily chosen to represent realistic conditions.

The second case, ‘Mechanism’, is an extension of the studies to include a more sophisticated vehicle model, which contains a *tilting mechanism* situated below the secondary suspensions, in essence providing tilt below the secondary suspension level. The deterministic specifications were based upon data used in [KE00], which are somehow different from the ‘ARB’ model. Moreover, this type of vehicle is currently used in practice by most tilting train operators. Table 4.1 lists the detailed specifications for the above two cases. Note that all active tilt control cases refer to high speed, i.e.

$58(\frac{m}{s})$ for both test cases.

Table 4.1: Tilt application test cases

		ARB	Mechanism	
		(CASE A)	(CASE B)	
Tilt compensation		60%	75%	
deterministic track*				(units)
maximum cant angle	$\theta_{o_{max}}$	6.00	5.84	(degrees)
maximum curve radius	R_{max}	1000.00	1200.00	(m)
transition length		145.00	145.00	(m) @ each end
track length		1200.00	1200.00	(m)
stochastic track†				
track roughness	Ω_l	0.33e-8	0.33e-8	(m)
track spatial spectrum	S_T	$\ddagger\Omega_l/f^3$	$\ddagger\Omega_l/f^3$	$(\frac{m^2}{(cycle/m)})$
track length		1200.00	1200.00	(m)
[(non-tilting) nominal speed: 45m/s], [(tilting) high speed: 58m/s]				

* curved track, † straight track lateral irregularities, ‡ see Chapter 3

The next step is to obtain appropriate models for the above vehicle configurations and design local, i.e. single vehicle based (without using precedence), tilt control structures based upon the above prerequisites. These concepts are discussed in the remaining parts of this thesis.

Part I

Active Anti-Roll Bar (ARB)
Studies

Chapter 5

Modelling of Vehicle Dynamics using Active ARB

Obtaining a correct model is essential in any simulation. Based on the design of the control model, conclusions for a number of cases can be drawn or predicted without the need of a real life experiment. After the required result is obtained, it can be appropriately applied in practice resulting in time and money saving.

A railway vehicle is a dynamically complex structure. It consists of: *a vehicle body, two bogies per vehicle and two wheelsets per bogie*. Each of the bodies is characterised by six degrees of freedom: *roll, lateral, yaw, pitch, longitudinal and vertical* modes. Flexibilities, non-linearities and parasitic effects can affect the dynamics and the behaviour of the vehicle in unexpected ways. In addition, many of the dynamic modes of the system are coupled and the coupling in certain situations is very significant which unavoidably causes difficulties in mode identification (i.e. vehicle *lateral* and *roll* modes) and also in control system design.

In this chapter mathematical models, based upon the Newtonian approach, of increasing complexity were developed to encapsulate the lateral and roll dynamics of the tilting vehicle system. The work was based upon linearised equivalents of the end-view of a vehicle, and in this part involved an *active anti-roll bar* system to provide the tilt action [PGP98]. The advantages of active ARBs results from their relative simplicity, i.e. *small weight increase, low cost, easily fitted as an optional extra to build or as a retro-fit*.

A simplified 2 D-o-F end-view vehicle model based upon the anti-roll bar model was

used for modal analysis. A non-linear model extension based upon the simplified end-view vehicle was used for basic vehicle dynamics validation. Throughout the work, advanced mathematical models were incorporated for model validation and control design.

5.1 Linear Two Degree-of-Freedom Endview Model

A simplified vehicle end-view model version is developed for modal analysis (no active control was considered for this part of the work) and is shown in Figure 5.1(a). Such a configuration represents a two degree-of-freedom model, lateral and roll motion of the vehicle body. For simplicity the bogie and the wheelsets were assumed to be fixed on the track, and the vertical motion is ignored. However the effects of the vertical suspensions on the vehicle roll motion is included by using a pair of airsprings. The model contains also the stiffness of an anti-roll bar connected between the body and the bogie frame. Referring to both Figure 5.1(a) and 5.1(b) a mathematical model for the system can be derived.

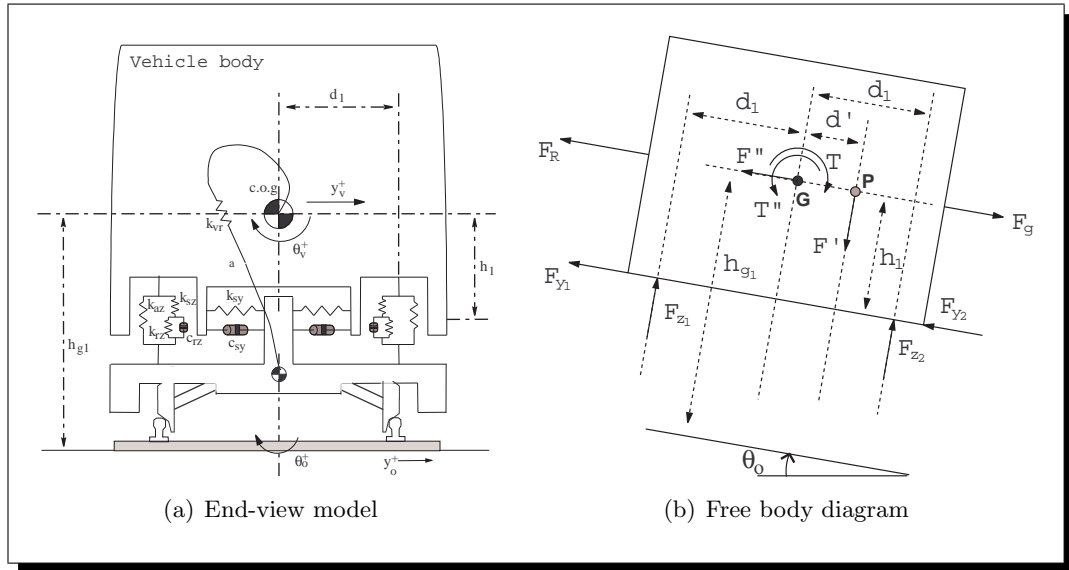


Figure 5.1: Two degree-of-freedom model

The body lateral degree-of-freedom is given by (using small angle approximation) the following expression

$$m_v \ddot{y}_v + \sum_{i=1}^2 F_{y_i} = -F_R + F_g - F'' \quad (5.1)$$

where,

$$F_{y_1} = k_{sy}(y_v - h_1\theta_v - y_o) + c_{sy}(\dot{y}_v - h_1\dot{\theta}_v - \dot{y}_o) \quad (5.2)$$

$$F_{y_2} = F_{y_1}, \quad F_R = m_v \frac{v^2}{R}, \quad F_g = m_v g \theta_o, \quad F'' = m_v h_{g_1} \ddot{\theta}_o \quad (5.3)$$

By incorporating equations (5.2) and (5.3) into (5.1), the lateral degree-of-freedom becomes

$$m_v \ddot{y}_v = -2k_{sy}(y_v - h_1\theta_v - y_o) - 2c_{sy}(\dot{y}_v - h_1\dot{\theta}_v - \dot{y}_o) - m_v \left(\frac{v^2}{R} - g\theta_o + h_{g_1} \ddot{\theta}_o \right) \quad (5.4)$$

Likewise for the equation which describes the body roll degree-of-freedom the following apply

$$i_{vr} \ddot{\theta}_v - h_1 \sum_{i=1}^2 F_{y_i} = T + d' F' + d_1 (F_{z_1} - F_{z_2}) - T'' \quad (5.5)$$

where,

$$F_{z_1} = -k_{az} d_1 \theta_v + k_{sz} d_1 (\theta_v - \theta_r) \quad (5.6)$$

$$F_{z_2} = -F_{z_1}, \quad T = -k_{vr} \theta_v, \quad F' = m_v g (y_v - y_o), \quad T'' = i_{vr} \ddot{\theta}_o \quad (5.7)$$

The incorporated extra roll state for the airspring linear model (see Appendix D.1.1) is governed by

$$\dot{\theta}_r = -\theta_r \frac{(k_{sz} + k_{rz})}{c_{rz}} + \frac{k_{sz}}{c_{rz}} \theta_v \quad (5.8)$$

Substituting (5.2), (5.6) and (5.7) in (5.5), the overall mathematical description of the body roll degree-of-freedom is as follows

$$i_{vr} \ddot{\theta}_v = 2h_1 (k_{sy}(y_v - h_1\theta_v - y_o) + c_{sy}(\dot{y}_v - h_1\dot{\theta}_v - \dot{y}_o)) - k_{vr} \theta_v - 2d_1^2 (k_{az} + k_{sz}) \theta_v + 2d_1^2 k_{sz} \theta_r + m_v g (y_v - y_o) - i_{vr} \ddot{\theta}_o \quad (5.9)$$

The above mathematical expressions correspond to local track references, and the translation and rotation of these reference axes associated with curves were allowed for, F'' and T'' , in the equations. Note that equation (5.9) includes an end moment effect, $F' = m_v g (y_v - y_o)$, which models the roll effect of the body weight due to the lateral displacement of its centre of gravity on the curve (a schematic representation of the cog is shown in Figure 5.3(a)). There exists significant coupling between the lateral and roll modes, which is depicted in the block diagram of Figure 5.1 (see page 44).

Now (5.4), (5.9) and (5.8) can be arranged to represent the model, for system analysis, in state space form

$$\dot{\mathbf{x}} = \mathbf{A}\mathbf{x} + \mathbf{\Gamma}\mathbf{w} \quad (5.10)$$

$$\mathbf{y} = \mathbf{C}\mathbf{x} + \mathbf{H}\mathbf{w} \quad (5.11)$$

Expression (5.10) is the *system state equation*, while (5.11) denotes the *system output equation* (which is not used in this section). The individual elements of (5.10) are

$$\dot{\mathbf{x}} = \begin{bmatrix} y_v & \theta_v & \dot{y}_v & \dot{\theta}_v & \theta_r \end{bmatrix}^T \quad \mathbf{w} = \begin{bmatrix} R^{-1} & \theta_o & \dot{\theta}_o & \ddot{\theta}_o & y_o & \dot{y}_o \end{bmatrix}^T \quad (5.12)$$

$$\mathbf{A} = \begin{bmatrix} 0 & 0 & 1 & 0 & 0 & 0 \\ 0 & 0 & 0 & 1 & 0 & 0 \\ \frac{-2k_{sy}}{m_v} & \frac{2k_{sy}h_1}{m_v} & \frac{-2c_{sy}}{m_v} & \frac{2h_1c_{sy}}{m_v} & 0 & 0 \\ \frac{2h_1k_{sy}+m_v g}{i_{vr}} & \frac{-(k_{vr}+2h_1^2k_{sy}+2d_1^2(k_{az}+k_{sz}))}{i_{vr}} & \frac{2h_1c_{sy}}{i_{vr}} & \frac{-2h_1^2c_{sy}}{i_{vr}} & \frac{2k_{sz}d_1^2}{i_{vr}} & 0 \\ 0 & \frac{k_{sz}}{c_{rz}} & 0 & 0 & \frac{-(k_{sz}+k_{rz})}{c_{rz}} & 0 \end{bmatrix} \quad (5.13)$$

$$\mathbf{\Gamma} = \begin{bmatrix} 0 & 0 & 0 & 0 & 0 & 0 \\ 0 & 0 & 0 & 0 & 0 & 0 \\ -v^2 & g & 0 & -h_{g1} & 0 & 0 \\ 0 & 0 & 0 & -1 & -g & 0 \\ 0 & 0 & 0 & 0 & 0 & 0 \end{bmatrix} \quad (5.14)$$

The system modes based upon the above representation and using the parameter values listed (see Appendix A.2.1).

Table 5.1: System modes of the two degree-of-freedom model

Mode	Eigenvalues	Damping(%)	Frequency(Hz)
1st (Lower sway)	$-1.13 \pm 4.6j$	24.0	0.75
2nd (Upper sway)	$-2.20 \pm 11.0j$	19.6	1.78
3rd (Airspring)	$-25.1 \pm 0.0j$	100.0	4.0

It can be seen from the table that the first two modes are not marked distinctively as ‘lateral’ and ‘roll’ instead they are referred to as ‘lower sway’ and ‘upper sway’. This situation appears due to the complex behaviour of the vehicle system and the coupling between the lateral and roll motions which become evident in the next section.

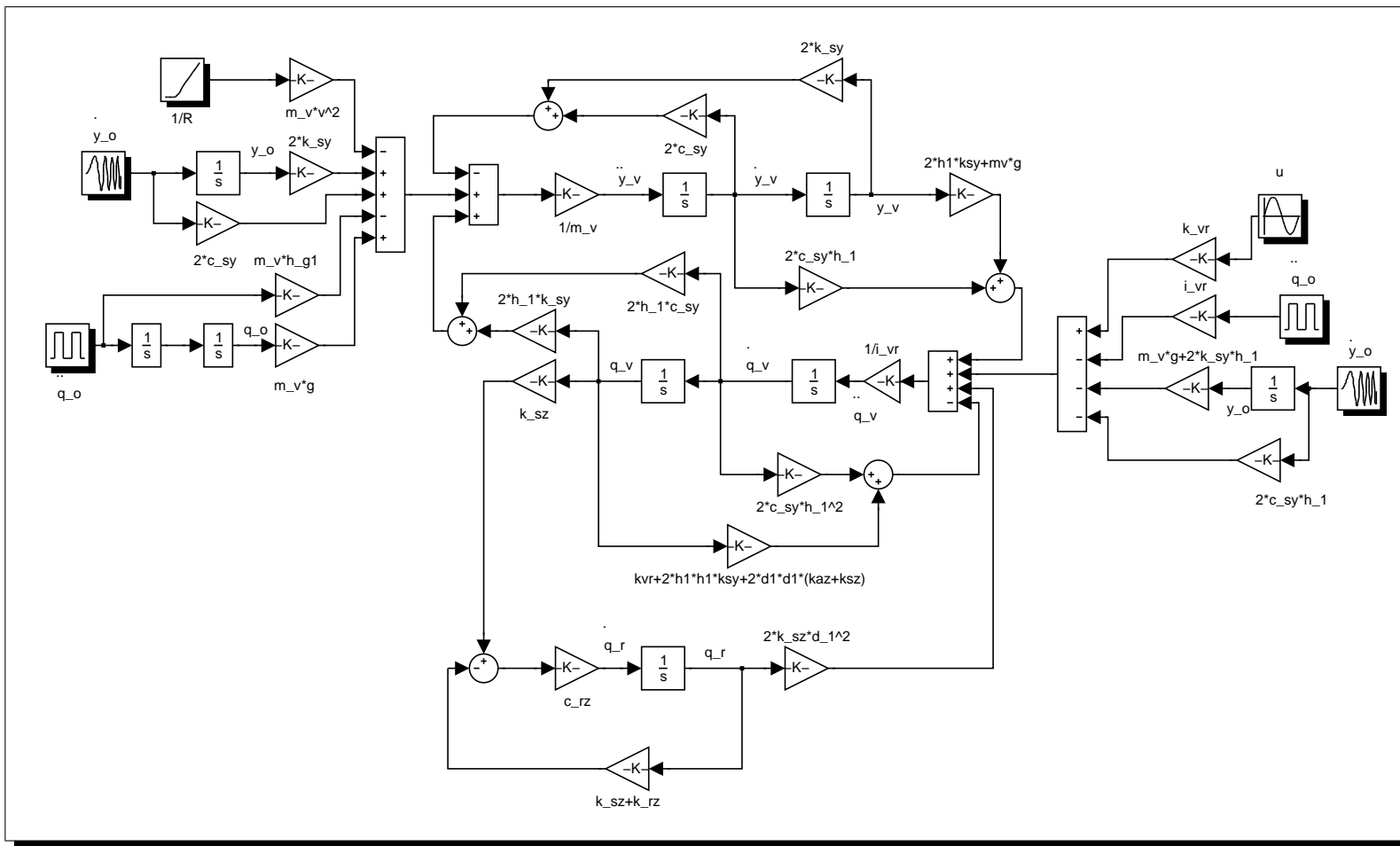


Figure 5.2: Block diagram of the two degree of model

5.2 Identification of Vehicle Sway Modes

Referring to the equations of motion in Section 5.1, it can be seen that there exists substantial coupling between the lateral and roll modes. This results in two modes, called ‘sway modes’ which combine both lateral and roll motion. Their centres of motion will be located at two points, called ‘motion centers’ or ‘nodes’, other than the vehicle body centre of gravity. No motion occurs at these nodes, i.e. a passenger situated at a node would not move if the vehicle was moving in the corresponding modal motion. In the case where the sway node appears above the vehicle body c.o.g, the mode is called ‘upper sway’ and its motion is predominantly roll (see Figure 5.5(a)). The location of the sway node below the c.o.g of the vehicle body incorporates a ‘lower sway’ mode characterised predominantly by a lateral motion (see Figure 5.5(b)). The analysis of node location can be very sensitive to slight parameter variations, and plays an important role in the selection of parameter values [Pal99].

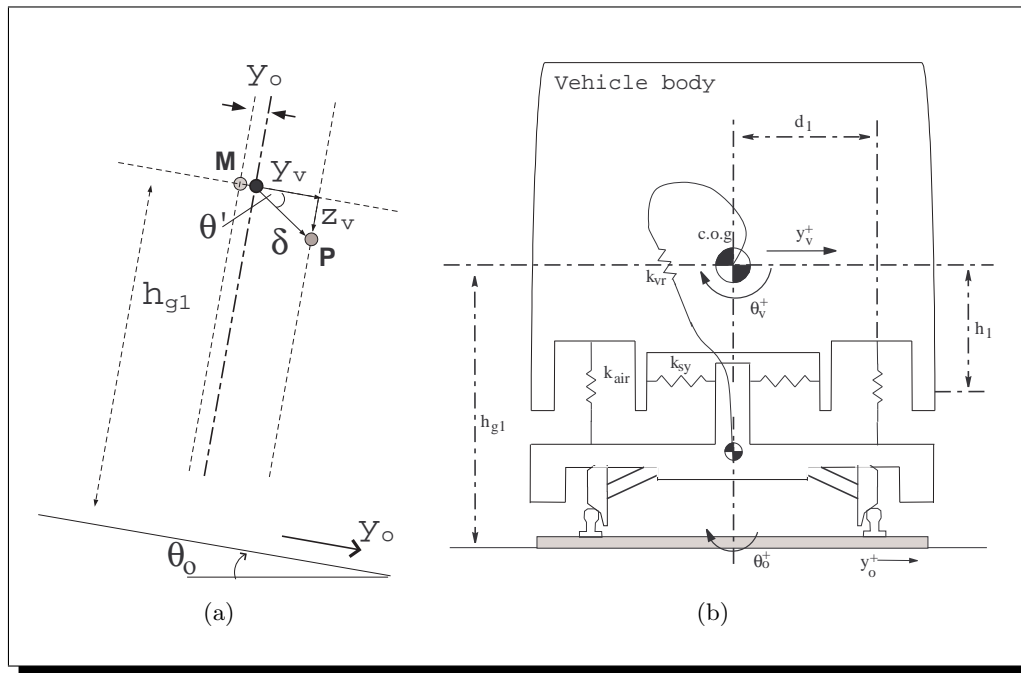


Figure 5.3: (a) Body cog displacement on curved track (2-DoF model). (b) Sway mode analysis model

The next step is to identify those modes based upon the equations of motion of the two degrees of freedom model, see Figure 5.3(b), (models of higher complexity would result in rather difficult analysis) with the following assumptions for simplicity:

1. Damping coefficients set to zero.

2. Inputs set to zero (free system response).

Note that item (1) will also result in a simpler airspring model representation (having a single airspring vertical stiffness).

Consider equations (5.4) and (5.9), by setting the damping coefficient and the inputs to zero (i.e. free vibration) , they become

$$m_v \ddot{y}_v + 2k_{sy}(y_v - h_1\theta_v) = 0 \quad (5.15)$$

$$i_{vr} \ddot{\theta}_v - 2h_1 k_{sy}(y_v - h_1\theta_v) + k_{vr}\theta_v + 2d_1^2 k_{air}\theta_v - m_v g y_v = 0 \quad (5.16)$$

Note that now $k_{air} = k_{az} + \frac{k_{sz}k_{rz}}{(k_{sz}+k_{rz})}$, which is the total airspring stiffness after the simplification made for the airspring reservoir ($c_{rz} = 0$). Collecting terms and re-writing (5.15) and (5.16) into differential form produces

$$(m_v s^2 + 2k_{sy})y_v - 2k_{sy}h_1\theta_v = 0 \quad (5.17)$$

$$-(m_v g + 2h_1 k_{sy})y_v + (i_{vr} s^2 + 2d_1^2 k_{air} + 2k_{sy}h_1^2 + k_{vr})\theta_v = 0 \quad (5.18)$$

Substitute $y_v(t) = A_1 e^{st}$ and $\theta_v(t) = A_2 e^{st}$ into (5.17) and (5.18) and cancel the e^{st} terms to get

$$(m_v s^2 + 2k_{sy})A_1 - 2k_{sy}h_1 A_2 = 0 \quad (5.19)$$

$$-(m_v g + 2h_1 k_{sy})A_1 + (i_{vr} s^2 + 2d_1^2 k_{air} + 2k_{sy}h_1^2 + k_{vr})A_2 = 0 \quad (5.20)$$

The solutions for A_1, A_2 will be non-zero iff the determinant

$$\begin{vmatrix} m_v s^2 + 2k_{sy} & -2k_{sy}h_1 \\ -(m_v g + 2h_1 k_{sy}) & (i_{vr} s^2 + 2d_1^2 k_{air} + 2k_{sy}h_1^2 + k_{vr}) \end{vmatrix} = 0 \quad (5.21)$$

Expanding the above determinant gives

$$(m_v s^2 + 2k_{sy})(i_{vr} s^2 + 2d_1^2 k_{air} + 2k_{sy}h_1^2 + k_{vr}) - 2k_{sy}h_1(m_v g + 2h_1 k_{sy}) = 0 \quad (5.22)$$

or

$$\begin{aligned} m_v i_{vr} s^4 + (m_v k_{vr} + 2m_v h_1^2 k_{sy} + 2i_{vr} k_{sy} + 2d_1^2 k_{air})s^2 \\ + 2k_{sy}[(k_{vr} + 2h_1^2 k_{sy} + 2d_1^2 k_{air}) - h_1(m_v g + 2h_1 k_{sy})] = 0 \end{aligned} \quad (5.23)$$

The polynomial in (5.23) is of fourth order and thus has four roots. It can be solved for s^2 using the quadratic formula because it is quadratic in s^2 (note that the s and s^3

terms are absent). The mode ratio can be obtained from either (5.19) or (5.20). By choosing (5.19) the ratio is given as

$$\frac{A_1}{A_2} = \frac{2k_{sy}h_1}{m_v s^2 + 2k_{sy}} \quad (5.24)$$

The mode ratio can be thought of as the ratio of the amplitudes of y_v and θ_v in that mode. It can be seen from Figure 5.2 that $\tan \psi = \frac{y_v}{\theta_v}$ and for small angle approximation

$$\frac{y_v}{\theta_v} = \frac{A_1}{A_2} \approx d_o \quad (5.25)$$

where d_o is the distance of the node for each mode. Note that the amplitude of y_v would be zero if $2k_{sy}h_1 = 0$, hence d_o would be zero and the modes would be uncoupled (the node for each mode would be at the vehicle c.o.g). This is not the case because both $k_{sy}, h_1 \neq 0$ and of course the modes are coupled.

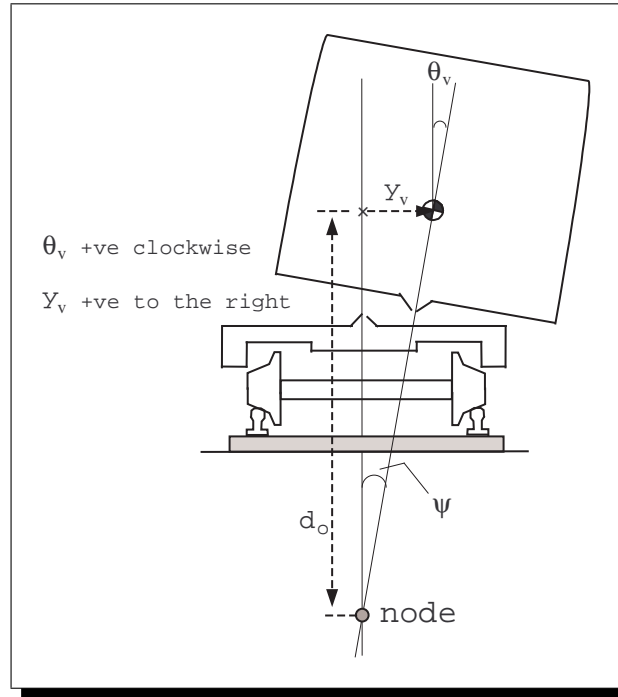


Figure 5.4: Location of nodes for the sway motions

Using the parameter values given in Appendix A.2.1 and dividing by $m_v i_{vr}$, the characteristic equation given by (5.23) becomes

$$s^4 + 149.17s^2 + 2688.8 = 0 \quad (5.26)$$

The roots in s^2 are $s_1^2 = -128.2$ and $s_2^2 = -20.97$ ($s_1 = \pm 11.32j$, $s_2 = \pm 4.58j$), while the corresponding frequencies are 1.8Hz and 0.73Hz respectively. Note that both modes are oscillatory. Substitute numerical values for the parameters into (5.24)

$$\frac{A_1}{A_2} = \frac{468}{19s^2 + 520} = \frac{y_v}{\theta_v} \approx d_o \quad (5.27)$$

1. For mode 1 ($s_1^2 = -128.2$) $\implies d_{o1} \approx \frac{24.632}{-128.2+27.368} = -0.244$.

This node is situated $0.244m$ above the vehicle c.o.g ($\frac{y_v}{\theta_v} < 0$, also distances are selected negative above the vehicle c.o.g and positive below the c.o.g for the mathematical modelling). The natural frequency for this mode is 1.8Hz and it is the ‘upper sway’ mode (Figure 5.5(a)).

2. For mode 2 ($s_1^2 = -20.97$) $\implies d_{o2} \approx \frac{24.632}{-20.97+27.368} = 3.852$.

This node is situated $3.852m$ below the vehicle c.o.g ($\frac{y_v}{\theta_v} > 0$). The natural frequency for this mode is 0.73Hz and it is the ‘lower sway’ mode (Figure 5.5(b)).

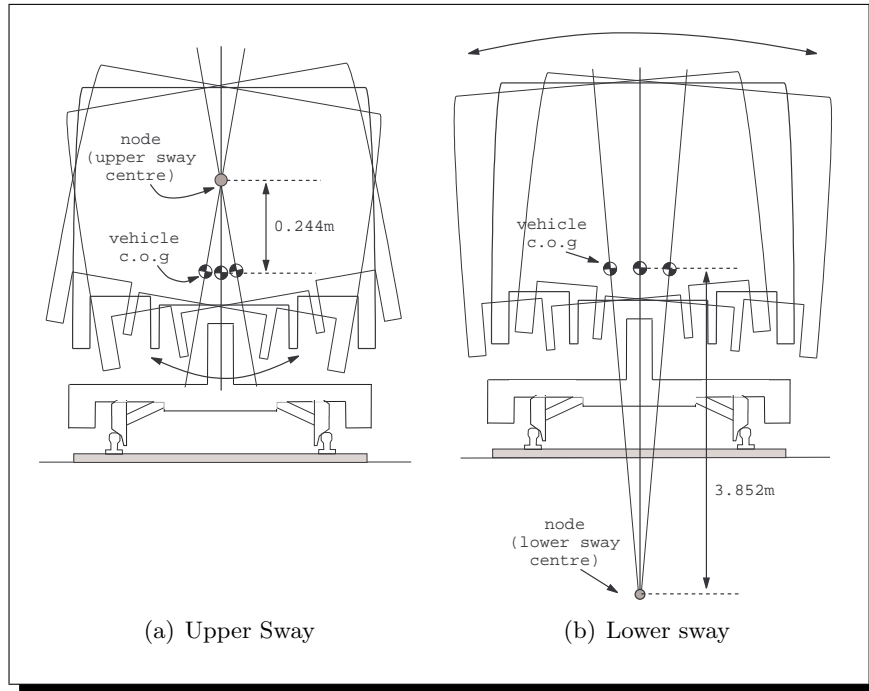


Figure 5.5: Sway mode centres

The analysis was based upon the assumption of zero damping coefficients. In reality the system includes *viscous* damping and this makes the modal analysis more difficult to accomplish. However there exist ways of simplifying the problems by re-arranging this damping into, a simpler in terms of study, proportional form [Ewi89, Gaw98].

5.3 Non-linear Three Degree-of-Freedom Endview Model

To extend the two degree-of-freedom model concept and also to validate the accuracy of the “local track reference” linear approach, a non-linear vehicle model was formulated to include three degrees of freedom: (i) vertical, (ii) lateral and (iii) roll, of the vehicle body. As in Section 5.1, the bogie and wheelsets of the vehicle formed a solid system directly connected to the track. Moreover, an appropriate representation of a pair of airsprings was included to comply with the non-linear approach. The stiffness of an anti-roll bar was also included, connected between the body and the bogie frames. The mathematical equations refer to absolute reference axis (i.e. the horizontal plane and not the canted track) and small angle approximation was applied when appropriate.

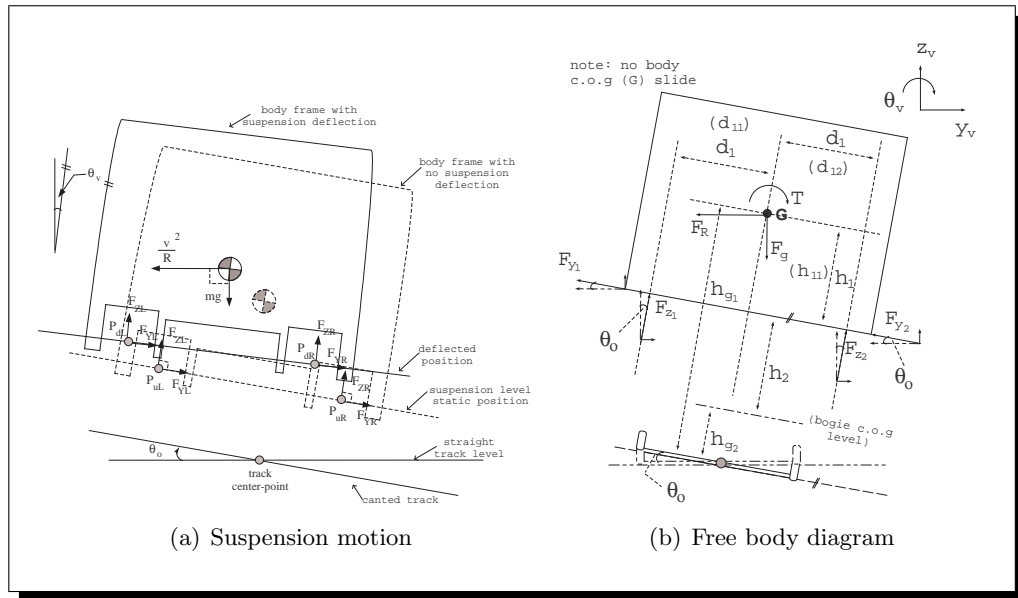


Figure 5.6: 3 D-o-F ARB model setup

The approach is based upon Figure 5.6(a) where the forces are calculated as follows: (i) $F_{zL} = \frac{mg}{2} + \delta_{zL}k_z$, $F_{zR} = \frac{mg}{2} + \delta_{zR}k_z$, where δ_{zL}, δ_{zR} are perpendicular relative movements with reference to the base of the suspension points, and k_z the vertical suspension stiffness. (ii) $F_{yL} = \delta_y k_y$, $F_{yR} = \delta_y k_y$, where δ_y is the relative movement parallel to the base, and k_y the overall lateral suspension stiffness.

In the vertical direction ($z \uparrow$)

$$\begin{aligned} m_v \ddot{z}_v &= \left\{ \left(\sum F \right)_{z \uparrow} \right\} \\ &= \left(\sum_{i=1}^2 F_{z_i} \right) \cos \theta_o + \left(\sum_{i=1}^2 F_{y_i} \right) \sin \theta_o - F_g \end{aligned} \quad (5.28)$$

In the lateral direction ($y \rightarrow$)

$$\begin{aligned} m_v \ddot{y}_v &= \left\{ \left(\sum F \right)_{y \rightarrow} \right\} \\ &= - \left(\sum_{i=1}^2 F_{y_i} \right) \cos \theta_o + \left(\sum_{i=1}^2 F_{z_i} \right) \sin \theta_o - F_R \end{aligned} \quad (5.29)$$

In the roll direction ($\theta \curvearrowright$)

$$m_v \ddot{\theta}_v = T + d_{11} F_{z1} - d_{12} F_{z2} + h_{11} (F_{y1} + F_{y2}) \quad (5.30)$$

where $d_{11} = d_1 + y_g$, $d_{12} = d_1 - y_g$, and $h_{11} = h_1 - z_g$. Variables y_g, z_g characterise the body c.o.g slide on curved track and are calculated from Figure 5.7. In more details y_g is the lateral displacement of the vehicle body c.o.g parallel and relative to the canted track, while z_g is the vertical displacement of the body c.o.g perpendicular and relative to the canted track. Note that in both cases is assumed that $F_{z1}, F_{z2}, F_{y1}, F_{y2}$ continue to act at the position before the c.o.g slide. In this case, the model takes into account the end moment effect implicitly compared to the linear models which include the effect explicitly. To get a correct comparison between the 2 D-o-F linear and this model, the vertical distance of the secondary suspension from the track is set to $\bar{h}_2 = h_2 + h_{g2}$ (note that it is the track that is moving in this case).

The individual elements of the above expressions are given by

$$F_{z1} = -k_{az} \delta_{za1} - k_{sz} \delta_{zs1} + \frac{mg}{2}, \quad F_{z2} = -k_{az} \delta_{za2} - k_{sz} \delta_{zs2} + \frac{mg}{2} \quad (5.31)$$

$$\delta_{za1} = z_v + d\theta_v - (z_o + d\theta_o), \quad \delta_{za2} = z_v - d\theta_v - (z_o - d\theta_o) \quad (5.32)$$

$$\frac{\delta_{zs1}}{\delta_{za1}}(s) = \frac{\delta_{zs2}}{\delta_{za2}}(s) = \frac{\frac{k_{rz}}{c_{rz}} + s}{\frac{k_{rz} + k_{sz}}{c_{rz}} + s} \quad (5.33)$$

More details on the airspring modelling procedure for this model version are presented in Appendix D.1.2. For F_{y1}, F_{y2} the following do apply

$$\begin{aligned} F_{y1} &= k_{sy}(\text{“lat. displ. @ deflected posn.”} - \text{“lat. displ. @ static posn.”}) \\ &\quad + c_{sy}(\text{“lat. velocity @ deflected posn.”} - \text{“lat. velocity @ static posn.”}) \end{aligned}$$

$$\begin{aligned}
m_v \ddot{y}_v = & -2k_{sy}(y_v - h_1\theta_v - y_o - \bar{h}_2\theta_o) \cos \theta_o - 2c_{sy}(\dot{y}_v - h_1\dot{\theta}_v - \dot{y}_o - \bar{h}_2\dot{\theta}_o) \cos \theta_o \\
& - k_{az}(z_v + d\theta_v - z_o - d\theta_o) \sin \theta_o - k_{az}(z_v - d\theta_v - z_o + d\theta_o) \sin \theta_o \\
& - k_{sz}\delta_{zs1} \sin \theta_o - k_{sz}\delta_{zs2} \sin \theta_o + m_v g \sin \theta_o - m_v \frac{v^2}{R} \quad (5.39)
\end{aligned}$$

$$\begin{aligned}
i_{vr} \ddot{\theta}_v = & -k_{vr}(\theta_v - \theta_o - \delta_a) + (d_1 + y_g)(-k_{az}(z_v + d\theta_v - z_o - d\theta_o) - k_{sz}\delta_{zs1} + \frac{mg}{2}) \\
& - (d_1 - y_g)(-k_{az}(z_v - d\theta_v - z_o + d\theta_o) - k_{sz}\delta_{zs2} + \frac{mg}{2}) \\
& + 2(h_1 - z_g)(k_{sy}(y_v - h_1\theta_v - y_o - \bar{h}_2\theta_o) + c_{sy}(\dot{y}_v - h_1\dot{\theta}_v - \dot{y}_o - \bar{h}_2\dot{\theta}_o)) \quad (5.40)
\end{aligned}$$

The system was developed in SIMULINK and the ‘parent’ diagram can be seen in Figure 5.10 (see page 55).

5.3.1 Comparison between the 2 D-o-F linear and 3 D-o-F non-linear models

The next step is to compare the two models in order to find how well does the 2-DoF linear approach match its 3-DoF extended non-linear equivalent. It is preferred for control design to use linear models, however recall that linear models should be a good representation of the real system for the control designs to apply.

It can be seen from Table 5.2 that the two models have identical major modes, i.e. Body upper, lower sway and Airspring vertical. The modes of the non-linear model were provided by a linearised state-space equivalent extracted from SIMULINK with the advanced linearisation method `linmod2`. The operating point is at 0, i.e. straight track, which is acceptable due to the fact the angles are small). The deterministic simulation

Table 5.2: Linear and Non-linear System modes

Linear 2 D-o-F			
<i>Mode</i>	<i>Eigenvalues</i>	<i>Damping(%)</i>	<i>Frequency(Hz)</i>
1st (Lower sway)	$-1.13 \pm 4.6j$	24.0	0.75
2nd (Upper sway)	$-2.20 \pm 11.0j$	19.6	1.78
3rd (Airspring)	$-25.1 \pm 0.0j$	100.0	4.0
Non-Linear 3 D-o-F			
<i>Mode</i>	<i>Eigenvalues</i>	<i>Damping(%)</i>	<i>Frequency(Hz)</i>
1st (Lower sway)	$-1.13 \pm 4.6j$	24.0	0.75
2nd (Upper sway)	$-2.20 \pm 11.0j$	19.6	1.78
3rd (Airspring)	$-25.1 \pm 0.0j$	100.0	4.0

results in Figure 5.8(a), Figure 5.8(b) show small to negligible differences between the

two models. This is expected because the non-linear model is relative to the horizontal track/global references, while the linear is relative to the canted track/local references. In the case of straight track, Figure 5.8(b), Figure 5.9(a), the behaviour is identical for

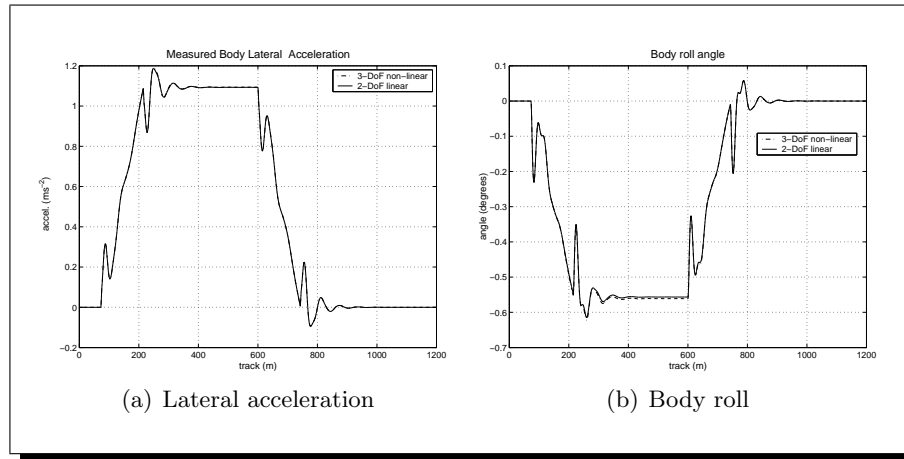


Figure 5.8: Time history results for deterministic track

both models. Note that on straight track the cant angle is zero and this does not really affect the way of modelling the system. The characteristics of the tracks used for this purpose are listed in Table 5.4 on page 60, and for correct model comparison no *vertical* and *cross-level* irregularities were used for straight track simulation in the non-linear case. Therefore, the linear approach is a good basis for designing control systems for

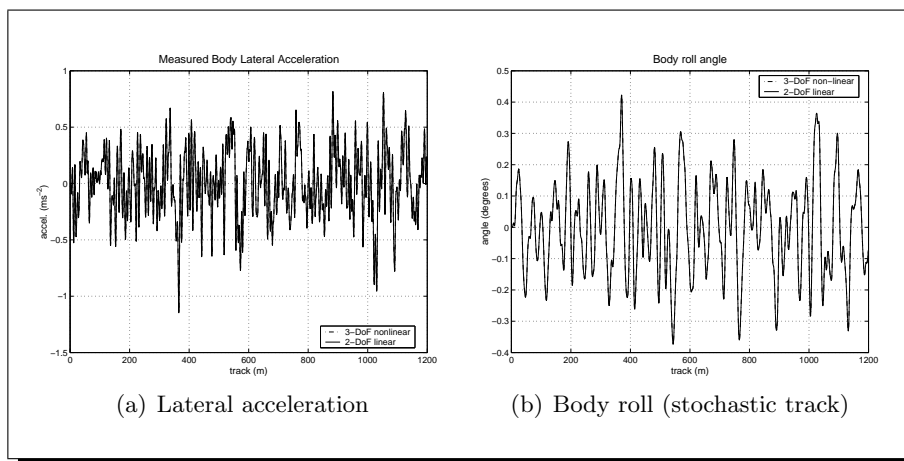


Figure 5.9: Time history results for stochastic track

the real system (it was not necessary to include a full non-linear vehicle for this part of the work). More details on linear/non-linear model comparison can be found in Part II which presents tilting vehicles using tilting bolsters. The next section introduces the

vehicle bogie into the system and implements a 4-DoF linear model which will be used for control system design.

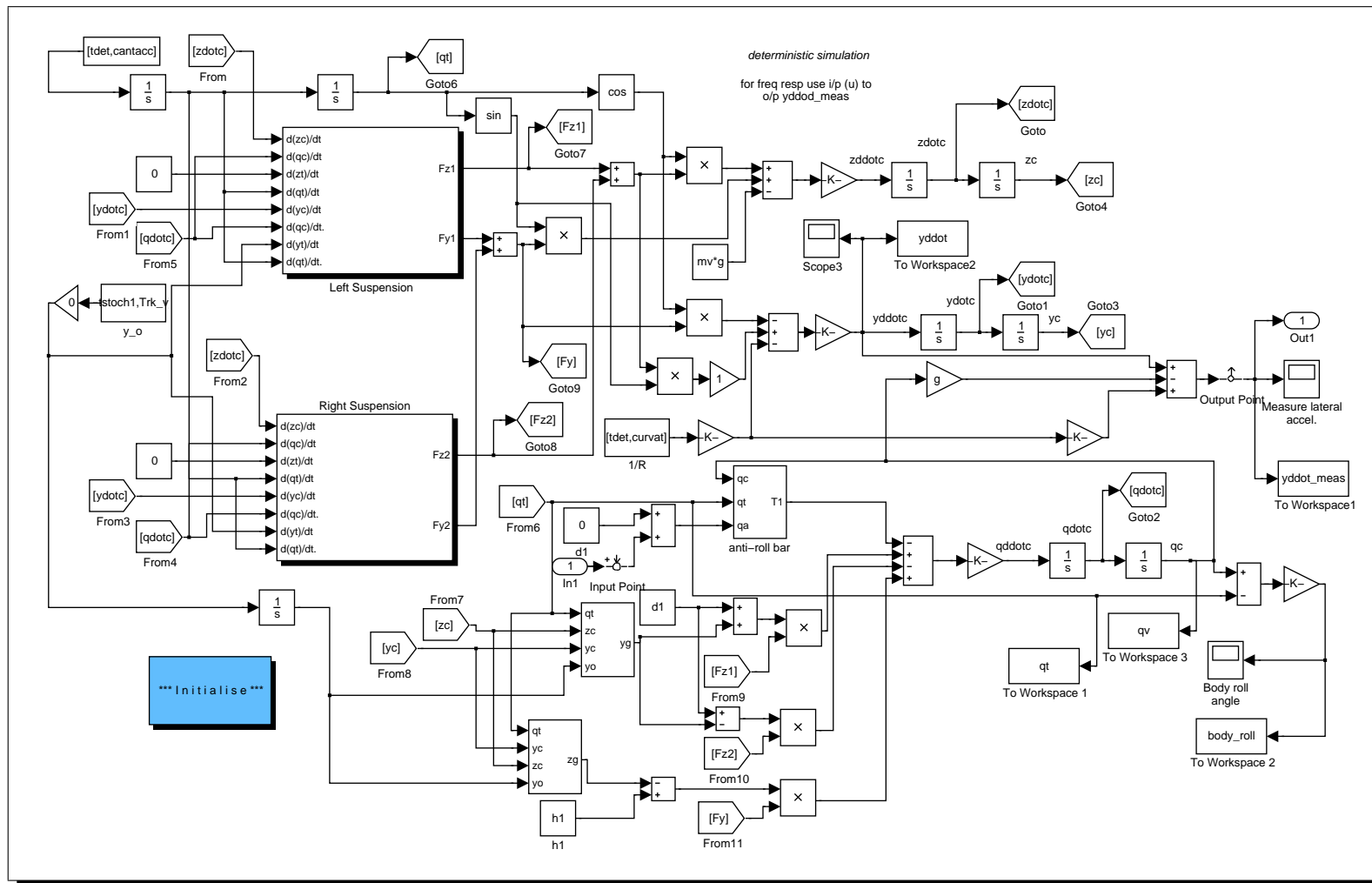


Figure 5.10: Non linear model Simulink

5.4 Linear Four Degree-of-Freedom Endview Model

This section develops a linear four degree-of-freedom vehicle model, which includes the lateral and roll dynamics of both the body and the bogie. As in Section 5.1 the vertical suspensions are represented by a pair of airsprings, which only contribute to the roll motion of the vehicle (vertical degrees of freedom are ignored). At this stage of the project it was not necessary to model the dynamics of the wheelsets, while their effect is taken in account for the simulation concerning track irregularities (i.e. low pass filtering of around 5Hz for the track input signal). The model now also contains the stiffness of an anti-roll bar connected between the body and the bogie frame. To provide active tilt a rotational displacement actuator, assumed to be an *ideal actuator* in this case, is included in series with the roll stiffness, i.e. the concept of an ‘active anti-roll bar’ [PGP98]. The list of parameter values used in this section can be found in Appendix A.2.1, while the description of the symbols can be found in the Glossary.

The mathematical model developed based on Figure 5.11(a) and 5.11(b) is presented below. The steps taken are very similar to the modelling of the simpler two degree-of-freedom end-view model. Note that small angle approximation is used throughout the procedure.

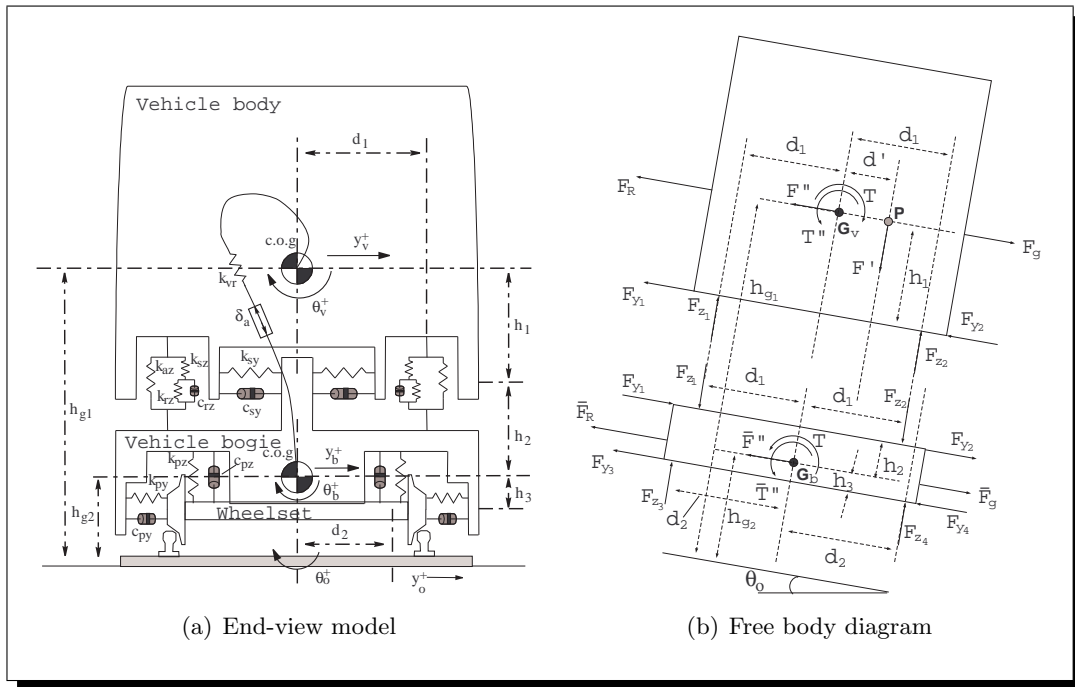


Figure 5.11: Four degree-of-freedom model

The equation of motion that describes the body lateral degree-of-freedom is given by

$$m_v \ddot{y}_v + \sum_{i=1}^2 F_{y_i} = -F_R + F_g - F'' \quad (5.41)$$

where the individual force components are,

$$F_{y_1} = k_{sy} \{y_v - h_1 \theta_v - (y_b + h_2 \theta_b)\} + c_{sy} \{\dot{y}_v - h_1 \dot{\theta}_v - (\dot{y}_b + h_1 \dot{\theta}_b)\} \quad (5.42)$$

$$F_{y_2} = F_{y_1}, \quad F_R = m_v \frac{v^2}{R}, \quad F_g = m_v g \theta_o, \quad F'' = m_v h_{g_1} \ddot{\theta}_o \quad (5.43)$$

Substitute (5.42) and (5.43) into (5.41) to get

$$m_v \ddot{y}_v = -2k_{sy} \{y_v - h_1 \theta_v - (y_b + h_2 \theta_b)\} - 2c_{sy} \{\dot{y}_v - h_1 \dot{\theta}_v - (\dot{y}_b + h_1 \dot{\theta}_b)\} - m_v \left(\frac{v^2}{R} - g \theta_o + h_{g_1} \ddot{\theta}_o \right) \quad (5.44)$$

Similarly the equation describing the body roll degree-of-freedom is as follows

$$i_{vr} \ddot{\theta}_v - h_1 \sum_{i=1}^2 F_{y_i} = T + d' F' + d_1 (F_{z_1} - F_{z_2}) - T'' \quad (5.45)$$

where,

$$F_{z_1} = -k_{az} d_1 (\theta_v - \theta_b) - k_{sz} d_1 (\theta_v - \theta_r) \quad (5.46)$$

$$F_{z_2} = -F_{z_1}, \quad T = -k_{vr} (\theta_v - \theta_b - \delta_a), \quad F' = m_v g (y_v - y_b), \quad T'' = i_{vr} \ddot{\theta}_o \quad (5.47)$$

The airspring reservoir roll state is characterised by (see Appendix D.1.3 for details)

$$\dot{\theta}_r = c_{rz}^{-1} \{-\theta_r (k_{sz} + k_{rz}) + k_{sz} \theta_v + k_{rz} \theta_b + c_{rz} \dot{\theta}_b\} \quad (5.48)$$

Substituting (5.42), (5.46) and (5.47) in (5.45), the overall equation for the body roll degree-of-freedom is

$$i_{vr} \ddot{\theta}_v = 2h_1 \{k_{sy} (y_v - h_1 \theta_v - y_b - h_2 \theta_b) + c_{sy} (\dot{y}_v - h_1 \dot{\theta}_v - \dot{y}_b - h_1 \dot{\theta}_b)\} - k_{vr} (\theta_v - \theta_b - \delta_a) - 2d_1^2 \{k_{az} (\theta_v - \theta_b) + k_{sz} (\theta_v - \theta_r)\} + m_v g (y_v - y_b) - i_{vr} \ddot{\theta}_o \quad (5.49)$$

The equations of motion describing the lateral and the roll degrees of freedom for the bogie are developed following a similar procedure. For the lateral degree-of-freedom the expression is

$$m_b \ddot{y}_b + \sum_{i=1}^4 F_{y_i} = -\bar{F}_R + \bar{F}_g - \bar{F}'' \quad (5.50)$$

or

$$m_b \ddot{y}_b - (F_{y_1} + F_{y_2} - F_{y_3} - F_{y_4}) = -\bar{F}_R + \bar{F}_g - \bar{F}'' \quad (5.51)$$

where F_{y_1} is given in (5.42) and,

$$F_{y_3} = k_{py}(y_b - h_3\theta_b - y_o) + c_{py}(\dot{y}_b - h_3\dot{\theta}_b - \dot{y}_o) \quad (5.52)$$

$$F_{y_2} = F_{y_1}, \quad F_{y_3} = F_{y_4}, \quad \bar{F}_R = m_b \frac{v^2}{R}, \quad \bar{F}_g = m_b g \theta_o, \quad \bar{F}'' = m_b h_{g_2} \ddot{\theta}_o \quad (5.53)$$

Thus substituting (5.42), (5.52) and (5.53) into (5.51) gives

$$\begin{aligned} m_b \ddot{y}_b = & 2k_{sy}\{y_v - h_1\theta_v - (y_b + h_2\theta_b)\} + 2c_{sy}\{\dot{y}_v - h_1\dot{\theta}_v - (\dot{y}_b - h_1\dot{\theta}_b)\} \\ & - 2k_{py}(y_b - h_3\theta_b - y_o) - 2c_{py}(\dot{y}_b - h_3\dot{\theta}_b - \dot{y}_o) - m_b\left(\frac{v^2}{R} - g\theta_o + h_{g_2}\ddot{\theta}_o\right) \end{aligned} \quad (5.54)$$

Concerning the bogie roll degree-of-freedom, the following apply

$$i_{vr}\ddot{\theta}_b - h_1 \sum_{i=1}^2 F_{y_i} - h_2 \sum_{i=3}^4 F_{y_i} = -T - d_1(F_{z_1} - F_{z_2}) + d_2(F_{z_3} - F_{z_4}) - \bar{T}'' \quad (5.55)$$

where T , F_{z_1} are given by (5.47) and (5.46) respectively (note that $F_{z_2} = -F_{z_1}$), and also (with no vertical degrees of freedom considered)

$$F_{z_3} = -k_{pz}d_2\theta_b - c_{pz}d_2\dot{\theta}_b \quad (5.56)$$

$$F_{z_4} = -F_{z_3}, \quad \bar{T}'' = i_{br}\ddot{\theta}_o \quad (5.57)$$

To get the overall equation of motion for the bogie roll mode, substitute (5.42), (5.52), (5.46), (5.56) and (5.57) into (5.55)

$$\begin{aligned} i_{br}\ddot{\theta}_b = & 2h_2\{k_{sy}(y_v - h_1\theta_v - y_b - h_2\theta_b) + c_{sy}(\dot{y}_v - h_1\dot{\theta}_v - \dot{y}_b - h_1\dot{\theta}_b)\} \\ & + 2h_3\{k_{py}(y_b - h_3\theta_b - y_o) + c_{py}(\dot{y}_b - h_3\dot{\theta}_b - \dot{y}_o)\} + k_{vr}(\theta_v - \theta_b - \delta_a) \\ & + 2d_1^2\{k_{az}(\theta_v - \theta_b) + k_{sz}(\theta_v - \theta_r)\} - 2d_2^2(k_{pz}\theta_b + c_{pz}\dot{\theta}_b) - i_{br}\ddot{\theta}_o \end{aligned} \quad (5.58)$$

The expression for θ_r is given in (5.48) (see Appendix D.1.3).

Local track references were used, and both the translation and rotation of these reference axes associated with curves were allowed for in the equations (F'' , \bar{F}'' and T'' , \bar{T}''). Moreover, equation (5.49) includes an end moment effect, $F' = m_v g(y_v - y_b)$, modelling the roll effect of the body weight due to the lateral displacement of its centre of gravity on the curve (based upon the schematic representation of Figure 5.12). However, this

that all necessary C and D output matrices, for control design, can be formed from the relevant rows (depending on the required outputs) of the given A and B matrices. For this reason a number of outputs is available such as displacements, velocities, accelerations of the vehicle body and bogies and also displacements, velocities of the active elements.

Table 5.3: Four D-o-F ARB vehicle model dynamic modes

Mode	Damping (%)	Frequency (Hz)
Body lower sway	16.5	0.67
Body upper sway	27.2	1.50
Bogie lateral	12.4	26.8
Bogie roll	20.8	11.1
Airspring	100.0	3.70

In order to verify the accuracy of the model, a series of tests is performed. First an analysis of the modes of the system guarantees compatibility with the full scale vehicle model. The modes present in the model are shown in Table 5.3, and they are very close to the industry norms. Next, a series of transient tests ensure that the vehicle behaves in a similar manner to its full scale equivalent (real) vehicle (for the passive model, the actuator is inactive). The track profiles, both deterministic and stochastic, used for this purpose can be seen in in Table 5.4.

A nominal vehicle speed of $v_o = 45 \frac{m}{s}$ ($162 \frac{km}{h}$) is assumed, and the designed cant deficiency at this speed is $\frac{v_o^2}{R} - g\theta_o = 5.83^\circ$ or $1.0(\frac{m}{s^2})$. Figure 5.13(a) shows the lateral acceleration and corresponding roll angle for the body mass.

Table 5.4: Track profiles for the 4 D-o-F ARB linear model

Curve Transition		
maximum cant angle	$\theta_{o_{max}}$	6.0 (degrees)
maximum curve radius	R_{max}	1000.0 (m)
transition length		145.0 (m) @ each end
sample track length		1200.0 (m)
Straight Track Lateral Irregularities		
track roughness	Ω_l	$0.33e - 8$ (m)
track spatial spectrum	S_T	Ω_l / f^3 $\left(\frac{m^2}{(cycle/m)} \right)$
sample track length		1200.0 (m)

The lateral acceleration level is what the passengers would experience on the curve transition, and it is provided by a lateral accelerometer placed on the vehicle body c.o.g. The peak value is $13.0\%g$, while the steady-state value is around $11.93\%g$ at a

forward vehicle speed of $45(m/s)$. The increase in lateral acceleration is because the lateral suspension acts significantly lower than the body centre of gravity, and as a consequence the body roll-outwards on curves (steady-state 1.0°).

In the case of the bogie mass, Figure 5.13(b), the roll-out is less (steady state value of 0.43°) due to the stiffer primary suspensions. The steady-state level of the bogie lateral acceleration of $10.7\%g$ is closer to the cant deficiency for which the track was designed by the civil engineers. Note that more high frequency components are now present due to the harsh environment of the bogie system.

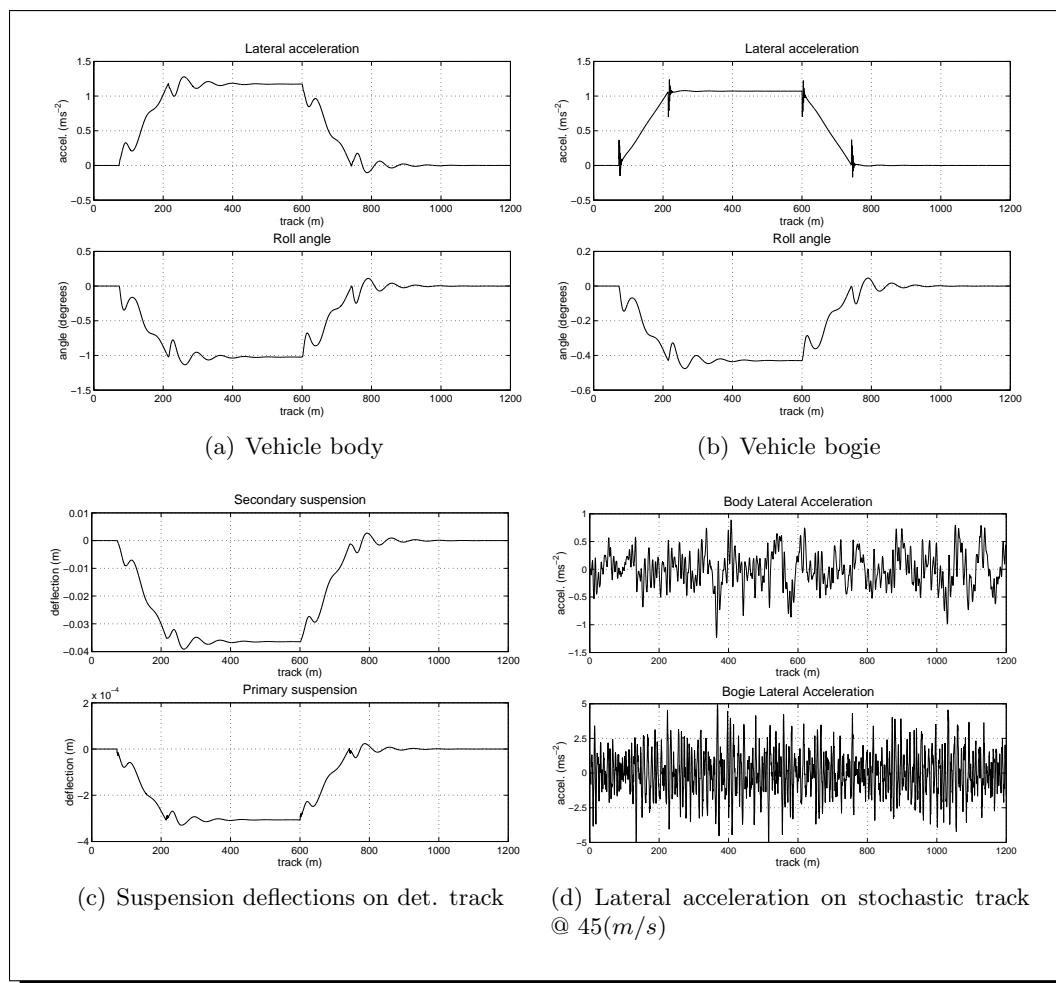


Figure 5.13: Vehicle body/bogie time histories @ $45(m/s)$

Figure 5.13(c) shows a comparison between the lateral displacements of the vehicle body and bogie. The effect of the two different sets of suspensions is clearly evident. The soft secondary suspensions cause a displacement of $36.5(mm)$ in steady-state, while the

primary suspensions owing to the high stiffness have hardly been displaced by $0.3(mm)$ in steady-state.

It is also important to test the behaviour of the vehicle model on the straight track irregularities, which are the primary cause of ride quality degradation. Figure 5.13(d) presents the time histories for the lateral acceleration of both the body and the bogie travelling on straight track. The nominal vehicle speed is assumed $45(m/s)$. The bogie due to its harsh environment has an R.M.S. value of lateral acceleration equal to $16.4\%g$, while the soft secondary suspensions filter out a large amount of high frequencies and leave the body with an R.M.S. lateral acceleration of $2.932\%g$.

Finally Table 5.5 presents the assessment of the passive model based upon the methods discussed in Chapter 3. The table presents a clear view of the suspension effects upon the model behaviour.

Table 5.5: Assessment of non-tilting vehicle @ $45(m/s)$

DETERMINISTIC		
Lateral accel. (actual vs ideal)	- steady-state	11.93 (%g)
	- R.M.S. deviation error	1.47 (%g)
	- peak value	13.02 (%g)
Roll gyroscope	- R.M.S. deviation	0.008 (rad/s)
	- peak value	0.044 (rad/s)
P_{CT} (P-factor)	- peak jerk level	5.55 (%g/s)
	- standing	38.13 (% of passengers)
	- seated	11.37 (% of passengers)
STOCHASTIC		
passenger comfort	- ride quality	2.932 (%g)

5.5 Summary

This chapter presented the issues on modelling the tilting vehicle using an anti-roll bar. The implementation of a 2-DoF linear model provided an insight into the coupling of the lateral and roll modes and their resultant sway motions. The comparison of the 2-DoF linear model with its extended 3-DoF non-linear version has shown that it can be a good basis for control system design to comply with the real system. The chapter concludes with the development of a 4-DoF linear vehicle model to include the lateral and roll degree-of-freedom for both the vehicle body and the bogie, which will be used for control system analysis and design.

Chapter 6

Basic Tilt Control Strategies for Active ARB

This chapter presents a classification of the basic tilt control strategies for the active ARB, listed in Section 1.3.4, before proceeding to the alternative advanced control studies proposed in this thesis. The purpose is to demonstrate the performance limitations of the early ‘nulling’ tilt control approach and to introduce the solution adopted by the major tilt vehicle manufacturers.

The chapter is divided into two sections, the first dealing with the early *nulling scheme*, the second with the development of the *command-driven approaches*. To allow the application of full tilt angle for partial compensation purposes, it was assumed that

1. the active anti-roll bar is able to provide tilt action up to the required amount of tilt angle, i.e. no limitation on tilt angles is imposed by suspension clearances (this can be possible in practice by having a single central airspring, rather than duo airsprings, which allows tilt angles up to 8° or 9°)
2. the secondary suspension deflection allowance is such that no bumpstop limits arise within the required interval of tilt action. However, it should be noted that this depends upon available *loading gauge*, i.e. a series of height and width profiles which are applied to a given route in order to ensure that a railway vehicle will not collide with a lineside or overline structure (such as station platforms, canopies, overhead power supplies (catenary) overbridges, tunnels). Moreover, loading gauge profiles vary by route, reflecting the constraints on rail vehicle size caused by the above structures, see Figure 6.1(a).

6.1 Basic Nulling Tilt Control

In this intuitively formulated control strategy, which is a classical application of SISO feedback control, the signal from a body-mounted lateral accelerometer is used to provide a measurement of the curving acceleration experienced by the passengers. The controller would drive the feedback signal to zero and therefore give 100% compensation, thus a portion of the suspension roll angle (i.e. the ‘actual tilt’) is included in the feedback, chosen to provide the specified 60% compensation Figure 6.1(b). This is actually referred to as ‘partial-nulling’, thus throughout this thesis the term ‘nulling’ will be referring to ‘partial-nulling’ for simplicity. For assessment purposes, the track input used is listed in Table 4.1 in column ‘ARB (Case A)’ on page 38 (the same as in the previous chapter, see Table 5.4). The advantage with the nulling strategies is that

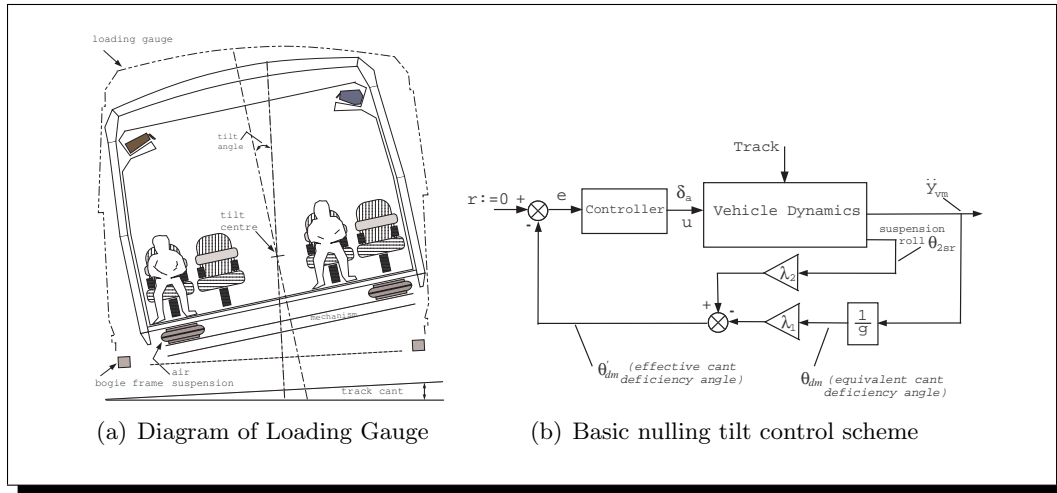


Figure 6.1: Loading gauge and basic nulling tilt

the sensors are mounted on the vehicle body and do not encounter the high levels of acceleration experienced on bogies (secondary suspensions act as a mechanical filter). However, it is worth mentioning that the sensor exists within the control loop and the tilt demand is continuously affected by the system dynamics, which imposes difficulties on controller design.

The control input comprises an angular displacement (δ_a) provided by a rotary actuator in series with the anti-roll bar, which in turn provides a torque to the vehicle body. Note that the reference signal is ‘zero’, i.e. the system is subject to track disturbances only. The feedback signal for partial tilt compensation is the *effective cant deficiency*

angle θ'_{dm} which is given by

$$\theta'_{dm} = \left(-\lambda_1 \frac{\ddot{y}_{vm}}{g} - \lambda_2 \theta_{2sr} \right) \quad (6.1)$$

where \ddot{y}_{vm} is the lateral acceleration felt by the passengers as measured from an accelerometer on the body c.o.g (6.1), and θ_{2sr} is the secondary suspension roll angle (6.2).

$$\ddot{y}_{vm} = \frac{v^2}{R} - g(\theta_o + \theta_v) + \ddot{y}_v \quad (6.2)$$

$$\theta_{2sr} = \theta_v - \theta_b \quad (6.3)$$

Note the effect of the deterministic track included in (6.1). Factors λ_1, λ_2 ensure partial tilt and for 60% compensation need to be set to 0.615 and 0.385 respectively, taking in account bogie roll-out in (6.3). The necessary C and D matrices can be easily formed from the relevant rows of state-space matrices A and B .

Remark 6.1.1. The sign of the feedback signal is inverted for correct application of negative feedback based upon the current axis system. Recall that all lateral motions (y) are positive inwards of the curve (i.e. to the right) and all roll motions (θ) positive clockwise. However, the lateral accelerometer, which is modelled as a mass on a spring, measures positive acceleration to the left (6.2) (i.e. outwards of the curve). Hence the acceleration is translated into a positive cant deficiency angle, combined with a portion of the suspension roll, and is then fed back (note that $\lambda_1 \frac{\ddot{y}_{vm}}{g} \geq \lambda_2 \theta_{2sr}$). The combined signal will of course be a positive angle, which if fed back using negative feedback causes the controller to provide a negative tilt angle (i.e. anti-clockwise rotation), consequently destabilising the system. Thus it is necessary to invert the sign of the feedback signal such that the controller receives a positive angle and rotates the body clockwise for correct compensation

Conclusions about the stability of the closed-loop may be drawn by investigating the open-loop frequency response of the system. The nominal open-loop frequency responses from $u := \delta_a$ to $y_1 := \theta'_{dm}$, and $y_2 := \theta_{2sr}$ can be seen in Figure 6.2. Note that, while gain reduction is required to stabilise the closed-loop system, the opposite applies in the case of fast tilt response. Hence, there must be a compromise between the tilt response and the ride quality.

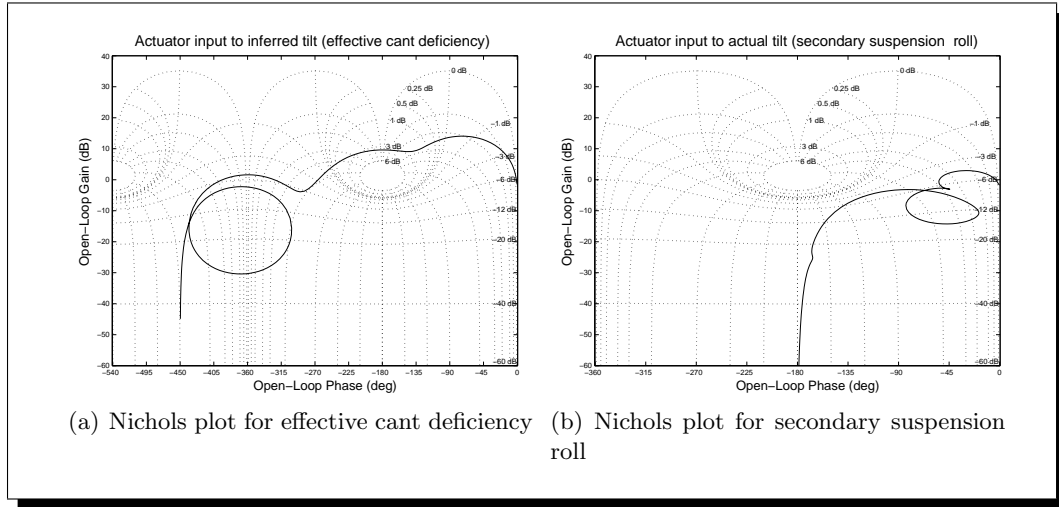


Figure 6.2: Nominal open-loop frequency responses

Table 6.1: Open-loop poles and zeros of $G_{y_1u}(j\omega)$

<i>OL poles</i>	<i>OL zeros</i>
$-20.87 \pm 167.34j$	$-2.41 \pm 125.94j$
$-14.57 \pm 68.38j$	$29.36 \pm 0.00j$
$-2.56 \pm 9.03j$	$-40.73 \pm 0.00j$
$-0.69 \pm 4.12j$	$-26.18 \pm 0.00j$
$-23.22 \pm 0.00j$	$6.02 \pm 0.00j$
-	$-3.83 \pm 3.13j$

A closer investigation of the open-loop poles and zeros of the transfer function $G_{y_1u}(s)$ reveals that, while the system is open-loop stable, is also *non-minimum* phase due to the existence of two RHP zeros at $(s - 29.4)$ and $(s - 6.02)$, Table 6.1. The pole-zero map of the uncompensated system $G_{y_1u}(s)$ can be seen in Figure 6.3(a). The presence of RHP-zeros imposes a fundamental limitation on control, and high controller gains induce closed-loop instability.

A classical root-locus analysis in Figure 6.3(b) shows clearly the limitation of controller design. Although the illustration involves only proportional gain, the case also holds for all *stable* dynamic SISO controllers due to the fact that the OL unstable zeros will still exist in the designed open-loop (gain path starts from OL poles and ends at OL zeros!). The combination of the two RHP zeros introduces extra phase lag as frequency increases, i.e. an extra -180° at $\omega \geq 29.36 \frac{\text{rads}}{\text{s}}$. A symbolic analysis - in Matlab based on the 2-DoF ARB linear model (described in Section 5.1) for simplicity - reveals that the cause for such a non-minimum phase system is the suspension dynamics

interaction, and the extra contribution of body roll (or tilt angle) in the body-mounted lateral accelerometer (detailed results can be found in Appendix B.3).

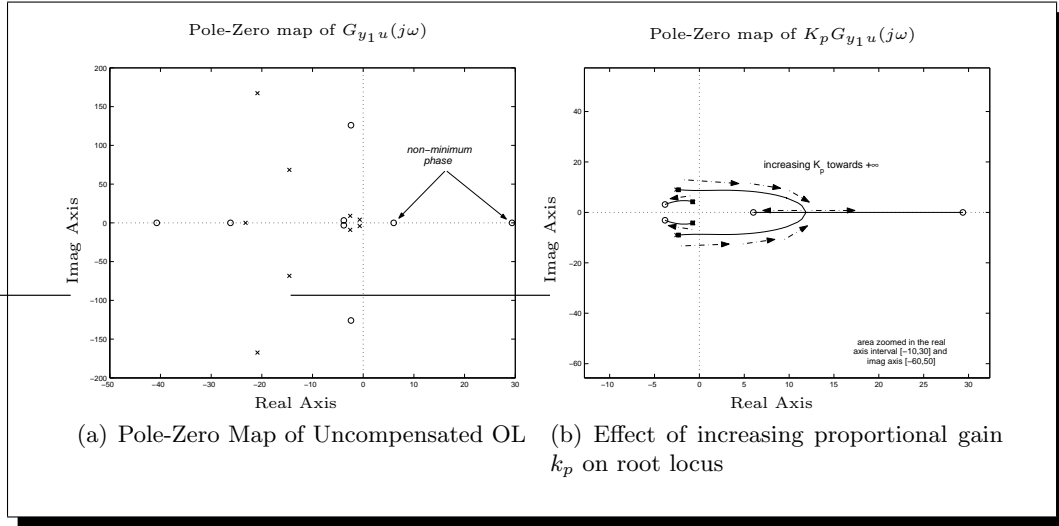


Figure 6.3: Non-minimum phase limitations

6.1.1 PI-control of the basic nulling tilt process

To guarantee a zero steady-state error, i.e. zero steady-state effective cant deficiency angle, integral action is necessary. Therefore, to remove the steady-state offset integral action is added in the form of a PI-controller, Figure 6.4, described by the following expression

$$K_{pi}(s) = k_g \left(1 + \frac{1}{s\tau_i} \right) \tag{6.4}$$

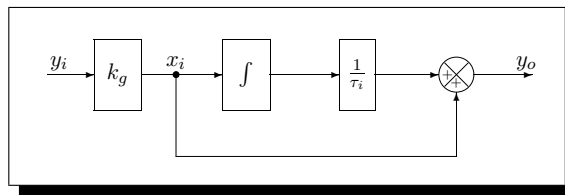


Figure 6.4: PI Block

It was necessary to include a ‘Proportional’ term to limit the phase-lag introduced as frequency increases (the system is already characterised by large phase-lag, thus is not desirable to introduce significant phase-lag especially at frequencies higher than $6.02 \frac{rads}{s}$). The settings for k_g and t_i were adjusted to suffice both the deterministic and stochastic criteria, with the best configuration being $k_g = 0.225$, $\tau_i = 0.4 \text{ s}$ (to at least

ensure appropriate stability margins, see Figure 6.6(a)). Table 6.2 presents the overall

Table 6.2: PI-control basic nulling approach assessment @ 58(m/s) - ($k_g = .225$, $\tau_m = 0.4$ s)

DETERMINISTIC		
Lateral accel. (actual vs ideal)	- steady-state	n/a (%g)
	- R.M.S. deviation error	5.555 (%g)
	- peak value	19.510 (%g)
Roll gyroscope	- R.M.S. deviation	0.032 (rad/s)
	- peak value	0.086 (rad/s)
P_{CT} (P-factor)	- peak jerk level	10.286 (%g/s)
	- standing	71.411 (% of passengers)
	- seated	22.640 (% of passengers)
STOCHASTIC		
Passenger comfort	- R.M.S. passive (equiv.)	3.778 (%g)
	- R.M.S. active	3.998 (%g)
	- degradation	5.802 (%)

controller assessment, while Figure 6.5 and Figure 6.6 present the simulation results on curved track and the corresponding frequency responses respectively. Clearly the response is very slow with the steady-state values for acceleration, roll angle and roll rate profiles not met. Note that, due to the vehicle body inertia at the start and the end of curve, the body roll angle initially has an inverse response and then rises slowly up to the required steady-state value. The difference between the control input δ_a and the body roll θ_v is due to the torque imposed by the secondary suspension subject to the curving forces on the vehicle body. Thus, additional control effort is demanded to overcome this extra torque and regulate the body roll (via the suspension roll portion) to the desired value. There is also great difficulty in controlling the roll rates appropriately, which has a detrimental effect on the overall system performance.

Recall that the actuator has no direct effect on the position of the secondary suspensions, thus the lateral deflection will increase due to the increased curving forces compared to the case of the low-speed non-tilting train, see Figure 6.5(d). The simulation yields a steady-state lateral secondary suspension deflection, for the tilting vehicle, of approximately -85mm (i.e. outwards of the curve). In theory the s.s. suspension deflection can be found from (5.44), which on steady-state is

$$0 = -2k_{sy}\{y_v - h_1\theta_v - (y_b + h_2\theta_b)\}\Big|_{ss} - m_v \left(\frac{v^2}{R} - g\theta_o \right) \Big|_{ss} \quad (6.5)$$

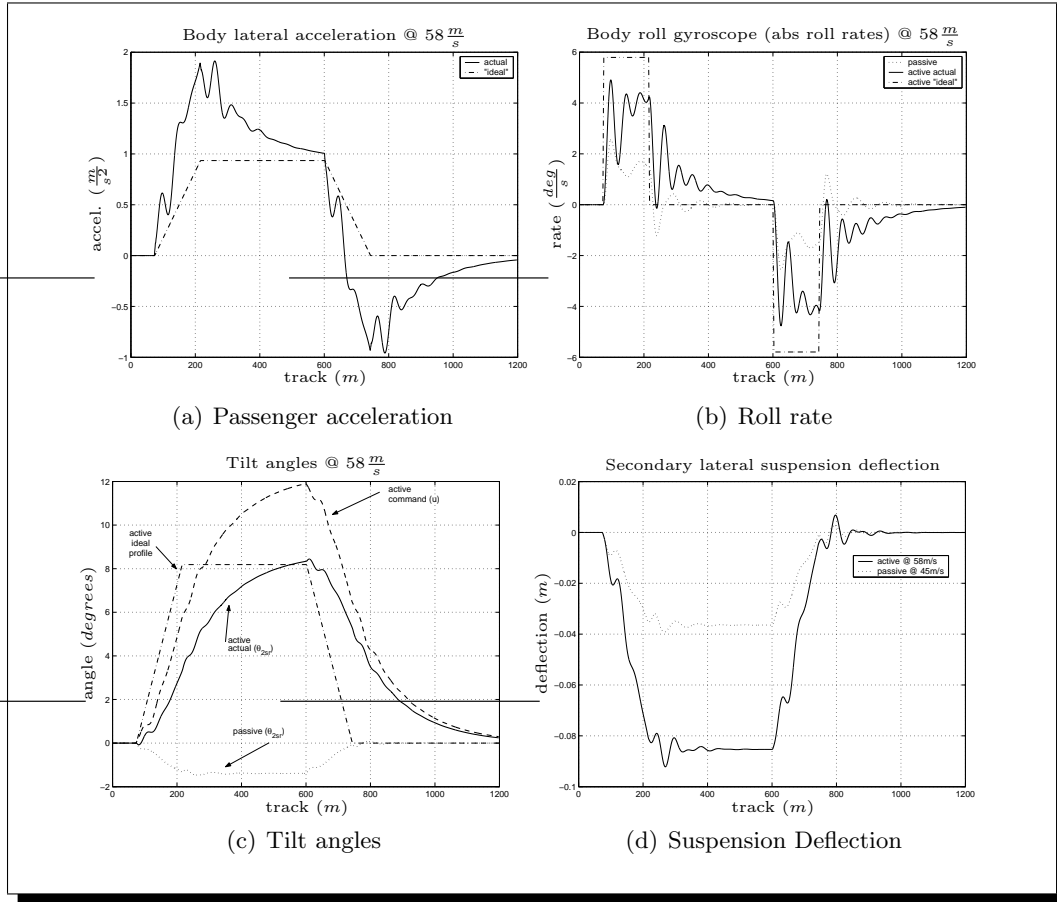


Figure 6.5: Basic nulling scheme with $P + I$ time history results for design track

and can be re-arranged as

$$x_{2dfl} \Big|_{ss} = - \frac{m_v (v^2 R^{-1} - g\theta_o)}{2k_{sy}} \Big|_{ss} \quad (6.6)$$

where $x_{2dfl} = \{y_v - h_1\theta_v - (y_b + h_2\theta_b)\}$. Substituting the appropriate values for each term in (6.6) gives a steady-state lateral secondary suspension deflection of $-85.38mm$ which agrees with the simulation results.

The *complementary sensitivity* T , in Figure 6.6(b), shows that the control action in the frequency range $[0.4(\frac{rads}{s}), 4(\frac{rads}{s})]$ does not affect the system, which causes a slow response (i.e. insufficient bandwidth). Moreover, higher frequency components enter owing to the sway mode resonances in the interval $[4(\frac{rads}{s}), 10(\frac{rads}{s})]$, with the control action incapable of improving the performance due to $|S| > 1$. The uncompensated and compensated open-loop responses are presented in Figure 6.6(a), with the latter emphasising the integral action at low frequencies.

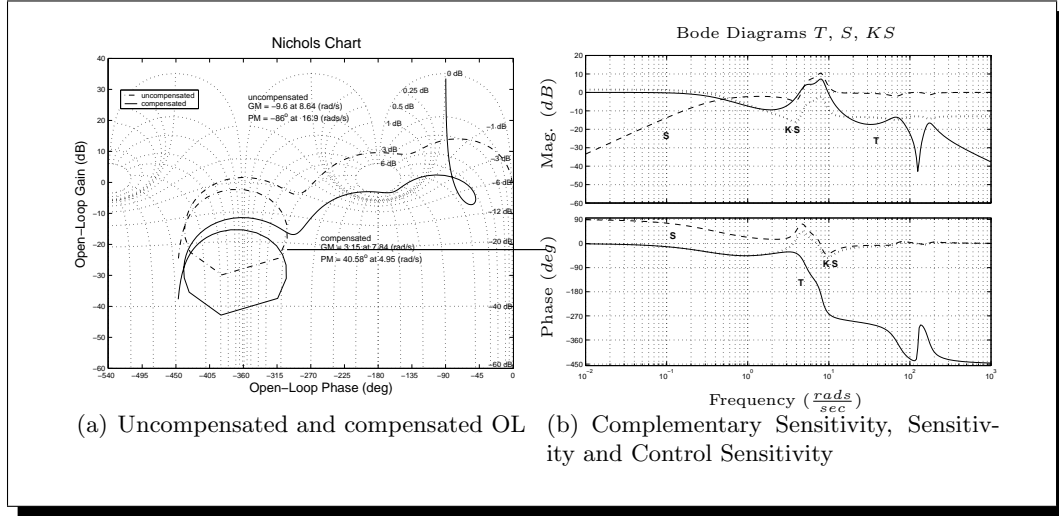


Figure 6.6: Basic nulling, designed system frequency responses

6.1.2 Complementary filter approach of the basic nulling tilt process

An alternative way to improve the tilt performance, still based upon the classical control approach, is to separate the measured acceleration (essentially the measured cant deficiency) into the (i) tilting component and (ii) the lower sway oscillations component. This can be achieved by using complementary *low pass* and *high pass* filters [BK82], and hence deal with each component separately by designing its own controller, as shown in Figure 6.1.2. Note that, since the two filters complement each other ($HP + LP = 1$), their net effect introduces *unity gain* and *zero phase shift* throughout the frequency range, i.e. $H_{HP}(s) + H_{LP}(s) = 1$.

The filters were chosen to have a second order flat “Butterworth response” ($\zeta = 0.707$), with a corner frequency of $w_c = 2\pi \times 0.3(\frac{rads}{s})$, such that the secondary feedback for lower sway will have some degree of control on the vehicle body modes.

$$H_{LP}(s) = \frac{w_c^2}{s^2 + 2\zeta w_c s + w_c^2} \quad (6.7)$$

$$H_{HP}(s) = \frac{s^2 + 2\zeta w_c s}{s^2 + 2\zeta w_c s + w_c^2} \quad (6.8)$$

The main loop, related to tilt performance, involved a $P+I+\{Phase\ Lead\}$ compensator given by

$$K_1(s) = \frac{0.225(0.2s + 1)}{0.2s} \times \frac{(s + 1.68)}{(0.42s + 1)} = \frac{(0.045s^2 + 0.30s + 0.378)}{s(0.084s + 0.2)} \quad (6.9)$$

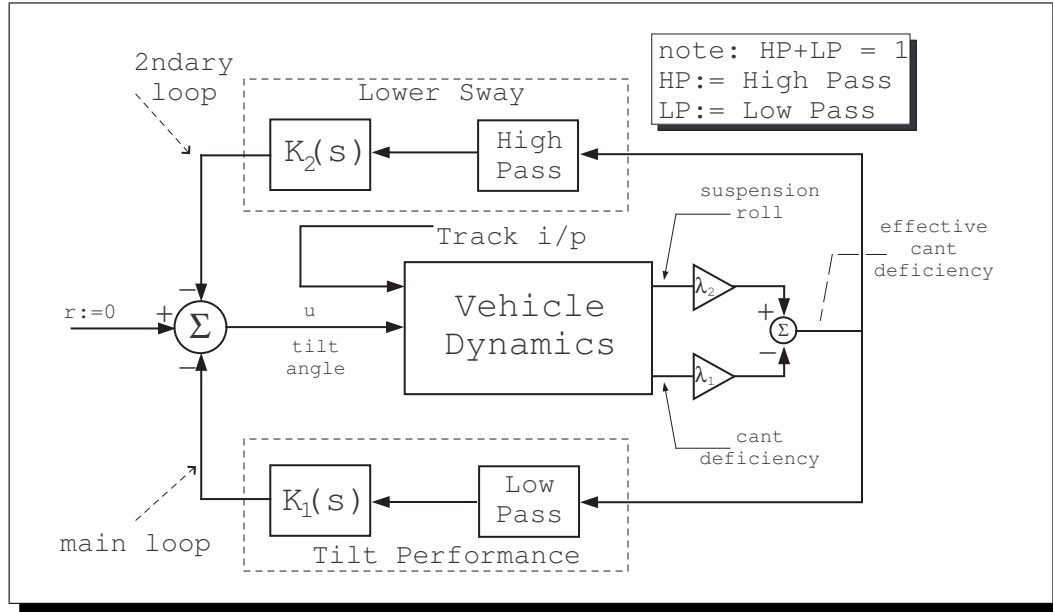


Figure 6.7: Complementary filter control approach

while the secondary loop, for lower sway control, incorporated a $P+\{Phase\ Lag\}$ controller given by

$$K_2(s) = \frac{0.175(0.1s + 1.428)}{(0.1428s + 1)} \quad (6.10)$$

The compensated OL frequency responses for both loops can be seen in Figure 6.8(c) and 6.8(d), while the related sensitivity and complementary sensitivity functions are presented in Figure 6.8(a) and 6.8(b).

In this case the control action is effective over a wider range of frequencies compared to the case in section 6.1.1, with the closed loop bandwidth (for the main loop) being approximately $\omega_{BT} = 0.6Hz^1$ based upon the complementary sensitivity T .

This approach provided some improvement in performance, see Table 6.3, with the secondary loop trying to minimise high frequency movements as shown in Figure 6.9 on page 73. However, the limitations from the basic nulling scheme still apply regarding the main feedback loop. The phase lags inherent in the feedback signal of the main loop induce insufficient stability margins for an acceptable tilt response (with the *robustness* of the system being questionable in some cases).

¹[SP00] suggests that ω_{BT} , i.e. the B/W based on T , may be misleading in some cases, the reason being that both its magnitude $|T|$ and phase $\angle T$ should be considered. Instead, it is recommended to rely on either ω_B , B/W in terms of S , or ω_c , B/W in terms of L , for a better indication of closed-loop performance (note that in the case of ω_B only $|S|$ needs to be considered).

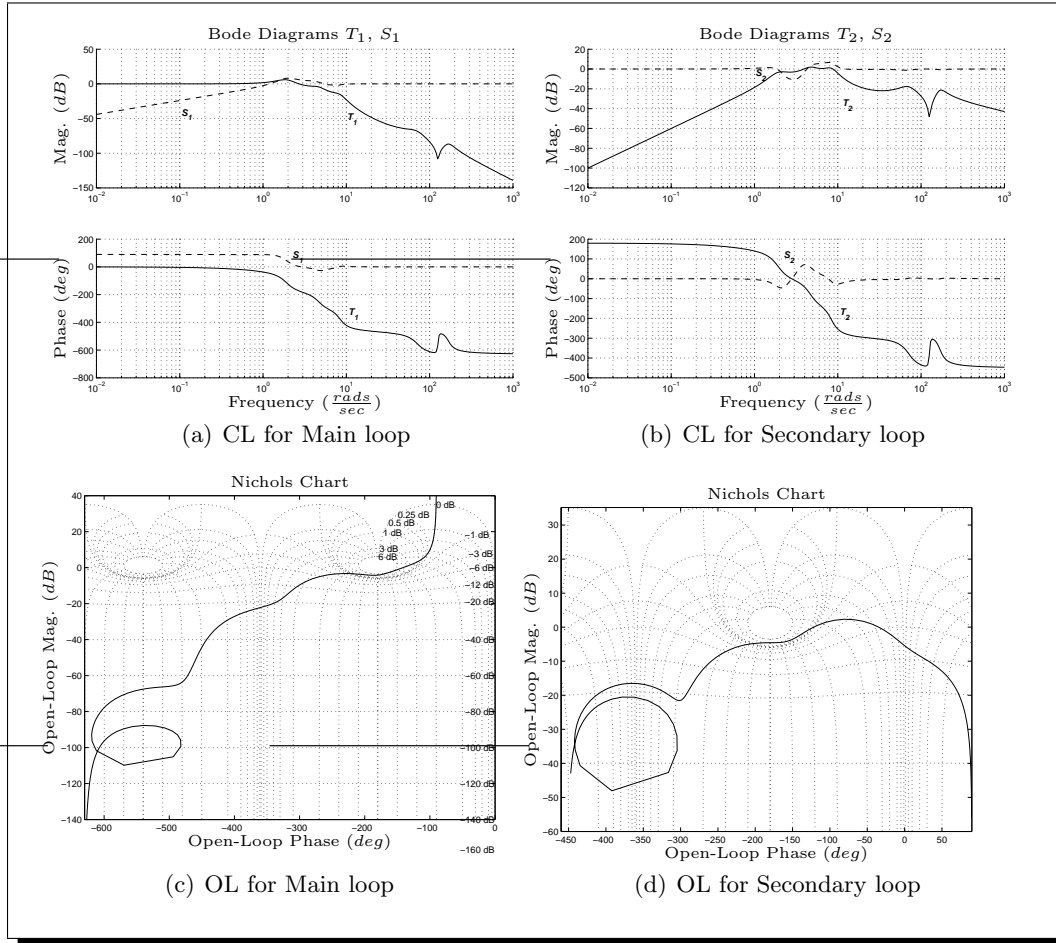


Figure 6.8: CF approach, designed system frequency responses

6.2 Basic Command-driven schemes

The difficulties of designing tilt controllers based upon a body-mounted accelerometer existing within the control loop led to the use of bogie-mounted accelerometers to provide the tilt reference command. All strategies in this category are called *command-driven* and include (i) *local command-driven* and (ii) *command-driven with precedence* (see Section 1.3.4 on page 8). The concept is illustrated in the following sections².

6.2.1 Local vehicle Command-driven

In the *local command-driven*, shown in Figure 6.10, the tilt command is provided by an accelerometer mounted on the bogie of the *local* vehicle, with low-pass filtering used to

²note that the controllers for this sections are designed for demonstration purposes only and they would be formed differently in the case where actuator dynamics are introduced.

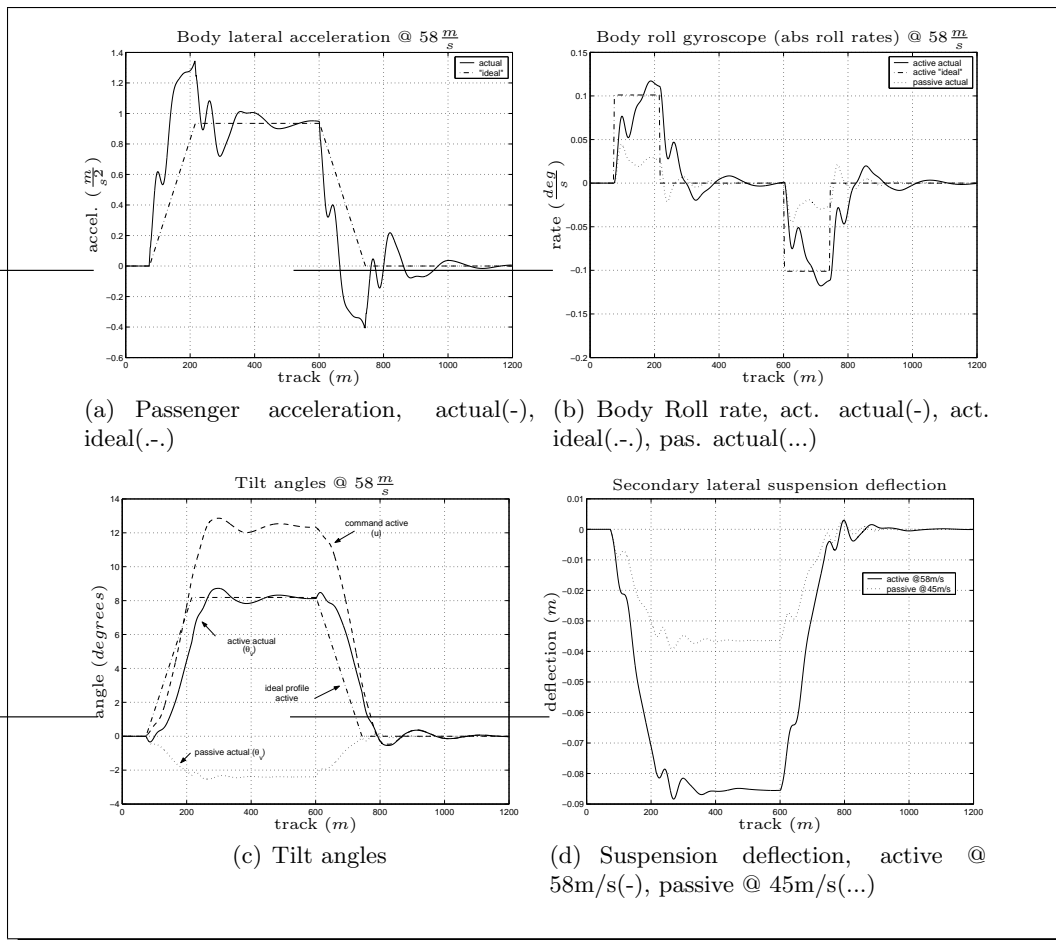
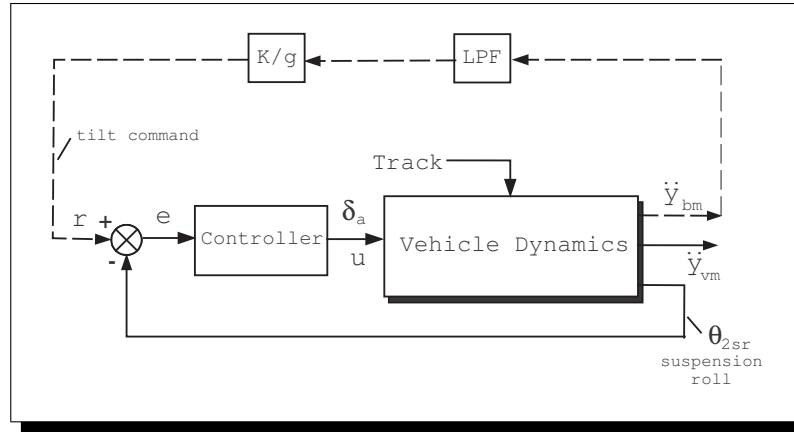


Figure 6.9: CF approach, simulation results on curved track

Table 6.3: Basic nulling complementary filter approach - assessment @ 58(m/s)

DETERMINISTIC		
Lateral accel. (actual vs ideal)	- steady-state	9.53 (%g)
	- R.M.S. deviation error	2.97 (%g)
	- peak value	13.70 (%g)
Roll gyroscope	- R.M.S. deviation	0.030 (rad/s)
	- peak value	0.117 (rad/s)
P_{CT} (P-factor)	- peak jerk level	8.000 (%g/s)
	- standing	57.773 (% of passengers)
	- seated	14.406 (% of passengers)
STOCHASTIC		
Passenger comfort	- R.M.S. passive (equiv.)	3.778 (%g)
	- R.M.S. active	3.983 (%g)
	- degradation	5.417 (%)

**Figure 6.10:** Local command-driven scheme

remove unwanted high frequencies due to the bogie harsh environment, while partial tilt is achieved by setting $K < 1$ (for 60% compensation $K = 0.6152$ taking in account bogie roll-out of $\approx 0.6^\circ$). The tilt action is controlled by utilising the secondary suspension roll angle as a feedback.

However the level of low-pass filtering required in practice, to achieve an adequate ride quality, introduces unacceptable delays in the tilt action on curve transition. Table 6.4 illustrates the effect of the low-pass filter corner frequency on both deterministic and stochastic tilt performance, while a set of relevant time history results for the deterministic case can be seen in Figure 6.11 included in the next page. The controller designed was chosen to be a $P+I$, for illustration purposes, given by $K_{pi}(s) = 2 \left(1 + \frac{1}{s0.5}\right)$.

It was found again very difficult to achieve all required objectives for tilt control based

Table 6.4: Effect of low-pass filtering on command-driven control ($v = 58(m/s)$)

LP ω_c (Hz)	P_{CT} stand. (% of passg)	(R.M.S.) determin. $ \dot{y}_m - \dot{y}_{m_i} $ (%g)	(R.M.S.) determin. $ \dot{\theta}_m - \dot{\theta}_{m_i} $ (rad/s)	Degradation stochastic (%)
2.000	45.39	1.68	0.016	149.132
1.000	46.44	1.96	0.020	37.64
0.500	54.50	2.61	0.024	18.00
0.250	65.39	4.07	0.033	6.588
0.125	76.74	6.37	0.040	2.255

upon this approach. The high frequency noise introduced by the vehicle bogie (which is there to guarantee running stability) requires heavy filtering to provide the clean signal of cant deficiency command. Thus, manufacturers proceeded to the concept of ‘precedence’ control to compensate for the time delays introduced by the filtering action and it is discussed in the next section.

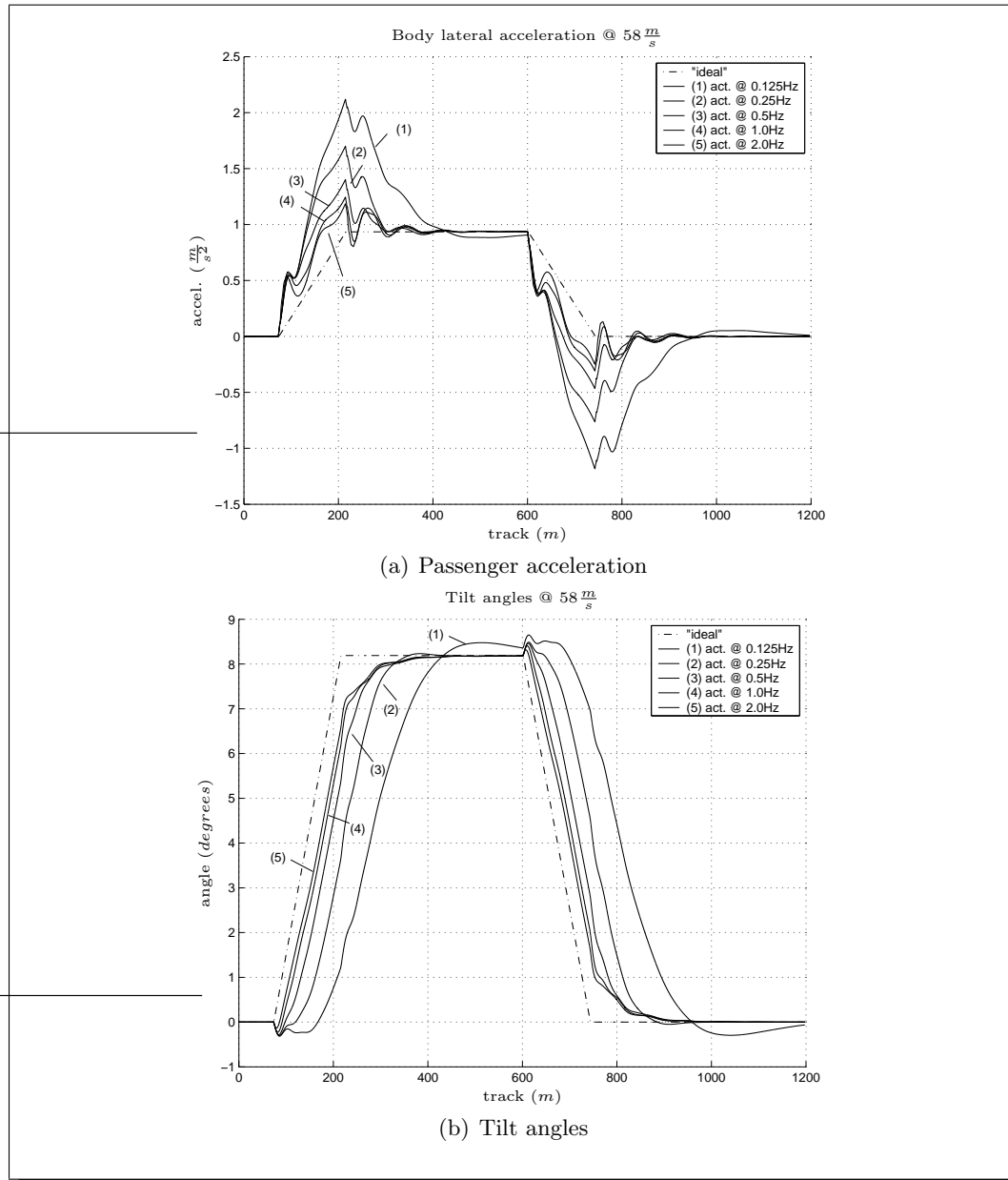


Figure 6.11: Command-driven tilt performance on design track

6.2.2 Command-driven with precedence

The evolution of the tilt control system, due to the problems of the local command-driven approach, led to the currently used *command-driven with precedence* scheme [Goo99] (see Section 1.3.4 on page 8 for more details). An accelerometer mounted on the leading bogie of the leading vehicle - for this purpose a preview of 29m, approximately 1.5 vehicle length (depending upon vehicle types), was assumed - provided the curving acceleration signal, passed via a 0.45Hz second-order low pass filter having a flat response ($\zeta = 0.707$) to remove high frequency elements, as shown in Figure 6.12(a). The schematic interpretation of the scheme for simulation purposes can be seen in Figure 6.12(b).

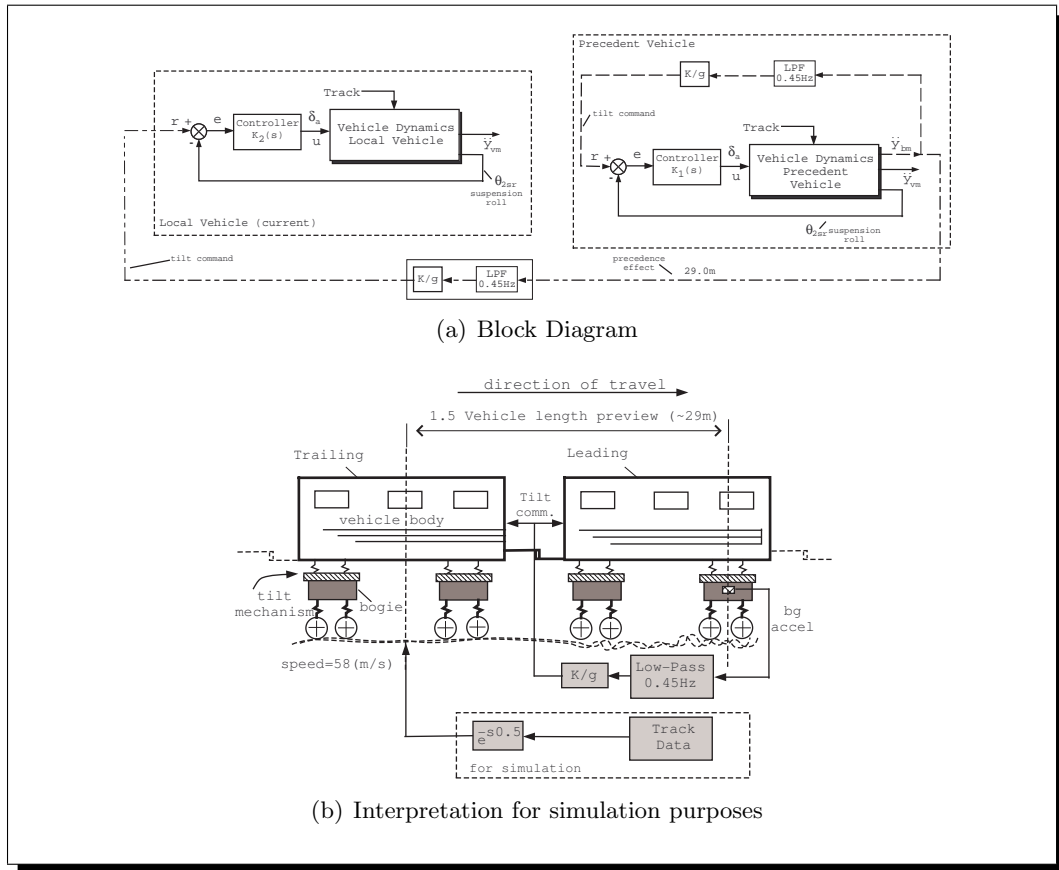


Figure 6.12: Command-driven with precedence approach

To obtain comparable results to the local tilt strategies, the filter delay was chosen to match the precedence time, however this can be changed to

emphasise precedence information if necessary. The transfer function of the LP filter is given by

$$H_{LP2}(s) = \frac{w_{c2}^2}{s^2 + 2\zeta_2 w_{c2} s + w_{c2}^2}, \quad w_{c2} = 2\pi \times 0.45, \quad \zeta_2 = 0.707 \quad (6.11)$$

and the time delay introduced is $t_{dLP} = \frac{2\zeta_2 w_{c2}}{w_{c2}^2}$ (see Appendix B.3.1), which for the current case is $0.5s$ delay. Thus for the *precedence* to match the *filter delay*, it takes $l = 58(\frac{m}{s}) \times 0.5s = 29m$ precedence, i.e. approximately 1.5 vehicle length as mentioned earlier. Note that the tilting response for the leading vehicle will be too late.

The leading vehicle controller is a $P+I$ given by $K_{pi}(s) = (1 + \frac{1}{s0.5})$. For the trailing vehicle, the controller designed to actively tilt the body is a PI compensator with a low-pass filter (LPF) in series (this will be redundant in the case of a non-ideal actuator, i.e. actuator with limited bandwidth³), in order to remove high frequencies from the secondary suspension roll (those are introduced due to the bogie roll contribution). The overall controller transfer function is listed below

$$K_{total}(s) = \left(\frac{1.5 + s0.75}{s0.5} \right) \times \frac{400}{s^2 + 28.28s + 400}$$

$$\therefore K_{total}(s) = \frac{300s + 600}{s(0.5s^2 + 14.14s + 200)} \quad (6.12)$$

The compensated and uncompensated open loop together with the overall compensator frequency response can be viewed in Figure 6.13(a). The corresponding sensitivity and complementary sensitivity of the closed loop system are presented in Figure 6.13(b), where it is evident that the control action influences the system over a wider range of frequencies compared to the previous cases.

A set of time-domain results for the deterministic track case is shown in Figure 6.14 (page 80), where it is obvious that the precedence scheme is superior to the previous basic approaches. The tilt controller performance is presented in Table 6.5 (page 79), and it is closer to the ideal performance expected in all cases. In the stochastic case it can be seen that there is an improvement in ride quality by the active system. When the precedence time matches the filter delay, which applies in this case, the reference and the track input will be uncorrelated and the tilt command will compensate for long wavelengths.

³i.e. electro-mechanical actuators have a bandwidth of up to approximately $5Hz$.

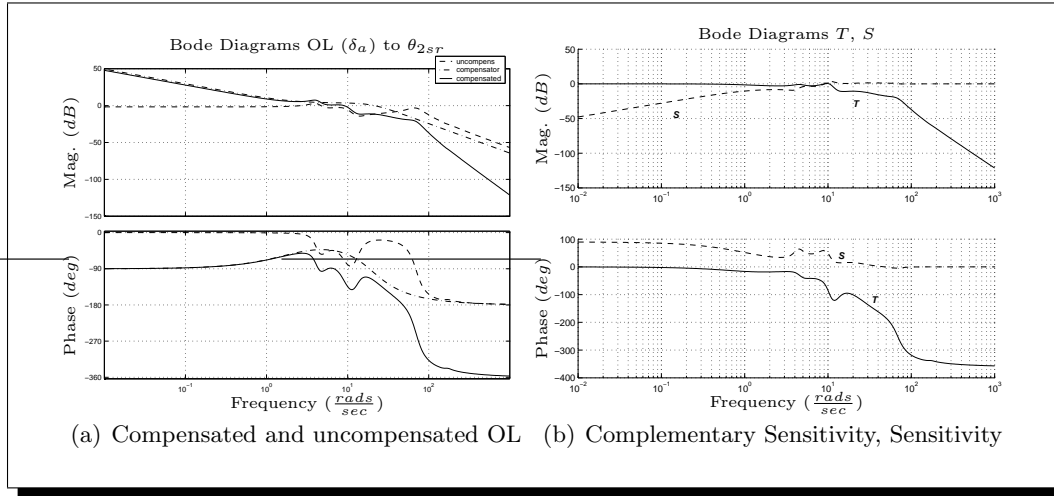


Figure 6.13: Basic nulling, designed system frequency responses

Table 6.5: Basic command-driven with precedence approach - assessment @ 58(m/s)

DETERMINISTIC		
Lateral accel. (actual vs ideal)	- steady-state	9.53 (%g)
	- R.M.S. deviation error	1.54 (%g)
	- peak value	12.18 (%g)
Roll gyroscope	- R.M.S. deviation	0.018 (rad/s)
	- peak value	0.104 (rad/s)
P_{CT} (P-factor)	- peak jerk level	6.80 (%g/s)
	- standing	47.62 (% of passengers)
	- seated	13.455 (% of passengers)
STOCHASTIC		
Passenger comfort	- R.M.S. passive (equiv.)	3.78 (%g)
	- R.M.S. active	3.31 (%g)
	- degradation	-12.12 (%)

Placing more emphasis on precedence information will improve the deterministic performance, subject of course to the amount of precedence used, i.e. too much precedence (over-precedence) can be disastrous for the normal operation of the train (tilt action will apply on straight track segments much sooner than the intended start of the curve!). In addition, the amount of precedence used will influence the stochastic ride quality either positively or negatively depending upon the correlation of the signals (in the case where the precedence time differs from the filter delay, the reference and track input signals are no longer uncorrelated). It should be noted that, even in the precedence schemes, sensors located on each vehicle (i.e. local sensors) are used to ensure the correct operation of the overall tilting system (the sensors are always present for safety purposes).

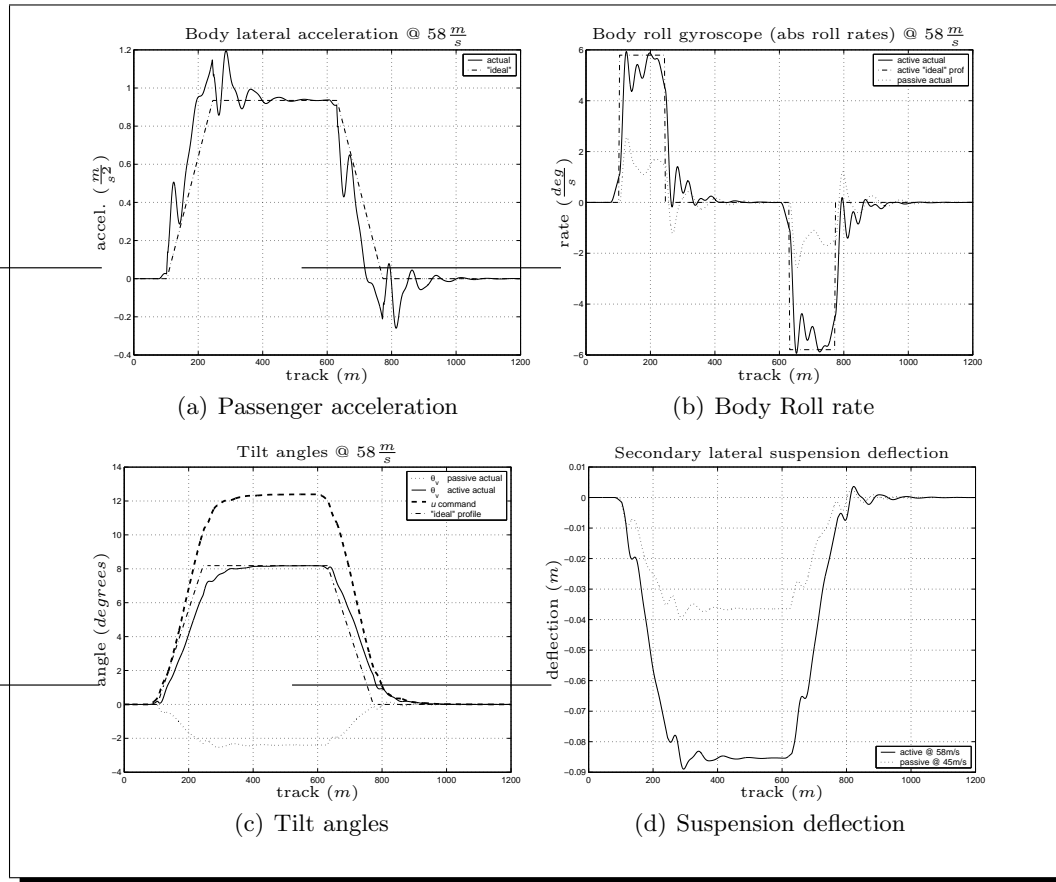


Figure 6.14: Command-driven with precedence basic approach, demonstration on curved track

6.3 Summary

This chapter presented the evolution of the *basic tilt control strategies* used by tilting train manufacturers. It included an investigation on the drawbacks of the early basic “nulling” scheme, and illustrated the advantages of using command-driven strategies with emphasis on precedence schemes - which are now mainly used by manufacturers. The next chapter proposes alternative control approaches to design local/vehicle based tilt controllers, i.e. without using precedence, by using rather more advanced control methods.

Chapter 7

Advanced Control Studies for Active ARB

The ‘nulling’ type classical control approach, described in Chapter 6, proved difficult to solve the tilt control problem in an effective manner. The very nature of this type of control means that it will be difficult to improve tilt performance while maintaining acceptable ride quality. Clearly a method is required to sustain the simplicity of ‘nulling’ control, and provide tilt performance comparable to the ‘precedence’ control scheme.

Modern control methods provide an approach where a number of objectives of the control problem can be simultaneously addressed. Undoubtedly classical control can be effectively applied to many SISO control-design problems, however modern control tackles a wider class of control problems including more complicated structures and especially MIMO systems. It is important to remember that space travel became possible only because of the advent of modern control theory. The theory is continuously evolving since the 1960s and has been applied in numerous practical applications, i.e. in the aerospace industry.

A number of modern control methods is available in control literature, however this thesis concentrates on the use of the following techniques: (i) optimal LQR, (ii) model-based estimation nulling control using Kalman filter, and (iii) Robust \mathcal{H}_∞ and $\mathcal{H}_\infty/\mathcal{H}_2$ schemes. The first method is based upon the use of state feedback optimal control to solve the *linear quadratic regulator* problem as it is widely known. It also extends the concept into designing an *optimal Proportional+Integral* controller. The Kalman filter is used for estimation of all necessary states, based upon the plant mathematical model,

in order to provide a more effective feedback signal, for the application of *model-based estimation nulling control*. Finally, the robust \mathcal{H}_∞ and $\mathcal{H}_\infty/\mathcal{H}_2$ techniques, usually referred as *post-modern* control methods, deal with control designs that guarantee system robustness. As in Chapter 6 the controllers are developed for the half vehicle model discussed in Section 5.4.

7.1 Linear-Quadratic Regulator (LQR) optimal control

Optimal control forms a particular branch of modern control theory, which offers a design solution supposed to be the best possible for a particular system type. *Linear optimal control* is a special type of optimal control, where the plant is assumed linear, and in addition the controller to be designed is constrained to be of a linear form. Such controller designs are solved by using quadratic performance indices, in terms of the control, regulation and/or tracking error variables.

Linear optimal control generally possesses a number of advantages compared to other forms of optimal control. Many engineering plants can in fact be considered to be linear and implementing linear controllers physically is a simple task. Also, the majority of linear optimal control problems have readily computable solutions, which often can be carried over to non-linear optimal control problems. The available literature on the optimal control problem is extensive [AM90, Fri86, Mac89], and only briefly covered in this thesis.

7.1.1 LQR Preliminaries - Full State Feedback

The standard description of the plant and output is given by the following equations (external disturbances or reference inputs not included)

$$\dot{\mathbf{x}} = \mathbf{A}\mathbf{x} + \mathbf{B}\mathbf{u} \quad (7.1)$$

$$\mathbf{y} = \mathbf{C}\mathbf{x} + \mathbf{D}\mathbf{u} \quad (7.2)$$

where \mathbf{x} is $(n \times 1)$, \mathbf{u} is $(m \times 1)$, \mathbf{y} is $(q \times 1)$. It is assumed that the system is *linear*, *time-invariant* (for simplicity), and *controllable*. It is desired to find a suitable linear control law

$$\mathbf{u} = -\mathbf{K}_r\mathbf{x} \quad (7.3)$$

where \mathbf{K}_r is a gain matrix, which minimises the following general form quadratic index

$$J = \lim_{T \rightarrow \infty} \frac{1}{T} E \left\{ \int_0^T [\mathbf{x}^T \mathbf{Q} \mathbf{x} + \mathbf{u}^T \mathbf{R}_k \mathbf{u}] d\tau \right\} \quad (7.4)$$

The weighting matrices \mathbf{Q} (state weighting matrix) and \mathbf{R}_k (control weighting matrix) must be symmetric (because J is a scalar), i.e. $\mathbf{Q}^T = \mathbf{Q}$ and $\mathbf{R}_k^T = \mathbf{R}_k$. There is no specific restriction about the form in which \mathbf{Q} and \mathbf{R}_k should appear, but in most cases they are diagonal matrices. If, instead of the states, the output \mathbf{y} is to be controlled then the quadratic performance index needs to be arranged into

$$J = \lim_{T \rightarrow \infty} \frac{1}{T} E \left\{ \int_0^T [\mathbf{y}^T \mathbf{Q}_o \mathbf{y} + \mathbf{u}^T \mathbf{R}_k \mathbf{u}] d\tau \right\} \quad (7.5)$$

where \mathbf{Q}_o is the output weighting matrix, and it can be easily shown that $\mathbf{Q} = \mathbf{C}^T \mathbf{Q}_o \mathbf{C}$ by setting $\mathbf{y} = \mathbf{C}\mathbf{x}$ for a strictly proper system.

The gain matrix \mathbf{K}_r is the solution of the following general form *matrix Riccati differential equation*

$$\mathbf{A}^T \mathbf{P}_c + \mathbf{P}_c \mathbf{A} + \dot{\mathbf{P}}_c + \mathbf{Q} = \mathbf{P}_c \mathbf{B} \mathbf{R}_k^{-1} \mathbf{B}^T \mathbf{P}_c \quad (7.6)$$

subject to given $\mathbf{A}, \mathbf{B}, \mathbf{C}, \mathbf{Q}$ and \mathbf{R}_k . Restricting ourselves in the time-invariant case, \mathbf{P}_c should be constant which states that $\dot{\mathbf{P}}_c = \mathbf{0}$. The *Riccati* equation is then simplified to

$$\mathbf{A}^T \mathbf{P}_c + \mathbf{P}_c \mathbf{A} + \mathbf{Q} - \mathbf{P}_c \mathbf{B} \mathbf{R}_k^{-1} \mathbf{B}^T \mathbf{P}_c = \mathbf{0} \quad (7.7)$$

and the solution of the gain matrix is given by

$$\mathbf{K}_r = \mathbf{R}_k^{-1} \mathbf{B}^T \mathbf{P}_c \quad (7.8)$$

subject to (\mathbf{A}, \mathbf{B}) being stabilisable, $\mathbf{R}_k > \mathbf{0}$ (positive definite, for finite control energy), $\mathbf{Q} \geq \mathbf{0}$ (positive semi-definite), and that (\mathbf{Q}, \mathbf{A}) has no *unobservable* modes on the imaginary axis [Fri86].

7.1.2 Partial-nulling Optimal P+I control with output regulation

For the current case of the tilt problem and based upon the ‘nulling’ type control approach, the vehicle is described by the following state-space expression

$$\dot{\mathbf{x}} = \mathbf{A}\mathbf{x} + \mathbf{B}\mathbf{u} \quad (7.9)$$

$$\mathbf{y} = \mathbf{C}\mathbf{x} \quad (7.10)$$

The state vector \mathbf{x} includes the vehicle states $\left[y_v \ \theta_v \ y_b \ \theta_b \ \dot{y}_v \ \dot{\theta}_v \ \dot{y}_b \ \dot{\theta}_b \ \theta_r \right]^T$ and $\mathbf{u} = [\delta_a]$. The plant is subject to constant external disturbances in the input (deterministic and stochastic track) and also an assumed constant reference input r

(which in this case is a zero reference, $r = 0$).

The design is based upon the feedback of the effective cant deficiency for 60% compensation, as in the case of basic ‘nulling’ tilt, θ_{dm} given by

$$\theta'_{dm} = \left(-0.615 \frac{\ddot{y}_{vm}}{g} - 0.385 \theta_{2sr} \right) \quad (7.11)$$

where \ddot{y}_{vm} is the lateral acceleration provided from the body lateral accelerometer (divided by g to convert into cant deficiency angle), and θ_{2sr} is the secondary suspension angle.

For disturbance rejection and reference tracking (which is zero in this case), a new state should be defined and this is the integral of the effective cant deficiency θ_{dm} . This approach will produce an optimal P+I controller [AM90] rather than a Proportional State feedback controller (recall that set point regulation is required as in the classical control case). Hence, the system is augmented to include $\int \theta'_{dm}$ as a state

$$\begin{pmatrix} \dot{\mathbf{x}} \\ \dot{x}' \end{pmatrix} = \begin{pmatrix} \mathbf{A} & 0 \\ C' & 0 \end{pmatrix} \begin{pmatrix} \mathbf{x} \\ x' \end{pmatrix} + \begin{pmatrix} \mathbf{B} \\ 0 \end{pmatrix} \mathbf{u} \quad (7.12)$$

where $x' = \int \theta'_{dm}$ and C' is the selector matrix for integral action and is found from $\theta'_{dm} = C' \mathbf{x}$. The control signal has the form

$$\mathbf{u} = - \begin{pmatrix} K_p & K_i \end{pmatrix} \begin{pmatrix} \mathbf{x} \\ x' \end{pmatrix} \quad (7.13)$$

and for output regulation the quadratic performance index is

$$J = \lim_{T \rightarrow \infty} \frac{1}{T} E \left\{ \int_0^T [\mathbf{y}^T \mathbf{Q}_o \mathbf{y} + \mathbf{u}^T \mathbf{R}_k \mathbf{u}] d\tau \right\} \quad (7.14)$$

where $\mathbf{y} = [(\dot{\theta}_v), \int \theta'_{dm}]$ and $\mathbf{u} = \delta_a$. In this case $Q_o(2, 2)$ is the most important weight concerning the speed of the response ($\int \theta'_{dm}$), while $Q_o(2, 2)$ takes care of unwanted oscillations. The overall concept is depicted in Figure 7.1 (see next page).

The selection of the quadratic weights Q_o, R_k is difficult and mainly depends on the experience of the designer. The translation of specifications into Q_o, R_k is often inaccurate and as a result the initial choices of Q_o, R_k may be inappropriate (usually the final selection is based on a trial and error process). There is an extensive discussion on this matter in [AM90], where a number of insights into choosing the weighting matrices is investigated. In this thesis, the elements in Q_o and R_k were initially chosen to represent

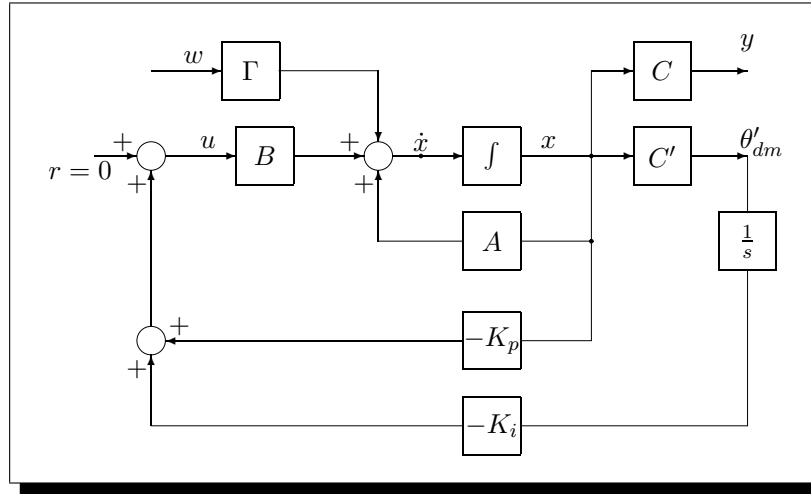


Figure 7.1: Optimal P+I output regulation

the square of the inverse of the expected value, $\frac{1}{(\text{expected value})^2}$, for each parameter. Thus, the controller can be tuned by varying the weighting factors and investigating the performance on both deterministic (the main issue) and straight track (see Chapter 3). The optimal gain is $K_r = R_k^{-1} B^T P_c$, with $K_r = [K_p \quad K_i]$, where P_c is the solution of the following algebraic Riccati equation

$$A^T P_c + P_c A + C^T Q_o C - P_c B R_k^{-1} B^T P_c = 0 \quad (7.15)$$

and matrix C represents $[(\dot{\theta}_v), \int \theta'_{dm}]$. Matlab functions `ARESOLV` (recommended) or `ARE`

- `[P1,P2,LAMP,PERR,WELLPOSED,P] = ARESOLV(A,Q,R,ARETYPE)`
- `P = ARE(A,B,C)`

provide a stable method to calculate P_c . Table 7.1 presents the controller performance for variable $Q_o(6,6)$ and fixed R_k and $Q_o(1,1)$.

Table 7.1: LQ output regulation controller performance, $v = 58(\frac{m}{s})$

R_k	$Q_o(1,1)$	$Q_o(2,2)$	Deterministic				Stochastic	
			$\ddot{y}_{e(rms)}$ (%g)	$\ddot{y}_{e(peak)}$ (%g)	$\dot{\theta}_{ge(rms)}$ (rad/s)	$\dot{\theta}_{ge(peak)}$ (rad/s)	$\ddot{y}_{m(rms)}$ (%g)	degradation (%)
$\frac{1}{0.215^2}$	0.01	1	9.53	23.89	0.038	0.053	3.80	0.6
$\frac{1}{0.215^2}$	0.01	$\frac{1}{0.5^2}$	6.89	21.30	0.035	0.069	3.71	-1.72
$\frac{1}{0.215^2}$	0.01	$\frac{1}{0.1^2}$	2.44	14.16	0.020	0.099	3.20	-15.35
$\frac{1}{0.215^2}$	0.01	$\frac{1}{0.05^2}$	1.85	12.8	0.017	0.103	3.13	-17.10

where $\ddot{y}_e = |\ddot{y}_m - \ddot{y}_{m_i}|$ and $\dot{\theta}_{ge} = |\dot{\theta}_m - \dot{\theta}_{m_i}|$. The degradation in straight track performance is compared to the passive train running at $58(\frac{m}{s})$ and is equal to approximately 3.78%g. As the value of $Q_o(2, 2)$ increases ($\int \theta'_{dm} \rightarrow 0$ faster), which emphasises extra integral action, the system response becomes faster (subject to fixed $R_k, Q_o(1, 1)$).

The selection of the values for the weighting factors is actually based on the deterministic case, however it enables both deterministic and stochastic aspects to be accommodated. Ideally the value of R_k should be as small as possible, however very small values will provide large feedback gains and result in a high closed loop bandwidth. The value of R_k in this case was chosen to be $\frac{1}{0.215^2}$, i.e. control input is expected to provide up to $0.215rad$ angle (indicated in the basic control cases where the ARB needs to overcome extra suspension forces). The weighting of the body roll velocity $Q_o(1, 1)$ is very useful in the stochastic case where it constrains the roll movement of body due to the irregularities input, its value was chosen $\frac{1}{5^2}$. High $Q_o(1, 1)$ degrades the transition performance, because there is no freedom for the roll velocity to increase quickly up to the required value during curve transition. Finally, the weight on the integral of the effective cant deficiency was set to $\frac{1}{0.1^2}$. The corresponding quadratic performance index is then

$$J = \lim_{T \rightarrow \infty} \frac{1}{T} E \left\{ \int_0^T \left(\frac{1}{5^2} \dot{\theta}_v + \frac{1}{0.1^2} \int \theta'_{dm} + \frac{1}{0.215^2} u^2 \right) d\tau \right\} \quad (7.16)$$

and the optimal gain for this configuration was found to be

$$K_r = [0.38 \ 0.07 \ -0.1 \ -0.04 \ 0.23 \ 0.09 \ -0.0003 \ 0.002 \ 0.07 \ 2.15] \quad (7.17)$$

The controller assessment for the current design is presented in Table 7.2, while the simulation results are shown in Figure 7.2 and Figure 7.3 in the next pages.

The controller is fast enough to accommodate all stochastic long wavelengths (low frequency), thus the improvement in ride quality. However, faster controller designs will unavoidably degrade curve transition performance because of both increased jerk and roll velocity levels. Extra regulated outputs were also considered such as body lateral velocity, body-bogie lateral rate, body roll angle, however they did not offer substantial improvement in controller design. Note that the body roll angle is inherently constrained by weighting its rate.

In the case where all required system states are not available for feedback, which may be difficult or even impossible to measure, a *Kalman filter* may be combined with the optimal controller to provide the necessary state estimates for state feedback [Fri86]

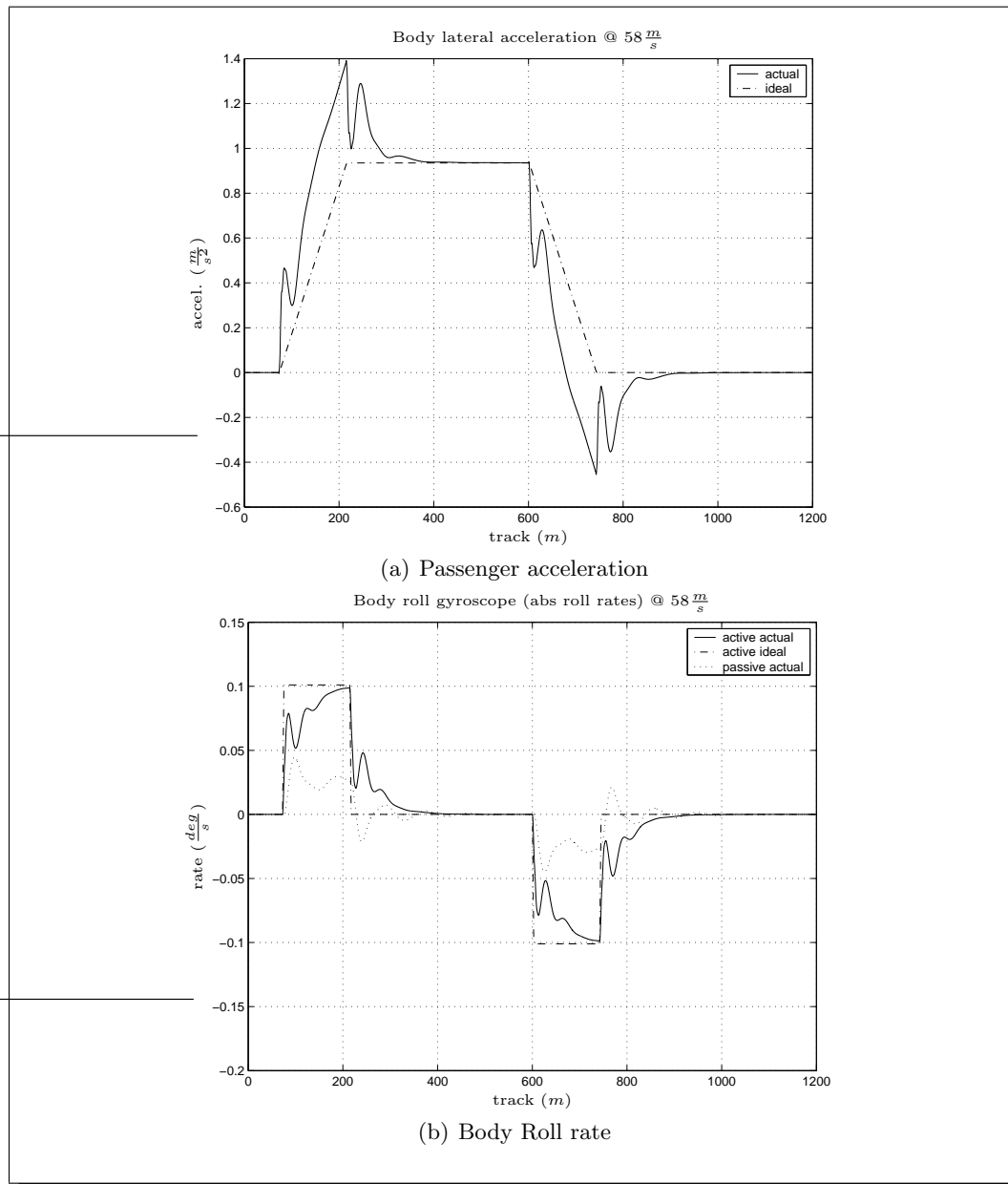


Figure 7.2: LQR with integral action transition performance, set 1

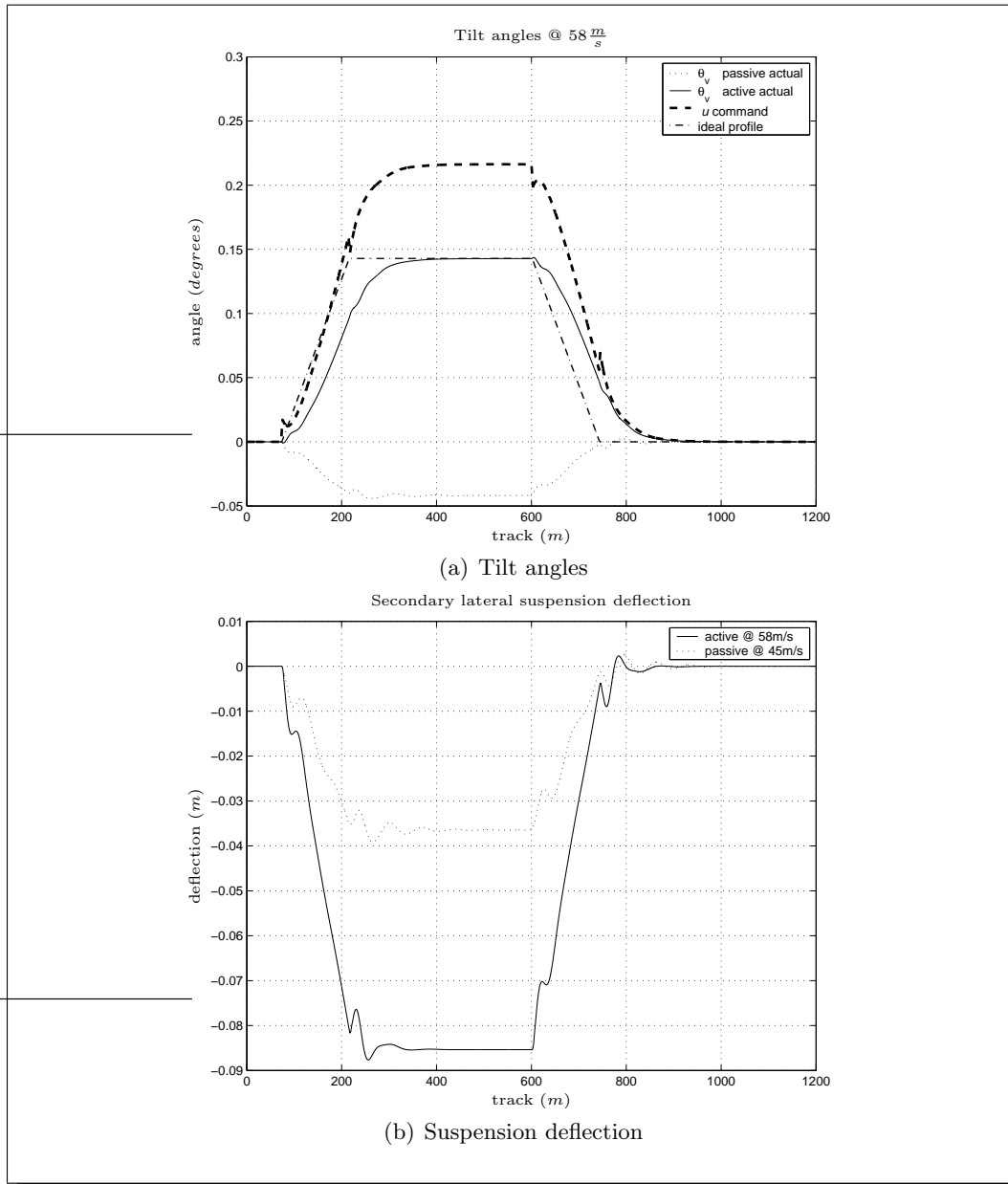
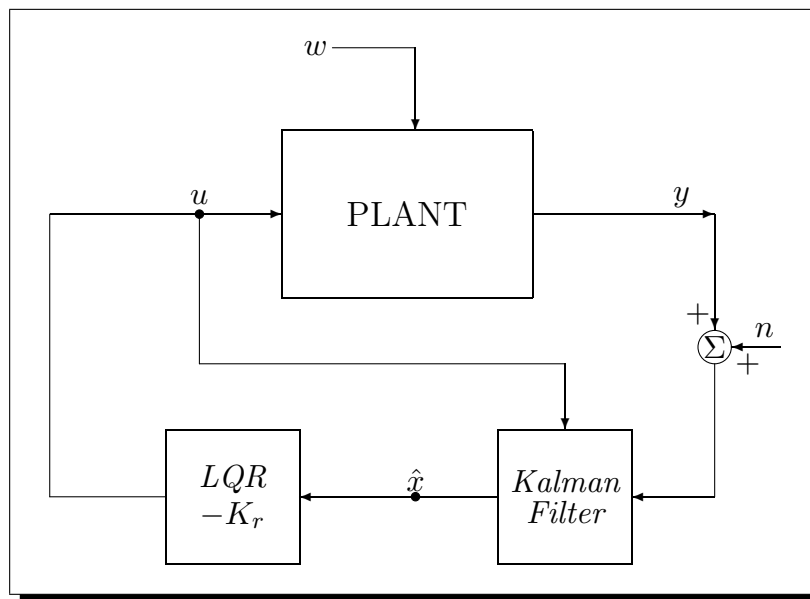


Figure 7.3: LQR with integral action transition performance, set 2

Table 7.2: (LQR) optimal P+I control assessment @ 58(m/s)

DETERMINISTIC		
Lateral accel. (actual vs ideal)	- steady-state	9.53 (%g)
	- R.M.S. deviation error	2.44 (%g)
	- peak value	14.18 (%g)
Roll gyroscope	- R.M.S. deviation	0.020 (rad/s)
	- peak value	0.099 (rad/s)
P_{CT} (P-factor)	- peak jerk level	7.16 (%g/s)
	- standing	53.75 (% of passengers)
	- seated	15.83 (% of passengers)
STOCHASTIC		
Passenger comfort	- R.M.S. passive (equiv.)	3.78 (%g)
	- R.M.S. active	3.19 (%g)
	- degradation	-15.66 (%)

(this approach produces very similar results to the LQR scheme). This is known as the *linear quadratic gaussian* or *LQG* problem, shown in Figure 7.4, and its solution is prescribed by the *separation principle* (or ‘certainty equivalence’ principle) [Mac89, SP00]¹.

**Figure 7.4:** Plant with Estimator (Kalman filter)

¹The separation principle reduces the LQG problem into two sub-problems: (i) find the state estimates and (ii) use these estimates for state feedback and solve the LQR problem. LQG controllers do not guarantee the robustness and performance properties of their LQR equivalent, however in certain cases there are procedures to overcome such difficulties i.e. *Loop Transfer Recovery* [Mac89, SP00].

7.2 Model Based Estimation ‘Nulling’ Control Incorporating a Kalman Filter

In the basic ‘nulling’ control scheme it was seen that the suspension dynamic interactions in the body cant deficiency constrained the controller design. This section proposes an alternative way to obtain the body cant deficiency unaffected by suspension dynamic interactions, in order to provide a more effective feedback signal for local tilt control.

7.2.1 Kalman Filter Preliminaries

Consider the following dynamic process

$$\dot{x} = Ax + Bu + \Gamma w \quad (7.18)$$

with known input u and output measurements given by

$$y = Cx + \nu \quad (7.19)$$

where w (process noise) and ν (measurement noise) are usually assumed to be uncorrelated white noise processes having known constant spectral density matrices W , V respectively. Their covariances are expressed by

$$E \{w(t)w(\tau)^T\} = W\delta(t - \tau) \quad (7.20)$$

$$E \{\nu(t)\nu(\tau)^T\} = V\delta(t - \tau) \quad (7.21)$$

$$E \{w(t)\nu(\tau)^T\} = 0, \quad E \{\nu(t)w(\tau)^T\} = 0 \quad (7.22)$$

where E defines the expectation operator and $\delta(t - \tau)$ the *delta function*.

The Kalman filter [Kal60, BS89] has the structure of an ordinary observer (state-estimator), shown in Figure 7.5, which is expressed by the following mathematical model

$$\dot{\hat{x}} = A\hat{x} + Bu + K_f(y - \hat{y}) \stackrel{(\hat{y}=C\hat{x})}{=} A\hat{x} + Bu + K_f(y - C\hat{x}) \quad (7.23)$$

$$\hat{y} = C\hat{x} \quad (7.24)$$

where \mathbf{K}_f is the optimally chosen observer gain matrix², minimising $E \{[x - \hat{x}]^T [x - \hat{x}]\}$, and given by

$$\mathbf{K}_f = \mathbf{P}_f \mathbf{C}^T \mathbf{V}^{-1} \quad (7.25)$$

²that is why many refer to Kalman filter as the *optimal estimator (observer)*.

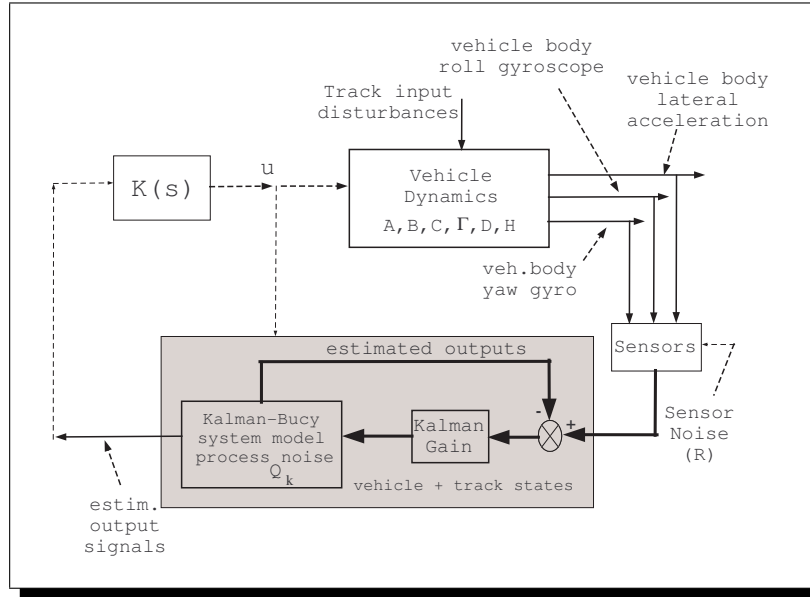


Figure 7.6: Model-based estimation control scheme

A Kalman-Bucy filter can be designed based upon (7.28) combined with the output equation which represents the measurements.

$$\dot{x} = Ax + Bu + \Gamma w \quad (7.28)$$

However, the curving acceleration feedback is associated with signals of the disturbance vector w . These signals are related to the track, on which the vehicle is travelling, for which no prior knowledge exists and also is not practical to measure such track parameters. Hence, the system state space should be re-formulated for the design of the Kalman-Bucy filter in order to treat w as states rather than disturbance inputs shown in equation (7.29), [HG99, SCW94].

$$\dot{x}_k = A_k x_k + B_k u + \Gamma_k w_k \quad (7.29)$$

where

$$x_k = \begin{bmatrix} x & \tilde{w} \end{bmatrix}^T \quad (7.30)$$

The output equation for the sensors is then given by:

$$y_k = C_k x_k + D_k u + \nu \quad (7.31)$$

where C_k and D_k are based upon the relative rows of A_k and B_k .

The selection of the extra states \tilde{w} depends on the application, the required feedback signals and the selected output measurements. In the current case of ‘*true*’ cant deficiency estimate θ_{td} , the application is mainly connected with the performance on design track, thus signals θ_o , R^{-1} should be incorporated as extra states. It has been found that only *three body measurements* were necessary for the Kalman filter design: (i) *body lateral accelerometer* (for cant deficiency information), (ii) *body roll gyroscope* (cant information) and (iii) *yaw gyroscope* (extra information about curvature). The body roll gyroscope measures absolute roll rate ($\dot{\theta}_v + \dot{\theta}_o$), thus $\dot{\theta}_o$ must be also included in the state estimates, making a total number of three extra states $\tilde{w} = [\theta_o \ \dot{\theta}_o \ R^{-1}]^T$. Hence, the re-formulated state vector becomes

$$x_k = \begin{bmatrix} x & \tilde{w} \end{bmatrix}^T \quad (7.32)$$

$$= \begin{bmatrix} y_v & \theta_v & y_b & \theta_b & \dot{y}_v & \dot{\theta}_v & \dot{y}_b & \dot{\theta}_b & \theta_r & \theta_o & \dot{\theta}_o & R^{-1} \end{bmatrix}^T \quad (7.33)$$

while,

$$w_k = \begin{bmatrix} \dot{R}^{-1} & \ddot{\theta}_o \end{bmatrix}^T \quad (7.34)$$

$$A_k = \begin{bmatrix} A & \tilde{\Gamma} \\ 0 & \Delta_{LP} \end{bmatrix} \quad B_k = \begin{bmatrix} B & 0_{3 \times 1} \end{bmatrix}^T \quad (7.35)$$

$$\Gamma_k = \begin{bmatrix} \Gamma_{w_k} & (0 \ 0) & (0 \ 1) & (1 \ 0) \end{bmatrix}^T \quad (7.36)$$

Appropriate low-pass filters were applied to the extra (track) estimates in the re-formulated matrix A_k , such that

$$\Delta_{LP} = \begin{bmatrix} 0 & 1 & 0 \\ -\epsilon^2 & -2\epsilon & 0 \\ 0 & 0 & -\epsilon \end{bmatrix} \quad (7.37)$$

defining, $\hat{\theta}_o = \frac{1}{(s+\epsilon)^2} \ddot{\theta}_o$ and $\hat{R}^{-1} = \frac{1}{(s+\epsilon)} \dot{R}^{-1}$, where $\epsilon = 2\pi \times \text{low-pass cut-off frequency}$. In reality ϵ should be set to zero, which corresponds to pure integration of the process ‘noise’ input as one would expect. However, a simple analysis reveals that the pair (C, A) is *detectable iff* $\epsilon \neq 0$. In this design, the value for ϵ was set to $0.001(\frac{\text{rads}}{\text{s}})$, corresponding to $2\pi \times (0.00016\text{Hz})$, and imposes minimal effects to the estimation results (see Figure 7.7). It has to be noted that the Kalman filter is principally a stochastic device, albeit the approach has been to develop the filter based upon the deterministic criteria. Any stochastic track inputs, i.e. signals related to track irregularities, were

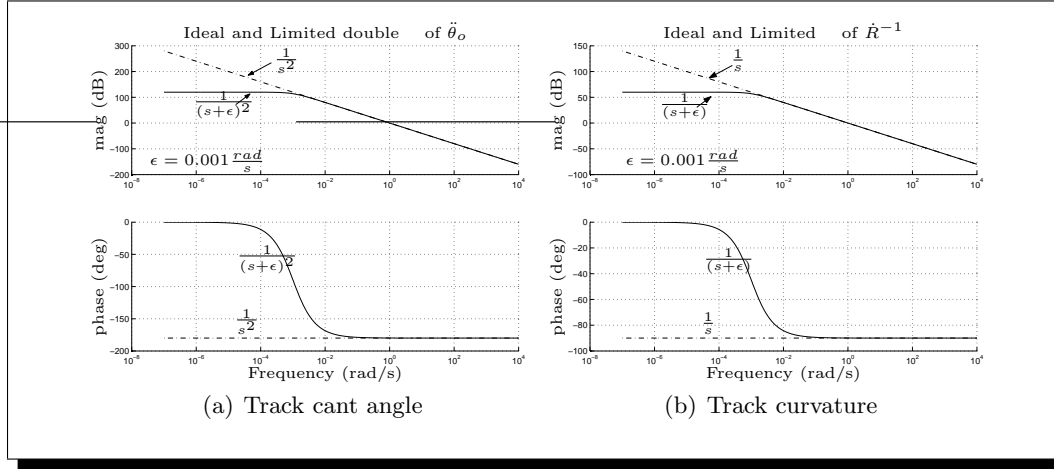


Figure 7.7: LQR with integral action transition performance

neglected in the filter design so it is expected that the filter would reject their effects³. Ultimately the filter design should be effective for both deterministic and stochastic inputs.

The Kalman-Bucy filter can be now designed off-line using Equations (7.29) and (7.31), while the state estimates can be calculated by solving the following differential equation

$$\dot{\hat{x}} = A_k \hat{x} + B_k u + K_f (y_k - C_k \hat{x} - D_k u) \quad (7.38)$$

where \hat{x} is the vector of the re-formulated state estimates and K_f is the Kalman-Bucy filter gain matrix which is designed off-line [BS89, Fri86]. The performance of the Kalman-Bucy filter can be thoroughly assessed by tuning the covariance matrix Q_k for the track process noises where $Q_k = \text{diag}(Q_{\ddot{\theta}_o}, Q_{\dot{R}^{-1}})$. The sensor noise levels are represented by vector ν and characterised by a covariance matrix R_{kf} .

The design aim is mainly connected to the deterministic performance of the tilt controller and the following procedure of choosing Q_{kf}, R_{kf} is used as a ‘rule-of-thumb’.

In this design, R_{kf} is a 3×3 diagonal matrix (cross-correlation terms are set to zero)

$$R_{kf} = \begin{bmatrix} R_{kf}(1,1) & 0 & 0 \\ 0 & R_{kf}(2,2) & 0 \\ 0 & 0 & R_{kf}(3,3) \end{bmatrix} \quad (7.39)$$

³In any case, it is extremely difficult to obtain correct estimates for the stochastic track signals based only upon body mounted sensors (secondary suspensions act as a low-pass filter). Additional *bogie-mounted* and *wheelset-mounted* sensors would provide information over a greater range of frequencies necessary for track irregularities estimation, however this approach is not a part of this thesis.

where $R_{kf}(1,1)$ is the covariance of the body lateral accelerometer sensor, $R_{kf}(2,2)$ the covariance of the body roll gyroscope sensor, and $R_{kf}(3,3)$ the covariance of the body yaw gyroscope sensor. The value for each of the covariances is set to

1% of the expected maximum value taken as, 3 times the true R.M.S. value of the sensor output signal on straight track with irregularities, plus the peak value on the pure curved track

which corresponds to high quality (realistic) sensors currently used in tilting trains. In reality, any detailed design would have a real sensor with actual noise values from the manufacturer, but the thesis uses a typical (sensible) level in the absence of detailed design information. Reducing the measurement noise will obviously improve the accuracy of the filter.

The values for matrix Q_{kf} were set to

1% of the total area of the process input signal during one transition on design track

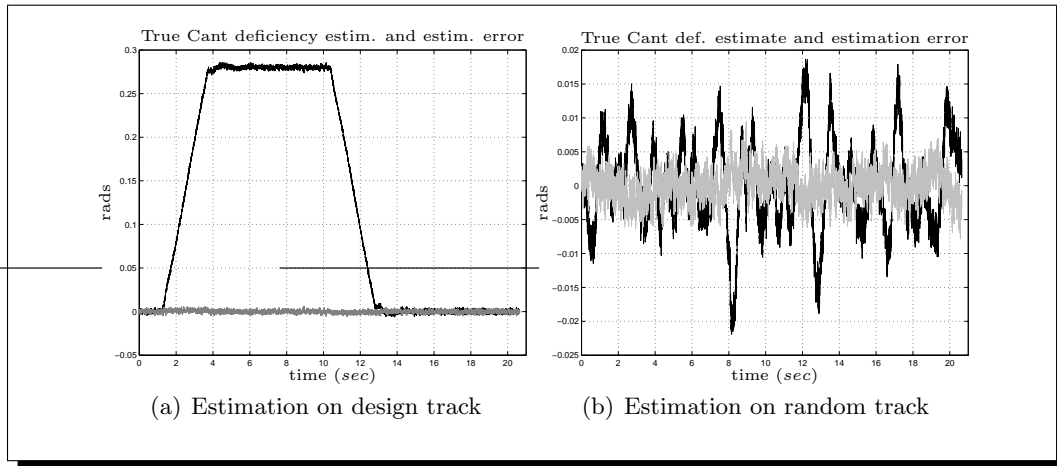


Figure 7.8: ‘True’ cant deficiency estimates, estimate (dark), error (grey)

Figure 7.8 illustrates the estimator performance for the ‘true’ cant deficiency estimate (7.27), at a speed of $58m/s$ for the above values of Q_{kf} , R_{kf} , which are equal to

$$R_{kf} = \begin{bmatrix} 1.6e-3 & 0 & 0 \\ 0 & 1.883e-6 & 0 \\ 0 & 0 & 1e-6 \end{bmatrix}, \quad Q_{kf} = \begin{bmatrix} 1e-5 & 0 \\ 0 & 8.5e-4 \end{bmatrix} \quad (7.40)$$

for both deterministic and stochastic track inputs, subject to sensor noise corruption. The Kalman gain obtained for the above configuration was

$$K_f = \begin{bmatrix} -0.18 & -3.033 & -0.23 \\ -0.08 & -2.734 & 0.033 \\ 0.0014 & 0.103 & -0.18 \\ -0.034 & -1.11 & 0.027 \\ -1.074 & 5.90 & -56.99 \\ -0.41 & 0.633 & -0.14 \\ 0.062 & -0.207 & -32.60 \\ -0.166 & 0.21 & 2.24 \\ -0.061 & -2.20 & 0.037 \\ 0.052 & 4.33 & -0.019 \\ 0.433 & 17.02 & -0.18 \\ 0.001 & -0.003 & 3.16 \end{bmatrix} \quad (7.41)$$

The results obtained from the estimator are very close to the true values, and the estimation error is mainly due to the sensor noise levels. An extra degree of error associated with the unknown information of the track signals was also expected especially for the stochastic case. This configuration provided the best estimation results and is used throughout this part of work. Note that the RMS value of the estimation error in the deterministic case was kept at around 0.0018(rads), while the RMS estimation error in the stochastic case was 0.0022(rads) (based upon the true cant deficiency (7.27)).

Trade-off sample curves can be obtained by varying the covariance of the deterministic $Q_{kf_{11}} = cov(\frac{1}{R})$ and $Q_{kf_{22}} = cov(\ddot{\theta}_o)$ as shown in Figure 7.9 (the simulation involves all three sensors including sensor noise with R_{kf} fixed). The selected range for $Q_{kf_{11}}, Q_{kf_{22}}$ was for $Q_{kf_{11}} = [0.84, 0.084, 8.4E-3, 8.4E-4, 8.4E-5, 8.4E-6, 8.4E-7, 8.4E-8, 8.4E-9]$ and for $Q_{kf_{22}} = [2E-6, 2E-7, 2E-8, 2E-9]$. It can be seen from the figure that with $Q_{kf_{11}}$ fixed decreasing $Q_{kf_{22}}$ eventually will degrade the maximum error on design track, although this degradation is less emphasised as $Q_{kf_{11}}$ decreases (due to cancellation between curvature and cant information). In terms of the R.M.S. value on stochastic initially there is associated degradation, however this improves as $Q_{kf_{22}}$ decreases (at high values of $Q_{kf_{11}}$ note that the R.M.S error stochastic is approximately fixed). High Q_{kf} means that much information for the states is available and the estimator will provide good results in the design track, however noise will penetrate the system and as a result it degrades the stochastic results. As Q_{kf} decreases then information especially for the design track signal (cant, curvature) is less effective which unavoidably degrades the deterministic estimation error, albeit improving or at least stabilising the stochastic R.M.S. error due to less noise in the system. Note that the trade-off

between the deterministic and stochastic results is not straightforward, thus extra care is required in selecting the best weights. It seems that both deterministic and stochastic errors are improved for high Q_{kf} , owing to cancellations between the curvature and cant information due to the deterministic design of the filter. Moreover, the maximum values of other signals exceed the desired limits - for high Q_{kf} - due to the excess of sensor noise.

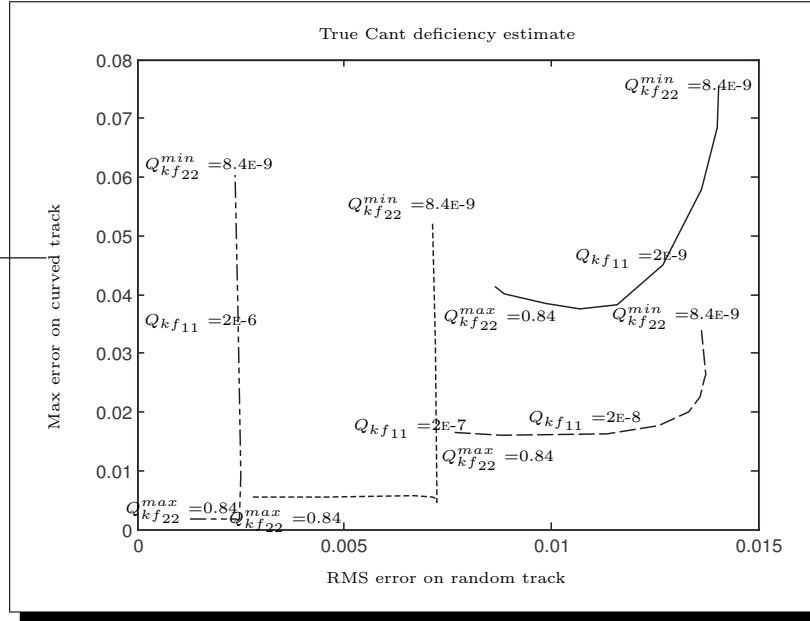


Figure 7.9: Stochastic-Deterministic weighting curves for KBF

Remark 7.3.1. Adding more sensors will always help the estimation process, however the system design complexity and cost increases. The above choice of three measurements (body accelerometer, roll gyro, yaw gyro) used in the estimation procedure gave a very satisfactory performance for both design and random track. The filter succeeds in rejecting the sensor noise, while keeps the extra errors in the stochastic case estimation sufficiently low. Trials with fewer sensors, i.e. combination of body lateral accelerometer and roll gyroscope or only lateral accelerometer, produced poorer performance due to the loss of the curvature information (it was necessary to increase Q_{kf} thus allowing more sensor noise to enter the system). Finally this Kalman filter design can be easily used in conjunction with the LQR optimal controller for LQG applications⁴.

⁴The results are approximately identical to the LQR application and are not included in the thesis.

7.3.1 Tilt Controller Design upon Model Based Estimator

The next step is to design a classical controller based upon the estimated ‘true’ cant deficiency to provide partial tilt as in the basic tilt control cases. The feedback signal for 60% *partial tilt* is given by (for negative feedback application)

$$\theta'_{td} = -0.6 \frac{v^2}{gR} + (0.6\theta_o + \hat{\theta}_t) \quad (7.42)$$

where θ_t being the tilt angle (actually the body roll angle estimate).

The scheme incorporates a $P+I+D$ controller given in (7.43) (with approximate derivative action and also a first order filter in series to attenuate high frequencies due to the derivative portion)

$$K_{PID}(s) = \frac{((k_d + k_p/N_d)s^2 + (k_p + k_i/N_d)s + k_i)}{(1/N_d)s^2 + s} \times \frac{w_c}{s + w_c} \quad (7.43)$$

where the parameters are set to: $k_d = .25, k_i = 3.33, k_p = 1, N = 100, w_c = 2\pi \cdot 25(\frac{rad}{s})$. The schematic diagram of the controller structure and the relative frequency response are shown in Figure 7.10.

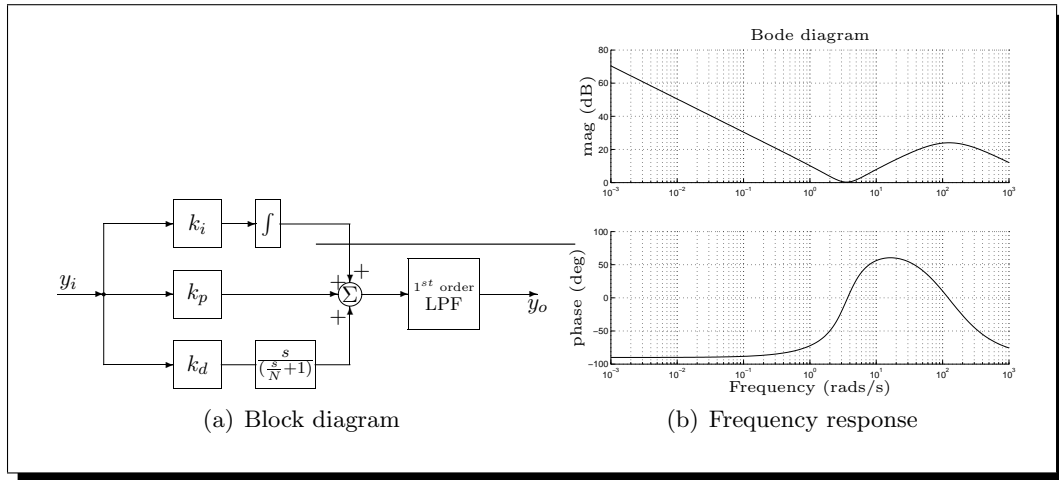


Figure 7.10: P+I+D with approximate derivative plus series LPF

Figure 7.11(a) on page 100 illustrates the frequency response of the designed open-loop system including the Kalman filter with the P+I+D type controller. It can be easily seen from the figure that the new feedback signal resulted in a much easier controller design compared to the previous basic control schemes. The dynamic complexity is still preserved via the body roll/tilt angle being taken in account by the control system, while the non-minimum phase characteristic has disappeared. The bandwidth of the

closed loop system has improved considerably compared to the basic nulling approach, as seen in Figure 7.11(b) page 100.

The time domain simulation results shown in Figures 7.12 and 7.13 on page 101 and 102 respectively, illustrate the effectiveness of the model based estimation control scheme on curved track. The system responds fast on curve and approaches the performance of a ‘precedence-type’ approach (precedence time = zero), see Table 7.3.

Table 7.3: Model-based estimation scheme assessment @ 58(m/s) - (PID approach)

DETERMINISTIC		
Lateral accel. (actual vs ideal)	- steady-state	9.53 (%g)
	- R.M.S. deviation error	1.62 (%g)
	- peak value	11.89 (%g)
Roll gyroscope	- R.M.S. deviation	0.014 (rad/s)
	- peak value	0.102 (rad/s)
P_{CT} (P-factor)	- peak jerk level	6.38 (%g/s)
	- standing	45.54 (% of passengers)
	- seated	12.74 (% of passengers)
STOCHASTIC		
Passenger comfort	- R.M.S. passive (equiv.)	3.778 (%g)
	- R.M.S. active	3.743 (%g)
	- degradation	-0.93 (%)

It also keeps the stochastic ride quality within acceptable values as shown in Table 7.3, with small errors introduced due to the estimation process as expected. Unfortunately even in this case the oscillations due to the lateral suspension effects still exist. This is mainly due to the coupling through the body roll, which the control system takes into account. Noticeably in the estimation case with two sensors (body accelerometer and roll gyroscope) in the Kalman filter design, the process cancels out some of the dynamic oscillations due to the estimation cancellations between $\frac{v^2}{gR}$ and θ_o in the ‘true’ cant deficiency expression.

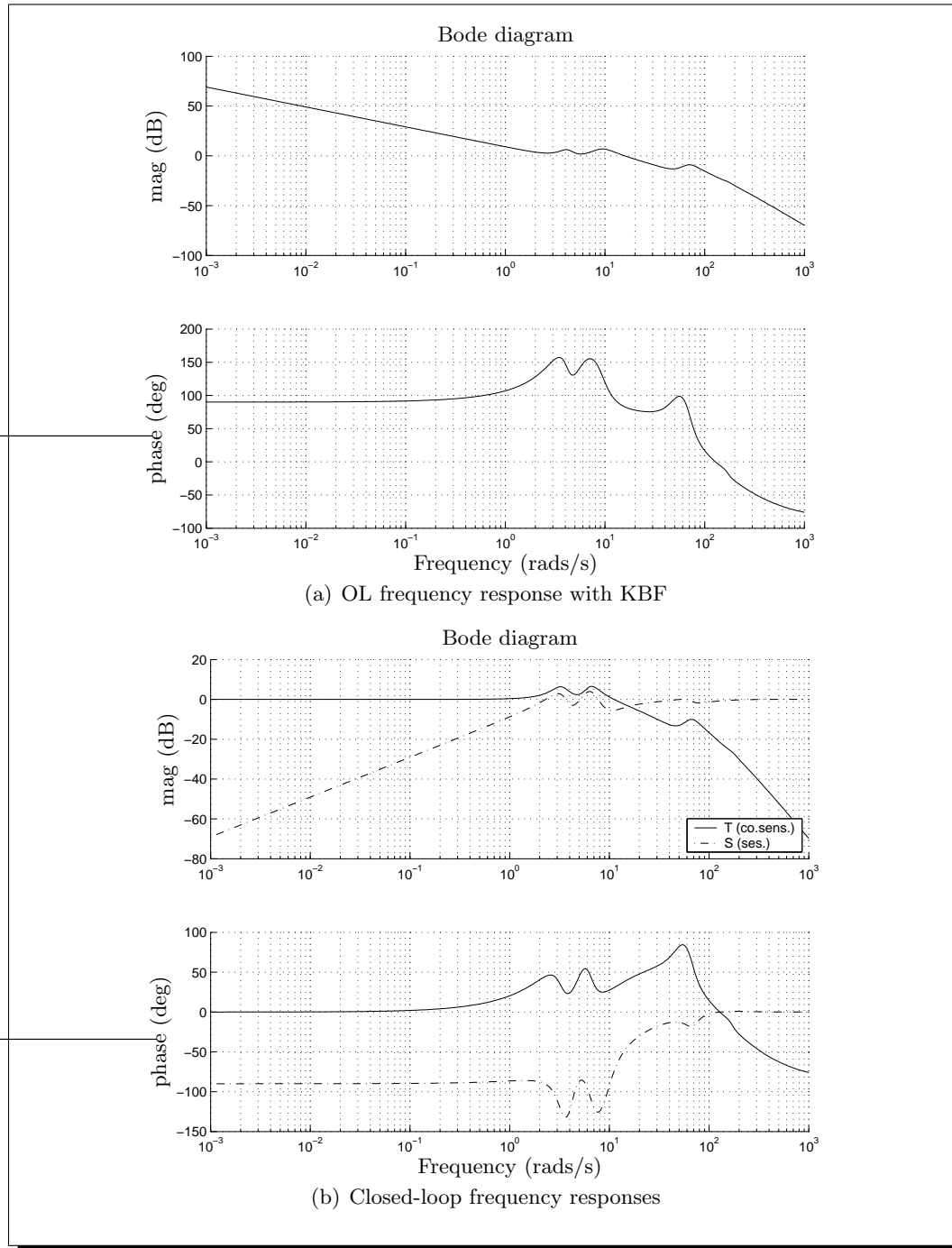


Figure 7.11: Frequency response analysis of MBE control designed system for partial 'true' cant deficiency

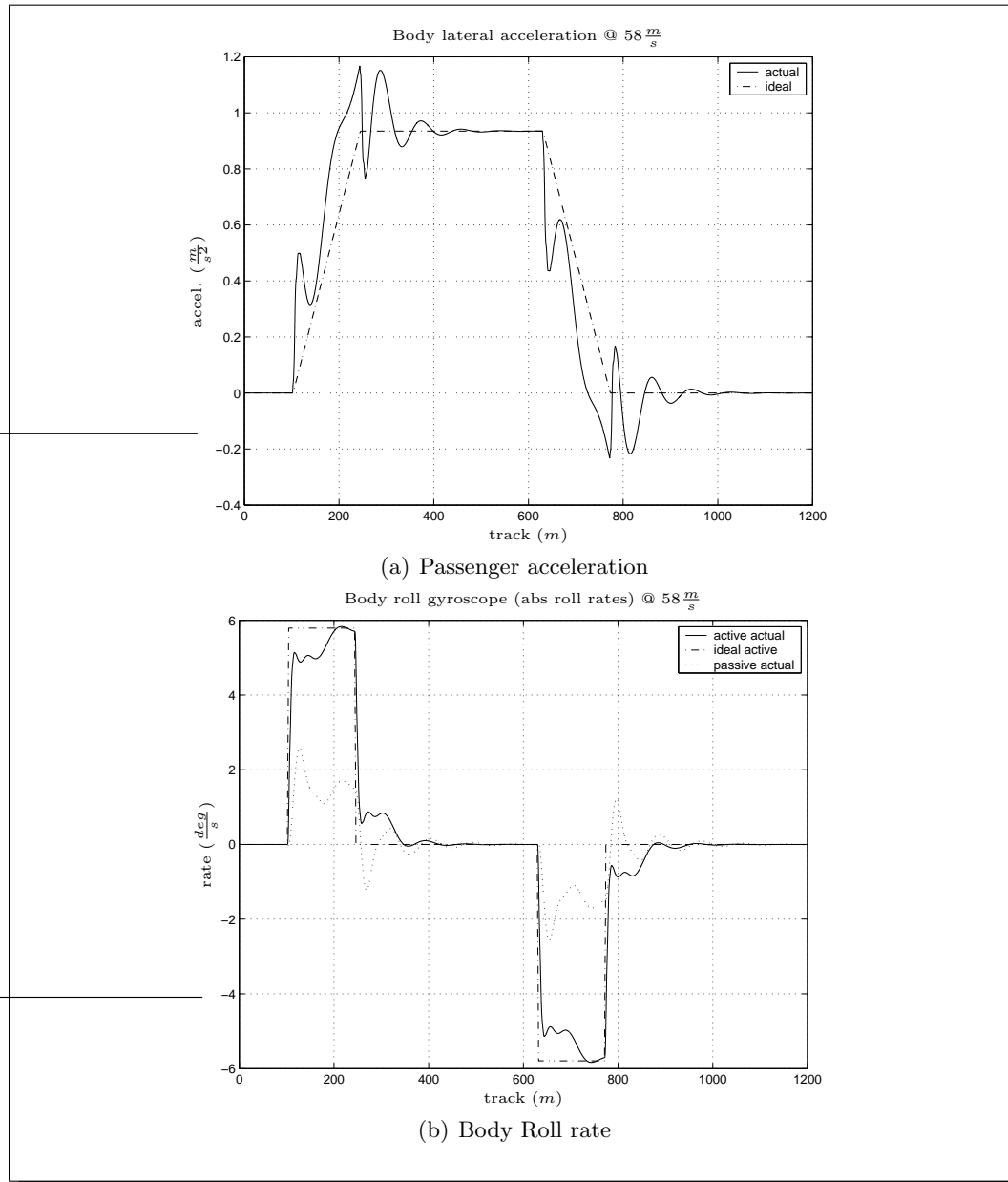


Figure 7.12: MBE 'nulling' approach, curved track simulation results, set 1

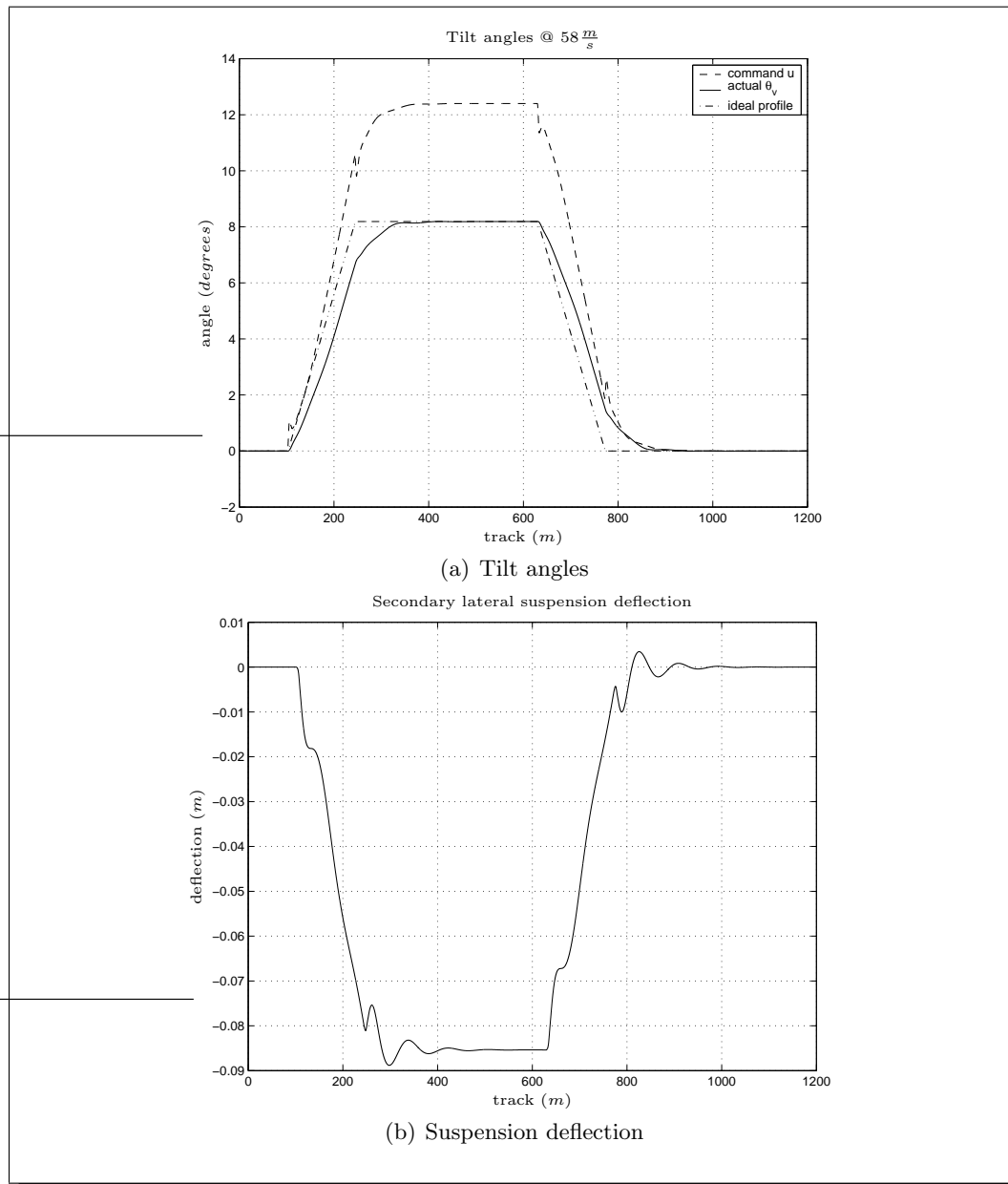


Figure 7.13: MBE 'nulling' approach, curved track simulation results, set 2

7.4 Robust \mathcal{H}_∞ -based Control Schemes

This section considers the application of robust \mathcal{H}_∞ -based techniques for 'nulling'-type tilt control. Robust controllers are designed for the so called nominal model, although yield acceptable performance for a certain plant uncertainty. The section starts with a brief overview of \mathcal{H}_∞ and introduces some basic notation. The use of robust control design is introduced via a mixed sensitivity \mathcal{H}_∞ control approach. Next a multi-objective $\mathcal{H}_\infty/\mathcal{H}_2$ LMI-based control design is proposed which offers a significant improvement in tilt performance. The design is based upon using only vehicle body measurements. The concept of uncertainty is not considered in many details in this thesis, however the robust controllers are assessed using a provided uncertainty set.

7.4.1 Preliminaries

Researchers began shifting towards \mathcal{H}_∞ optimisation for robust control during the 1980s, the reason being the weakness of LQG (Linear Quadratic Gaussian) control to deal with good robustness properties and also its interpretation of uncertain disturbances based upon white noise (which is often unrealistic). Early concepts of \mathcal{H}_∞ optimisation were encountered in Helton [Hel76], however the most influential work was that of Zames [Zam81]. Owing to its frequency-domain nature and the systematic incorporation of uncertainty, \mathcal{H}_∞ has become a widely used method in controller design since the 1990s. Although theory behind \mathcal{H}_∞ is now established, very few practical implementations have been reported.

Initial applications on \mathcal{H}_∞ have been considered in the SISO case, and later extended in the multivariable case [SP00]. The most useful designs however resulted from *mixed type* \mathcal{H}_∞ problems such as mixed sensitivity approaches [Cas93]. However, all designs were concentrated on a complete design methodology and many criticised this approach by referring to the complexity of selecting the frequency-dependent weights especially in the overlapping frequency areas. Hence, McFarlane and Glover [MG90] proposed a \mathcal{H}_∞ approach for loop shaping which is purely based upon providing robust stability within a classical open loop design.

Recent developments incorporated the use of Linear Matrix inequalities in the \mathcal{H}_∞ framework [G⁺94] which can provide effective solutions especially in the case of multi-objective design problems. Unavoidably the computation required for designing \mathcal{H}_∞ controllers can be intense but there is available software which is used for this purpose such as `Matlab` (The Mathworks, Inc.) and `Scilab` (INRIA, France).

7.4.2 Basic Notation

Before proceeding to the main design considerations, a brief introduction to some basic notation necessary for implementing the controllers is presented.

A continuous time, linear time invariant, state space system is given by

$$\dot{x}(t) = Ax(t) + Bu(t) \quad (7.44)$$

$$y(t) = Cx(t) + Du(t) \quad (7.45)$$

where $A \in \Re^{n \times n}$, $B \in \Re^{n \times m}$, $C \in \Re^{p \times n}$ and $D \in \Re^{p \times m}$. The above state space system is characterised by the following transfer function with dimension $p \times n$

$$G(s) = C(sI - A)^{-1}B + D \quad (7.46)$$

This thesis adopts the following conventional state-space representation to represent $G(s)$

$$G(s) \stackrel{s}{=} \left[\begin{array}{c|c} A & B \\ \hline C & D \end{array} \right] \quad (7.47)$$

Note also that the complex conjugate of $G(s)$ is given by

$$G^*(s) = G^T(-s) \stackrel{s}{=} \left[\begin{array}{c|c} -A^T & -B^T \\ \hline C^T & D^T \end{array} \right] \quad (7.48)$$

and if $G(s)G^*(s) = I = G^*(s)G(s)$ for all $s \in j\Re$, then $G(s)$ is said to be *all-pass*.

Finally if matrix D is invertible, then $G^{-1}(s)$ is given by⁵

$$G^{-1}(s) \stackrel{s}{=} \left[\begin{array}{c|c} A - BD^{-1}C & BD^{-1} \\ \hline -D^{-1}C & D^{-1} \end{array} \right] \quad (7.49)$$

• Frequency Domain Spaces and Norms

This part introduces the meaning of frequency domain spaces and norms of real rational, matrix valued, transfer functions. For a more comprehensive study the reader is referred to McFarlane and Glover [MG90] and also Zhou and Doyle [ZD98].

Let \mathcal{R} denote the space of all real rational transfer function matrices. The $\mathcal{L}_2/\mathcal{H}_2$ norm of $G(s)$ is given by

$$\|G\|_2 \triangleq \sqrt{\frac{1}{2\pi} \int_{-\infty}^{\infty} \text{tr}(G^*(j\omega)G(j\omega)) d\omega} \quad (7.50)$$

⁵Using the **matrix inversion lemma**:

$$(A_1 + A_2A_3A_4)^{-1} = A_1^{-1} - A_1^{-1}A_2(A_4A_1^{-1}A_2 + A_3^{-1})^{-1}A_4A_1^{-1}.$$

which is used to define the following spaces

- (i). \mathcal{RL}_2 refers to the space of all real rational transfer function matrices with no poles on the imaginary axis and is characterised by a finite \mathcal{L}_2 norm.
- (ii). \mathcal{RH}_2 defines the space of all transfer function matrices in \mathcal{RL}_2 with no poles in $Re(s) > 0$.

The $\mathcal{L}_\infty/\mathcal{H}_\infty$ norm of $G(s)$ is given by

$$\|G\|_\infty \triangleq \sup_{\omega \in \Re} \bar{\sigma}[G(j\omega)] \quad (7.51)$$

and

- (i). \mathcal{RL}_∞ refers to the space of all real rational transfer function matrices with no poles on the imaginary axis (with finite \mathcal{L}_∞ norm).
- (ii). \mathcal{RH}_∞ defines the space of all transfer function matrices in \mathcal{RL}_∞ with no poles in $Re(s) > 0$.

Also, the \mathcal{H}_∞ norm of a stable transfer function $G(s)$ is its largest input/output RMS gain

$$\|G\|_\infty \triangleq \sup_{\substack{u \in \mathcal{L}_2 \\ u \neq 0}} \frac{\|y\|_{\mathcal{L}_2}}{\|u\|_{\mathcal{L}_2}} \quad (7.52)$$

where \mathcal{L}_2 is the space of signals having finite energy and y is the output of the system G for a given input u . Thus, for any input u of unit energy, the output energy in y is bounded by the \mathcal{H}_∞ norm of $G(s)$.

• Linear Fractional Transformations

The basic concept of *Linear Fractional Transformations* is outlined in this section. *Linear Fractional Transformations* (LFT) are frequently used in the area of \mathcal{H}_∞ optimisation as well as in other areas of control theory. They do represent a means of standardising a wide variety of feedback arrangements [MG90, ZD98].

Let $P(s)$ define a transfer function matrix with the following state-space representation

$$P(s) \stackrel{s}{=} \left[\begin{array}{c|cc} A & B_1 & B_2 \\ \hline C_1 & D_{11} & D_{12} \\ C_2 & D_{21} & D_{22} \end{array} \right] \quad (7.53)$$

which can be also partitioned as

$$P(s) \stackrel{s}{=} \left[\begin{array}{c|c} P_{11} & P_{12} \\ \hline P_{21} & P_{22} \end{array} \right] \quad (7.54)$$

where

$$P_{ij}(s) = C_i(sI - A)^{-1}B_j + D_{ij} \quad (7.55)$$

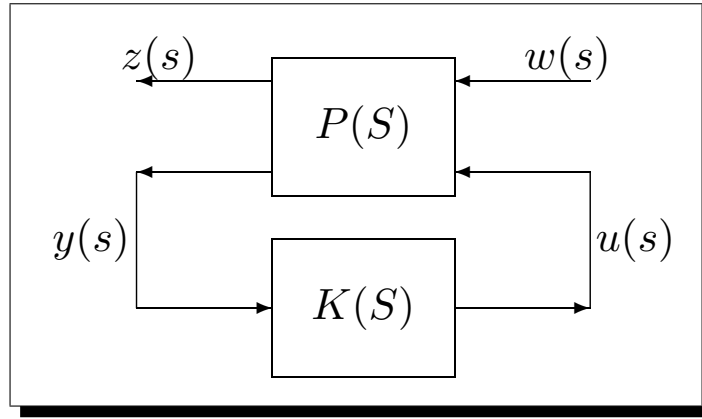


Figure 7.14: The Generalised Regulator Configuration

Referring to Figure 7.14, which presents the generalised regulator configuration, the (lower) linear fractional transformation⁶ of P and K is given by

$$\mathcal{F}_L(P, K) \triangleq P_{11} + P_{12}K(I - P_{22}K)^{-1}P_{21} \quad (7.56)$$

for $\det(I - P_{22}K) \neq 0$. $P(s)$ represents the “generalised plant”, consisting of the nominal model $G(s)$ combined with all frequency weightings appropriately chosen to shift the emphasis with frequency between different design objectives. In addition, the signals are: u the control variables, w the exogenous inputs such as disturbances w_d and commands r , y the measured variables and z the regulated outputs, i.e. the signals need to minimise to meet the design objectives. In fact $\mathcal{F}_L(P, K)$ represents the transfer function between w and z in Figure 7.14, i.e.

$$z(s) = [P_{11} + P_{12}K(I - P_{22}K)^{-1}P_{21}] w(s) \quad (7.57)$$

\mathcal{H}_∞ and \mathcal{H}_2 control implies the minimisation of the \mathcal{H}_∞ -norm and the \mathcal{H}_2 -norm of $\mathcal{F}_L(P, K)$ respectively, and this is considered in the following sections.

⁶There is also the concept of the upper LFT which is employed in representing uncertainties in a system. This is not considered in this thesis work, however details can be found in [MG90, ZD98].

7.4.3 \mathcal{H}_∞ Mixed Sensitivity Design

Mixed-sensitivity refers to closed loop transfer function shaping problems where the sensitivity S is shaped together with other closed loop transfer functions like KS (control sensitivity) and/or T (complementary sensitivity) [SP00].

Setpoint regulation is employed, i.e. to reject any disturbances which enter at the plant output and keep the feedback signal to zero in steady-state as shown in Figure 7.15 (measurement noise is assumed insignificant). The basis for this design is a *pseudo-reference* or a ‘virtual’ reference signal set to zero (in reality the track is the input that excites the system, however it is not considered for this design). Note that the configuration in Figure 7.15 employs positive feedback for design purposes, which is widely used in \mathcal{H}_∞ generalised regulator robust control problems.

It is required to keep the steady-state cant deficiency, or in this case the steady-state effective cant deficiency (6.1) for partial tilt, equal to zero unaffected by disturbances at the output.

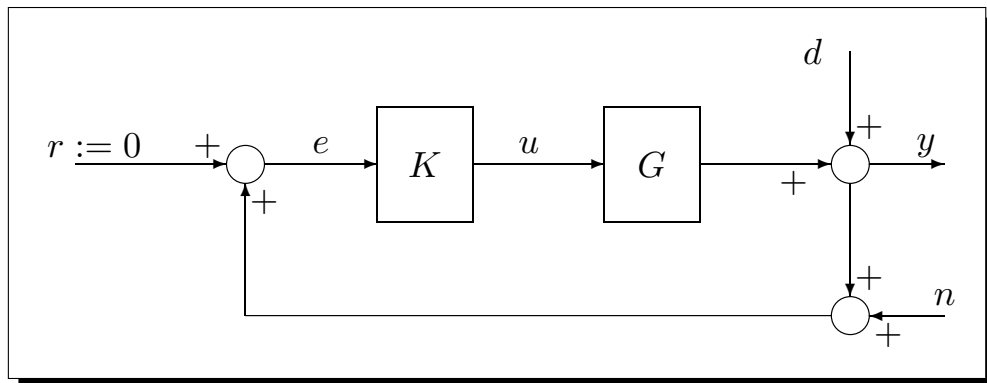


Figure 7.15: A general regulation control problem

The problem is then to design a fixed-structure (model-based) controller $K(s)$, based upon the \mathcal{H}_∞ framework, to meet several requirements such as closed loop stability, good tracking or disturbance rejection performance and robust stability in the presence of modelling discrepancies in $G(s)$.

Consider the system in Figure 7.15 where the output of the system can be written as

$$\begin{aligned}
 y &= d + Gu \\
 &= d + GKe \\
 &= d + GK(r + y + n) \\
 y &= \underbrace{(I - GK)^{-1}}_S d + \underbrace{[(I - GK)^{-1} GK]}_T (r + n)
 \end{aligned} \tag{7.58}$$

where the term '(s)' is withdrawn for simplicity.

The sensitivity function S represents the transfer function between the disturbance and the output, and also the transfer function from r to the error e . The complementary sensitivity T is the transfer function between r and y and also between n and y . The complementary sensitivity and the sensitivity functions are related by (note positive feedback)

$$S - T = I \tag{7.59}$$

For good tracking, disturbance rejection and robust tracking it is required to minimise $\|S\|_\infty$. In addition, for sensor noise attenuation and good robust stability to output model uncertainty is useful to minimise $\|T\|_\infty$. Finally, limited control bandwidth and good robust stability due to additive perturbations in the plant model requires the minimisation of $\|KS\|_\infty$. Thus, the minimisation problem can be summarised as

$$\min_{K \in \mathbb{S}} \left\| \begin{array}{c} (I - GK)^{-1} \\ GK (I - GK)^{-1} \\ K (I - GK)^{-1} \end{array} \right\|_\infty \tag{7.60}$$

where \mathbb{S} is the set of all internally stabilising controllers.

It is not possible to achieve all design objectives simultaneously, because there is a fundamental trade-off between S and T as shown in (7.59). However, this problem is overcome by incorporating appropriate shaping filters to emphasise the minimisation of each individual transfer function at different frequency ranges of interest. Disturbance rejection is usually required at low frequencies, thus S can be minimised at low frequency range. Moreover, both T and KS can be minimised at higher frequencies where sensor noise attenuation and limited control action are practically required.

• Mixed sensitivity for tilt control

The block diagram in Figure 7.16 illustrates the general control problem configuration for tilt control.

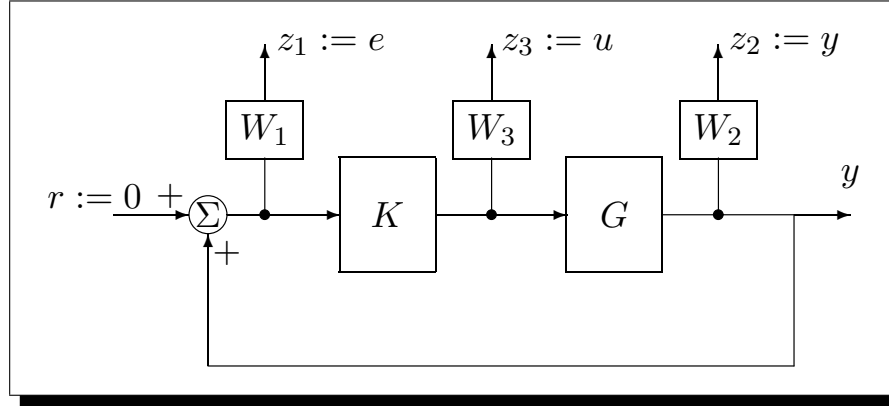


Figure 7.16: $S/KS/T$ mixed-sensitivity General Control problem formulation for tilt control

The exogenous input w represents a setpoint zero reference command r , and the regulated outputs are z_1 the effective cant deficiency (e.c.d.) error signal, z_2 the e.c.d. output signal and z_3 the control signal u , i.e.

$$\begin{bmatrix} z_1 \\ z_2 \\ z_3 \end{bmatrix} = \begin{bmatrix} (r + \theta'_{dm}) \\ \theta'_{dm} \\ \delta_a \end{bmatrix} \quad (7.61)$$

where, $z_1 = \theta'_{dm} = \left(-0.615 \frac{\ddot{y}_{vm}}{g} - 0.385 \theta_{2sr}\right)$. Note that regulating z_1 to zero will provide the required 60% tilt compensation, while the regulation of z_2, z_3 will satisfy control limitation and noise attenuation at high frequencies. The state vector used for the design of the controller is given by

$$x = \left[y_v \quad \theta_v \quad y_b \quad \theta_b \quad \dot{y}_v \quad \dot{\theta}_v \quad \dot{y}_b \quad \dot{\theta}_b \quad \theta_r \right]^T \quad (7.62)$$

The associated closed loops from w to z are given by

$$\begin{bmatrix} z_1 \\ z_2 \\ z_3 \end{bmatrix} = \begin{bmatrix} W_1 (I - GK)^{-1} \\ W_2 GK (I - GK)^{-1} \\ W_3 K (I - GK)^{-1} \end{bmatrix} w \quad (7.63)$$

From (7.57)

$$\mathcal{F}_L(P, K) = \begin{bmatrix} W_1 (I - GK)^{-1} \\ W_2 GK (I - GK)^{-1} \\ W_3 K (I - GK)^{-1} \end{bmatrix} \quad (7.64)$$

and expanding the row of the sensitivity function gives

$$\mathcal{F}_L(P, K) = \begin{bmatrix} W_1 \left[I + GK (I - GK)^{-1} \right] \\ W_2 GK (I - GK)^{-1} \\ W_3 K (I - GK)^{-1} \end{bmatrix} \quad (7.65)$$

or similarly

$$\mathcal{F}_L(P, K) = \begin{bmatrix} W_1 \\ 0 \\ 0 \end{bmatrix} + \begin{bmatrix} W_1 G \\ W_2 G \\ W_3 \end{bmatrix} \left[K (I - GK)^{-1} \right] \quad (7.66)$$

Now the elements of the generalised plant P can be easily obtained as

$$\left[\begin{array}{c|c} P_{11} & P_{12} \\ \hline P_{21} & P_{22} \end{array} \right] = \left[\begin{array}{c|c} W_1 & W_1 G \\ \hline 0 & W_2 G \\ \hline 0 & W_3 \\ \hline I & G \end{array} \right] \quad (7.67)$$

The main problem of designing the \mathcal{H}_∞ controller is now the selection of the weighting filters. As discussed above, in general W_1 should be a low pass filter, whereas W_2, W_3 appropriate high pass filters. Actually, it was found very difficult to satisfy both deterministic and stochastic criteria for the tilt problem using the mixed-sensitivity formulation.

W_1 was chosen to be a low-pass filter with a very low cut-off frequency essentially to enforce integral action on z_1 . In contrast W_2, W_3 were chosen as high-pass filters with pole and zero cut-off frequencies.

$$W_1(s) = k_{w1} \left(\frac{1 + s/30}{1 + s/10^{-4}} \right) \quad (7.68)$$

$$W_2(s) = k_{w2} \left(\frac{1 + s/0.1}{1 + s/300} \right) \quad (7.69)$$

$$W_3(s) = k_{w3} \left(\frac{1 + s/0.01}{1 + s/30} \right) \quad (7.70)$$

where k_{w1}, k_{w2}, k_{w3} are the filter gains to be tuned for appropriate frequency based S, T, KS infinity norm minimisation. Results are presented for two sets of filter gains: (i) compromise between deterministic and stochastic criteria and (ii) improved curving performance. The LMI Matlab toolbox [G⁺94] was used for the design of the \mathcal{H}_∞ controllers, and both the Riccati and LMI approaches provided the same results.

However, it should be noted that the actual procedure followed is to specify a maximum value of γ for the closed loop RMS gain and find all stabilising controllers which ensure

$$\min_{K \in \mathbb{S}} \|\mathcal{F}_L(P, K)\|_\infty < \gamma \quad (7.71)$$

This problem is known as the *suboptimal* \mathcal{H}_∞ problem and γ is referred to as the *prescribed* \mathcal{H}_∞ performance [G⁺94]. The associated Matlab files for the controller design can be found in Appendix H.

SET 1: Compromise between deterministic and stochastic criteria. The gains for the filters in this design were tuned as follows

$$\begin{bmatrix} k_{w1} \\ k_{w2} \\ k_{w3} \end{bmatrix} = \begin{bmatrix} 900.0 \\ 0.032 \\ 0.0032 \end{bmatrix}, \Rightarrow \begin{aligned} W_1(s) &= 900 \left(\frac{1+s/30}{1+s/10^{-4}} \right) \\ W_2(s) &= 0.032 \left(\frac{1+s/0.1}{1+s/300} \right) \\ W_3(s) &= 0.0032 \left(\frac{1+s/0.01}{1+s/30} \right) \end{aligned} \quad (7.72)$$

The (sub-)optimal \mathcal{H}_∞ controller was designed using Matlab function `hinfric()`⁷, which implements the Riccati-based approach and produced the following result:

Gamma-Iteration:

Gamma	Diagnosis
1.7321	: feasible
0.0721	: infeasible (Hx has imaginary axis eigenvalues)
0.3533	: feasible
0.2127	: infeasible (X is not positive semi-definite)
0.2830	: feasible
0.2479	: feasible
0.2303	: feasible
0.2215	: infeasible (X is not positive semi-definite)
0.2259	: feasible
0.2237	: feasible

Best closed-loop gain (GAMMA_OPT): 0.223702

It can be seen that after few iterations the optimum value for γ was set to approximately $\gamma_{opt} = 0.224$. The resulting controller can be found in Appendix F.1.1.

The magnitude Bode plot of the selected weighting functions and the singular values of the associated controller can be seen in Figure 7.17. At low frequencies the minimisation

⁷The same results are produced by also using `hinfli()` which implements the LMI-based approach. The only difference is that `hinfli()` does not have some regularity rejections attached to `hinfric()`, and it is used often in large problems. Both functions are offered in the LMI toolbox.

of the sensitivity function is dominant (W_1), thus providing the required integral action, while after approximately 0.5rads the cost function takes in account both T (W_2) and KS (W_3) as expected. It is expected that such a controller will be sufficiently robust to changes in the plant, however the response on design track will unavoidably be slow. The time history results which are presented in Figure 7.18 (page 114) illustrate the performance of the designed controller. It more or less resembles the performance of the classical $P + I$ controller, albeit having better robustness properties. However, it is slow on design track and cannot meet the required objectives regardless of whether it keeps the stochastic criteria within acceptable values, see Table 7.4 (next page).

SET 2: Improved curving performance. To improve the speed of the response, the weightings need to be adjusted such that the minimisation of S is dominant over a wider range of frequencies. To achieve this, the gain of each filter was changed to

$$\begin{bmatrix} k_{w1} \\ k_{w2} \\ k_{w3} \end{bmatrix} = \begin{bmatrix} 900.0 \\ 3.2e - 4 \\ 3.2e - 5 \end{bmatrix}, \Rightarrow \begin{aligned} W_1(s) &= 900 \left(\frac{1+s/30}{1+s/10^{-4}} \right) \\ W_2(s) &= 3.2e - 4 \left(\frac{1+s/0.1}{1+s/300} \right) \\ W_3(s) &= 3.2e - 5 \left(\frac{1+s/0.01}{1+s/30} \right) \end{aligned} \quad (7.73)$$

The resulting weightings can be seen in Figure 7.19(a), where the crossover between the different elements of the cost function has been shifted at approximately 4.5rads . It is expected that the controller will offer an improvement to the tilt response on curved track.

The Riccati-based approach returned the following results in Matlab:

Gamma-Iteration:

Gamma	Diagnosis
1.7321	: feasible
0.0721	: feasible
0.0147	: infeasible (X is not positive semi-definite)
0.0434	: feasible
0.0291	: infeasible (X is not positive semi-definite)
0.0362	: infeasible (X is not positive semi-definite)
0.0398	: feasible
0.0380	: infeasible (X is not positive semi-definite)
0.0389	: feasible
0.0385	: infeasible (X is not positive semi-definite)
0.0387	: infeasible (X is not positive semi-definite)

Best closed-loop gain (GAMMA_OPT): 0.038912

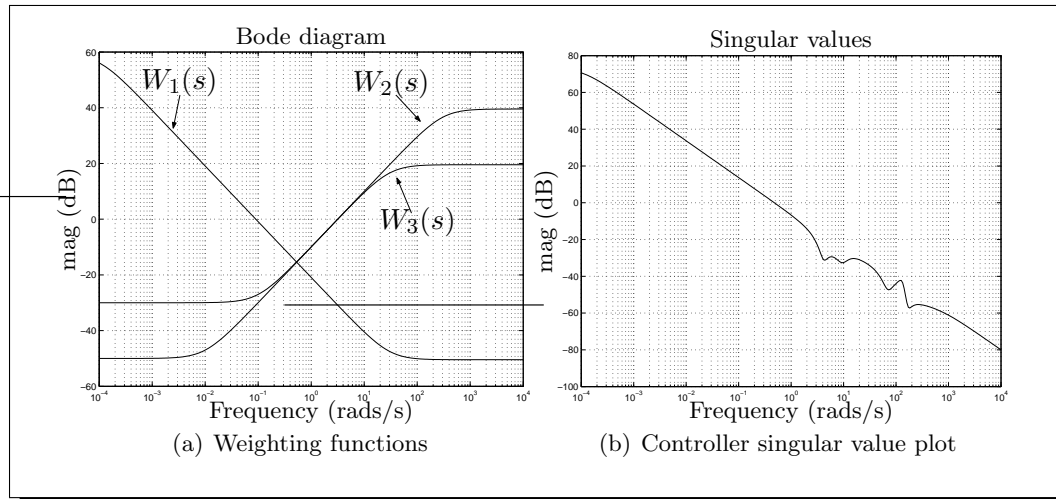


Figure 7.17: Mixed sensitivity design set 1

Table 7.4: Mixed Sensitivity \mathcal{H}_∞ approach, weightings set 1, @ 58(m/s)

DETERMINISTIC		
Lateral accel. (actual vs ideal)	- steady-state	n/a (%g)
	- R.M.S. deviation error	6.78 (%g)
	- peak value	21.4 (%g)
Roll gyroscope	- R.M.S. deviation	0.038 (rad/s)
	- peak value	0.073 (rad/s)
P_{CT} (P-factor)	- peak jerk level	10.55 (%g/s)
	- standing	75.2 (% of passengers)
	- seated	24.22 (% of passengers)
STOCHASTIC		
Passenger comfort	- R.M.S. passive (equiv.)	3.78 (%g)
	- R.M.S. active	4.01 (%g)
	- degradation	6.2 (%)

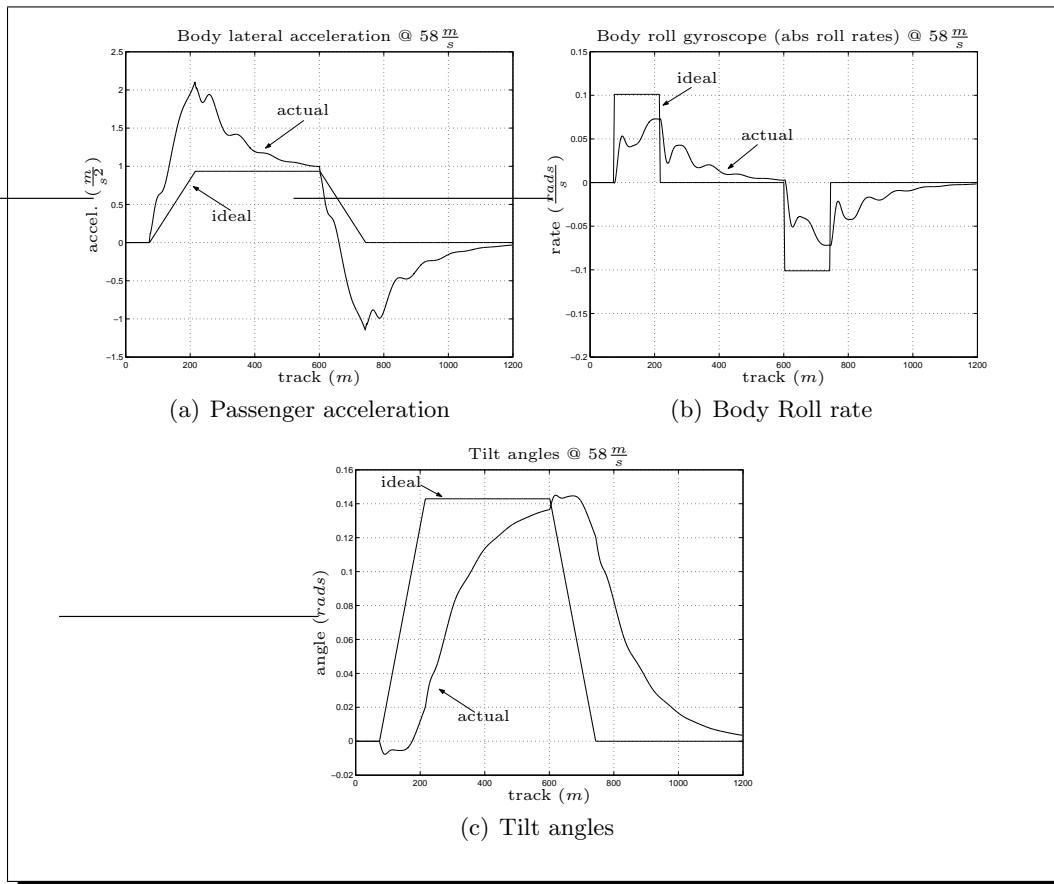


Figure 7.18: Design track time history results for mixed sensitivity weightings set 1

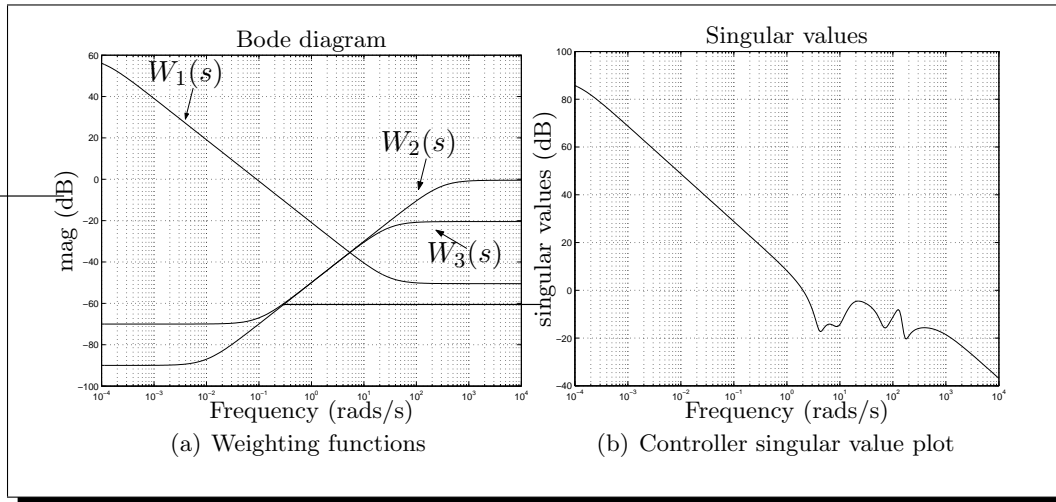


Figure 7.19: Mixed sensitivity design set 2

The decrease on the the magnitudes of W_2, W_3 weights causes the optimal value of γ to reduce to $\gamma_{opt} = 0.0389$. The resulting controller for this design is presented in Appendix F.1.2, while the singular values are plotted in Figure 7.19(b).

Table 7.5: Mixed Sensitivity \mathcal{H}_∞ approach, weightings set 2, @ 58(m/s)

DETERMINISTIC		
Lateral accel. (actual vs ideal)	- steady-state	9.53 (%g)
	- R.M.S. deviation error	2.08 (%g)
	- peak value	12.23 (%g)
Roll gyroscope	- R.M.S. deviation	0.022 (rad/s)
	- peak value	0.111 (rad/s)
P_{CT} (P-factor)	- peak jerk level	6.8 (%g/s)
	- standing	49.5 (% of passengers)
	- seated	13.74 (% of passengers)
STOCHASTIC		
Passenger comfort	- R.M.S. passive (equiv.)	3.78 (%g)
	- R.M.S. active	5.02 (%g)
	- degradation	32.86 (%)

From Figure 7.20 (page 117) it can be obtained that the response of the system has been significantly improved compared to the previous set. The curved performance is acceptable with the required steady-state compensation achieved as shown in Table 7.5. However, more oscillations have entered to the system as a result of the higher bandwidth. This also further degrades the stochastic ride quality, due to the fact that the fast controller excites the suspension modes on random track, Table 7.5.

In the \mathcal{H}_∞ mixed sensitivity approach of this section, the problem encountered is that the formulation proves too restrictive for control design. It is very difficult to design the controller for both acceptable deterministic and stochastic performance based upon the choice of r as the unique exogenous input. Trials with additional sensors, i.e. body roll gyroscope and suspension deflection, did not provide significant improvement. Thus, it is required to somehow separate the two objectives for the deterministic and stochastic criteria in the problem formulation and this is discussed in the following section.

7.4.4 Multi-objective $\mathcal{H}_\infty/\mathcal{H}_2$ Robust Control via LMI approach

Initial designs using \mathcal{H}_∞ optimisation were found adequate in terms of providing either good deterministic or stochastic performance to the closed-loop system; however it was found difficult to satisfy both objectives simultaneously as discussed earlier. This difficulty was attributed to modelling assumptions of external disturbances implicit in the \mathcal{H}_∞ optimality criterion.

Recall that the \mathcal{H}_∞ norm of a system represents the worst-case energy transfer between (bounded energy) disturbances to (bounded-energy) regulated outputs, and as a result can be conservative when disturbances are naturally modelled as persistent or white noise signals. In such cases, provided that the interests falls upon minimising the RMS value of a regulated output, the \mathcal{H}_2 norm [ZD98] of the corresponding closed-loop transfer function is a more appropriate measure of stochastic performance. This section considers the multiple-objective $\mathcal{H}_\infty/\mathcal{H}_2$ design method for local/vehicle tilt control [ZHG00].

The design objectives are formulated as an optimisation problem, defined in the generalised -regulator setting shown in Figure 7.21, where $P(S)$ and $K(s)$ are the generalised plant (inclusive of all weighting factors) and the controller to be designed. The vector of external disturbances was set to $w = [w_1 \ w_2]^T$, where w_1 denotes $(\frac{1}{R})$ the (deterministic) track-curvature (low-frequency) disturbance signal and w_2 is the (stochastic) lateral track position (high-frequency) signal y_o . Scaling factors W_{i_1}, W_{i_2} emphasise the relative weight between the two disturbances for the design. Outputs y_1 and y_2 are the measured lateral acceleration and the secondary suspension roll angle, respectively. It was chosen for the output vector to replicate the sensors used in the basic classical nulling control. To meet both deterministic and stochastic requirements, the following

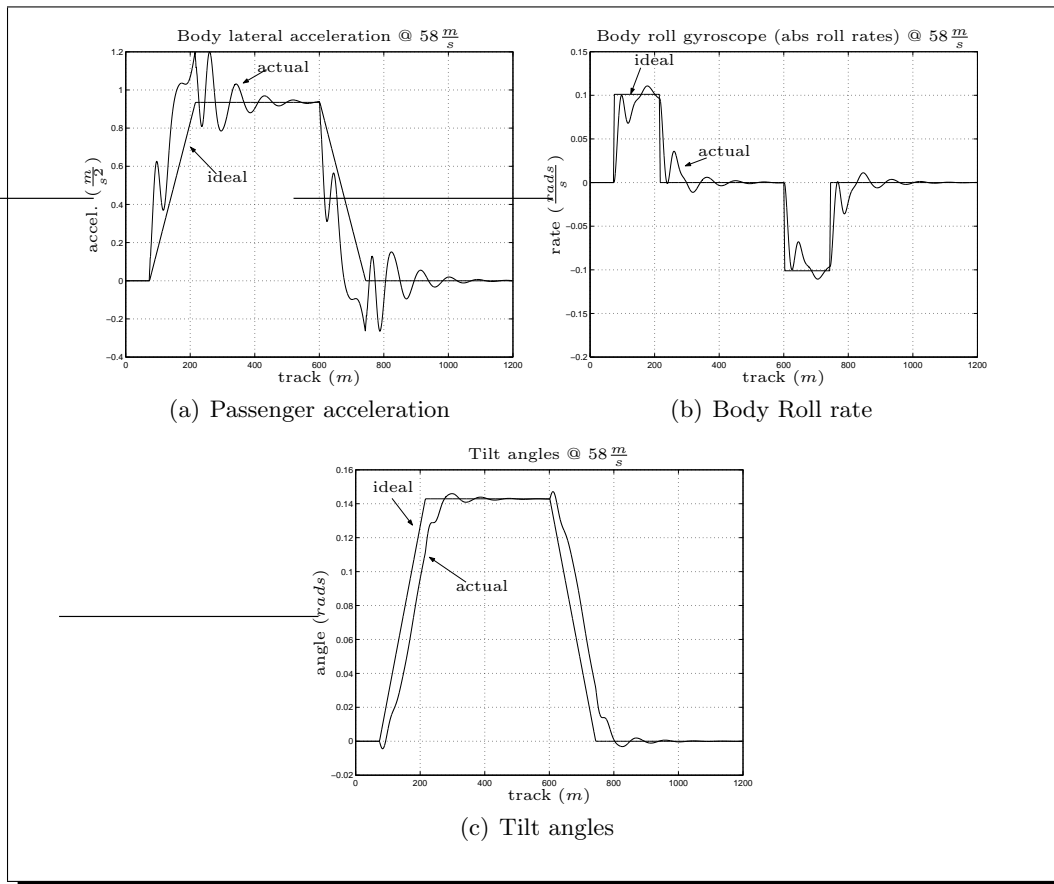


Figure 7.20: Design track time history results for mixed sensitivity weightings set 2

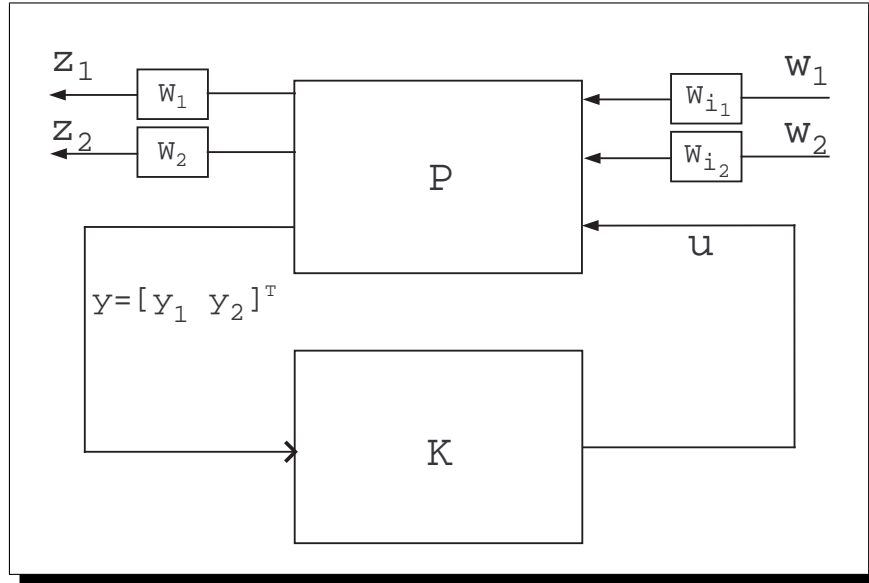


Figure 7.21: The Generalised Regulator Configuration for multi-objective control

multi-objective optimisation problem was formulated

$$\min_{K \in \mathbb{S}} \alpha \|W_1 T_{z_1 w}\|_{\infty}^2 + \beta \|W_2 T_{z_2 w}\|_2^2 \quad (7.74)$$

in which \mathbb{S} denotes the set of all internally stabilising controllers. The first regulated output z_1 for infinity-norm minimisation, was chosen as the effective cant deficiency $z_1 = \theta'_{dm}$ (6.1). For the minimisation of the 2-norm, z_2 was chosen as the control input u denoting the actuator roll angle δ_a . Regulating z_1 to zero corresponds to 60% tilt compensation and thus attains the desired (steady-state) level of acceleration on steady state curve. $T_{z_i w}$ ($i = 1, 2$) denotes the (closed-loop) transfer functions between signals w and z_1, z_2 respectively.

Remark 7.4.1. Multi-objective optimisation typically refers to the joint optimisation of a vector consisting of two or more functions, typically representing conflicting objectives. Common types of multi-objective optimisation problems include “Pareto-optimal” (non-inferior) optimality criteria, minimax optimality criteria, etc.

In the context of this work, the term “multi-objective” refers simply to the fact that the cost function of the optimisation problem involves two different types of norms, capturing the deterministic and stochastic objectives of the design. The two different norms that are used here are the *two-norm* and the *infinity norm*. Thus, typical examples of multi-objective problems in our context include:

1. Constrained minimisation:

Minimise $\|W_1 T_{xy}\|_2$ subject to $\|W_2 T_{zw}\|_\infty < \gamma$,

2. Unconstrained minimisation:

Minimise $\beta \|W_1 T_{xy}\|_2 + \alpha \|W_2 T_{zw}\|_\infty$, and

3. Feasibility problem: Find a stabilising $K(s)$ (if one exists) such that

$\|W_1 T_{xy}\|_2 \leq \gamma_1$ and $\|W_2 T_{zw}\|_\infty \leq \gamma_2$

Here T_{xy} and T_{zw} represent two general closed-loop transfer functions, weighted via W_1 and W_2 .

Scalars α and β , in (7.74), are positive definite design parameters which may be used to shift the emphasis of the optimisation problem between the minimisation of the $\|T_{z_1 w}\|_\infty$ term (deterministic objective) and the $\|T_{z_2 w}\|_2$ term (stochastic objective). The frequency-domain weights W_1 and W_2 have been chosen as:

$$W_1(s) = 10^4 \frac{\frac{s}{200} + 1}{\frac{s}{0.0001} + 1} \quad (7.75)$$

$$W_2(s) = 0.5 \frac{s^3 + 1.59s^2 + 0.58s + 0.06}{s^3 + 13.81s^2 + 38.4s + 2.98} \quad (7.76)$$

W_1 is essentially a low-pass filter with a very low pole cut-off frequency ($10^{-4} \frac{rads}{s}$) and high gain at low frequencies, Figure 7.22(a). Thus W_1 emphasises minimisation of the $\|T_{z_1 w}\|_\infty$ term in the low frequency range and effectively enforces integral control on the regulated output (z_1). W_2 is a high-pass filter with pole ($10 \frac{rads}{s}$) and zero ($0.2 \frac{rads}{s}$) cut-off frequencies. A lead/lag network is also included in W_2 , in the range of $[.1 \frac{rads}{s}, 6 \frac{rads}{s}]$, which found to have a positive effect on controller design (by enhancing the cross-over frequency of W_1, W_2), Figure 7.22(a). By limiting the high-frequency components of the control input (z_2), effectively places a limit on the closed-loop bandwidth of the system, which in turn limits the RMS acceleration on random track (stochastic case). Additional benefits include a smoother control signal and improved robustness properties of the controller when the effects of uncertainty in $P(s)$ and in the actuator dynamics are taken into account. Moreover, the relative weighting between w_1 and w_2 involved the unity matrix, i.e.

$$W_i = \begin{bmatrix} W_{i_1} & 0 \\ 0 & W_{i_2} \end{bmatrix} = \begin{bmatrix} 1 & 0 \\ 0 & 1 \end{bmatrix} \quad (7.77)$$

Thus the energy of either of the signals is equally incorporated in the cost function. Increasing either W_{i_1} or W_{i_2} with respect to the other will put more emphasis on the

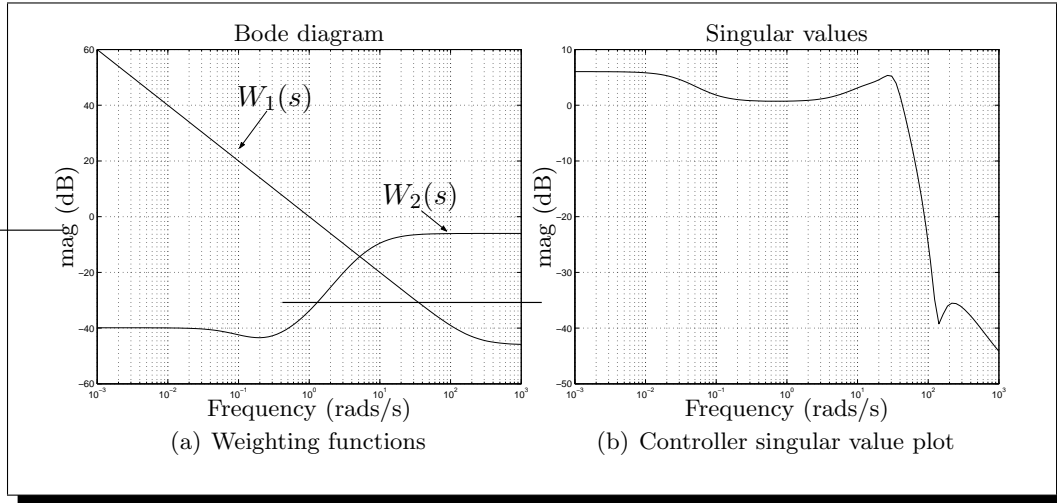


Figure 7.22: Multi-objective $\mathcal{H}_\infty/\mathcal{H}_2$ LMI approach scheme

deterministic or the stochastic track respectively. However, the current choice of W_i provided the best results based upon the specifications in this thesis.

The minimisation problem in (7.74) was solved in Matlab using the LMI approach [G⁺94]. LMIs represent the problem in a set of Linear Matrix Inequalities and follow a convex optimisation approach. This technique has very attractive computational properties and is widely used in systems and control theory and more details can be found in [B⁺94].

For controller design, the generalised plant was formulated as follows

$$\begin{aligned} \dot{x} &= Ax + B_1w + B_2u \\ z_\infty &= C_\infty x + D_{\infty 1}w + D_{\infty 2}u \end{aligned} \quad (7.78)$$

$$z_2 = C_2x + D_{21}w + D_{22}u \quad (7.79)$$

$$y = C_yx + D_{y1}w \quad (7.80)$$

where all matrices can be formed based upon the A,B,C,D state space matrices in Appendix E.1 and the specifications in the generalised plant. Note that the state vector incorporates the same states as in the mixed sensitivity design. The controller can be then found by using matlab function `hinfmix()`.

The optimisation problem was solved for a few combinations of the α and β parameters and the results can be seen in Table 7.6. The results shown in the table clearly illustrate the fundamental trade-off between the deterministic and the stochastic objectives of

Table 7.6: α - β combinations for the $\mathcal{H}_\infty/\mathcal{H}_2$ problem

α	β	<i>RiQu – Deg.</i> (%)	<i>Dev – Det.</i> (%g)
1	1	21.7	1.95
1	2.5	10	2.15
1	5	4.95	2.37
1	10	3.4	2.62
1	20	2.1	2.9

RiQu – Deg.: ride-quality degradation @58m/s of active system compared to passive @58m/s (straight track)
Dev – Det.: RMS acceleration deviation from the ideal response of an ideal tilting controller @58m/s (curved track)

the design.

As expected, increasing the value of β relative to α puts more emphasis on the stochastic aspects of the design, and as a result the RMS acceleration on straight track is reduced. This is at the expense of deterministic performance and, therefore, the curved track response becomes slower (larger deviations from the ideal tilt response). Since it is required that stochastic performance deteriorates by no more than 7.5% compared to the passive system, the “best” design was obtained for $\alpha = 1$ and $\beta = 5$. The result returned in Matlab for the “best” configuration is shown below

```
Optimization of 1.000 * G^2 + 5.000 * H^2 :
```

```
-----  
Solver for linear objective minimization under LMI constraints
```

```
Iterations : Best objective value so far
```

```
1  
2  
3  
4  
5  
6  
7  
8  
9  
10  
11  
12  
13  
14
```

```
15
16
* switching to QR
17
18
19
20
21
22
23
24
25
26
27
28
29
30
31
32
33
34
35
36          1.018621e+005
37          1.018621e+005
38          6.830550e+004
39          6.830550e+004
40          5.029532e+004
41          5.029532e+004
42          4.475980e+004
43          4.226245e+004
***          new lower bound: 3159.072336
44          4.067042e+004
45          3.932891e+004
***          new lower bound: 7515.082450
46          3.869554e+004
***          new lower bound: 1.337229e+004
47          3.813935e+004
***          new lower bound: 2.126712e+004
48          3.768442e+004
***          new lower bound: 2.417974e+004
49          3.731571e+004
***          new lower bound: 2.648882e+004
50          3.731571e+004
***          new lower bound: 2.831748e+004
51          3.669343e+004
***          new lower bound: 2.858709e+004
52          3.654895e+004
***          new lower bound: 3.010962e+004
53          3.634128e+004
***          new lower bound: 3.236723e+004
54          3.617982e+004
```

```

***          new lower bound: 3.294263e+004
55          3.611540e+004
***          new lower bound: 3.334488e+004
56          3.611540e+004
***          new lower bound: 3.392420e+004
57          3.519640e+004
***          new lower bound: 3.393568e+004
58          3.510891e+004
***          new lower bound: 3.406173e+004
59          3.507050e+004
***          new lower bound: 3.416366e+004
60          3.503430e+004
***          new lower bound: 3.424687e+004
61          3.496769e+004
***          new lower bound: 3.431505e+004
62          3.493807e+004
***          new lower bound: 3.437031e+004
63          3.488358e+004
***          new lower bound: 3.441555e+004
64          3.483742e+004
***          new lower bound: 3.450646e+004

```

```

Result: feasible solution of required accuracy
        best objective value: 3.483742e+004
        guaranteed relative accuracy: 9.50e-003
        f-radius saturation: 88.219% of R = 1.00e+008

```

```

Guaranteed Hinf performance: 1.54e+002
Guaranteed H2 performance: 4.68e+001

```

Note that, in the first few iterations, the algorithm does not find any solutions for the problem, however the solution converges soon after. The resulting controller is of 2-input/1-output dimension due to the two measurements used in the formulation, and can be found in Appendix F.2. The singular value plot is shown in Figure 7.22(b).

The performance of the designed system is assessed in Table 7.7, where it can be seen that it is very good even if the scheme is based upon “nulling”-type control. This approach offers a significant improvement compared to the mixed sensitivity, by distinguishing the design objectives in the cost function. The associated time history analysis for the design track is presented in Figure 7.23, with clearly improved system damping by the fixe-structure \mathcal{H}_∞ controller.

A further step is to test the controller designed for the nominal plant under *parametric changes*, which involved two assumed cases

1. **Perturbed (1)**: 20% increase in body mass with 10% increase in secondary suspension stiffness and 20% decrease in secondary suspension damping ratio.
2. **Perturbed (2)**: 40% increase in body mass with 20% increase in secondary

Table 7.7: $\mathcal{H}_\infty/\mathcal{H}_2$ multi-objective LMI approach @ 58(m/s)

DETERMINISTIC		
Lateral accel. (actual vs ideal)	- steady-state	9.53 (%g)
	- R.M.S. deviation error	2.37 (%g)
	- peak value	13.66 (%g)
Roll gyroscope	- R.M.S. deviation	0.023 (rad/s)
	- peak value	0.101 (rad/s)
P_{CT} (P-factor)	- peak jerk level	7.07 (%g/s)
	- standing	51.7 (% of passengers)
	- seated	14.93 (% of passengers)
STOCHASTIC		
Passenger comfort	- R.M.S. passive (equiv.)	3.78 (%g)
	- R.M.S. active	3.96 (%g)
	- degradation	4.95 (%)

suspension stiffness and 40% decrease in secondary suspension damping ratio.

The above cases were chosen such that they represent realistic parametric changes. However, the decrease in damping was included to observe the performance of the controller under reduced damping in the passive system. It should be noted at this point that system uncertainty was not considered in the robust controller design procedure.

Results are illustrated for the passenger acceleration on design track in Figure 7.24 in page 126. The system is stable in all cases and also the transition performance does not change significantly even though the uncertainty was not taken in account in the design. There is of course a small change in the steady-state, however this is a function of the system parameters rather than the tilt controller. Moreover, the stochastic ride quality was within the required 7.5% degradation margin in all test cases. Thus, the controller provides sufficient performance and also acceptable robust stability.

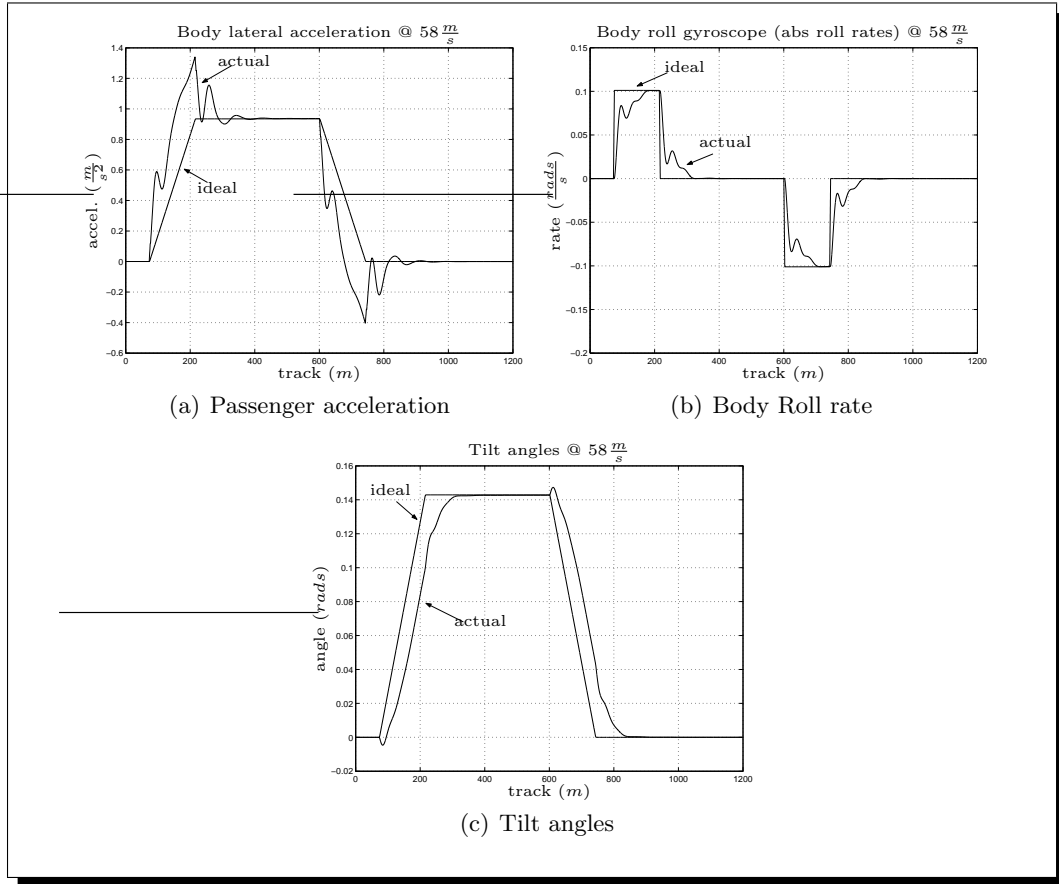


Figure 7.23: Design track time history results for $\mathcal{H}_\infty/\mathcal{H}_2$ "best" design

7.5 Concluding remarks

This chapter has considered the design of local/vehicle tilt controllers based upon advanced control concepts. It has been shown that the optimal LQR with integral action approach provides a significant improvement in all aspects of the tilt control problem. It especially illustrates the advantage of using state feedback in the controller design. The controller has a fast response on design track while improving the ride quality in the stochastic case and this illustrates the validity of the cost function in the design. However, in reality a state estimator is required for implementation properties due to the weakness of measuring all states (LQG control), which does not guarantee the prescribed robustness properties of the LQR controller.

Moreover, a model-based estimation scheme was proposed to provide a more effective feedback signal for control design. The work concentrated upon Kalman estimators

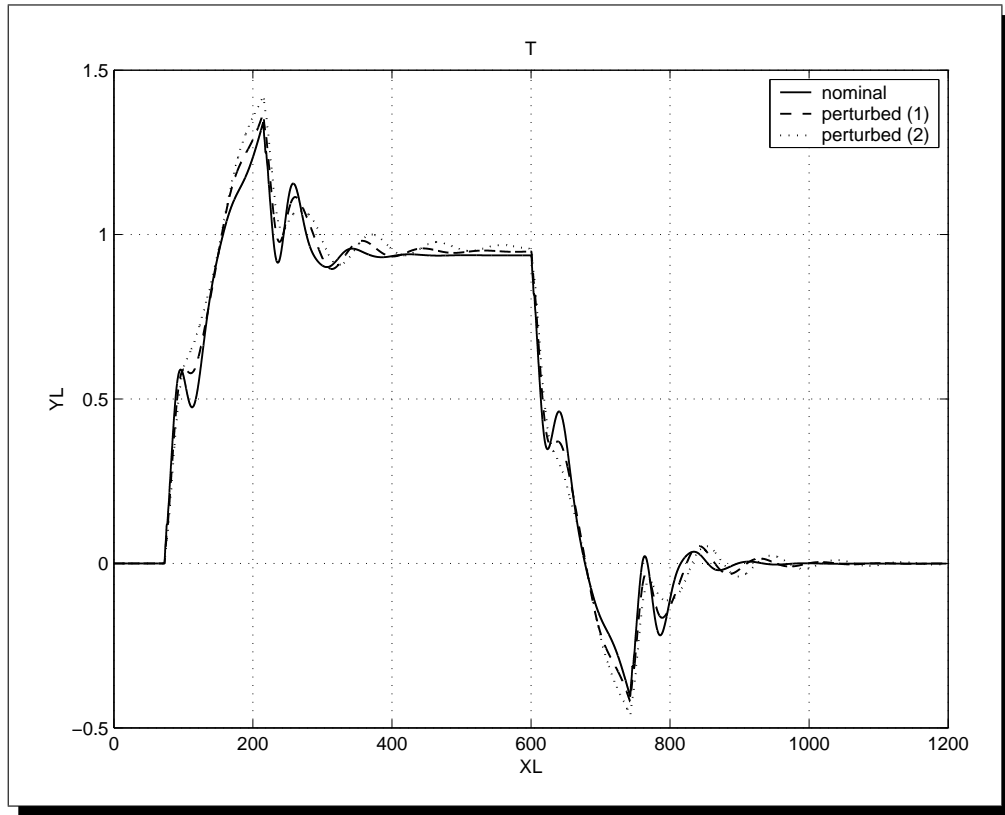


Figure 7.24: Controller performance with parametric change

and results have illustrated the effectiveness of the method. The estimator performed remarkably well although the deterministic and stochastic track features are unknown and not included with the vehicle dynamics. A simple PID controller completed the design in order to achieve the required tilt angles. Trials with added sensor noise had minimal effects on the estimator performance and on the overall designed system. This estimator can be easily incorporated in the LQR approach for LQG control.

The chapter has also considered the design of \mathcal{H}_∞ controllers for application to the tilt control problem. The method was illustrated by using the mixed sensitivity approach based upon a pseudo-reference command, however it proved too difficult to attain both deterministic and stochastic criteria. This problem was overcome by using a multi-objective $\mathcal{H}_\infty/\mathcal{H}_2$ approach based upon a direct connection of the cost function to the two different track profiles. The problem formulation was solved using the LMI approach, a technique which recently emerges in a variety of control methods. The $\mathcal{H}_\infty/\mathcal{H}_2$ controller offers a very good tilt performance with low overshoots and fast settling times. Uncertainty was not taken in account during the design stage, albeit

tests shown that the controller provides good robust stability in the presence of plant uncertainty. The main problem with such closed-loop based approaches is the selection of weights which can be a complex procedure.

The next part investigates the tilt control problem in a vehicle configuration which is widely used in the tilting train industry. It is based upon the use of a tilt mechanism to provide tilt action. The problem is similar to the previous case of the ARB vehicle model but the vehicle structure is more complex. The part includes modelling and also the extension of the control studies for the new model.

Part II

Tilt Mechanism Studies below Secondary Suspensions

Chapter 8

Modelling of Vehicle Dynamics using tilting bolster

8.1 Tilt Mechanism Preliminaries

As noted earlier in the thesis, the amount of tilt tends to be rather restricted in the case of tilting across the secondary suspensions, i.e. via airsprings or by using active ARBs. Most systems now use what is called a *tilting mechanism*, connected to the bogie via swing links (see Section 1.3.3) effectively providing a tilting bolster with the conventional secondary suspension placed below or above the mechanism.

Modern tilting trains mainly employ mechanisms with the secondary suspension situated on top, where tilt action is provided below the suspension level. In this arrangement the secondary suspension acts between the tilting bolster and the vehicle body, as a consequence the lateral suspension does not have to react to the increased curving forces which reduces the suspension deflections. There are still issues with bogie weight and complexity as well as with increased actuator force, albeit available technology can overcome such problems (though such structures are more expensive compared to simpler forms of tilt). Note that the inclined swing links imply that the effective tilt centre is still above the vehicle body floor level even if the tilt action is applied below the vehicle body.

The actuator technology in the early mechanism configurations involved mainly *hydraulic* actuators (i.e. X2000 tilt), though trials for the British APT (during the 1980s) made use of electro-mechanical actuators [Goo99]. However, most European

manufacturers now tend to replace hydraulic with *electro-mechanical* actuator solutions, i.e. VT612 (Adtranz), FIAT-SIG for Virgin West Coast. Details on these vehicle configurations can be found in [Goo99]¹.

8.2 Vehicle Modelling

The mathematical modelling in this part of the research work is based upon a demonstration vehicle assembled in VAMPIRE rail vehicle dynamics software package [KE00]. The generated full non-linear vehicle model is illustrated in Figure 8.2², where the tilting bolster is represented by the mass between the bogie and the body elements.

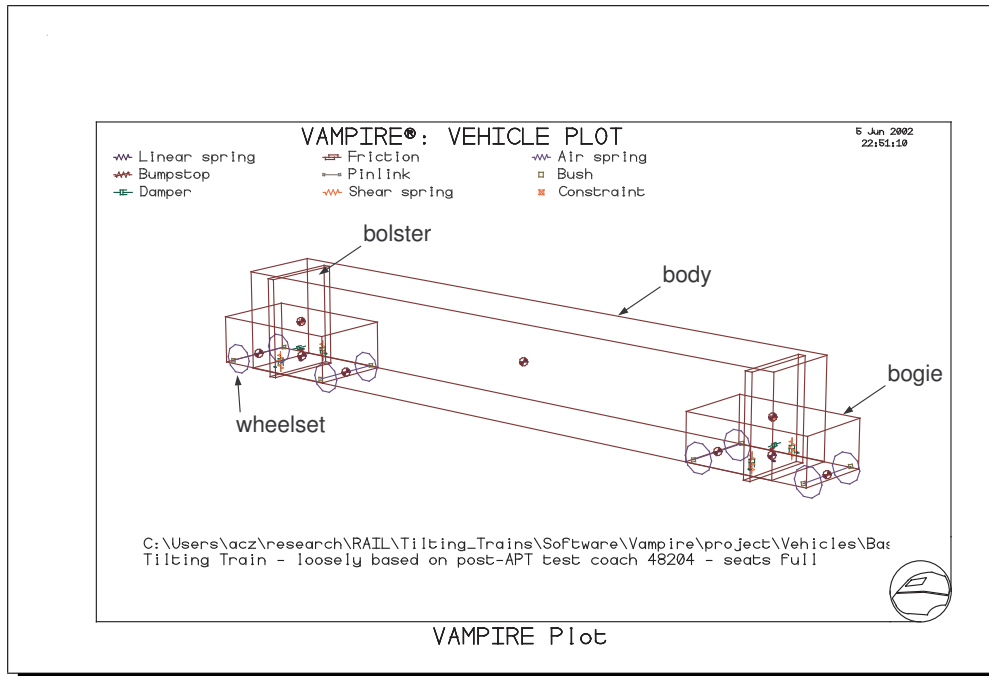


Figure 8.1: Vampire model of the tilting train (single vehicle)

Although the VAMPIRE model is a full non-linear vehicle dynamic model, involving 39-DoF without and 51-DoF with the bolster, this section develops a linear model approximation to represent the main vehicle dynamic modes essential for tilt control design (using the half-vehicle model). The linear model comprises both the lateral and roll degrees-of-freedom for both the body and the bogie masses, subject to the following

¹there is also a website including information on railway technology and related projects, and can be found at <http://www.railway-technology.com>.

²the author wishes to thank Jeremy Evans (AEA Technology) for providing the VAMPIRE vehicle model and parameter values. An overview of the VAMPIRE software package can be found in <http://www.aeat.co.uk/rail/pdf/vampire.pdf>.

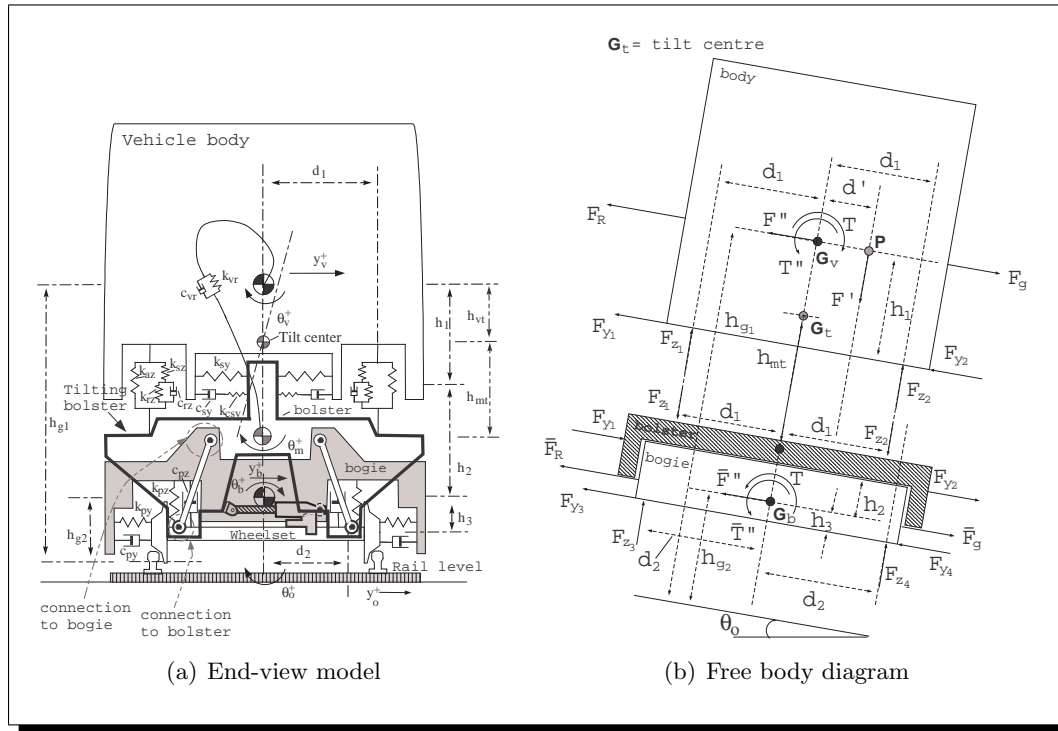


Figure 8.2: Vehicle with tilt mechanism below secondary

considerations:

- both vertical and lateral, primary and secondary suspension are characterised by pairs of spring/damper parallel combinations. *Damper end-stiffness* was also included in the case of the secondary lateral suspensions.
- also included is the stiffness of an anti-roll bar connected between the body and the combined bogie/bolster masses (using additional roll damping).
- active tilt is provided by the “tilting bolster” mounted on the bogie mass, with the tilt action applied between the bolster and the bogie frame via a roll actuator. The mechanical arrangement is for *tilt below secondary suspension*, with the motion illustrated in Figure 8.3(a).
- the actuation system is represented by a position servo in series with the mechanism (see Figure 8.3(b)). The parameters were chosen such that they gave $3.5Hz$ bandwidth and 50% damping closed-loop position servo mechanism. The tilting bolster is able to provide the maximum tilt required, i.e. up to 10 degrees.
- detailed wheelset dynamics were not included for simplicity, however the associated effects are incorporated in the model by using an appropriate 2nd order LP

filter (bogie lateral kinematics). The filter was characterised by a $5Hz$ cut-off frequency and 20% damping.

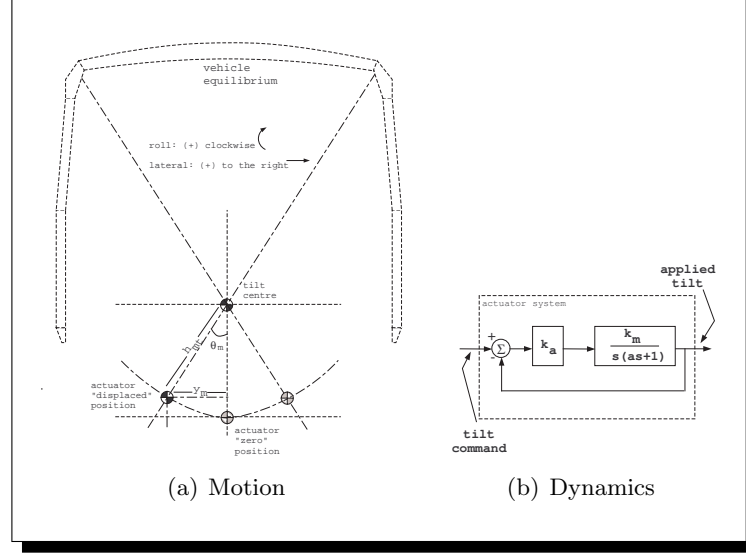


Figure 8.3: Actuator configuration

The modelling procedure is very similar to the previous one followed in Section 5.4. The vehicle model is characterised by the following set of equations of motion (corresponding to local reference axis, with the rotation and translation associated with curves allowed for in the equations).

$$m_v \ddot{y}_v = -2k_{sy} y_v + 2k_{sy} h_1 \theta_v + 2(k_{sy} + k_{csy}) y_b + 2(k_{sy} + k_{csy}) h_2 \theta_b - 2k_{csy} y_{es} - [2h_{mt}(k_{sy} + k_{csy}) - m_v g] \theta_m + m_v g \theta_o - \frac{m_v v^2}{R} - m_v h_{g1} \ddot{\theta}_o \quad (8.1)$$

$$i_{vr} \ddot{\theta}_v = (2h_1 k_{sy} + m_v g) y_v - [k_{vr} + 2h_1^2 k_{sy} + 2d_1^2 (k_{az} + k_{sz})] \theta_v - [2h_1 (k_{sy} + k_{csy}) + m_v g] y_b + [k_{vr} + 2d_1^2 k_{az} - 2h_1 h_2 (k_{sy} + k_{csy})] \theta_b - c_{vr} \dot{\theta}_v + c_{vr} \dot{\theta}_b + 2k_{sz} d_1^2 \theta_r + 2h_1 k_{csy} y_{es} + [k_{vr} + 2d_1^2 k_{az} + 2(k_{sy} + k_{csy}) h_1 h_{mt}] \theta_m + c_{vr} \dot{\theta}_m - i_{vr} \ddot{\theta}_o \quad (8.2)$$

$$m_b \ddot{y}_b = 2k_{sy} y_v - 2h_1 k_{sy} \theta_v - 2[(k_{sy} + k_{csy}) + k_{py}] y_b - 2[h_2 (k_{sy} + k_{csy}) - h_3 k_{py}] \theta_b - 2c_{py} \dot{y}_b + 2h_3 c_{py} \dot{\theta}_b + 2k_{csy} y_{es} + 2k_{py} y_w + 2c_{py} \dot{y}_w + 2h_{mt} (k_{sy} + k_{csy}) \theta_m + m_b g \theta_o - \frac{m_b v^2}{R} - m_b h_{g2} \ddot{\theta}_o \quad (8.3)$$

$$\begin{aligned}
i_{br}\ddot{\theta}_b = & 2h_2k_{sy}y_v + [k_{vr} - 2h_2h_1k_{sy} + 2d_1^2(k_{az} + k_{sz})] \theta_v - 2[h_2(k_{sy} + k_{csy}) - h_3k_{py}] y_b \\
& - [k_{vr} + 2h_2^2(k_{sy} + k_{csy}) + 2h_3^2k_{py} + 2d_2^2k_{pz} + 2d_1^2k_{az}] \theta_b + c_{vr}\dot{\theta}_v + 2h_3c_{py}\dot{y}_b \\
& - (c_{vr} + 2d_2^2c_{pz} + 2h_3^2c_{py}) \dot{\theta}_b - 2k_{sz}d_1^2\theta_r + 2h_2k_{csy}y_{es} - 2h_3k_{py}y_w - 2h_3c_{py}\dot{y}_w \\
& - [k_{vr} + 2d_1^2k_{az} - 2(k_{sy} + k_{csy})h_2h_{mt}] \theta_m - c_{vr}\dot{\theta}_m - i_{br}\ddot{\theta}_o \quad (8.4)
\end{aligned}$$

- Additionally, for the actuator and the bogie kinematics respectively:

$$\frac{\theta_m}{\theta_{m_i}}(s) = \frac{483.6}{s^2 + 22s + 483.6}, \quad \frac{y_w}{y_o}(s) = \frac{987}{s^2 + 12.57s + 987} \quad (8.5)$$

- and also for the damper end-stiffness state and the airspring state respectively:

$$\dot{y}_{es} = c_{sy}^{-1}(k_{csy}y_b + h_2k_{csy}\theta_b + c_{sy}\dot{y}_v - c_{sy}h_1\dot{\theta}_v - k_{csy}h_{mt}\theta_m - k_{csy}y_{es}) \quad (8.6)$$

$$\dot{\theta}_r = c_{rz}^{-1}\{-\theta_r(k_{sz} + k_{rz}) + k_{sz}\theta_v + k_{rz}(\theta_b + \theta_m) + c_{rz}(\dot{\theta}_b + \dot{\theta}_m)\} \quad (8.7)$$

The model parameter values are listed in Appendix A.2.2, with all other symbols listed in the Glossary. Furthermore, an end-moment effect, similar to the case of the ARB model, $m_v g(y_v - y_b)$ (see Figure 5.12 on page 59), was also included to model the roll contribution of the body c.o.g. displacement on curved track (due to the soft secondary suspensions). The system is still highly complex with the lateral and roll mode coupling strongly present, however the actuator has now a direct effect on the lateral motion (compared to the ARB case) which provides reduced suspension deflection (in the active case) and some improvement in tilt performance.

It is now a matter of re-arranging the equations into a state space form for system analysis and control design as follows

$$\dot{\mathbf{x}} = \mathbf{A}\mathbf{x} + \mathbf{B}\mathbf{u} + \mathbf{\Gamma}\mathbf{w} \quad (8.8)$$

$$\mathbf{y} = \mathbf{C}\mathbf{x} + \mathbf{H}\mathbf{w} \quad (8.9)$$

where,

$$\begin{aligned}
\dot{\mathbf{x}} = & [y_v \ \theta_v \ y_b \ \theta_b \ \dot{y}_v \ \dot{\theta}_v \ \dot{y}_b \ \dot{\theta}_b \ \theta_r \ y_{es} \ y_w \ \dot{y}_w \ \theta_m \ \dot{\theta}_m]^T, \dots \\
\mathbf{u} = & [\theta_{m_i}], \quad \mathbf{w} = [R^{-1} \ \dot{R}^{-1} \ \theta_o \ \dot{\theta}_o \ \ddot{\theta}_o \ y_o \ \dot{y}_o]^T. \quad (8.10)
\end{aligned}$$

For simulation purposes only, disturbance signals \dot{R}^{-1} , θ_o , $\dot{\theta}_o$, y_o should be incorporated into the state vector. The associated A and B matrices can be seen in Appendix E.2, with more details available in the relevant `matlab` files. The analysis of the system modes ensures compatibility between the `matlab` and `vampire` models listed in Table 8.1 (indicating the major system modes).

Table 8.1: Tilt mechanism vehicle model dynamic modes

Matlab linear model		
Mode	Damping(%)	Frequency(Hz)
Lower sway	21.8	0.48
Upper sway	20.9	1.35
Bogie lateral	9.95	16.7
Bogie roll	28.3	7.26
Vampire full non-linear model		
Mode	Damping(%)	Frequency(Hz)
Lower sway	22.5	0.44
Upper sway	21.3	1.44
Bogie lateral	11.76	16.0
Bogie roll	30.46	6.6

Table 8.2: Track profiles for the tilting mechanism linear model

Curve Transition		
maximum cant angle	$\theta_{o_{max}}$	5.84 (degrees)
maximum curve radius	R_{max}	1200.0 (m)
transition length		145.0 (m) @ each end
sample track length		1200.0 (m)
Straight Track Lateral Irregularities		
track roughness	Ω_l	0.33e - 8 (m)
track spatial spectrum	S_T	$\Omega_l/f^3 \left(\frac{m^2}{(cycle/m)} \right)$
sample track length		1200.0 (m)

Table 8.3: Assessment of passive (tilt mechanism) vehicle @ 45(m/s)

DETERMINISTIC		
Lateral accel. (actual vs ideal)	- steady-state	8.89 (%g)
	- R.M.S. deviation error	1.49 (%g)
	- peak value	9.67 (%g)
Roll gyroscope	- R.M.S. deviation	0.007 (rad/s)
	- peak value	0.040 (rad/s)
P_{CT} (P-factor)	- peak jerk level	3.85 (%g/s)
	- standing	25.0 (% of passengers)
	- seated	6.73 (% of passengers)
STOCHASTIC		
passenger comfort	- ride quality	2.114 (%g)

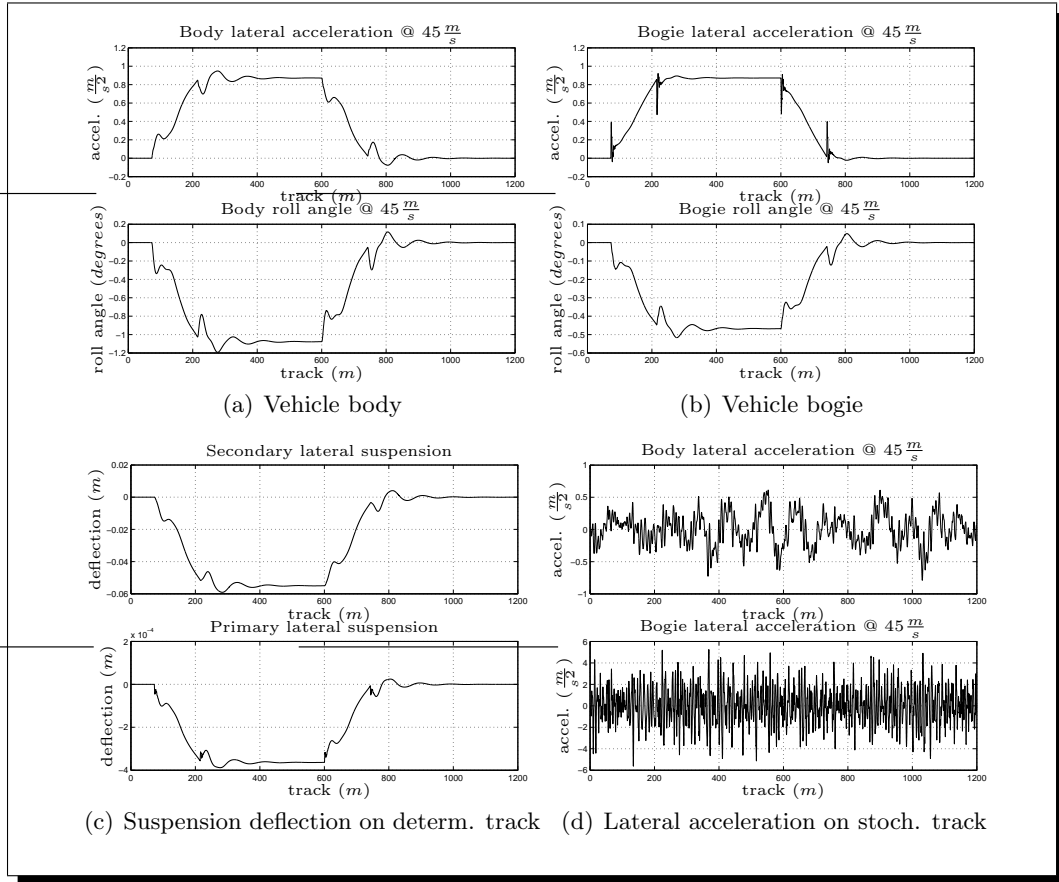


Figure 8.4: Simulations results for the passive (tilt mechanism) vehicle

Figure 8.4 presents a set of simulation results for the linear model for both the deterministic and stochastic case, with the track profile characteristics listed in Table 8.2. With the nominal vehicle speed assumed $v_o = 45 \frac{m}{s}$, the designed cant deficiency is $\frac{v_o^2}{R} - g\theta_o = 4.0^\circ$ or $0.686(\frac{m}{s^2})$. However, the steady-state body lateral acceleration is $0.8725(\frac{m}{s^2})$ due to the body roll-out of 1.1° , while the peak acceleration reaches a value of $0.95(\frac{m}{s^2})$ (Figure 8.4(a)). In the stochastic case, the R.M.S. value of the body lateral acceleration is $2.114(\%g)$. The overall assessment of the passive model is presented in Table 8.3 (previous page).

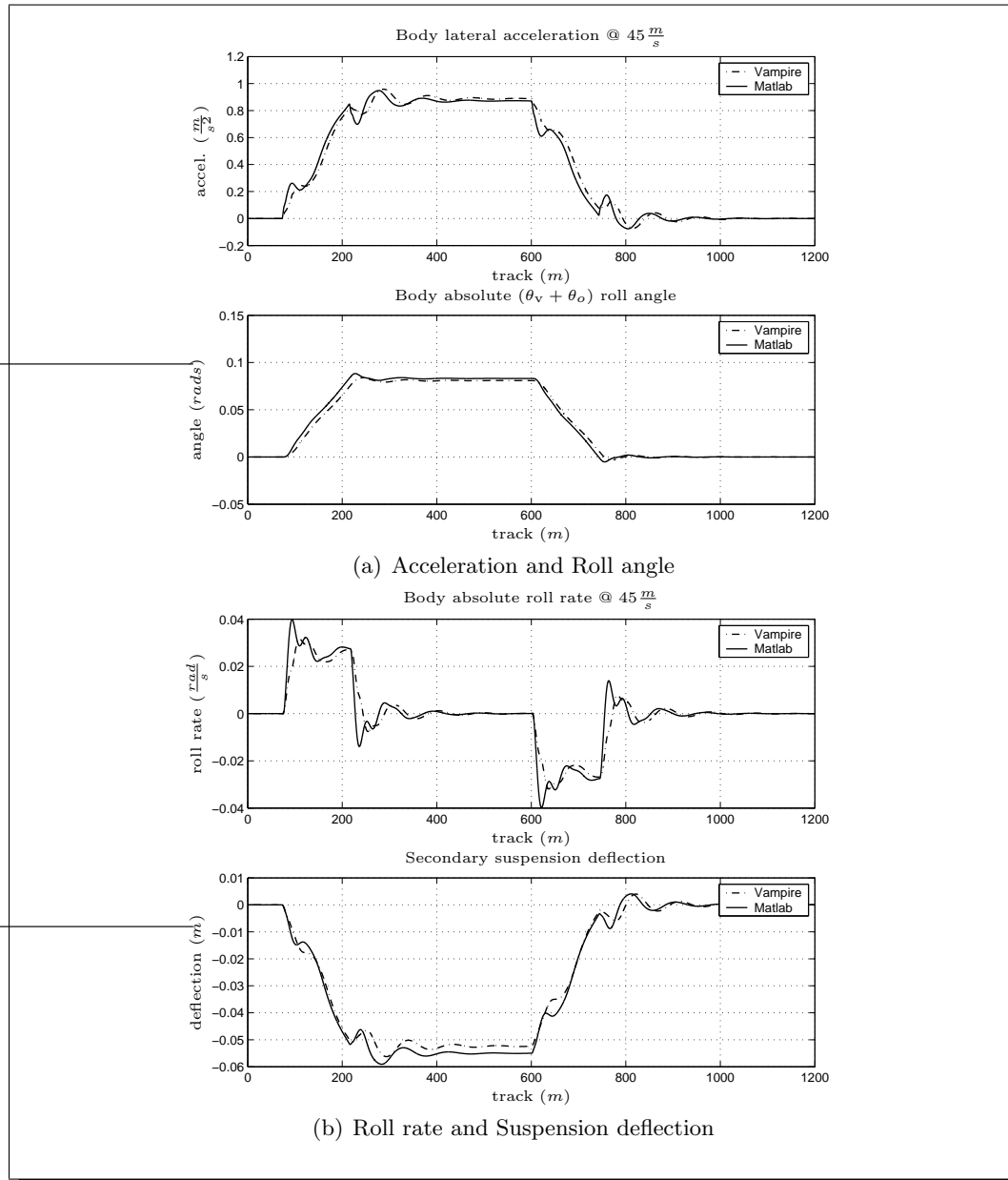


Figure 8.5: Comparison of Vampire (dash-dotted) and Matlab (solid) generated models for the deterministic case based on the vehicle body

In addition, the accuracy of the linear model was further verified via a comparison with the non-linear `vampire` model based on the above track profile for the deterministic case³. It can be easily seen from the results in Figure 8.5 (previous page) that the linearised model forms a very good approximation of the non-linear model structure.

8.3 Summary

This chapter discussed on the modelling of a vehicle structure with a tilting bolster used for active tilt control. It also presented an overview of tilting mechanisms used in railway vehicles. The developed linearised model was based upon a full non-linear vehicle generated in `Vampire` software package. Moreover, a series of transient tests demonstrated the compatibility between these two models, and shown that the linear approximation can be an effective basis for system analysis and control design.

³the stochastic track profile specified in `matlab` was found to be incompatible with `vampire`, thus a thorough comparison between the two models was not possible. For these reasons the stochastic track case was not considered.

Chapter 9

Control Studies for the Tilt Mechanism Application

This chapter describes the control strategies applied for the railway vehicle including the tilt mechanism. It includes an outline of the basic tilt control methods to accommodate the tilt mechanism, and also extends and adapts the advanced control concepts already implemented in the anti-roll bar case (Chapter 7), to the tilt mechanism model. Moreover, it extends the above advanced approaches to further improve the active tilt performance based upon the tilt mechanism.

9.1 Basic control approaches

The evolution of the basic control approaches to overcome the tilt control problems has been already presented in Chapter 6, the same applies in this case with minor adjustments to accommodate the tilt mechanism structure. The procedure is briefly illustrated for the *basic partial-nulling* and *basic precedence* strategies.

The tilt application for this model case is based upon 75% partial tilt compensation on steady curve at a high speed of 58(m/s), and relates to a nonlinear simulation study presented in [KE00]. The track profile is given in column ‘Mechanism (Case B)’ Table 4.1 on page 38 (it is also listed in Table 8.2 in the previous chapter).

9.1.1 Basic Partial-nulling control

The basic partial-nulling control structure for the mechanism model is depicted in Figure 9.1, which is very similar to the ARB model case in Chapter 6. However, the feedback signal, effective cant deficiency (9.1), now incorporates a portion of the

actuator roll angle, rather than the vehicle roll, which forms a more direct measurement of vehicle tilt (it is easier to fit sensors on the active elements of the vehicle, i.e. the tilt mechanism model in this case).

$$\theta'_{dmm} = -k_1 \frac{\ddot{y}_{vm}}{g} - k_2 \theta_a \quad (9.1)$$

where, $\ddot{y}_{vm} = \frac{v^2}{R} - g(\theta_o + \theta_v) + \ddot{y}_v$. For the purposes of 75% tilt compensation, factors k_1, k_2 were adjusted to 0.7652 and 0.2348 respectively in order to accommodate any discrepancies from the secondary suspension roll due to the remaining curving forces. For the explanation regarding the sign used for feedback the reader is referred to remark 6.1.1 on page 65 (replacing θ_{2sr} with θ_m).

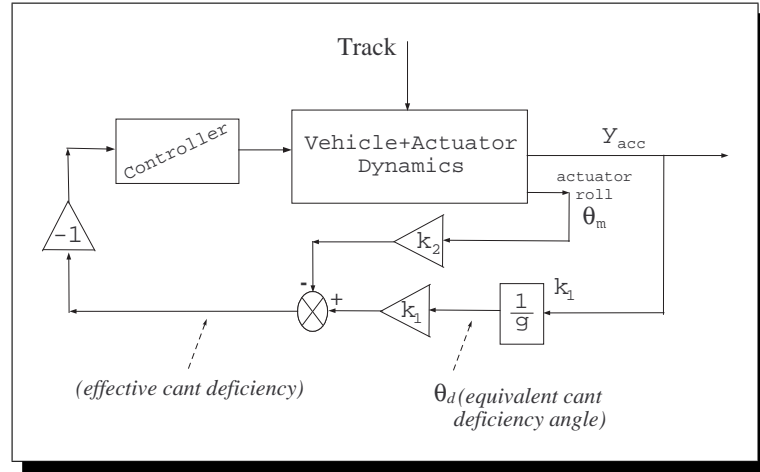


Figure 9.1: Basic partial-nulling scheme for vehicle with tilting bolster

The control input comprises the angular displacement (θ_{m_i}) provided by the tilting bolster, which in turns provides a rotary and an associated lateral displacement to the vehicle body. The uncompensated OL frequency response for the controller design is shown in Figure 9.2 and the system is still characterised by two RHP-zeros (a complex pair) at 5.08 ± 4.2 , which as described in earlier chapters limits the control design.

A typical controller design based upon classical methods would incorporate a P+I compensator (9.2), setting $k = 0.2, \tau = 0.4sec$, to guarantee the required steady-state tilt compensation and limit higher frequency phase lag due to the RHP zeros.

$$K_{PI}(s) = \frac{k(1 + s\tau)}{s\tau} \quad (9.2)$$

The resulted compensated OL together with the associated complementary sensitivity and sensitivity functions are shown in Figure 9.3(a) and Figure 9.3(b) respectively (page 141).

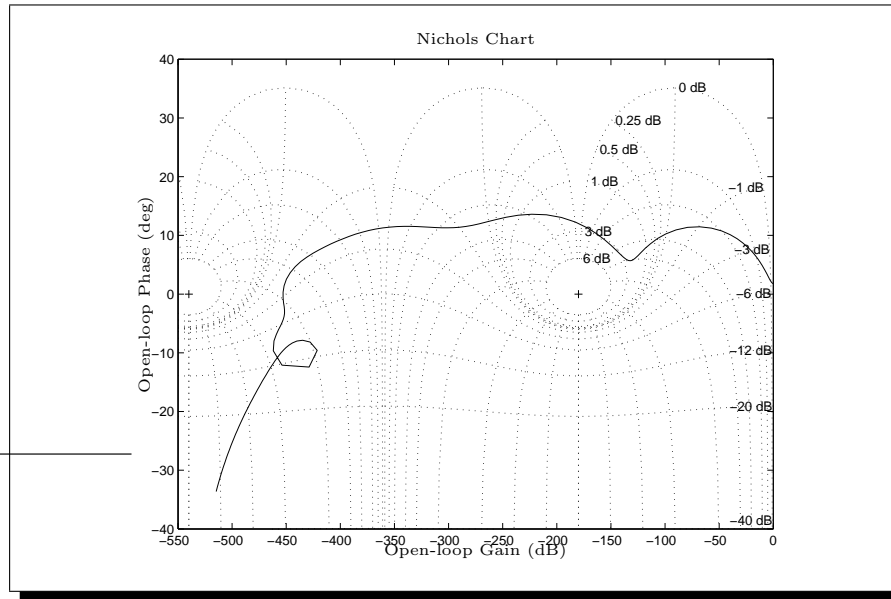


Figure 9.2: Uncompensated OL frequency response from u to effective cant deficiency

The time domain results are shown for the curved track in the set of Figure 9.4 and Figure 9.5 (page 142, 143), and the overall assessment in Table 9.1. The controller does not perform well (which is expected due to classical control limitations with this scheme), still failing to provide the steady-state value of tilt and including significant oscillations in the roll rates (poor gain margin).

Table 9.1: Mechanism basic nulling scheme assessment @ 58(m/s) - (PI approach)

DETERMINISTIC		
Lateral accel. (actual vs ideal)	- steady-state	n/a (%g)
	- R.M.S. deviation error	4.65 (%g)
	- peak value	13.02 (%g)
Roll gyroscope	- R.M.S. deviation	0.03 (rad/s)
	- peak value	0.093 (rad/s)
P_{CT} (P-factor)	- peak jerk level	6.95 (%g/s)
	- standing	47.87 (% of passengers)
	- seated	13.98 (% of passengers)
STOCHASTIC		
Passenger comfort	- R.M.S. passive (equiv.)	2.725 (%g)
	- R.M.S. active	2.888 (%g)
	- degradation	5.97 (%)

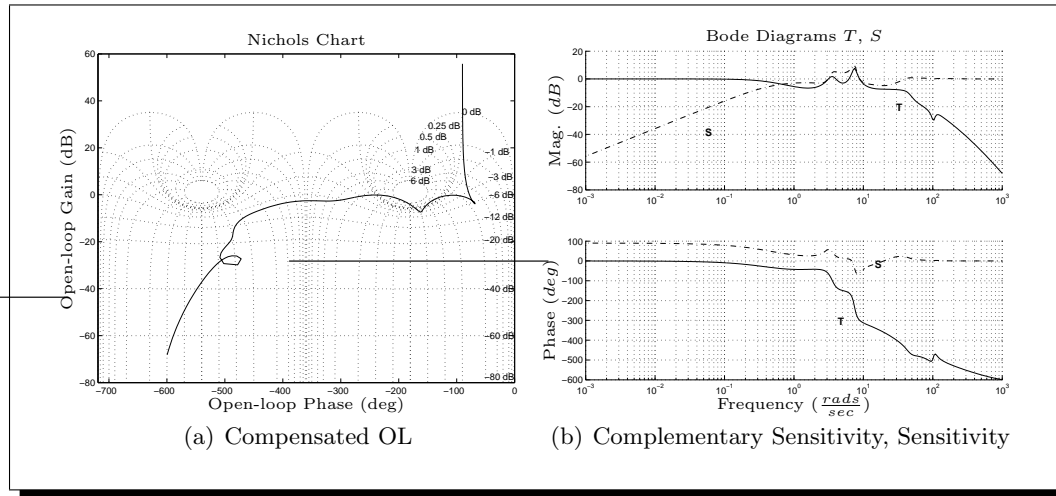


Figure 9.3: Basic nulling for mechanism, designed system frequency responses

9.1.2 Basic Command-Driven with Precedence Control

This scheme is used by all tilting train manufacturers, where the tilt signal in most cases is provided from the first vehicle and transmitted digitally with appropriate time delays to the rest of the coaches, see Figure 9.6(a).

In this case there is no need to include an extra feedback of tilt angle, which is taken in account by the mechanism itself which acts just like a servo (see Figure 8.3(b) on page 132). Simply, the mechanism output angle will closely follow the provided command input tilt command, subsequently providing the required tilt action to the vehicle body. Hence, the control design is redundant (unless a more complex design is extra required) and the only prerequisite is a prefilter to guarantee a tilt command for 75% compensation. The above idea is illustrated in Figure 9.6(b).

The designed prefilter involves a second order low pass filter to remove high frequencies from the bogie-based acceleration signal. An extra proportional term of $0.75/g$ converts the acceleration into cant deficiency and provides the command for 75% tilt compensation. The cut-off frequency of the low pass filter is set to 0.45Hz with damping factor equal to 0.707, which introduces a 0.5sec delay. Note that the preview time is chosen to match the filter delay for comparable results with all other localised control strategies, however it can be up to the designer to decide how much preview is needed for further improvement in tilt performance.

From an assessment point of view the results are in Table 9.2, and as in the ARB case

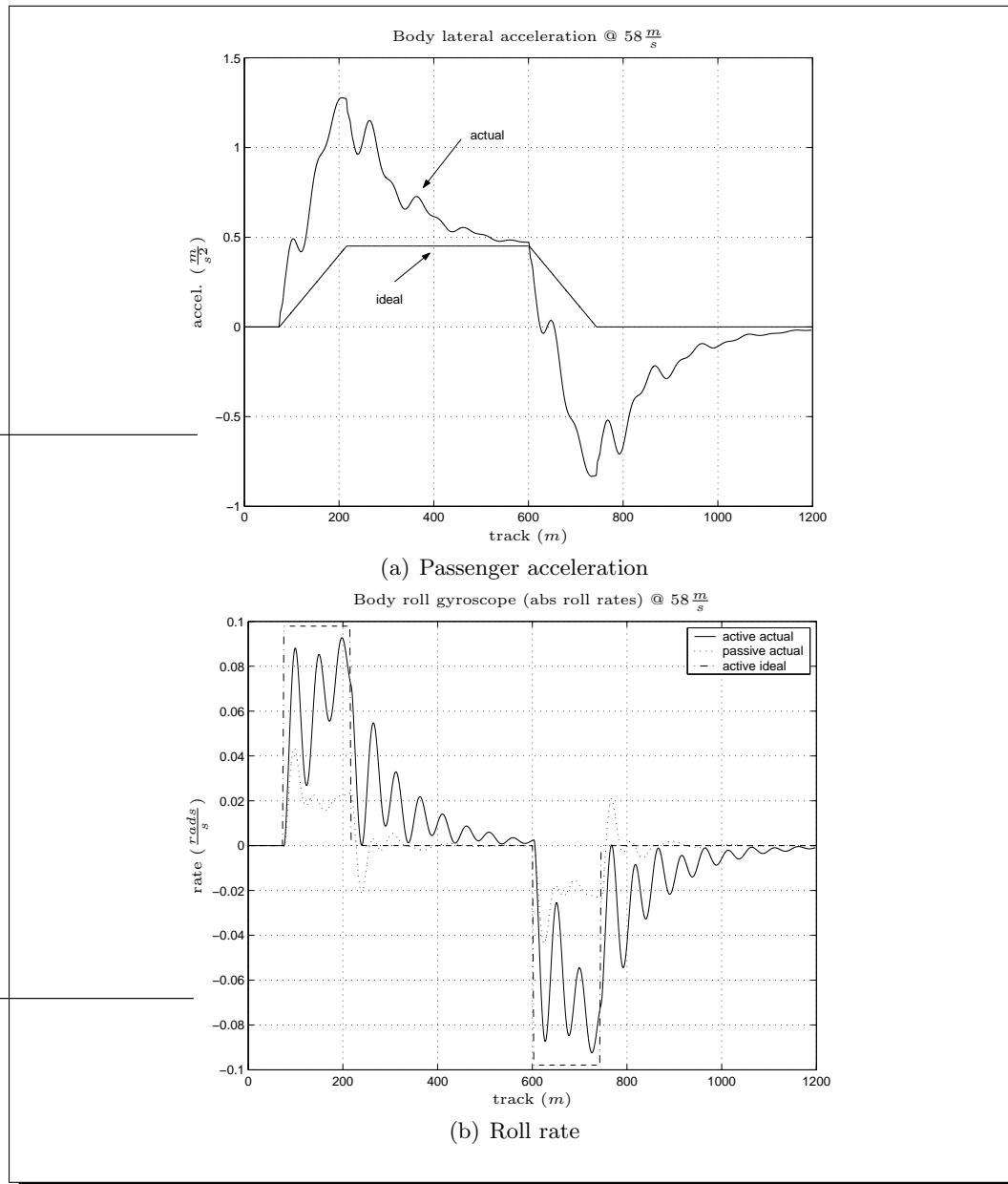


Figure 9.4: Mechanism basic nulling scheme with $P + I$ time history results (design track), set 1

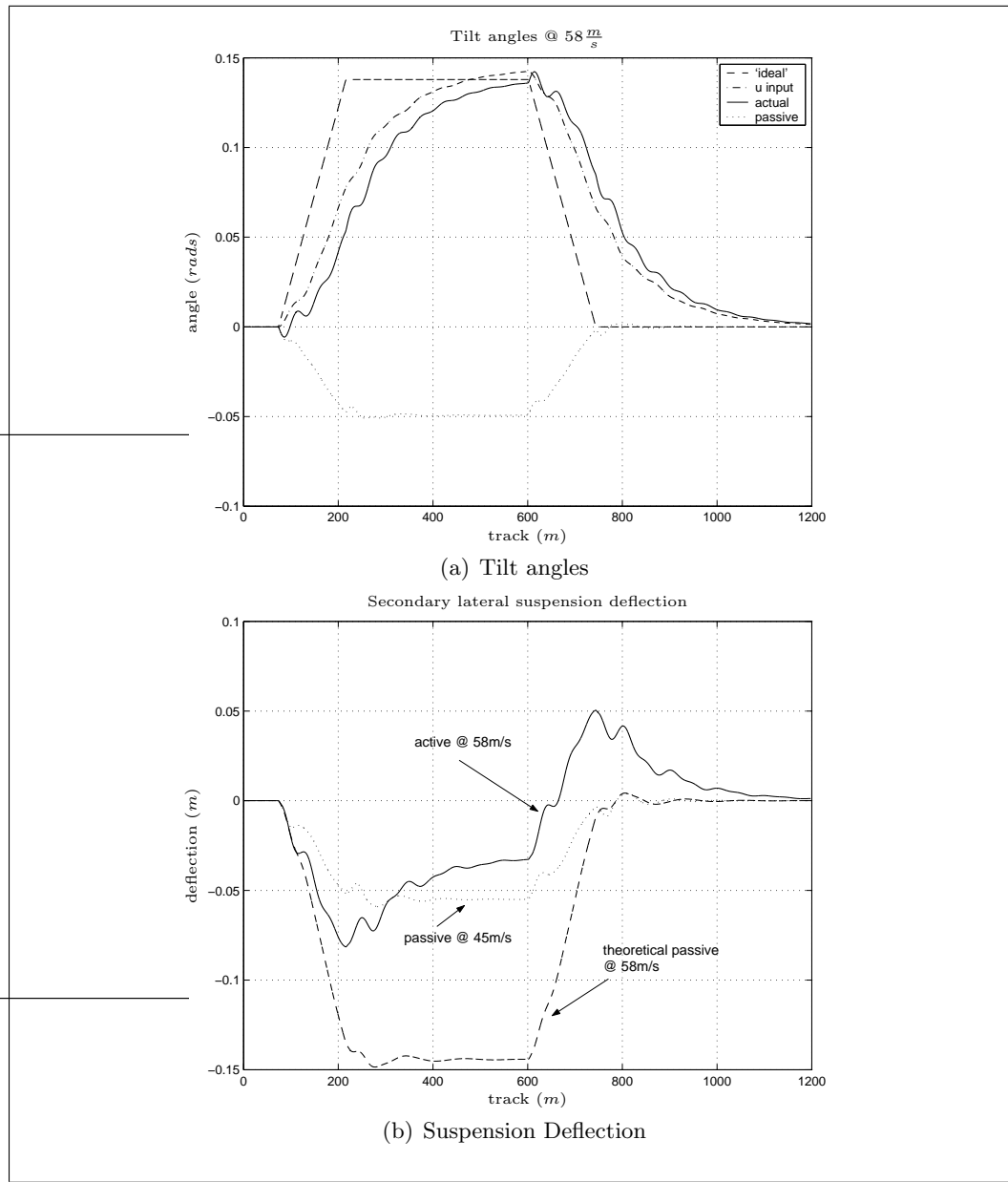


Figure 9.5: Mechanism basic nulling scheme with $P + I$ time history results (design track), set 2

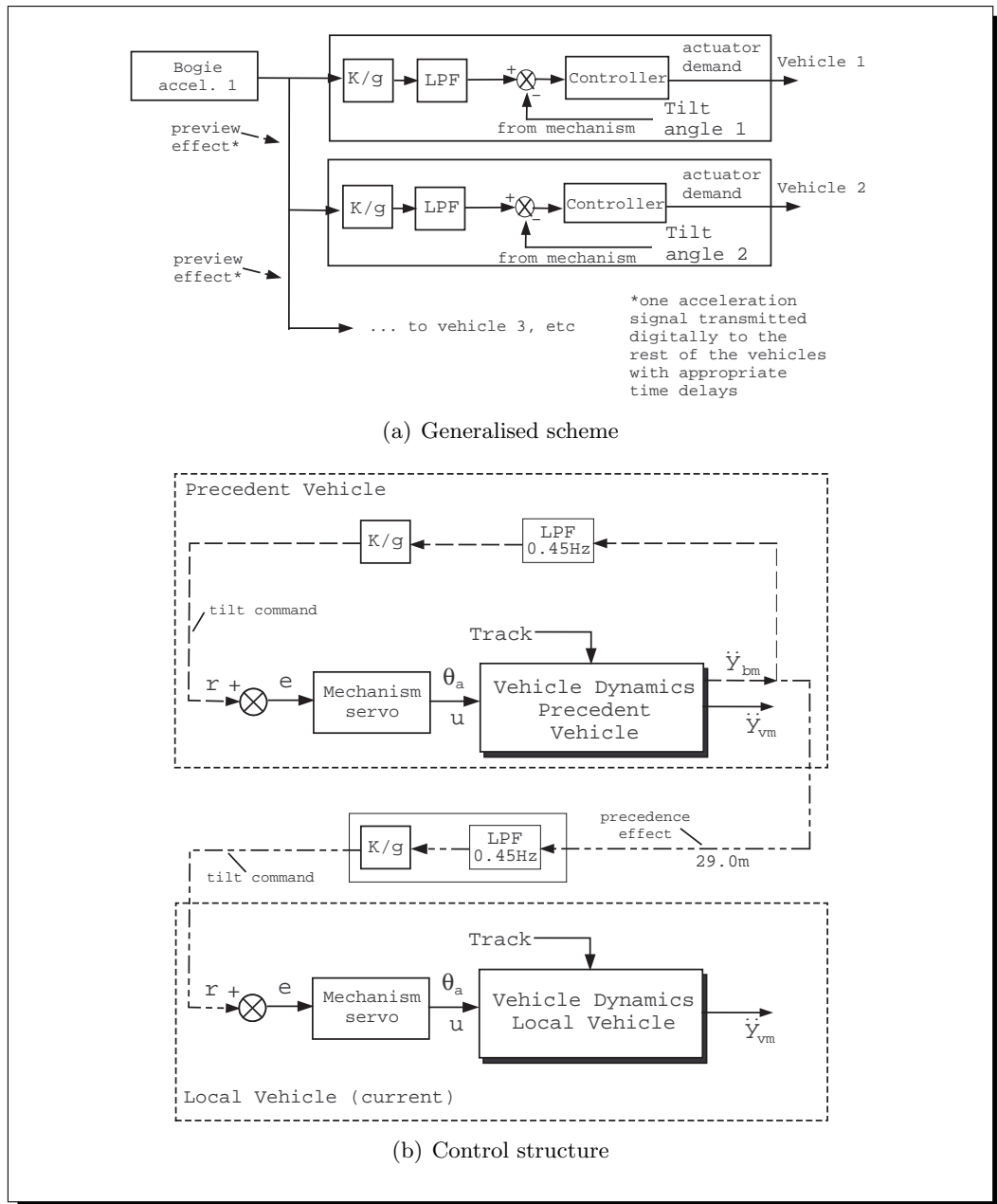


Figure 9.6: Mechanism Basic Precedence Tilt

performs very well for both curves and random track. In the latter case, the correlation between the input command and the random track input produces the best results (due to preview time = filter delay). The design track simulation results are shown in Figure 9.7, Figure 9.8 in the next pages. The advantage of using a mechanism can be seen from Figure 9.8(b), where the active system keeps the suspension deflection low compared to the theoretical passive configuration at the same speed. Moreover, Figure 9.8(a) illustrates how the body roll closely follows the mechanism tilt command. There are of course other more complex control approaches for such precedence scheme, however they are not a part of this thesis.

Table 9.2: Mechanism basic precedence scheme assessment @ 58(m/s)

DETERMINISTIC		
Lateral accel. (actual vs ideal)	- steady-state	4.6 (%g)
	- R.M.S. deviation error	0.725 (%g)
	- peak value	5.342 (%g)
Roll gyroscope	- R.M.S. deviation	0.015 (rad/s)
	- peak value	0.11 (rad/s)
P_{CT} (P-factor)	- peak jerk level	3.047 (%g/s)
	- standing	22.06 (% of passengers)
	- seated	4.04 (% of passengers)
STOCHASTIC		
Passenger comfort	- R.M.S. passive (equiv.)	3.122 (%g)
	- R.M.S. active	2.269 (%g)
	- degradation	-27.31 (%)

9.2 Advanced Control I (Modern Control)

This section presents the first part of the advanced control concepts proposed in this thesis, and presents the extension of the *LQR nulling* and *Model Based Estimation* for the mechanism model case.

9.2.1 LQR (Optimal P+I) Nulling Tilt Strategy for Tilt Mechanism Model

The concept of this scheme and also the theory behind it are well discussed in Chapter 7, and the following example presents how it can be adapted to work for the tilt mechanism model. The design makes use of output regulation, which is more a realistic approach, however state regulation can be also employed if required.

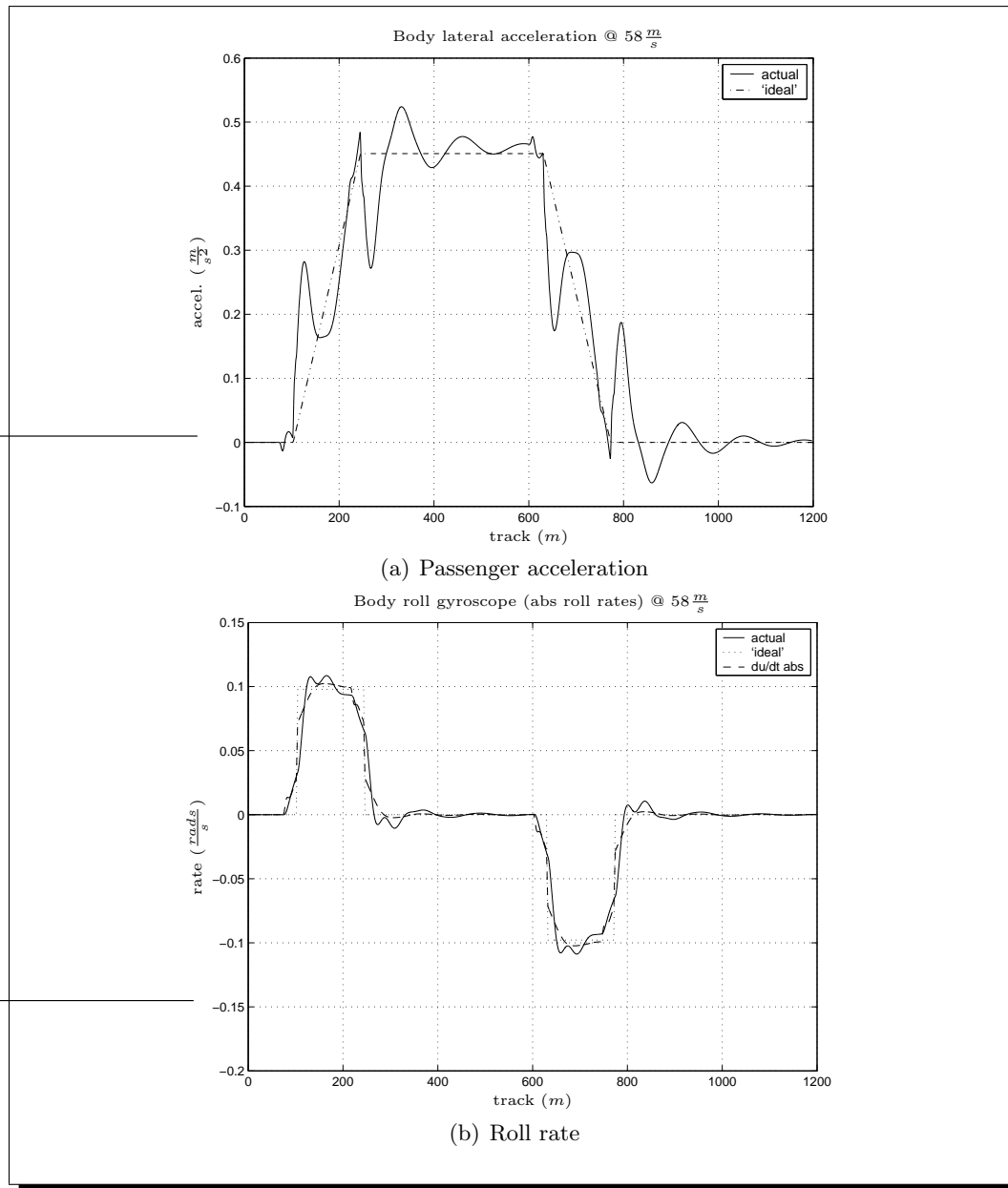


Figure 9.7: Mechanism basic precedence scheme time history results (design track), set 1

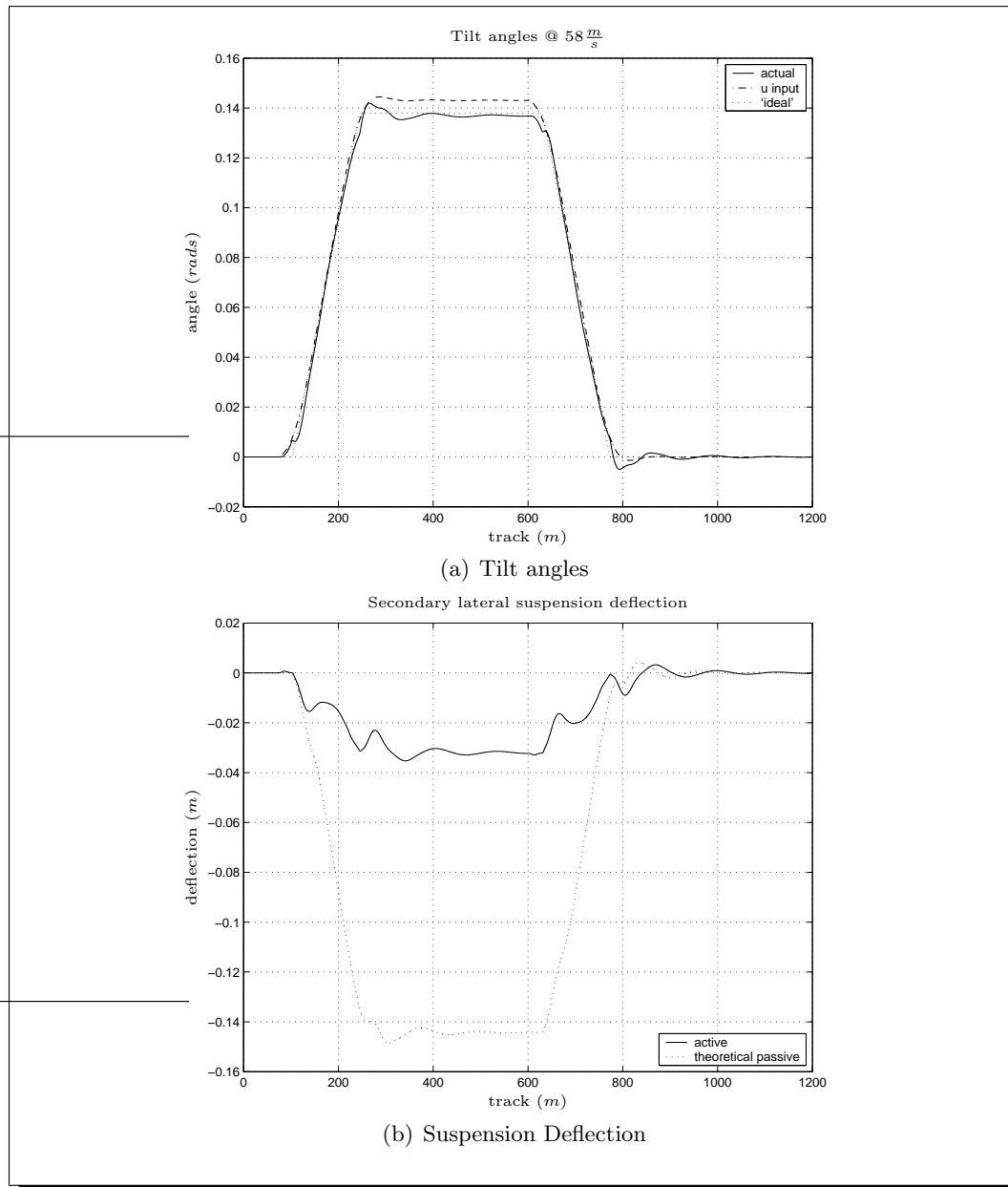


Figure 9.8: Mechanism basic precedence scheme time history results (design track), set 2

For correct tilt compensation and also good disturbance rejection, the required extra state introduced is the *effective cant deficiency* based upon the mechanism model (9.3). This structure results in an optimal P+I controller.

$$\theta'_{dmm} = -k_1 \frac{\ddot{y}_{vm}}{g} - k_2 \theta_m \quad (9.3)$$

where, $k_1 = 0.75$, $k_2 = 0.25$ and $\ddot{y}_{vm} = \frac{v^2}{R} - g(\theta_o + \theta_v) + \ddot{y}_v$. Thus the augmented system is now of the form

$$\begin{pmatrix} \dot{\mathbf{x}} \\ \dot{\mathbf{x}}' \end{pmatrix} = \begin{pmatrix} \mathbf{A} & 0 \\ \mathbf{C}' & 0 \end{pmatrix} \begin{pmatrix} \mathbf{x} \\ \mathbf{x}' \end{pmatrix} + \begin{pmatrix} \mathbf{B} \\ 0 \end{pmatrix} \mathbf{u} \quad (9.4)$$

where $\mathbf{x}' = \int \theta'_{dmm}$ and \mathbf{C}' is the selector matrix for integral action and is found from $\theta'_{dmm} = \mathbf{C}' \mathbf{x}$. All the above are based upon the state space matrices for the vehicle model with the tilt mechanism listed in Appendix E.2. Note that the state vector \mathbf{x} now includes the following vehicle states (for the new model):

$$\left[y_v \quad \theta_v \quad y_b \quad \theta_b \quad \dot{y}_v \quad \dot{\theta}_v \quad \dot{y}_b \quad \dot{\theta}_b \quad \theta_r \quad y_{es} \quad y_w \quad \dot{y}_w \quad \theta_m \quad \dot{\theta}_m \right]^T$$

and also $\mathbf{u} = [\theta_{m_i}]$. The control signal is

$$\mathbf{u} = - \begin{pmatrix} K_p & K_i \end{pmatrix} \begin{pmatrix} \mathbf{x} \\ \mathbf{x}' \end{pmatrix} \quad (9.5)$$

and the quadratic performance index for output regulation is

$$J = \lim_{T \rightarrow \infty} \frac{1}{T} E \left\{ \int_0^T [\mathbf{y}^T \mathbf{Q}_o \mathbf{y} + \mathbf{u}^T \mathbf{R}_k \mathbf{u}] d\tau \right\} \quad (9.6)$$

where $\mathbf{y} = [(\dot{\theta}_v - \dot{\theta}_m), \int \theta'_{dmm}]$ and $\mathbf{u} = \theta_{m_i}$. The weight of $\int \theta'_{dmm}$ emphasises the system speed, while the weight of $(\dot{\theta}_v - \dot{\theta}_m)$ minimises the oscillations between body-mechanism (recall that the secondary suspensions are situated on top of the bolster).

The weights Q_o, R_k were initially set to represent the square of the inverse of the expected value, $\frac{1}{(\text{expected value})^2}$, for each parameter of interest. The controller can be easily designed by varying the above weights until a satisfactory design arises. The tuning process is the same as the one followed in the ARB case, and this section only illustrates the results from the best system design.

The weights for the best design were set to the following values

$$Q_o = \begin{pmatrix} \frac{1}{0.5^2} & 0 \\ 0 & \frac{1}{0.05^2} \end{pmatrix}, \quad R_k = \frac{1}{0.14^2}$$

making the corresponding performance index to be minimised equal to

$$J = \lim_{T \rightarrow \infty} \frac{1}{T} E \left\{ \int_0^T \left(\frac{1}{0.5^2} (\dot{\theta}_v - \dot{\theta}_m) + \frac{1}{0.05^2} \int \theta'_{dmm} + \frac{1}{0.14^2} u^2 \right) d\tau \right\} \quad (9.7)$$

and finally the optimal gain for this above setup was found to be ($K_r = [K_p \ K_i]$)

$$K_r = [.94 \ -1.8 \ .25 \ -.07 \ .43 \ .075 \ .006 \ .015 \ .131 \ -.16 \ .06 \ -.004 \ 2.53 \ .26 \ -2.8] \quad (9.8)$$

The controller assessment in Table 9.3 shows that this scheme works well for the mechanism model, even if it is based upon the nulling approach. The controller can also accommodate all low frequency elements in the random track offering an improved ride quality. The designed OL singular value plot can be seen in Figure 9.9(c), while the tilt performance is illustrated in Figure 9.9(a) and Figure 9.9(b). In addition, the choice of the relative body roll-mechanism roll rates proved effective in minimising unwanted oscillations.

Table 9.3: Mechanism LQR+I advanced control scheme assessment @ 58(m/s)

DETERMINISTIC		
Lateral accel. (actual vs ideal)	- steady-state	4.6 (%g)
	- R.M.S. deviation error	2.34 (%g)
	- peak value	9.34 (%g)
Roll gyroscope	- R.M.S. deviation	0.02 (rad/s)
	- peak value	0.1 (rad/s)
P_{CT} (P-factor)	- peak jerk level	5.05 (%g/s)
	- standing	34.9 (% of passengers)
	- seated	9.11 (% of passengers)
STOCHASTIC		
Passenger comfort	- R.M.S. passive (equiv.)	3.2 (%g)
	- R.M.S. active	3.0 (%g)
	- degradation	-5.86 (%)

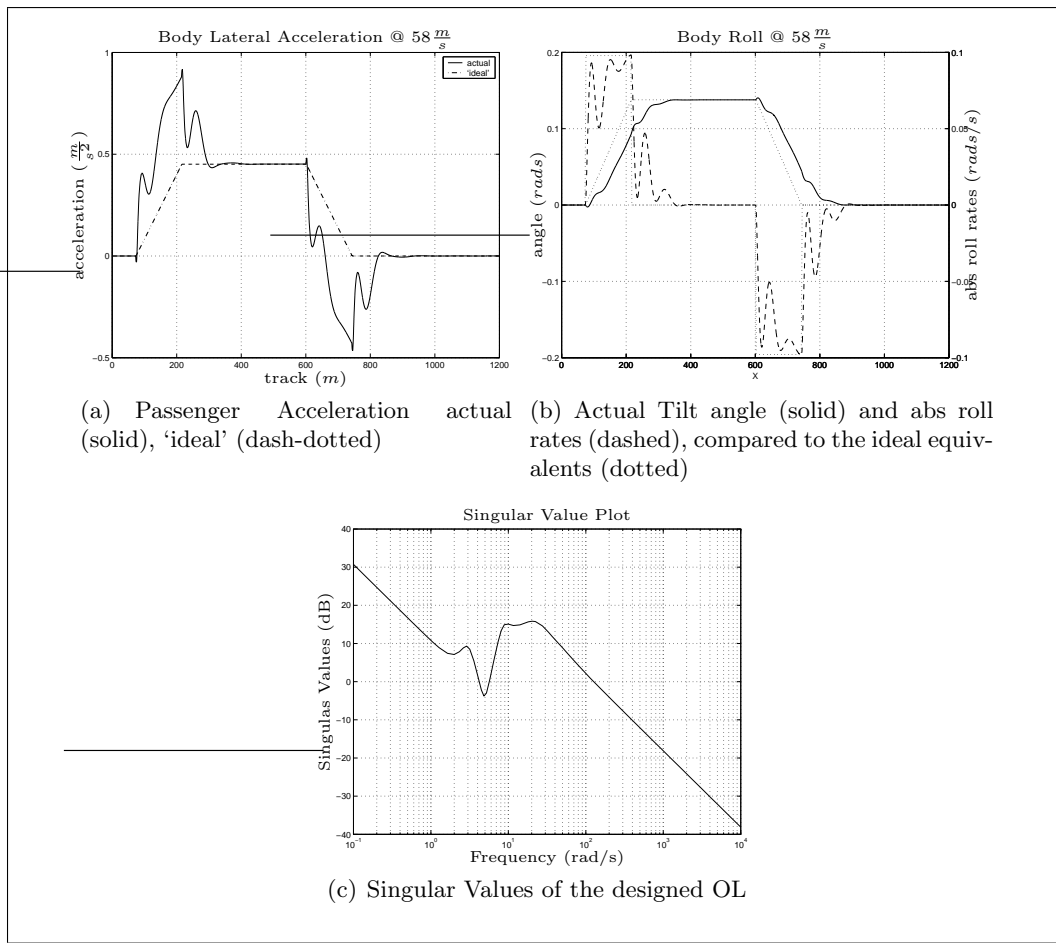


Figure 9.9: Mechanism advanced LQR+Integral scheme results (design track)

9.2.2 Extension of Model-Based Estimation Control for Tilt Mechanism Model

This work extends the successful MBE control scheme, designed for the ARB model, to apply in the vehicle model with the tilt mechanism [ZGH01]. It should be noted that the true cant deficiency signal for the mechanism case is given by

$$\theta_{tdm} = \frac{v^2}{gR} - (\theta_o + \theta_m) \quad (9.9)$$

which employs the mechanism roll as a measurement of tilt angle rather than the body roll itself.

The design of the Kalman estimator is very similar to the one followed in Section 7.3, however there are some different aspects to be considered with the new model structure for controller design and those are presented below.

• Estimator Design

The estimator design was again based upon three sensors measuring: body lateral acceleration, body absolute roll rate and body yaw rate. Recall, that the system should be re-formulated to include a set of track signals as states for correct estimation of the feedback signals. The procedure is identical to the ARB case (see section 7.3), with the model matrices in this case corresponding to the new model with the mechanism. Note that the state vector of the re-formulated system now holds the following states

$$x_k = \left[y_v \quad \theta_v \quad y_b \quad \theta_b \quad \dot{y}_v \quad \dot{\theta}_v \quad \dot{y}_b \quad \dot{\theta}_b \quad \theta_r \quad y_{es} \quad y_w \quad \dot{y}_w \quad \theta_m \quad \dot{\theta}_m \quad \theta_o \quad \dot{\theta}_o \quad R^{-1} \right]^T \quad (9.10)$$

and also the process noise is characterised by

$$w_k = \left[\dot{R}^{-1} \quad \ddot{\theta}_o \right]^T \quad (9.11)$$

The values for matrices R_{kf} , Q_{kf} were set, based upon the guide of page 95, as follows

$$R_{kf} = \begin{bmatrix} 1.1e-3 & 0 & 0 \\ 0 & 1.42e-6 & 0 \\ 0 & 0 & 1e-6 \end{bmatrix}, \quad Q_{kf} = \begin{bmatrix} 8.3-6 & 0 \\ 0 & 8.32e-4 \end{bmatrix} \quad (9.12)$$

which provided the best estimator design results (see Figure 9.10). The Kalman gain was given by

$$K_f = P_f C^T V^{-1} \quad (9.13)$$

where P_f is the unique positive semi-definite, $P_f = P_f^T \geq 0$, of the following algebraic Riccati equation

$$P_f A^T + A P_f - P_f C^T V^{-1} C P_f + \Gamma W \Gamma^T = 0 \quad (9.14)$$

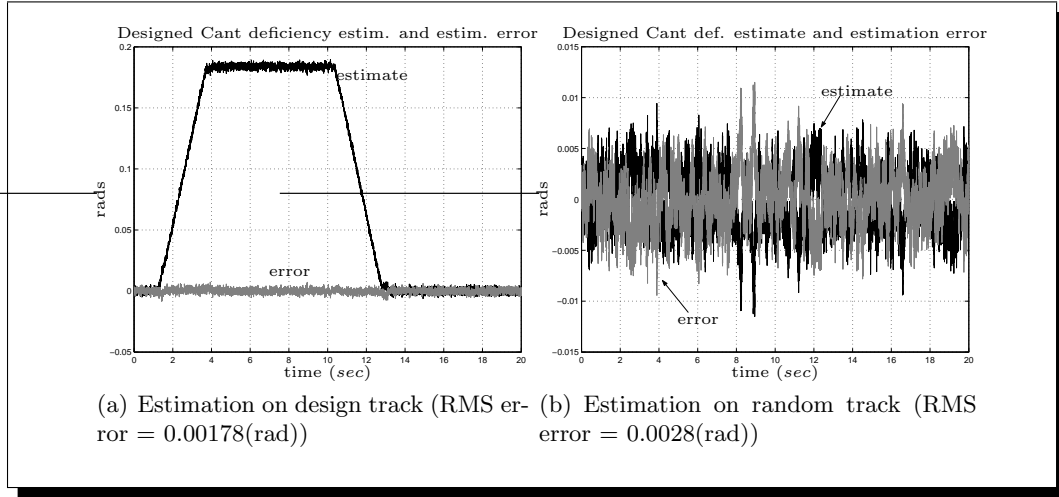


Figure 9.10: ‘True’ cant deficiency estimate

and the values obtained for the current configuration were

$$K_f = \begin{bmatrix} -0.289 & -3.734 & -0.304 \\ -0.102 & -2.952 & 0.0125 \\ -0.0112 & -0.219 & -0.246 \\ -0.0464 & -1.121 & -0.0193 \\ -1.519 & 1.889 & -57.62 \\ -0.4879 & -1.85 & -0.0758 \\ 0.0592 & -0.575 & -41.41 \\ -0.22 & -1.561 & -4.244 \\ -0.0737 & -2.11 & -0.014 \\ -0.0254 & -0.491 & -0.275 \\ -3.698e-015 & -2.1306e-015 & -2.0679e-013 \\ 1.605e-013 & 6.4297e-013 & 1.6618e-012 \\ 4.178e-015 & -2.1598e-014 & -4.2143e-013 \\ -4.339e-014 & 1.4898e-013 & 1.3174e-012 \\ 0.0735 & 4.55 & -0.00767 \\ 0.523 & 19.39 & -0.0627 \\ 0.000396 & -0.00169 & 2.886 \end{bmatrix} \quad (9.15)$$

The results can be seen in Figure 9.10 (sensor noise is included) and are very close to the true values. The estimation error is mainly due to the sensor noise levels (plus a

small percentage due to the effect of the stochastic track signals). The signal employed is the designed cant deficiency estimate, i.e. $\frac{v^2}{gR} - \hat{\theta}_o$ because still the passive model is used. The estimator can now be used for further control design.

• Tilt Controller Design based upon Model Based Estimator

The control scheme applied in this section is depicted in Figure 9.11 where two loops are employed: the main loop for tilt performance and the secondary loop for suppressing unwanted oscillations. The main loop incorporates the feedback signal required for 75% tilt compensation

$$\hat{\theta}'_{tdm} = 0.78 \frac{v^2}{gR} - (0.78\hat{\theta}_o + \hat{\theta}_t) \quad (9.16)$$

where $\hat{\theta}_t$ in this case is the actual roll angle of the tilt mechanism $:= \theta_m$. The secondary loop uses the estimate of the absolute body roll rate ($\hat{\theta}_v + \hat{\theta}_o$). Initially only the main loop was considered, however trials with the secondary loop shown that the overall performance is much improved. Note that the compensation factor in (9.16) was set to 0.78 to accommodate the remaining 25% of uncompensated acceleration on the vehicle body, which forces the body to roll slightly out compared to the mechanism.

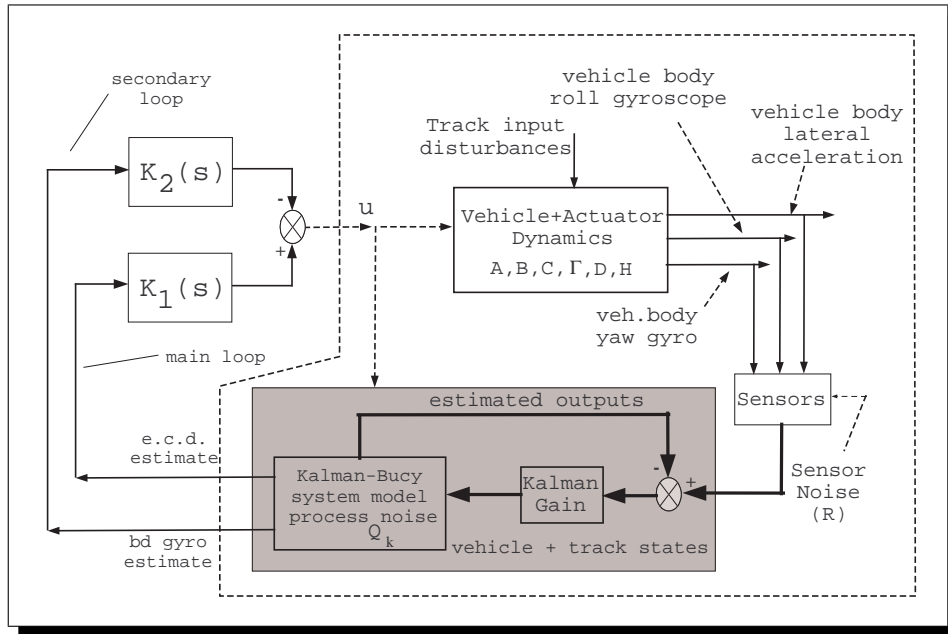


Figure 9.11: MBE-based control approach for tilt mechanism model

The main loop incorporates a P+I control configuration, $K_1(s)$ (9.17), for zero steady-state error. The secondary loop involves a P+D controller, $K_2(s)$ (9.18), to feedback

a portion of the absolute body roll rate to the system and improve the transient behaviour. Note that the main loop is closed using positive feedback due to the notation used, i.e. positive tilt angle is required to tilt the body inwards.

$$K_1(s) = \frac{0.675s + 2.25}{0.3s} \tag{9.17}$$

$$K_2(s) = \frac{0.01s + 0.2}{0.01s + 1} \tag{9.18}$$

Figure 9.12 illustrate the uncompensated and compensated open loop for the main and the secondary loop respectively. In reality only the mechanism roll incorporates dynamics in the system and the design is based upon that, the other two signals in the true e.c.d. do not have any associated dynamics. Moreover, the closed loop system for the main loop can be seen in Figure 9.13 (improved CL bandwidth compared to the previous schemes). Note that the Kalman filter is already incorporated in the system.

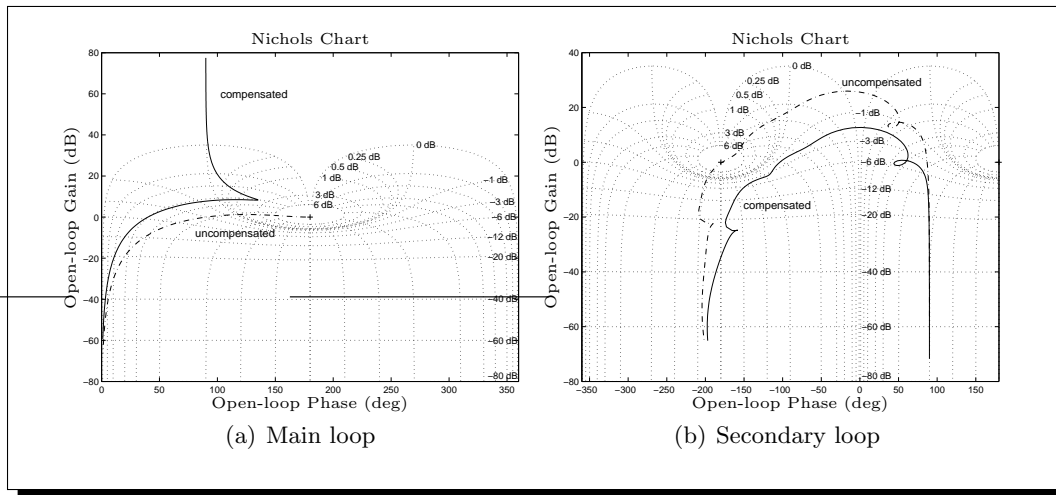


Figure 9.12: MBE control design - Open loop

Figure 9.14, page 156, illustrates the performance of the controlled system on design track in the time domain. The body roll smoothly achieves the required amount of required tilt $0.138(rads)$ approx. 7.9° , as expected (recall that this scheme mimics the precedence-type)¹.

However, there are still oscillations on the acceleration felt by the passengers due to the secondary suspension. Some of the oscillations can be accommodated by increasing the complexity of the overall controller, however an extra active element is the ideal

¹The mechanism will roll slightly more in order to force the required body tilt angle, due to the remaining 25% uncompensated cant deficiency forces (approximately 0.35° more).

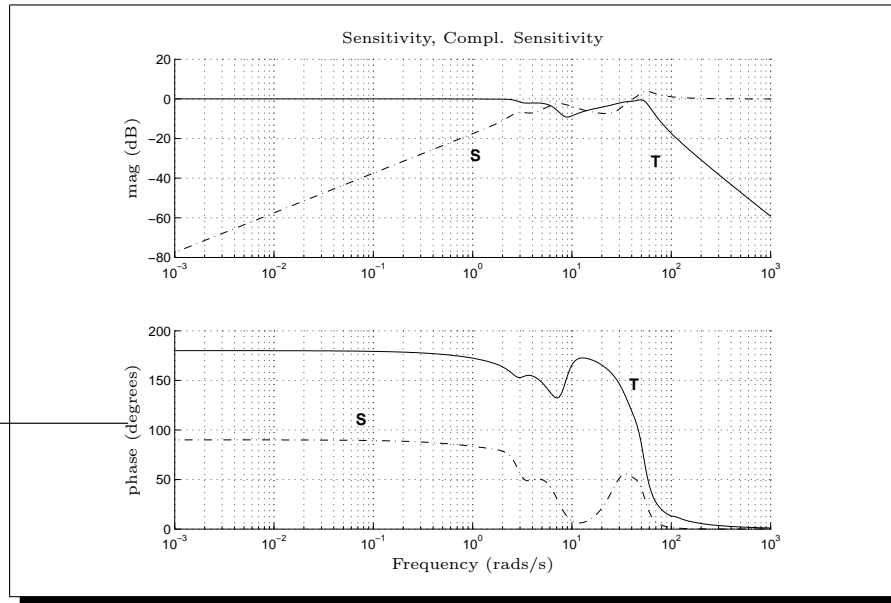


Figure 9.13: Main Closed Loop designed system

solution for this problem.

The assessment in Table 9.4 on page 156 reveals in more details the performance of the controller. It can be seen that the designed system performs well in both design and random track. It actually provides improved ride quality, while maintaining very good passenger comfort on curve transition. Note that the system does not include sensor noise for correct comparison with all other schemes. However, sensor noise does not have a significant effect on the controller performance and all above characteristics are maintained.

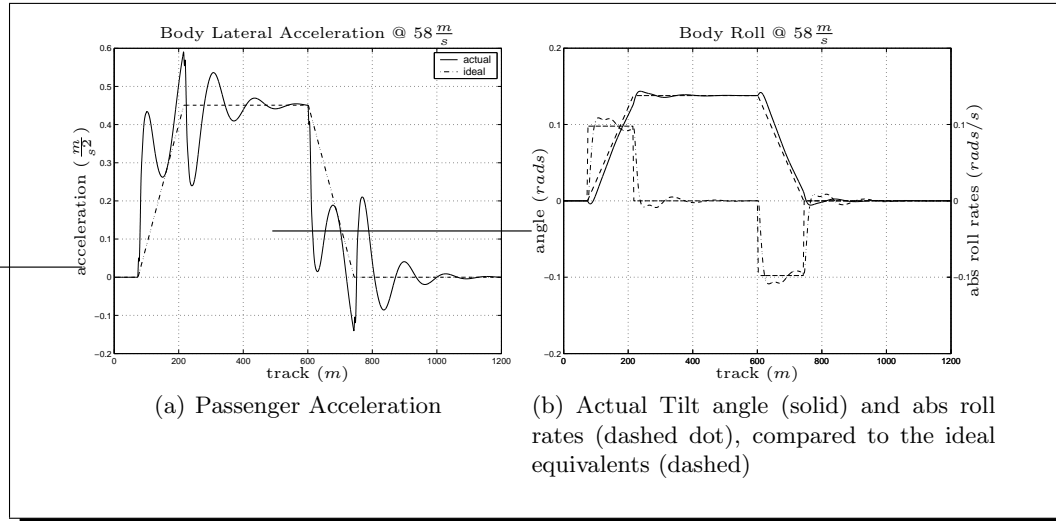


Figure 9.14: Mechanism advanced MBE scheme results (design track)

Table 9.4: MBE-based advanced control scheme assessment @ 58(m/s)

DETERMINISTIC		
Lateral accel. (actual vs ideal)	- steady-state	4.6 (%g)
	- R.M.S. deviation error	1.23 (%g)
	- peak value	6.02 (%g)
Roll gyroscope	- R.M.S. deviation	0.018 (rad/s)
	- peak value	0.109 (rad/s)
P_{CT} (P-factor)	- peak jerk level	4.42 (%g/s)
	- standing	26.78 (% of passengers)
	- seated	5.95 (% of passengers)
STOCHASTIC		
Passenger comfort	- R.M.S. passive (equiv.)	3.2 (%g)
	- R.M.S. active	3.04 (%g)
	- degradation	-4.89 (%)

9.3 Advanced Control II (Post-Modern Control)

Previous work presented in Chapter 7 involved mixed sensitivity and also a multi-objective approach within the \mathcal{H}_∞ framework for the ARB model. Those designs incorporated the formulation of the control problem in closed-loop and as such the weights selection proved a difficult task. Studies in this section are based upon a robust control approach proposed in [MG90], which makes use of \mathcal{H}_∞ methods to provide robust stability in an open loop shaping framework to achieve certain specifications for the closed loop system.

9.3.1 \mathcal{H}_∞ Loop Shaping Robust-Control Design via the Co-Prime Factorization Method

The design of the controller was based on the normalized coprime-factor plant description introduced by McFarlane and Glover [MG90]. In this method, the nominal plant is factored as $G = M^{-1}(s)N(s)$, where $M(s)$ and $N(s)$ are stable transfer functions representing a left coprime factorization of $G(s)$. Coprime factorizations are not unique; however, it is always possible to make the factors $M(s)$ and $N(s)$ essentially unique (i.e. unique up to left multiplication by a unitary matrix), by forcing them to satisfy the normalization equation $NN^* + MM^* = I$. In this setting, the perturbed plant is described by the set:

$$G_\Delta = \{(M + \Delta_M)^{-1}(N + \Delta_N) \mid \|[\Delta_M \ \Delta_N]\|_\epsilon < \epsilon\} \quad (9.19)$$

where ϵ quantifies the “size” of model uncertainty. In the context of robust stabilization, left and right coprime factor descriptions were first proposed by Vidyasagar [Vid85]. Their main advantage over alternative descriptions of unstructured uncertainty (e.g. additive, multiplicative, etc) is that the corresponding robust-stabilisation results are free from the assumption that the nominal and perturbed systems have the same number of poles in the right-half plane. The robust-stabilization problem associated with (9.19) can now be posed as follows: “*Given a fixed ϵ , does there exist a feedback controller $K(s)$ which internally stabilizes the closed-loop system of Figure 9.15 for every $G \in G_\Delta$?*”. The corresponding maximum robust stabilization problem is: “*Find the largest $\epsilon = \epsilon_o$ so that the feedback loop of Figure 9.15 is internally stable for all $G \in G_\Delta$, and the corresponding set of all optimal controllers $K(s)$* ”.

It turns out that, when the normalization condition is imposed on the coprime factors, the two problems have surprisingly simple solutions. In particular, the maximum stability radius ϵ_o and the set of all optimal controllers can be obtained in closed form, i.e.

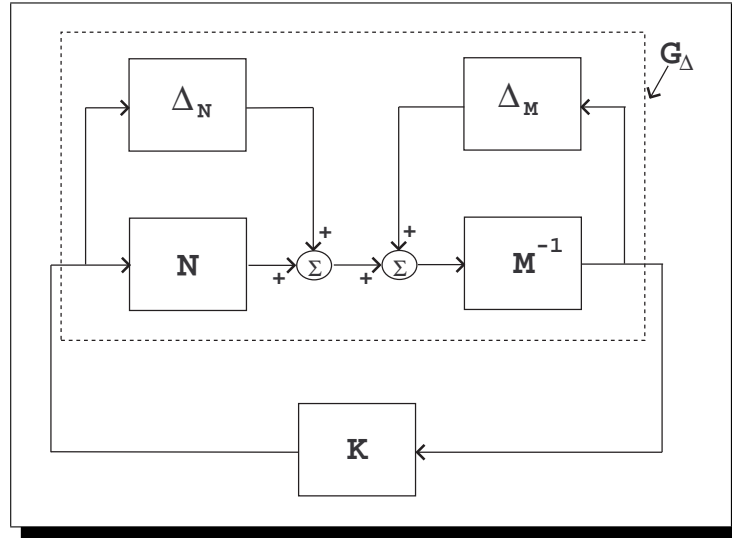


Figure 9.15: Coprime factor robust stabilisation problem

without the need to carry out an iterative procedure (“ γ -iteration”), typically characterising \mathcal{H}_∞ problems of this type. If one insists on the exact optimal solution however, the derivation of a state-space realisation for the optimal controller is slightly complicated due to a pole/zero cancellation phenomenon occurring at optimality [MG90]; in this case, a singular perturbation procedure is needed to obtain the required realizations. To avoid this procedure, a slightly sub-optimal approach can be adopted, by setting the robust-stabilization radius to $\epsilon = (1 - \delta)\epsilon_o$, where $\delta = 0.01$. The corresponding (slightly sub-optimal) controller has one state that is almost non-minimal, and can be removed with minimal effect on the controller’s frequency-response characteristics.

The solution to the normalized coprime-factor robust stabilization problem is summarized by the following result [MG90]:

Theorem 9.3.1. [McFarlane & Glover]: Let $G(s)$ have a minimal state-space realization (A, B, C, D) and let X and Z be the unique stabilizing solutions to the generalized control and filtering algebraic Riccati equations,

$$(A - BS^{-1}D^*C)^*X + X(A - BS^{-1}D^*C) - XBS^{-1}B^*X + C^*R^{-1}C = 0$$

and

$$(A - BD^*R^{-1}C)Z + Z(A_BD^*R^{-1}C)^* - ZC^*R^{-1}CZ + BS^{-1}B^*$$

respectively, where $R = I + DD^*$ and $S = I + D^*D$. Define further the control gain matrix $F = -S^{-1}(D^*C + B^*X)$. Then:

- (i). The maximum robust stability radius is given by $\epsilon_o = (1 + \lambda_{max}(ZX))^{-\frac{1}{2}}$.
- (ii). For each $\epsilon < \epsilon_o$ the ϵ -suboptimal central controller has a state-space realization (A_k, B_k, C_k, D_k) where $A_k = A + BF + \epsilon^{-2}W_1^{-*}ZC^*(C + DF)$, $B_k = \epsilon^{-2}W_1^{-*}ZC^*$, $C_k = B^*F$ and $D_k = -D^*$, in which $W_1 = I + (XZ - \epsilon^{-2}I)$.

The design procedure based on this method proceeds by shaping the open-loop characteristics of the plant by means of a weighting function $W(s)$ (see Figure Figure 9.16(a)). The plant is temporarily redefined as $\hat{G}(s) = W(s)G(s)$ and Theorem 9.3.1 is applied to \hat{G} to find the \mathcal{H}_∞ optimal controller $\hat{K}(s)$; finally the weighting function is absorbed into the controller by defining $K(s) = \hat{K}(s)W(s)$ as shown in Figure 9.16(b).

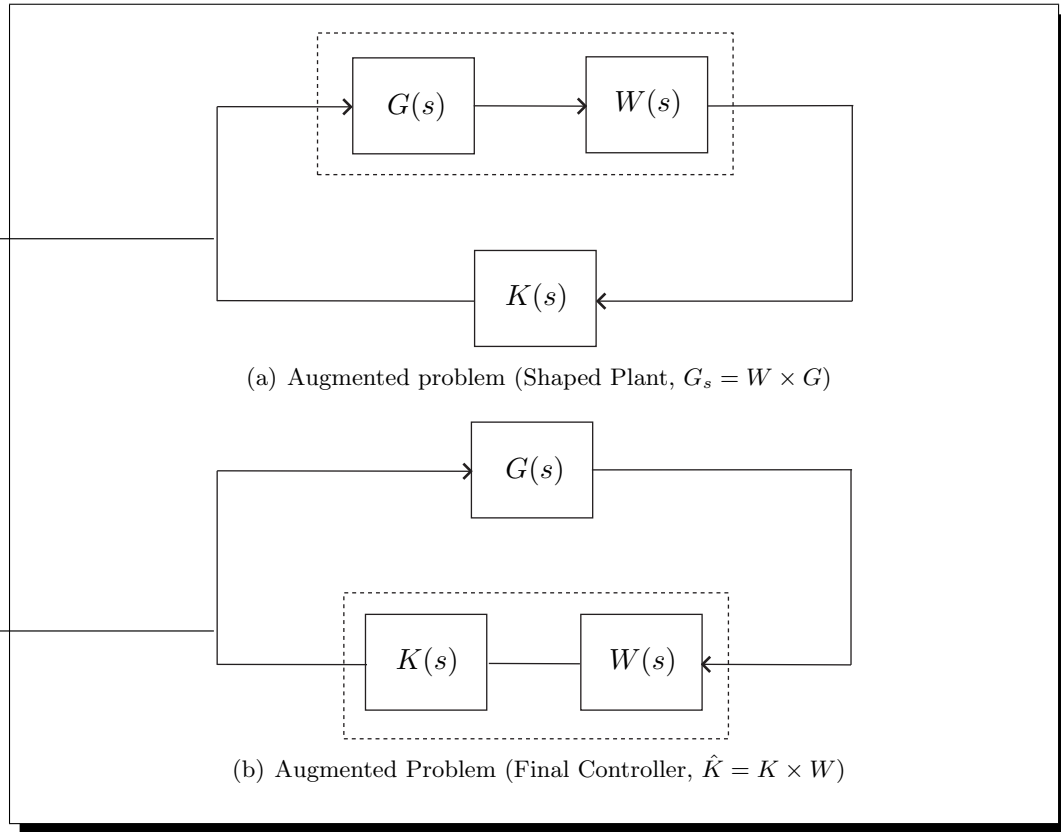


Figure 9.16: Coprime factors loop shaping design process

- \mathcal{H}_∞ coprime factorisation for tilt control

The work on control design involved a number of plant output configurations based on body-mounted sensors and those were:

[**Case 1**] (y_1) combined signal (effective cant deficiency) for 75% partial tilt compensation

[**Case 2**] (y_1) combined signal (effective cant deficiency) for 75% partial tilt compensation, plus (y_2) body roll gyroscope

[**Case 3**] (y_1) combined signal (effective cant deficiency) for 75% partial tilt compensation, plus (y_2) body roll gyroscope, plus (y_3) tilt angle (actual mechanism roll)

In addition, the state vector for control design incorporated the following states

$$x = \left[y_v \quad \theta_v \quad y_b \quad \theta_b \quad \dot{y}_v \quad \dot{\theta}_v \quad \dot{y}_b \quad \dot{\theta}_b \quad \theta_r \quad y_{es} \quad y_w \quad \dot{y}_w \quad \theta_m \quad \dot{\theta}_m \right]^T \quad (9.20)$$

Trials with only one output ('case 1') were unsuccessful as very little information was available to design a sufficiently fast controller. System performance has been significantly improved by using two outputs for the design procedure ('case 2'), while the three outputs ('case 3') produced very similar results to 'Case 2'. Hence, the design procedure is illustrated for the second case with the two outputs configuration. Note that plant uncertainty was again not represented in detail in the design procedure, rather the controller was designed based upon the nominal model and then tested for robust stability.

Using two outputs for controller design (effective cant deficiency signal and body roll gyroscope) will require the weighting function $W(s)$ to be a two by two matrix, each channel of $W(s)$ corresponding to a separate measurement. For the current case $W(s)$ was chosen as:

$$W(s) = \begin{pmatrix} \frac{k_1(1+sT)}{sT} & 0 \\ 0 & \frac{k_2}{1+s/\omega_c} \end{pmatrix}, \quad T = 0.25s \quad \omega_c = 30\left(\frac{rad}{s}\right) \quad (9.21)$$

$W_{11}(s)$ forces integral action in the controller, which guarantees the correct level of steady-state acceleration on curved track, i.e. 75% tilt compensation. The additional pole in $W_{22}(s)$ introduced at $\omega_c = 30\frac{rad}{s}$ increases the roll-off rate of the open-loop at high frequencies and thus helps to suppress any high frequencies of the output signal of roll rate. Note that the dynamic behaviour of the roll gyroscope depends only upon the body roll velocity part of the roll gyroscope signal.

The gain factors k_1, k_2 included in $W(s)$ may be used to adjust the (target) open-loop bandwidth of the design, by placing emphasis on either the first or the second output, and thus the speed of transient response, and also, indirectly, the level of RMS acceleration on straight track due to track irregularities. Table 9.5 presents a

comparison for different values of k_1 by fixing k_2 . The reason for doing this is that k_1 governs the speed of the system, while k_2 relates to the extra amount of damping to be introduced and in that case the comparison with a varying k_2 would not be as straightforward. Note that the fourth column of the table is the RMS error between the actual body lateral acceleration signal and the ideal lateral acceleration profile as described in Chapter 3. The final column represents the *robust stability radius* ' ϵ '.

Table 9.5: Trade-off of coprime factorisation with variable k_1 (@ 58m/s)

k_2	k_1	peak accel. determ. (%g)	error accel. determ. (%g)	degrad. stoch. (%)	ϵ
0.3	0.1	20.0	8.81	-6.1	0.55
0.3	0.5	10.4	3.17	-3.1	0.38
0.3	1.0	8.74	2.39	1.9	0.26
0.3	1.25	8.43	2.25	4.9	0.22
0.3	1.75	8.13	2.1	9.6	0.17
0.3	2.0	8.05	2.06	11.2	0.15
0.3	5.0	7.8	1.94	17.6	0.06

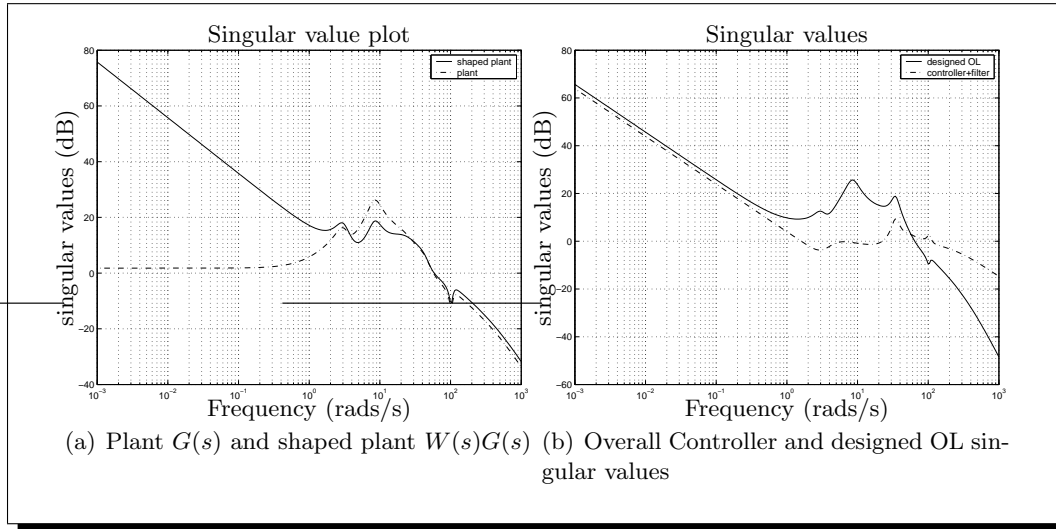


Figure 9.17: Best design for coprime factorisation \mathcal{H}_∞ method frequency responses

The design may be used successfully to trade-off performance and robust-stability requirements for the deterministic characteristics of the design (i.e. curved track). Note, however, that if the target open-loop bandwidth is set too high (large k values), the robust stability margins are reduced, and the stochastic performance index starts deteriorating excessively. In addition, it was found that very fast designs tend to produce unstable controllers, which is clearly impractical.

To comply with the design objectives required in the controller assessment of the thesis, the best design was obtained for $k_1 = 1.25$ and $k_2 = 0.3$. The singular value plot of the original and shaped plant, $G(s)$ and $W(s)G(s)$ respectively, are shown in Figure 9.17(a) (page 161). Note that the type of weight chosen forces integral action in the controller as expected. The designed controller and also the designed open loop are shown in Figure 9.17(b) (page 161), while the controller structure can be found in Appendix F.3. The `matlab` file which implements the design is listed in Appendix H.

The detailed assessment of the controller performance has revealed some interesting results, Table 9.6. The performance is very much improved even if the scheme is just based on an open-loop shaping procedure without directly including information about the track disturbances. The stochastic ride quality is successfully kept within acceptable limits, while the tilt performance is acceptably fast on curved track. It should be noted that the choice of the weights is by far easier compared to the mixed sensitivity case of previous chapters.

Table 9.6: \mathcal{H}_∞ coprime approach controller assessment “best” design @ 58(m/s)

DETERMINISTIC		
Lateral accel. (actual vs ideal)	- steady-state	4.6 (%g)
	- R.M.S. deviation error	2.25 (%g)
	- peak value	8.43 (%g)
Roll gyroscope	- R.M.S. deviation	0.023 (rad/s)
	- peak value	0.10 (rad/s)
P_{CT} (P-factor)	- peak jerk level	5.606 (%g/s)
	- standing	33.69 (% of passengers)
	- seated	8.88 (% of passengers)
STOCHASTIC		
Passenger comfort	- R.M.S. passive (equiv.)	2.725 (%g)
	- R.M.S. active	2.86 (%g)
	- degradation	4.9 (%)

Results from the simulation of the controller on design track can be viewed in Figure 9.18, and are very closely connected to Table 9.6. Initially, there is a small delay for the controller to start reacting to the start of the curve transition as shown in Figure 9.18(c) but soon after quickly provides the required tilt action. The controller provides the full amount of required tilt angle equal to approximately 7.9 degrees, however the mechanism tilts slightly more in order to compensate for the remaining 25% curving forces. The effect of the controller on the roll rates is also evident from Figure 9.18(b) due to the incorporation of the roll gyroscope in the design. Thus, by rejecting high

frequency components, the controller controls the roll rates in such a way that damping in the system is highly improved (this is also expected by referring to the stability radius $\epsilon = 0.22$). Of course, the robust stability radius can be increased in the expense of tilt performance.

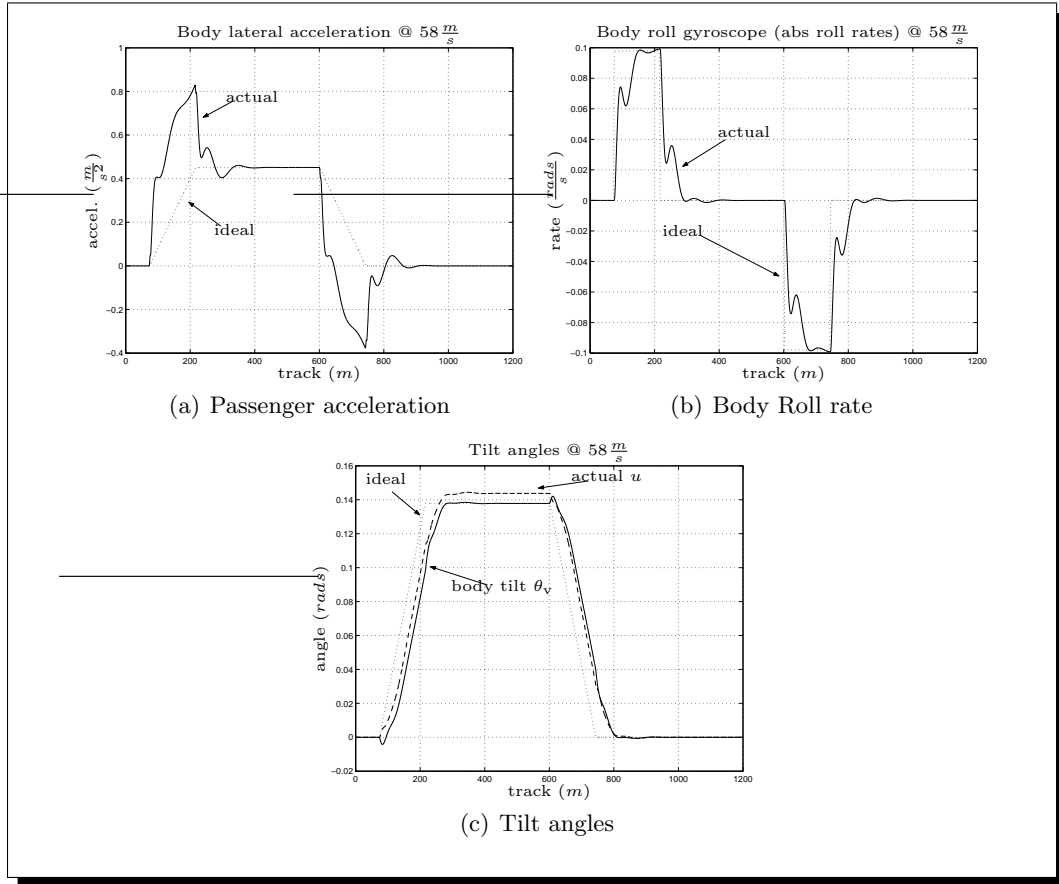


Figure 9.18: Design track time history results for \mathcal{H}_∞ coprime “best” design

The above design attains both deterministic and stochastic design objectives. The degree of the controller may be reduced, if required, by following the closed-loop model reduction method introduced in [MG90].

Testing the controller. The designed controller was also tested in the presence of parametric uncertainty even if uncertainty was not an integral part in the current design procedure. The cases were chosen similar to the ones in the \mathcal{H}_∞ design of Chapter 7:

1. **Perturbed (1):** 20% increase in body mass with 10% increase in secondary suspension stiffness and 20% decrease in secondary suspension damping ratio.

2. **Perturbed (2)**: 40% increase in body mass with 20% increase in secondary suspension stiffness and 40% decrease in secondary suspension damping ratio.

The two cases represent realistic parametric changes, with the decrease in damping to observe the performance of the controller under reduced damping in the passive system. The controller was simulated for the perturbed cases together with the nominal case and results are presented for the passenger acceleration and the body roll rates on design track in Figure 9.19 (in the next page).

The system is stable in all cases and also the transition performance does not change significantly for the nominal and the first perturbed model. There is of course a small change in the steady-state, however this is a function of the system parameters rather than the tilt controller. However, it can be seen that in the second perturbed model, oscillations appear and those are contributed by the lateral modes of the system. The overall system is still stable and the oscillations eventually die out.

The problem was further investigated by running simulation tests on the ‘perturbed (2)’ passive model and those oscillations were still evident. Modal analysis of the passive model has revealed that the lower sway was poorly damped, which in reality will be an unrealistic situation. Thus, the problems are introduced because of the passive model structure. This enforces the effectiveness of such a robust controller, which sustains acceptable robust stability even in a ‘worst case’ model situation.

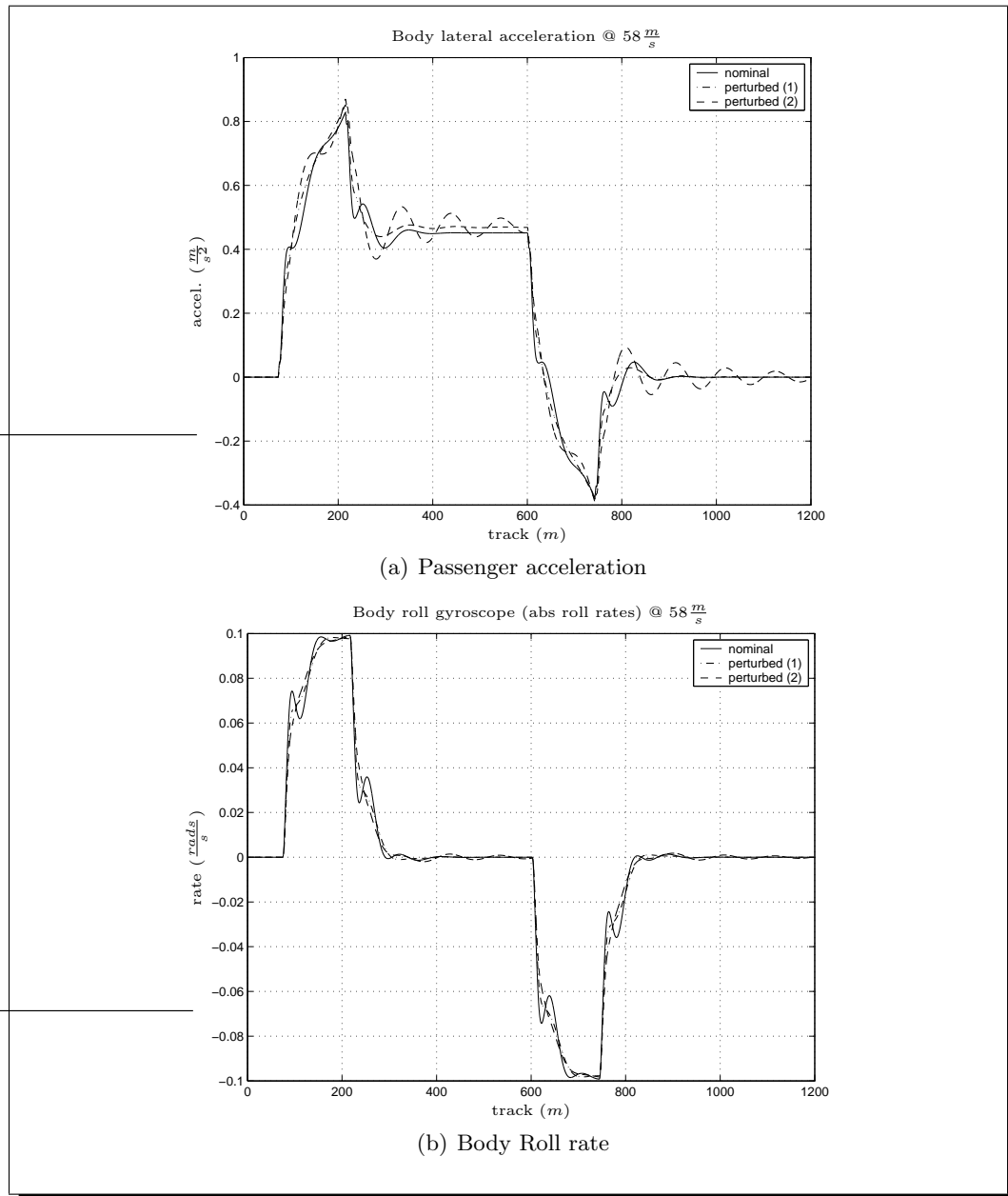


Figure 9.19: Robust performance test for coprime \mathcal{H}_∞ design

9.4 Concluding remarks

This chapter included an introduction to the basic tilt control for the new vehicle model of the tilt mechanism and also proposed new schemes for local/vehicle tilt comparable with the basic precedence scheme currently used by manufacturers.

It has been shown that the LQR and Model Based Estimation control schemes can be extended for the tilt mechanism model case. They both offer substantial improvement in tilt performance and in some cases compensate for stochastic ride quality even at high speeds. The MBE scheme provides results very similar to the basic precedence scheme, although the deterministic and stochastic track features are unknown and not included with the vehicle dynamics. It was possible to achieve higher system bandwidth based upon the above proposed schemes, without being affected by tilt limitations encountered in the basic control cases.

A further investigation into \mathcal{H}_∞ control revealed the possibility of using the coprime factorisation method for tilt control design. The scheme follows a straightforward open-loop shaping method to design the controller for robust stability and performance. Results have illustrated the potential of the design method in solving the localised tilt control problem. It should be noted that the controller manages to sustain good robust performance even in the worst case uncertainty, although detailed uncertainty modelling was not included.

Chapter 10

Conclusions and Future Work

10.1 Conclusions

Since the 1980s there have been varying levels of interest in employing active suspensions for railway vehicles. Significant use however has only emerged during the 1990s with the advent of tilting trains in service operation, which is now approaching the stage of being accepted as a standard for numerous high speed passenger trains and increasingly for regional/cross-country services. The clear commercial benefit of tilting trains is that offers substantial reduction in journey times on *conventional* railway infrastructure.

Early tilt control designs using classical methods with local vehicle measurements proved limited in terms of system performance. Thus, manufacturers were forced to employ measurements for precedent vehicles in order to improve tilt performance, known as “precedence” tilt control. However, these schemes tend to be rather complex with signal connections between vehicles, direction-sensitive, while the tilt system is optimised for a specific route. Additionally, the performance of the first vehicle remains inferior due to the lack of precedence. A similar solution is provided by employing track databases for providing ‘precedence’ tilt information, nevertheless this approach is still under investigation and its use is limited in few tilt applications.

Generally, literature in tilt control design is mainly concentrated upon the use of precedence signals or signals provided by track databases for tilt control, with only few papers in the detailed theoretical formulation. However, tilt control based upon localised vehicle measurements may provide simpler and more straightforward, in terms of solutions compared to the currently used approaches.

This thesis re-visits the idea of early local ‘nulling’-type tilt control and concentrates on a number of problems associated with these schemes and the use of advanced control concepts in improving the tilt performance. Some very interesting results have been obtained and these are discussed in this section. In addition, the thesis refers to the partial-nulling tilt case, i.e. where the passenger acceleration is partially compensated on steady curves, in order to comply with what is used in practice by tilting train operators.

In general, tilt control assessment methods were mainly concentrated upon human responses and motion sickness. An assessment approach is proposed in this thesis which may be used (and has been used throughout this research work) for assessing the performance of tilt system controllers. The method is connected to established methods of tilt assessments, i.e. P_{CT} factor evaluation, for practical validation of the control schemes.

The author has concentrated his research work on detailed linear tilt vehicle system models for control analysis and design. Two tilt configurations were developed, one using an active anti-roll bar for tilt application across the secondary suspensions, while the second involved a tilt mechanism structure for tilt below the secondary suspensions. The latter model is used to compensate for the large suspension deflections when large amounts of tilt are necessary within limited track gauge. The validity of the linear models was proved by appropriate modal analysis and realistic time history tests compared to full non-linear equivalents. This permits the assumption that the simulation responses of the linearised models represent the true responses of a real train.

The first part of the work incorporated control studies on the vehicle with the active anti-roll bar structure, and this model was actually used for the majority of the proposed control systems. A simplified linear model was developed in order to introduce the important vehicle modes for tilt control design, namely the body upper and lower sway. However, the control designs were based upon a more detailed linear model to include the lateral and roll modes of both the body and the vehicle bogie.

The evolution of the basic control approaches was illustrated via appropriate control design examples to show how the system performs in these schemes. The work included a detailed theoretical analysis of the fundamental problem of using straightforward classical methods for local nulling-type tilt. From a control point of view, the body-mounted accelerometer which provides the main information introduces RHP zeros which pose

significant limitations on control design. Further symbolic analysis in Matlab software, based upon a simplified vehicle model, has revealed that the RHP zeros are introduced due to the measurement of absolute vehicle acceleration with respect to the horizontal (not canted) level of the track. It seems that problems like this are unavoidable in “pendulum”-like structures (usual system instabilities and/or RHP zeros). Solutions given by the command-driven schemes, and especially the ‘precedence’ approach, were presented. The latter was set as a basis for comparison with the proposed control strategies.

The linear quadratic regulator (LQR) has always been used in regulation control problems. An LQR controller was designed for the tilt control problem, with the addition of integral action for elimination of steady-state errors, and promises a great deal. Theoretically it offers stability and tilt performance superior to the classical control, and also manages to significantly improve ride quality on random track geometry. Issues are raised concerning the implementation, because in practice an estimator is needed for providing state estimates. Though, assessment of the LQG equivalent controller has proved that the controller manages to perform sufficiently well even with representative parametric changes in the model.

It was seen that the accelerometer used to provide the feedback signal in the basic ‘nulling’ control was affected by suspension interaction and caused limitations in control design. For that reason a model based estimation approach was developed, utilising a Kalman filter, to estimate the (pure) cant deficiency which is unaffected by such unwanted interactions. In practice this would be very similar to the signal which is provided in ‘precedence’-type controllers, but derived locally rather than being transmitted from an adjacent vehicle. The estimator not only estimates the vehicle states but also the unknown track signals required for correct estimation of cant deficiency. Only practical body-mounted sensors were used and it was found that three measurements were sufficient for the estimation. A classical PID controller finalised the design, and the overall controller (+ estimator) performed exceptionally well in both deterministic and stochastic track. It is worth noting that the stochastic track was not taken in account during the design procedure. The closed-loop bandwidth was highly improved (approx. 12-15 rads/s) and consequently the tilt performance. Trials with sensor noise shown minimal effects on the overall controller, especially in stochastic ride quality. The designed estimator may be used with an LQR controller for the purposes of LQG control, although an LTR (Loop Transfer Recovery) approach should be followed to guarantee robustness performance.

Compared to classical and some well known modern control methods (LQR, Model Based Estimation) very few robust controllers exist in tilt control literature. Within the robust control field, the area currently receiving most interest is the subject of \mathcal{H}_∞ control. A reason for this lack of practical applications of \mathcal{H}_∞ control theory is that, at first, the theory and the design procedure itself seem rather complex and computationally intensive. However, there is a number of software routines currently available for solving such problems that they now become less complex. This research work suggested two \mathcal{H}_∞ -based control approaches, based upon the idea of ‘nulling’ control by only using body-mounted sensors.

The first approach followed the common \mathcal{H}_∞ mixed sensitivity control method. This method refers to the minimisation of the infinity norm of the appropriately weighted sensitivity and complementary sensitivity functions to reduce the effects of disturbances and sensor noise in the system. For tilt control design the control sensitivity function was also added in the cost function for control bandwidth limitation and also to guarantee robustness properties in terms of additive uncertainty in the model. Unfortunately, the scheme could not achieve both deterministic and stochastic criteria simultaneously and this was attributed in difficulty of the method to distinguish successfully between the design and random track inputs.

The second \mathcal{H}_∞ approach was concentrated upon forming the tilt control requirements into a multi-objective optimisation problem. This approach incorporated directly into the design both the deterministic and stochastic track ‘disturbances’ and formed appropriate closed-loop transfer functions to tackle the problem of improving tilt performance. It was found that while infinity norms (with the appropriate weightings) can improve tilt performance, the two norm (2-norm) is a better measurement for the stochastic criterion. The problem was formed and solved by using the LMI (Linear Matrix Inequalities) approach, which is widely used in the control community for solving such classes of control problems. Simulation have revealed promising results and also superb controller performance in the presence of model parametric uncertainty, even if this was not included in details during the design process. It is worth mentioning that both this approach and the mixed sensitivity approach result in fixed-structure controllers usually larger in size than to the plant models due to the additional weighting function required. This is an unavoidable consequence, because weights are required for appropriate frequency-shaping of the sensitivity, complementary sensitivity and control sensitivity. In addition both of those \mathcal{H}_∞ schemes fall within a closed-loop shaping

framework and as such the choice of the weighting functions are not straightforward and usually require some trial and error procedure.

The second part of this thesis presented an extension of the research studies over a vehicle model which involves a tilting bolster or tilt mechanism situated below the secondary suspension level. This type of vehicle is more complex compared to the ARB equivalent but provides full amounts of tilt angles and also small suspension deflection. The latter being very important for railway operators concerned with limited track gauge.

A detailed linearised model of the vehicle structure was developed for control system analysis and design. In addition, the passive model was compared to a full non-linear vehicle implemented in a non-linear railway vehicle simulation package called 'Vampire'. The two models shown very similar behaviour, with minor difference especially on steady state curved track due to modelling assumptions during the linearisation process.

The concept of basic control strategies was also presented this model, especially for the 'nulling' and the 'precedence' approaches for the purposes of introducing the differences between the tilt mechanism and the anti-roll bar. For example, in the tilt mechanism model the feedback signal can now incorporate the roll angle of the mechanism which is a much straightforward signal to be measured compared to the secondary suspension roll angles.

The tilt control problem is very similar in both the ARB and mechanism model cases and this was demonstrated by extending the LQR and the Model Based Estimation schemes to the mechanism model. As expected the results were very similar in both cases and this proved the validity of the strategies for the new model.

It was seen that the weightings function in previous \mathcal{H}_∞ controllers, for the ARB model, were not as straightforward to define. A contribution of this research work has been to develop a \mathcal{H}_∞ scheme for robust control design by formulating the problem of tilt control within an open loop shaping framework. The approach is slightly simpler than the mixed sensitivity and multi-objective method and is based on what is known as 'coprime factorisation' method, which incorporates the solutions of appropriate Riccati equations for the controller and the weighting functions. This approach was also based upon the idea of 'nulling' control and used only body-mounted sensors. The computation of the \mathcal{H}_∞ optimal controller was very fast and simulations shown very good

performance on both design and random tracks. The controller was also tested under parametric changes in the plant model and performed very efficiently, even if one test case involved a worst uncertainty set.

Throughout the research work, the proposed assessment of tilt controllers has provided a useful means of comparing the various control schemes. Work has proved that advanced control schemes can offer great potential of using local vehicle tilt controllers simple to implement with results comparable to ‘precedence’-type control. The author attempts a classification of the proposed control strategies relative to their potential for localised tilt control design and this is summarised in Table 10.1 on page 173. The scale chosen for this purpose is in the range of [1 to 5], with 1 : 5 being ‘very low potential’ while 5 : 5 refers to ‘very high potential’.

Table 10.1: Overall research classification of proposed tilt control strategies

TILT CONTROL STRATEGIES RESEARCH SUMMARY				
<i>Strategy</i>	<i>Active ARB-across secondary</i>		<i>Tilt Mechanism-below secondary</i>	
	Attempted	Development prospective	Attempted	Development prospective
Partial-Nulling type				
Model Based Estim. (body sensors)	Yes	5 : 5	Yes	5 : 5
Optimal LQR	Yes	3 : 5	Yes	3 : 5
\mathcal{H}_∞ mixed sens.	Yes	2 : 5	No	
$\mathcal{H}_\infty/\mathcal{H}_2$ multi-obj.	Yes	5 : 5	No	
\mathcal{H}_∞ coprime factors	No		Yes	5 : 5

*N.B.: The above classification is based upon the author's personal opinion.

10.2 Suggestions for Future Work

From the results obtained for the optimal LQR control scheme it was seen that the method provides an efficient way of tackling the tilt control problem and also ride quality. Moreover, Kalman estimator designs, from the MBE control scheme, show that the sensor noise has minimal effects on the estimator performance. Thus, the next step would be a detailed investigation of the LQG equivalent control based upon LTR methods to guarantee sufficient robust performance.

Fault detection studies for the Kalman filter structure in the model-based estimation scheme would be necessary for future practical implementation and especially to guarantee overall tilt system safety. The Kalman filter could be also extended to estimate uncertain parameters such as body mass or inertia. In addition, if there are issues of increased controller size, then designs of reduced order controllers could be followed. Digital implementation would be necessary as the majority of real applications use some form of digital control.

Studies of the assessment of ride quality on both stochastic and design curved tracks are concentrated on the human perspective and motion sickness. Based upon this, the proposed assessment procedure could be extended in order to associate it with human motion sickness criteria.

Uncertainty was not included in a detailed manner during control system design. An extension of the concept would be to introduce structured (parametric) and maybe unstructured uncertainty, i.e. uncertainty between non-linear to linear models, and follow a theoretical investigation of robust control system design which can be based on the *μ -analysis and synthesis method*. This will guarantee good robustness approach regardless of the uncertainty within the system.

\mathcal{H}_∞ -based controllers result in fixed-structure controllers, which may be of larger size compared to the plant model due to the extra weighting factors required for control design. However, there are many controller reduction techniques which can be used in order to accommodate this problem such as *Balanced Truncation*, *Schur model reduction*, *Hankel norm approximation*. In addition, more computational power is becoming available and computers can easily solve even complex computational problems. Thus \mathcal{H}_∞ controllers can be easily incorporated for practical implementation of tilt controllers.

An important next step would be to test the controllers with a full non-linear vehicle model using a multi-body software such as **VAMPIRE**, although in present Matlab routines cannot be used directly and it is necessary to convert them into a “user subroutine”.

Part III

Bibliography/References

Bibliography

- [A⁺95] E. Andersson et al., *Allowing higher speeds on existing tracks - design considerations of the X2000 train for the Swedish State Railways*, Proceeding, Institution of Mechanical Engineers, Part F **209** (1995), no. 2, 93–104. 2.2.2
- [AH99] E. Andersson and L. Halling, *Running gear for tilting trains*, Proceedings, Interactive Conference 'Can your Railway Benefit From Tilting Train Technology?', Part: Rolling Stock (1999). 2.2
- [AM90] B. D. O. Anderson and J. B. Moore, *Optimal control: Linear quadratic methods*, Prentice-Hall Inc., 1990. 7.1, 7.1.2, 7.1.2
- [And94] E. Andersson, *Improvements in the tilt and bogie dynamics*, Seminar S181, Institution of Mechanical Engineers, Vehicle Track Interface Dynamics (1994). 2.2
- [Ano70] Anonymous, *Tilting coaches to raise speeds on curves*, Railway Gazette **126** (1970), 655–659. 2.2
- [Ano98a] ———, *Railway applications; ride comfort for passengers; measurement and evaluation*, European Pre-Standard ENV 12299 (1998). 3.3.1
- [Ano98b] ———, *Tilting trains hold the key to Virgin's ambitious franchise*, Railway Gazette International (1998), 707–710. 2.2
- [Aut99] Various Authors, *Conference Proceedings, Can your railway benefit from tilting train technology?, Part: commercial benefits*, Interactive Conference, Paris (1999). 2.2
- [AW95] M. Appleyard and P. E. Wellstead, *Active suspensions some background*, Proceedings, Institution of Electrical Engineers - Control Theory and Applications **142/2** (1995), 123–128. 2.1

-
- [B⁺94] S. Boyd et al., *Linear matrix inequalities in system and control theory*, SIAM Society for Industrial & Applied Mathematics, 1994. 7.4.4
- [Bär99] W. Bär, *Predictive knowledge-based coach tilting control*, Proceedings, European Control Conference (ECC) (1999). 2.2.1
- [Bin87] H. Binnewies, *Body tilt passenger coaches*, Rail International **12** (1987), no. 3, 21–25. 2.2
- [BK82] D. Boocock and B. L. King, *The development of the Prototype Advanced Passenger train*, Proceedings, Institution of Mechanical Engineers **196** (1982), 35–46. 2.2, 6.1.2
- [BS89] K. Brammer and G. Siffing, *Kalman-bucy filters*, Artech House, 1989. 7.2.1, 7.2.1, 7.3
- [Cas93] R. D. Cashmore, *Adaptive and robust control of a flexible manipulator system*, Ph.D. thesis, University of Leeds (UK), Department of Electronic and Electrical Engineering, 1993. 7.4.1
- [CPM96] C. Casini, G. Piro, and G. Mancini, *The Italian tilting train ETR460*, Proceedings, Institution of Mechanical Engineers, Conf STech96 **C514-058-9620** (1996), 35–46. 2.2.2
- [E⁺95] E. M. Elbeheiry et al., *Advanced ground vehicle suspension systems - a classified bibliography*, Vehicle System Dynamics **24** (1995), 231–258. 2.1
- [Eli97] A. Elia, *Fiat Ferroviaria Group - the PENDOLINO tilting systems, international experiences, state of the art, development, perspectives*, Proceedings Seminar S479, Institution of Mechanical Engineers - Railway Division, “Tilting Trains in the UK?” (1997). 2.2
- [Ewi89] D. J. Ewins, *Modal testing: Theory and practice*, Research Studies Press (RSP), 1989. 5.2
- [FL88] J. S. Freudenberg and D. Looze, *Frequency domain properties of scalar and multivariable feedback systems, (lecture notes in control and information sciences)*, vol. 104, Springer-Verlag, Berlin, 1988. B.3
- [For95] R. Ford, *SIG blows away the mystique of tilt*, Railway Gazette International (1995), 367–368. 2.2.2

- [För00] J. Förstberg, *Ride comfort and motion sickness in tilting trains: Human responses to motion environments in train and simulation experiments*, Ph.D. thesis, Railway Technology, Department of Vehicle Engineering, Royal Institute of Technology KTH, Sweden, 2000. 3.1, 3.4
- [Fri86] B. Friedland, *Control System Design - an introduction to state space methods*, McGraw Hill, 1986. 7.1, 7.1.1, 7.1.2, 7.2.1, 7.3, B.1, B.1, B.1
- [G⁺94] P. Gahinet et al., *Lmi control matlab toolbox manual*, The Mathworks, Inc., 1994. 7.4.1, 7.4.3, 7.4.3, 7.4.4
- [G⁺98] J. F. Garcia et al., *A new tilting strategy based on the knowledge of the train position*, Congreso VTVDF '98, Universidad Politécnica de Cataluña (1998). 2.2.1
- [Gaw98] W. K. Gawronski, *Dynamics and control of structures, a modal approach*, Mechanical Engineering Series, Springer, 1998. 5.2
- [GJ] R. Gawthorpe and T. Jonhson, *Aerodynamics considerations for high-speed tilting trains*, Tech. report. 2.2
- [GK83] R. M. Goodall and W. Kortüm, *Active control in ground transportation - a review of the state of the art and future potential*, Proceedings 11th IFAC World Congress, Tallinn (Estonia) **12** (1983), 225–258. 2.1
- [GK90] ———, *Active suspension for railway vehicles - an unavoidable luxury or an inevitable consequence?*, Proc. 11th IFAC World Congress, Tallinn (Estonia) **12** (1990), 219–225. 2.1
- [Goo93] R. M. Goodall, *Performance limits for active secondary railway suspensions*, Proceedings, International Conference on Speed-Up Technology for Railway and Maglev Vehicles, STECH 93, Yokohama (Japan) **2** (1993), 81–86. 2.1
- [Goo97] ———, *Active railway suspensions: Implementation status and technological trends*, Vehicle System Dynamics **28** (1997), 87–117. 1.2, 2.2, 2.2.2
- [Goo99] ———, *Tilting trains and beyond - the future for active railway suspensions, part 1 improving passenger comfort*, Computing and Control Engineering Journal IEE (1999), 153–160. 2.2, 6.2.2, 8.1
- [GZE00] R.M. Goodall, A. Zolotas, and E. Evans, *Assessment of the performance of tilt system controllers*, The Railway Conference at Railtex '00, NEC Birmingham (UK), November 2000. 3.3.1, 3.3.1, 3.3.2

-
- [H⁺91] H. Higaki et al., *An active pneumatic tilting system for railway cars*, Proceedings, Vehicle System Dynamics Supplement, Dynamics of Vehicles on Roads from Tracks, 12th Symposium, Lyon-FRANCE **20** (1991), 254–268. 2.2.1, 2.2.2
- [Har86] P. R. Harborough, *Passenger comfort during high speed curving - summary report*, Tech. Report 260-386-038, British Rail Research (BRR), May 1986. 1.3.4, 1.4, 3.3.1
- [Hel76] J. Helton, *Operator theory and broadband matching*, In Proceedings of the 11th Allerton Conference on Communications, Control and Computing, 1976. 7.4.1
- [Her81] J. K. Herdrick, *Railway vehicle active suspensions*, Vehicle System Dynamics **10** (1981), 267–283. 2.1
- [HG99] L. Hong and R. M. Goodall, *State estimation for active steering of railway vehicles*, IFAC '99 (1999). 7.3
- [HSS98] N. R. Harris, F. Schmid, and R. A. Smith, *Introduction: Theory of tilting train behaviour*, Proceedings, Institution of Mechanical Engineers **212** (1998), no. F1, 1–5. 2.2
- [Hub97] B. H. Huber, *The bogie-based tilt option - simplicity and flexibility*, Proceedings, Institution of Mechanical Engineers **212** (1997), no. F1, 19–32. 2.2
- [K⁺93] Y. Kurokawa et al., *Limited angle tilt control systems by air-springs*, Proceedings, STECH93, JSME **2** (1993), 361–364. 2.2.2
- [Kal60] R. E. Kalman, *A new approach to linear filtering and prediction problems*, Journal of Basic Engineering, Trans. ASME Series D **82** (1960), 35–45. 7.2.1
- [Kar78] D. C. Karnopp, *Are active suspension really necessary?*, The American Society of Mechanical Engineers Winter Meeting (San Francisco), Paper 78-WA/DE-12 (1978). 2.1
- [Kay74] U. Kayserling, *Power bogies of the DB 200 km/h ET 403 incorporating body-tilt through the secondary suspension*, Rail Engineering International **4** (1974), no. 9, 414–418. 2.2
- [KCH74] D. C. Karnopp, M. J. Crosby, and R. A. Harwood, *Vibration control using semi-active force generators*, Journal of Engineering for Industry (1974), 619–626. 2.1

- [KE00] S. Kent and J. Evans, *Hardware-in-loop simulation of railway vehicles with tilting and active suspension systems*, Vehicle System Dynamics, Supplement **33** (2000). 2.2.1, 4.4, 8.2, 9.1
- [KH91] D. C. Karnopp and G. Hees, *Electronically controlled vehicle suspensions*, Vehicle System Dynamics **20** (1991), 207–217. 2.1
- [Kof70] J. L. Koffman, *Higher speeds through curves*, Railway Gazette **126** (1970), 61–64. 2.2
- [Mac89] J. M. Maciejowski, *Multivariable feedback design*, Addison-Wesley, 1989. 7.1, 7.1.2, 1
- [MG90] D.C. McFarlane and K. Glover, *Robust controller design using normalised coprime factor plant descriptions, lecture notes in control and information sciences*, vol. 138, Springer-Verlag, 1990. 7.4.1, 7.4.2, 7.4.2, 6, 9.3, 9.3.1, 9.3.1, 9.3.1
- [MH99] Y. Mingli and Z. HanQuan, *Robust \mathcal{H}_∞ control to active tilting train: An experimental research*, Proceedings of the IEEE International Vehicle Electronics Conference **1** (1999), 290–293. 2.2.1
- [N⁺72] A. Nishio et al., *A high speed powered tilting vehicle with air-springs*, The Sumitomo Search (1972), no. 7, 70–77. 2.2.1, 2.2.2
- [N⁺97] Y. Nishioka et al., *Tilting control system for railway vehicles using long-stroke air-spring*, The Sumitomo Search (1997), no. 59, 102–107. 2.2.1, 2.2.2
- [Pad95] J. E. Paddison, *Advanced control strategies for maglev suspension systems*, Ph.D. thesis, Loughborough University (UK), Department of Electronic and Electrical Engineering, 1995. 3.4.1, 3.4.2
- [Pal99] W. J. III Palm, *Modelling, analysis, and control of dynamic systems*, John Wiley & Sons, Inc, 1999, 2nd Edition. 5.2
- [PGP98] J. T. Pearson, R. M. Goodall, and I. Pratt, *Control system studies of an active anti-roll bar tilt system for railway vehicles*, Proceedings, Institution of Mechanical Engineers **212** (1998), no. F1, 43–60. 1.3.3, 2.2.1, 5, 5.4
- [PP83] K.W. Pennington and M. G. Pollard, *The development of an electro-mechanical tilt system for the advanced passenger train*, Conference, Institution of Mechanical Engineers, Electric vs Hydraulic Drives **C299-83** (1983), 21–28. 2.2.2

- [Pra96] I. Pratt, *Active suspension applied to railway trains*, Ph.D. thesis, Loughborough University (UK), Department of Electronic and Electrical Engineering, 1996. 2.1, 3.2.1, A.1
- [S+96] A. Suescun et al., *Use of inverse dynamics in the development of tilt control strategies for rail vehicles*, *Vehicle System Dynamics, Supplement* **25** (1996), 655–667. 2.2.1, 2.2.2
- [San74] Ing. O. Santanera, *FS and RENFE try out tilt-body prototype trains*, *Railway Gazette International* **130** (1974), 101–104. 2.2
- [Sau96] B. Sauer, *The BR 611 DMU with new tilting technology*, *Proceedings, Institution of Mechanical Engineers, International Conference Railtech 96* **C511-8-076-96** (1996). 2.2.2
- [Sch97] F. Schmid, *Control and operation of tilting train services*, *Proceedings, Institution of Mechanical Engineers* **212** (1997), no. F1, 73–84. 2.2
- [SCW94] K. Sharma, D. A. Crolla, and D. A. Wilson, *The design of a fully active suspension system incorporating a kalman filter for state estimation*, *IEE Control 1994 Conference Publication* (1994), no. 389. 7.3
- [Shu99] X. Shu, *On the adaptive control of railway tilting coaches*, *Proceedings, IFAC 14th World Congress* (1999), no. P-8b-02-5, 515–520. 2.2.1
- [SP00] S. Skogestad and I. Postlethwaite, *Multivariable feedback control: Analysis and design*, Wiley, 2000, Reprinted Version. 1, 7.1.2, 1, 7.4.1, 7.4.3, B.2.1, B.3
- [Str97] A. Stribersky, *The development of an integrated suspension control technology for passenger trains*, *Seminar S479, Institution of Mechanical Engineers, Tilting Trains in the UK* (1997). 2.2.2
- [Tho93] W. T. Thomson, *Theory of vibration with applications*, Chapman & Hall, 1993, 4th Edition. 3.4.1
- [Vid85] M. Vidyasagar, *Control system synthesis - a coprime factorisation approach*, MIT Press, 1985. 9.3.1
- [Wat99] H. Waters, *The commercial benefits of tilting trains - VIRGIN's strategy for the new WEST COAST and CROSSCOUNTRY fleets*, *Proceedings, Interactive Conference 'Can your Railway Benefit From Tilting Train Technology?'*, Part: COMMERCIAL BENEFITS (1999). 2.2

- [Wic92] A. H. Wickens, *A review progress in the application of active suspension to railway vehicles*, IEE Colloquium - Active Suspension Technology for Automotive and Railway Applications (1992), 1/1–1/3. 2.1
- [Wil86] R. A. Williams, *Comparison of classical and optimal active suspension control system*, Ph.D. thesis, Loughborough University (UK), Department of Electronic and Electrical Engineering, 1986. 2.1
- [Zam81] G. Zames, *Feedback and optimal sensitivity, model reference transformations, multiplicative seminorms, and approximate inverse*, IEEE Transactions on Automatic Control **AC-26** (1981), 301–320. 7.4.1
- [ZD98] K. Zhou and J. C. Doyle, *Essentials of robust control*, Prentice Hall International Editions, 1998. 7.4.2, 7.4.2, 6, 7.4.4
- [ZG00] A. C. Zolotas and R. M. Goodall, *Advanced control strategies for tilting railway vehicles*, UKACC Control 2000, Cambridge UK, UKACC (UK), September 2000. 7.3
- [ZGH01] A.C. Zolotas, R.M. Goodall, and G.D. Halikias, *New control strategies for tilting trains*, 17th Symposium Dynamics of Vehicles on road and tracks IAVSD 2001, Copenhagen(Lyngby) (DK), Int'l Association for Vehicle System Dynamics, August 2001. 9.2.2
- [ZHG00] A.C. Zolotas, G.D. Halikias, and R.M. Goodall, *A comparison of tilt control approaches for high speed railway vehicles*, Proceedings ICSE 2000, Coventry UK, ICSE, September 2000, pp. 632–636. 7.4.4

Please note: All URLs included in this thesis were operational when this thesis was produced. The author accepts no responsibility in case any of the referenced URLs does not either operate properly or for some reason its operation is terminated in the future.

** The figure in the dedication page (page ii) presents an example of an ancient greek column/pillar found in ancient Greek temples. It is of Ionic order found in the Greek islands and Eastern/North-Eastern Greece. [source: <http://www.ancientgreece.com>]*

Part IV

Appendices

Appendix A

Summary of Track Profiles and Vehicle Parameter Values

This Appendix list the time history profiles of the track inputs used for both the anti-roll bar and tilt mechanism studies. In addition it includes a list of the vehicle parameter values for the tilt vehicle models developed in this thesis.

A.1 Track Profiles

A.1.1 Anti-Roll Bar studies

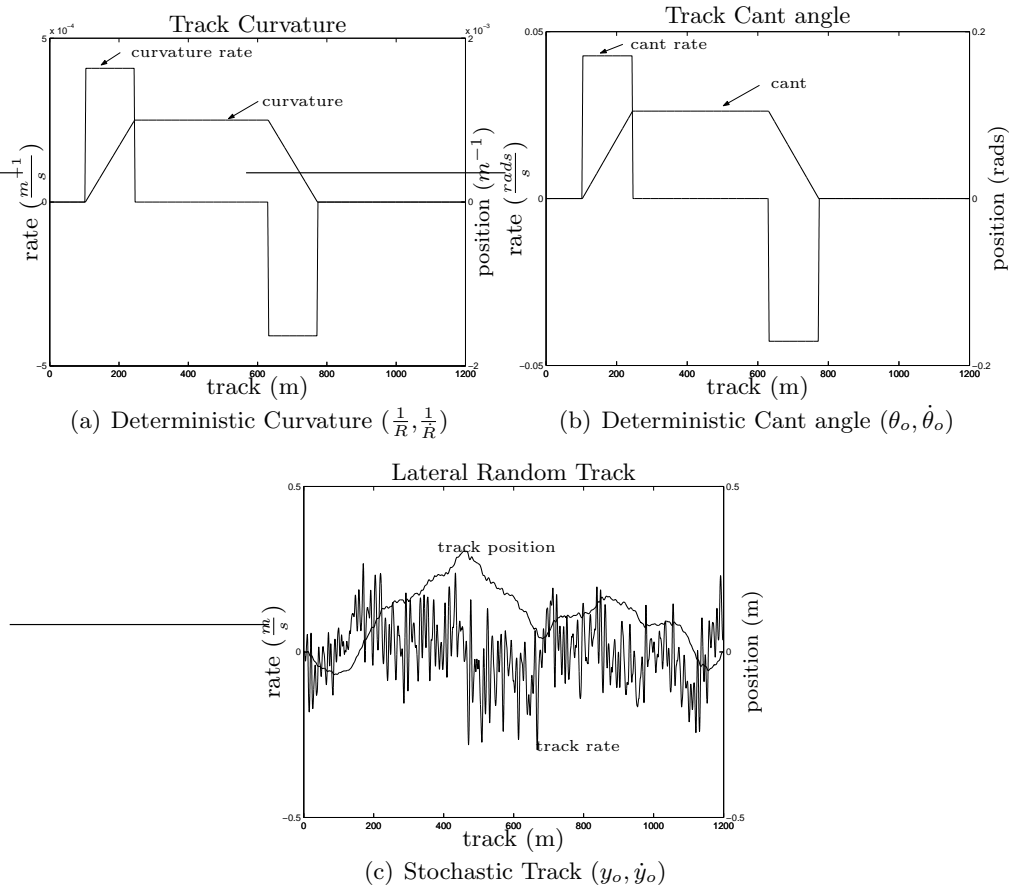


Figure A.1: Track features for anti-roll bar studies

A.1.2 Tilt Mechanism Studies

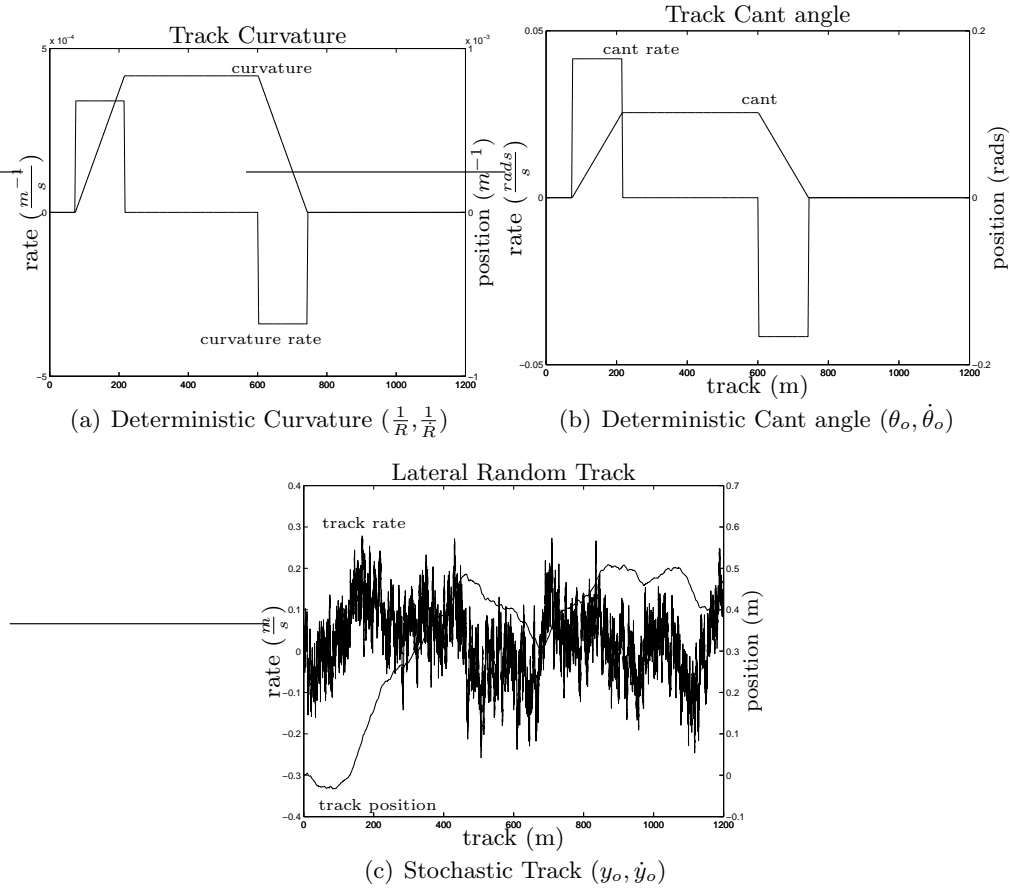


Figure A.2: Track features for tilt-mechanism studies

A.2 Vehicle Parameter Values

A.2.1 Vehicle with Active Anti-Roll Bar

Table A.1: Parameters based upon the Bombardier Pro Rail current best configuration

m_v, i_{vr}	HALF BODY: mass, 19,000(kg), roll inertia, 25,000(kgm^2)
m_b, i_{br}	BOGIE: mass, 2,500(kg), roll inertia, 1,500(kgm^2)
	* Values per bogie side *
k_{az}	Airspring area stiffness, 210,000($\frac{N}{m}$)
k_{sz}	Airspring series stiffness, 620,000($\frac{N}{m}$)
k_{rz}	Airspring reservoir stiffness, 244,000($\frac{N}{m}$)
c_{rz}	Airspring reservoir damping, 50,000($\frac{Ns}{m}$)
k_{sy}	Secondary lateral stiffness, 260,000($\frac{N}{m}$)
c_{sy}	Secondary lateral damping, 33,000($\frac{Ns}{m}$)
k_{vr}	Anti-roll bar stiffness per bogie, 2,000,000($\frac{Nm}{rad}$)
k_{pz}	Primary vertical stiffness, 3,000,000($\frac{N}{m}$)
c_{pz}	Primary vertical damping, 25,000($\frac{Ns}{m}$)
k_{py}	Primary lateral stiffness, 35,000,000($\frac{N}{m}$)
c_{py}	Primary lateral damping, 16,000($\frac{Ns}{m}$)
d_1	Airspring semi-spacing, 0.9(m)
d_2	Primary vertical suspension semi-spacing, 1.00(m)
h_1	Secondary lateral suspension spacing (bogie cog), 1.0(m)
h_2	Secondary lateral suspension spacing (bogie cog), 0.25(m)
h_3	Primary lateral suspension spacing (bogie cog), -0.09(m)
h_{g1}	Height ARL of body cog, 1.520(m)
h_{g2}	Height ARL of bogie cog, 0.37(m)

source: [Pra96], PhD Thesis, Loughborough University (UK)

A.2.2 Vehicle with Tilting Mechanism below Secondary Suspension

Table A.2: Parameters based loosely based on post-appt test coach 48204 (seats full) with slightly increased lateral stiffness

m_v, i_{vr}	HALF BODY: mass, 16,000(kg), roll inertia, 20,000(kgm^2)
m_b, i_{br}	BOGIE: mass, 3,680(kg), roll inertia, 2,500(kgm^2)
* Values per bogie side *	
k_{az}	Airspring area stiffness, 201,500($\frac{N}{m}$)
k_{sz}	Airspring series stiffness, 300,000($\frac{N}{m}$)
k_{rz}	Airspring reservoir stiffness, 201,000($\frac{N}{m}$)
c_{rz}	Airspring reservoir damping, 20,000($\frac{Ns}{m}$)
k_{sy}	Secondary lateral stiffness, 100,000($\frac{N}{m}$)
c_{sy}	Secondary lateral damping, 18,000($\frac{Ns}{m}$)
k_{csy}	Secondary lateral damper end-stiffness, 8,000,000($\frac{N}{m}$)
k_{vr}	Anti-roll bar stiffness per bogie, 1,500,000($\frac{Nm}{rad}$)
c_{vr}	Anti-roll bar damping per bogie, 18,200($\frac{Nsm}{rad}$)
k_{pz}	Primary vertical stiffness, 1,600,000($\frac{N}{m}$)
c_{pz}	Primary vertical damping, 20,000($\frac{Ns}{m}$)
k_{py}	Primary lateral stiffness, 18,600,000($\frac{N}{m}$)
c_{py}	Primary lateral damping, 20,000($\frac{Ns}{m}$)
d_1	Airspring semi-spacing, 0.835(m)
d_2	Primary vertical suspension semi-spacing, 1.00(m)
h_1	Secondary lateral suspension spacing (bogie cog), 0.844(m)
h_2	Secondary lateral suspension spacing (bogie cog), 0.252(m)
h_3	Primary lateral suspension spacing (bogie cog), 0.194(m)
h_{mt}	Mechanism c.o.g. vertical separation from effective tilt centre, 0.6(m)
h_{g1}	Height ARL of body c.o.g., 1.696(m)
h_{g2}	Height ARL of bogie c.o.g., 0.6(m)

source: Jeremy Evans, AEA Technology, Derby (UK)

Appendix B

Theory Supplement

The topics in this Appendix are included as background material for the thesis.

B.1 Covariance analysis of systems excited by white noise inputs

Consider the state-space representation, Figure B.1, of the following general linear system [Fri86]

$$\dot{x} = Ax + Bu + \Gamma w \quad (\text{B.1})$$

$$y = Cx + H\nu \quad (\text{B.2})$$

where w, ν represent Gaussian white noise processes. For simplicity ignore both the measurement noise ν and the control input u . Therefore the focus of the analysis is the effect of the process noise w on the output y .

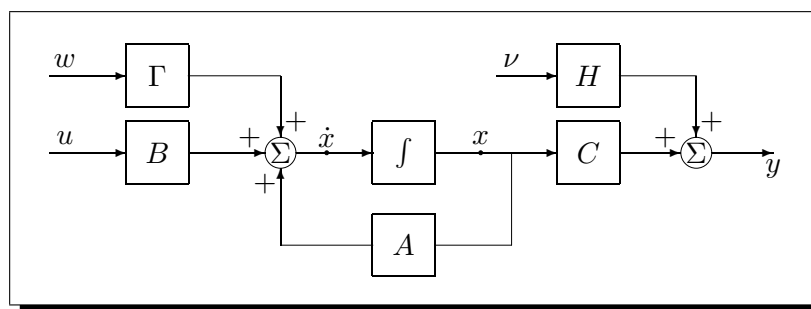


Figure B.1: General linear system

The system is simplified to

$$\dot{x} = Ax + \Gamma w \quad (\text{B.3})$$

$$y = Cx \quad (\text{B.4})$$

which is asymptotically stable (i.e. all $\text{Re}(\text{eig}\{A\}) < 0$) and strictly proper.

The solution of (B.3) in terms of the transition matrix is given by

$$x(t) = \Phi(t, t_0)x(t_0) + \int_{t_0}^t \Phi(t, \psi)F(\psi)w(\psi)d\psi \quad (\text{B.5})$$

where t_0 is a fixed initial time.

The expected value of the states is $E \{x(t)x^T(\tau)\}$ (assuming zero mean, i.e. $\overline{x(t)} = 0$), where the product $x(t)x^T(\tau)$ is

$$\begin{aligned} x(t)x^T(\tau) &= \Phi(t, t_0)x(t_0)x^T(t_0)\Phi^T(t, t_0) \\ &+ \Phi(t, t_0)x(t_0) \cdot \int_{t_0}^t w^T(\psi)F^T(\psi)\Phi^T(t, \psi)d\psi \\ &+ \int_{t_0}^t \Phi(t, \psi)F(\psi)w(\psi)d\psi \cdot x^T(t_0)\Phi^T(t, t_0) \\ &+ \int_{t_0}^t \int_{t_0}^{\tau} \Phi(t, \psi)F(\psi)w(\psi)w^T(\mu)F^T(\mu)\Phi^T(t, \mu)d\psi d\mu \end{aligned} \quad (\text{B.6})$$

Recall that w is a white noise process with zero mean $E \{w(t)\} = 0$, thus

$$\begin{aligned} E \left\{ \Phi(t, t_0)x(t_0) \cdot \int_{t_0}^t w^T(\psi)F^T(\psi)\Phi^T(t, \psi)d\psi \right\} = \\ \Phi(t, t_0)x(t_0) \cdot \int_{t_0}^t E \{w^T(\psi)\} F^T(\psi)\Phi^T(t, \psi)d\psi = 0 \end{aligned} \quad (\text{B.7})$$

the same applies to $E \left\{ \int_{t_0}^t \Phi(t, \psi)F(\psi)w(\psi)d\psi \cdot x^T(t_0)\Phi^T(t, t_0) \right\}$.

Hence $E \{x(t)x^T(\tau)\}$ reduces to the following correlation state matrix

$$\begin{aligned} R_x(t, \tau) &= E \{x(t)x^T(\tau)\} = \Phi(t, t_0)E \{x(t_0)x^T(t_0)\} \Phi^T(t, t_0) \\ &+ \int_{t_0}^t \int_{t_0}^{\tau} \Phi(t, \psi)F(\psi)E \{w(\psi)w^T(\mu)\} F^T(\mu)\Phi^T(t, \mu)d\psi d\mu \end{aligned} \quad (\text{B.8})$$

Define the covariance matrix of $x(t_0)$, $P_x(t_0) = E \{x(t_0)x^T(t_0)\}$, and also recall that

$$E \{w(\psi)w^T(\mu)\} = Q_w(\psi)\delta(\psi - \mu) \quad (\text{B.9})$$

Thus

$$\int_{t_0}^t \int_{t_0}^{\tau} \Phi(t, \psi) F(\psi) E \{ w(\psi) w^T(\mu) \} F^T(\mu) \Phi^T(t, \mu) d\psi d\mu = \int_{t_0}^t \Phi(t, \psi) F(\psi) Q_w(\psi) \left\{ \int_{t_0}^{\tau} \delta(\psi - \mu) F^T(\mu) \Phi^T(t, \mu) d\mu \right\} d\psi \quad (\text{B.10})$$

where

$$\int_{t_0}^{\tau} \delta(\psi - \mu) F^T(\mu) \Phi^T(t, \mu) d\mu = \begin{cases} F^T(\mu) \Phi^T(t, \mu) & \text{for } \mu \in (t_0, t), \\ 0 & \text{otherwise.} \end{cases} \quad (\text{B.11})$$

Therefore

$$R_x(t, \tau) = \Phi(t, t_0) P_x(t_0) \Phi^T(\tau, t_0) + \int_{t_0}^{\bar{t}} \Phi(t, \psi) F(\psi) Q_w(\psi) F^T(\psi) \Phi^T(\tau, \psi) d\psi \quad (\text{B.12})$$

with $\bar{t} = \min(t, \tau)$

Note that the state transition matrix $\Phi(t, \tau)$ has the property $\Phi(t_1, t_3) = \Phi(t_1, t_2) \Phi(t_2, t_3)$, $\forall t_1, t_2, t_3$ [Fri86]. Thus

$$\begin{aligned} \Phi^T(\tau, t_0) &= [\Phi(\tau, t) \Phi(t, t_0)]^T = \Phi^T(t, t_0) \Phi^T(\tau, t) \\ \Phi^T(\tau, \psi) &= [\Phi(\tau, t) \Phi(t, \psi)]^T = \Phi^T(t, \psi) \Phi^T(\tau, t) \end{aligned}$$

Substitute the above expressions into (B.12) to get

$$R_x(t, \tau) = P_x(t) \Phi^T(\tau, t), \quad \text{for } \tau \geq t \quad (\text{B.13})$$

where

$$P_x(t) = \Phi(t, t_0) P_x(t_0) \Phi^T(t, t_0) + \int_{t_0}^t \Phi(t, \psi) F(\psi) Q_w(\psi) F^T(\psi) \Phi^T(t, \psi) d\psi \quad (\text{B.14})$$

$P_x(t)$ is the covariance matrix of the state $x(t)$ at time t . Note that (B.14) holds only for $\tau \geq t$, however the symmetry property $R_x(t, \tau) = R_x^T(\tau, t)$ can be used to find $R_x(t, \tau)$ for $t \geq \tau$ using (B.13) [Fri86].

Differentiating both sides of (B.14) w.r.t. time gives

$$\begin{aligned} \frac{\partial P_x}{\partial t} &= \frac{\partial \Phi(t, t_0)}{\partial t} P_x(t_0) \Phi^T(t, t_0) + \Phi(t, t_0) P_x(t_0) \frac{\partial \Phi^T(t, t_0)}{\partial t} \\ &\quad + \frac{\partial}{\partial t} \left(\int_{t_0}^t \Phi(t, \psi) F(\psi) Q_w(\psi) F^T(\psi) \Phi^T(t, \psi) d\psi \right) \quad (\text{B.15}) \end{aligned}$$

and hence the differential equation for P_x is

$$\dot{P}_x = AP_x + P_xA^T + \Gamma Q_w \Gamma^T \quad (\text{B.16})$$

using Leibnitz's rule of differentiating integrals $\frac{\partial}{\partial t} \int_0^t f(t, \lambda) d\psi = f(t, t) + \int_0^t \frac{\partial f(t, \lambda)}{\partial t} d\psi$ and also the property of $\frac{\partial \Phi(t, \tau)}{\partial t} = A(t)\Phi(t, \tau)$, $\forall t, \tau$.

For time-invariant systems $\dot{P} = 0$ thus (B.16) simplifies to

$$AP_x + P_xA^T = -\Gamma Q_w \Gamma^T \quad (\text{B.17})$$

which is the Lyapunov stability matrix equation. P_x is a positive definite square matrix, and also symmetric subject to $\Gamma Q_w \Gamma^T$ being symmetric. The positive definite P_x exists only for *stable* systems and is finite when the system is *strictly proper*.

For the correlation matrix regarding the output $y(t)$ the following applies

$$y(t) = C(t)x(t)$$

which then becomes

$$y(t)y^T(t) = C(t)x(t)x^T(t)C^T(t)$$

Take expectations on both sides

$$E \{y(t)y^T(t)\} = C(t)E \{x(t)x^T(t)\} C^T(t)$$

Finally

$$P_y(t) = C(t)P_x(t)C^T(t) \quad (\text{B.18})$$

Matlab Implementation of (i) covariance, (ii) frequency response and (iii) time history analysis

```
(i) function [rmsv,Qo,Xs] = rMSC(sys,Qw)
%
% RMSC          : function [rmsv,Qo,Xs] = rMSC(sys,Qw)
%
% RMS value based upon Covariance Analysis (C).
% Input assumed white noise with flat spectrum.
%
% rmsv : rms value
% Qo  : output covariance matrix
% Xs  : state covariance from Lyapunov eqn
%
% sys: system with appropriate i/o selection
```

```

% Qw : track spectrum covariance input
%

% minimal realisation (using default tolerance=sqrt(eps))
sys_om = minreal(sys);
%
[A_om,G_om,C_om,D_om] = ssdata(sys_om); % get ss data from sys_om
%
% stationary covariance solution (Lyapunov eqn)
Xs = lyap(A_om,G_om*Qw*G_om');
%
Qo = C_om*Xs*C_om'; % curving accel o/p
%
rmsv = sqrt(abs(diag(Qo))); % rms value(s)

```

```

(ii) function [rms_value] = rmsf(sys_asiso,w,Qn)
% RMSF      : function [rms_value] = rmsf(sys_asiso,f,Qn)
%
% RMS value based upon Frequency Response Analysis (F).
% Input assumed white noise with flat spectrum.
%
% Inputs:
%   sys_asiso ..... LTI SISO system
%   w ..... Frequency range (rads/s)
%   Qw ..... Track spectrum covariance input
%              in terms of cycles (Hz)
%
% Outputs:
%   rms_value ..... RMS value from frequency analysis
%
% minimal realisation
sys = minreal(sys_asiso);

[mag,phase] = bode(sys,w); % frequency still in rads/s
mag2 = mag.^2;

% Initialise integration
m1 = 0; w1 = 0; Area = 0;
for i=1:max(size(f));
    Area = Area+(w(i)-w1)*(m1+mag2(i))/2;
    m1 = mag2(i);
    w1 = w(i);
end

% multiply by 2 due to double sided integral
% and get correct value by dividing variance with (2*pi)
rms_value = sqrt(2*Qn*Area/(2*pi));

```

```

(iii) function [rms_value] = findrms(vector_in)
% FINDRMS      : function [rms_value] = rmsf(vector_in)
%
% RMS value based upon Time history analysis (T).
%
% Inputs:
%   vector_in ..... Input time history vector
%
% Outputs:
%   rms_value ..... RMS value from time history analysis
%
rms_value = sqrt(mean(vector_in.^2));

```

B.2 Basic Control Theory

B.2.1 Feedback Control Systems

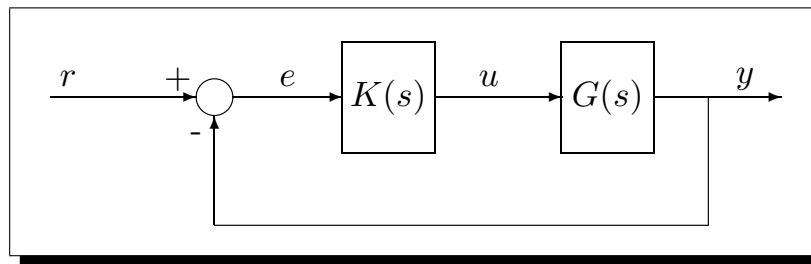


Figure B.2: One-degree of freedom feedback control system

From Figure B.2 the input to the plant is

$$u = K(s)(r - y) \quad (\text{B.19})$$

where, r is the setpoint or reference input, e the control error, u the control input and y the plant output. Moreover, the plant model can be written as

$$y = G(s)u \quad (\text{B.20})$$

or by substituting (B.19) into (B.20)

$$y = G(s)K(s)(r - y) \quad (\text{B.21})$$

or

$$(I + GK)y = GK r \quad (\text{B.22})$$

and finally

$$y = \underbrace{(I + GK)^{-1}GK}_T r \quad (\text{B.23})$$

Note also that the control error is

$$e = r - y = r - GK e \Rightarrow e = \underbrace{(I + GK)^{-1}}_S r \quad (\text{B.24})$$

And the corresponding control input to the plant is

$$u = KS r \quad (\text{B.25})$$

To summarise

$L = GK$	Loop Transfer Function
$S = (I + GK)^{-1}$	Sensitivity Function
$T = (I + GK)^{-1}GK = GK(I + GK)^{-1}$	Complementary Sens. Function
$KS = K(I + GK)^{-1}$	Control Sensitivity Function
Note that $S + T = I$.	

If positive feedback arrangement is used then

$L = GK$	Loop Transfer Function
$T = (I - GK)^{-1}GK = GK(I - GK)^{-1}$	Complementary Sens. Function
$S = (I - GK)^{-1}$	Sensitivity Function
$KS = K(I - GK)^{-1}$	Control Sensitivity Function
and also $S - T = I$ or $T - S = -I$.	

For more details on practical feedback control the reader is referred to [SP00].

B.3 Non-Minimum Phase System Symbolic Analysis

The symbolic analysis, carried out in Matlab, is based upon the 2-DoF ARB linear model described in Section 5.1. For simplicity, the model does not include airsprings and damper elements.

Matlab results

```
!!!!!!!!!!!!!!!!!!!!!!!!!!!!!!!!!!!!!!!!!!!!!!
! NO AIRSPRING INCLUDED IN THE MODEL !
!!!!!!!!!!!!!!!!!!!!!!!!!!!!!!!!!!!!!!!!!!!!!!
```

```
*****
* Case 1: not including damping coefficient "c_sy" *
*****
```

```

A =
[ 0, 0, 1, 0]
[ 0, 0, 0, 1]
[ -2*k_sy/m_v, 2*k_sy*h_1/m_v, 0, 0]
[(2*k_sy*h_1+m_v*g)/i_vr, (-k_vr-2*h_1^2*k_sy)/i_vr, 0, 0]

C =
[ -2*k_sy/m_v, 2*k_sy*h_1/m_v-g, 0, 0]

D =
0

I =
    1    0    0    0
    0    1    0    0
    0    0    1    0
    0    0    0    1

% G = C*inv(s*I-A)*B+D

G =
(-4*k_sy^2/m_v*h_1/(s^4*m_v*i_vr+s^2*m_v*k_vr+2*s^2*m_v*h_1^2*k_sy...
+2*k_sy*s^2*i_vr+2*k_sy*k_vr-2*k_sy*h_1*m_v*g)*i_vr...
+(2*k_sy*h_1/m_v-g)*(s^2*m_v+2*k_sy)/(s^4*m_v*i_vr+s^2*m_v*k_vr+2*s^2*m_v*h_1^2*k_sy...
+2*k_sy*s^2*i_vr+2*k_sy*k_vr-2*k_sy*h_1*m_v*g)*i_vr)*k_vr/i_vr

nG =
-i_vr*m_v*(-2*k_sy*h_1*s^2+m_v*g*s^2+2*g*k_sy)*k_vr

dG =
m_v*(s^4*m_v*i_vr+s^2*m_v*k_vr+2*s^2*m_v*h_1^2*k_sy+2*k_sy*s^2*i_vr+2*k_sy*k_vr...
-2*k_sy*h_1*m_v*g)*i_vr

G =
-(-2*k_sy*h_1*s^2+m_v*g*s^2+2*g*k_sy)*k_vr/(s^4*m_v*i_vr+s^2*m_v*k_vr...
+2*s^2*m_v*h_1^2*k_sy+2*k_sy*s^2*i_vr+2*k_sy*k_vr-2*k_sy*h_1*m_v*g)

nG =
-(-2*k_sy*h_1*s^2+m_v*g*s^2+2*g*k_sy)*k_vr

```

dG =

$$s^4 m_v i_{vr} + s^2 m_v k_{vr} + 2 s^2 m_v h_1^2 k_{sy} + 2 k_{sy} s^2 i_{vr} \dots \\ + 2 k_{sy} k_{vr} - 2 k_{sy} h_1 m_v g$$

nG_c =

$$-(-2 k_{sy} h_1 + m_v g) k_{vr} s^2 - 2 g k_{sy} k_{vr}$$

r =

$$\left[\frac{1}{-2 k_{sy} h_1 + m_v g} * (-(-4 k_{sy} h_1 + 2 m_v g) g k_{sy})^{1/2} \right]$$

$$\left[-\frac{1}{-2 k_{sy} h_1 + m_v g} * (-(-4 k_{sy} h_1 + 2 m_v g) g k_{sy})^{1/2} \right]$$

Solutions

$$\begin{aligned} & \left[\begin{array}{c} 1/2 \\ (-(-4 k_{sy} h_1 + 2 m_v g) g k_{sy}) \\ \hline -2 k_{sy} h_1 + m_v g \end{array} \right] \\ & \left[\begin{array}{c} 1/2 \\ (-(-4 k_{sy} h_1 + 2 m_v g) g k_{sy}) \\ \hline -2 k_{sy} h_1 + m_v g \end{array} \right] \end{aligned}$$

=> Normally in railway vehicles $(2 k_{sy} h_1) > (m_v g)$

There are two solutions for the numerator (i.e. two system zeros) of the SISO system transfer function from u (actuator input angle) to y (lateral accelerometer signal) given $\pm \sqrt{\frac{2gk_{sy}}{2k_{sy}h_1 - m_v g}}$, with the positive being the *non-minimum phase zero*. This imposes limitations on controller design, subsequently leading to system instability for high controller gains [FL88]. The solutions are becoming more complex by increasing the complexity of the system dynamics. Additional details on non-minimum phase system limitations on control design, and especially bandwidth limitation can be found in [SP00].

B.3.1 Calculation of Time Delay Introduced by Low-Pass Filters

Assume the following second-order low-pass filter structure

$$H(s) = \frac{\alpha}{\gamma s^2 + \beta s + \alpha} \quad (\text{B.26})$$

Next, consider the situation portrayed in Figure B.3.1, where a *ramp* input (with laplace transform $x(s) = \frac{1}{s^2}$) is fed into the low-pass filtered and then compared to its original version.

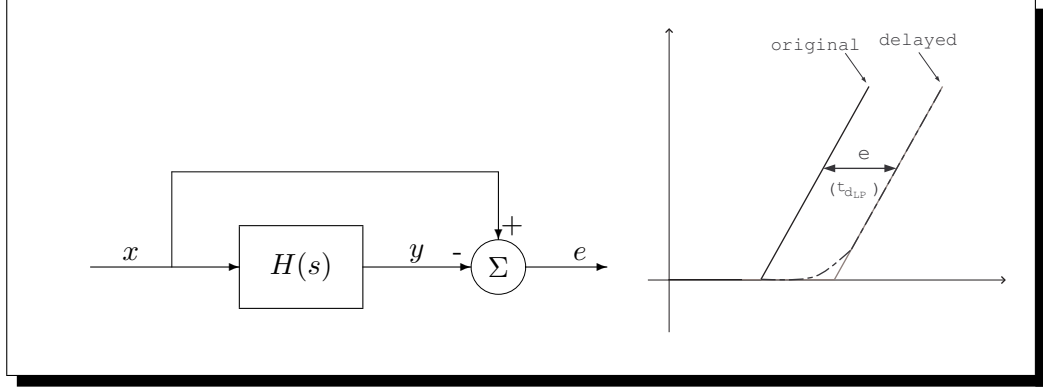


Figure B.3: Open-loop system including original and LP delayed signals for comparison

The error between the original signal $x(s)$ and the low-pass filtered signal $y(s)$ is given by

$$e(s) = x(s) - y(s), \quad \text{where } y(s) = H(s)x(s) \quad (\text{B.27})$$

Thus,

$$e(s) = (1 - H(s))x(s) \quad (\text{B.28})$$

From the above, the *time delay* can be found by

$$t_{dLP} = \lim_{s \rightarrow 0} \left(s \left[\left(1 - \frac{\alpha}{\gamma s^2 + \beta s + \alpha} \right) \times \frac{1}{s^2} \right] \right) \quad (\text{B.29})$$

$$\therefore t_{dLP} = \frac{1}{s} \left(\frac{\gamma s^2 + \beta s}{\gamma s^2 + \beta s + \alpha} \right) \Bigg|_{s \rightarrow 0} = \frac{\gamma s + \beta}{\gamma s^2 + \beta s + \alpha} \Bigg|_{s \rightarrow 0}$$

Therefore,

$$t_{dLP} = \frac{\beta}{\alpha} \quad (\text{B.30})$$

Appendix C

Evaluation for curve transition passenger comfort

C.1 P_{CT} Factor Calculation

$$P_{CT} = (A\ddot{y} + B\dot{\ddot{y}} - C)_{\geq 0} + D(\dot{\theta})^E \quad (C.1)$$

where A , B , C , D , E are constants defined below:

Condition	A	B	C	D	E
Standing passengers	2.80	2.03	11.1	0.185	2.283
Seated passengers	0.88	0.95	5.9	0.120	1.626

and

P_{CT} = passenger comfort index on curve transition, representing the percentage of passengers that will feel discomfort

\ddot{y} = maximum vehicle body lateral acceleration, in the time interval between the beginning of the curve transition and 1.6sec after the end of the transition (expressed in %'age of g), g denotes gravity (see Figure C.1 next page)

$\dot{\ddot{y}}$ = maximum lateral jerk level, calculated as the maximum difference between two subsequent values of \ddot{y} no closer than 1sec, in the time interval between 1sec before the start of the curve transition and the end of the transition (expressed in %'age of g per second) (see Figure C.1 next page)

$\dot{\theta}$ = maximum absolute value of vehicle body roll speed, in the time interval between the beginning of the curve transition to the end of the curve transition (expressed

in degrees per second), dot denotes the derivative with respect to time t (see Figure C.1 below)

Graphical interpretation

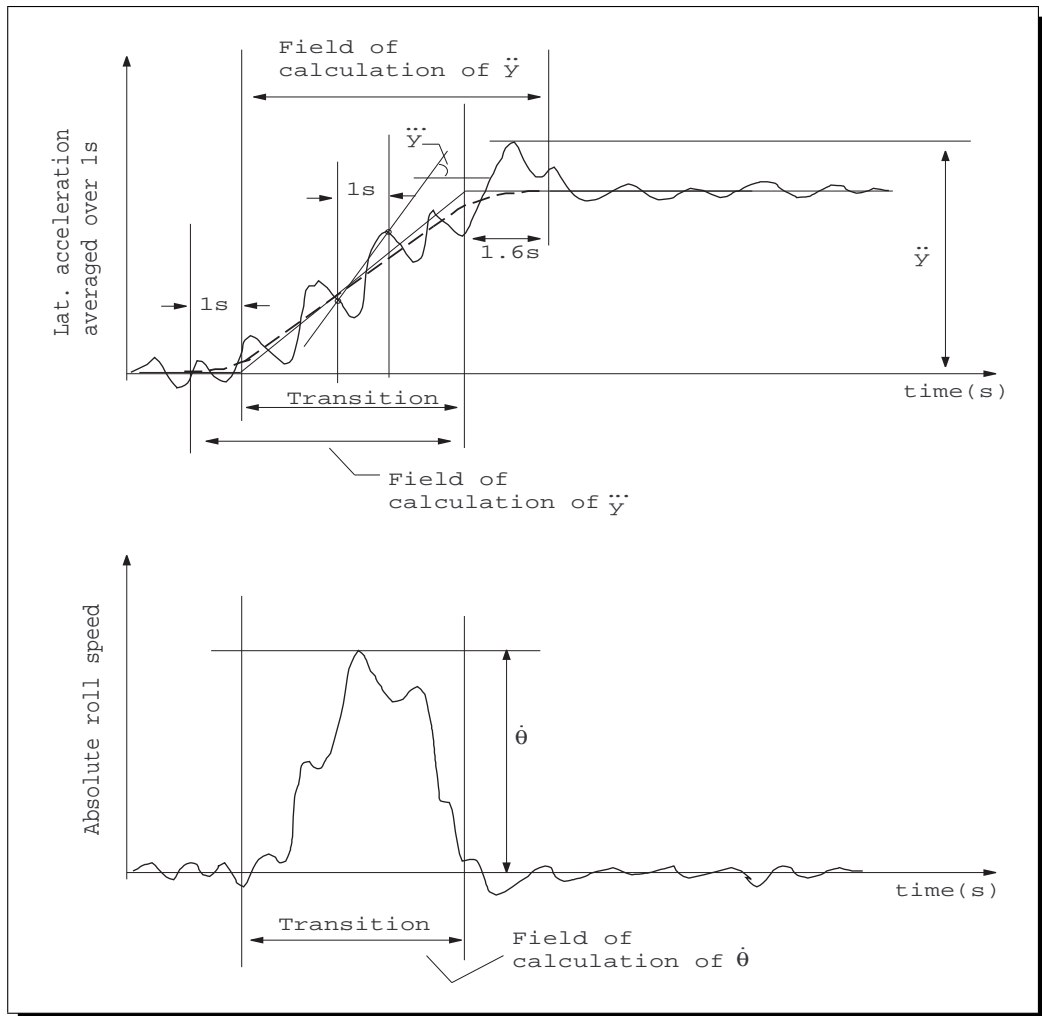


Figure C.1: Calculation of quantities \ddot{y} , \dot{y} and $\dot{\theta}$ for P_{CT} factor evaluation

Appendix D

Suspension Components Modelling

D.1 Airspring Modelling

D.1.1 Model One

This model is relevant for the case of the 2 D-o-F vehicle model (ARB).

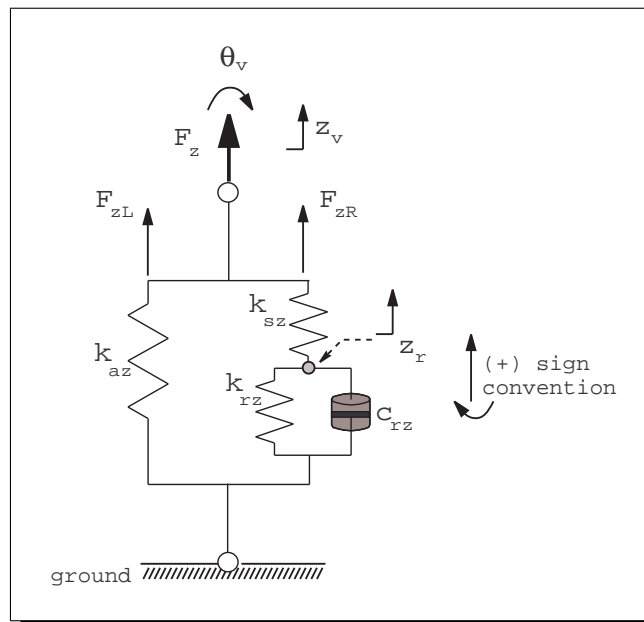


Figure D.1: Airspring Model 1

The total airspring force is given by

$$F_z = F_{zL} + F_{zR} \quad (\text{D.1})$$

where

$$F_{zL} = -k_{az}(z_v + d_1\theta_v) \quad (\text{D.2})$$

$$F_{zR} = -k_{sz}(z_v + d_1\theta_v - z_r) \quad (\text{D.3})$$

An equivalent expression for F_{zR} is

$$F_{zR} = -k_{rz}z_r - c_{rz}\dot{z}_r \quad (\text{D.4})$$

From (D.3) and (D.4) an expression for \dot{z}_r can be easily obtained

$$\dot{z}_r = c_{rz}^{-1}\{-z_r(k_{sz} + k_{rz}) + k_{sz}(z_v + d_1\theta_v)\} \quad (\text{D.5})$$

It is assumed that vertical degrees of freedom are ignored and also z_r is replaced by the equivalent $d_1\theta_r$ (roll contribution). Thus (D.5) changes to

$$\dot{\theta}_r = c_{rz}^{-1}\{-\theta_r(k_{sz} + k_{rz}) + k_{sz}\theta_v\} \quad (\text{D.6})$$

Finally the airspring force becomes

$$F_z = -k_{az}d_1\theta_v - k_{sz}d_1(\theta_v - \theta_r) \quad (\text{D.7})$$

The notation used is as follows d_1 is the airspring semi-spacing, subscript ‘v’ denotes vehicle body, subscript ‘r’ denotes airspring reservoir.

D.1.2 Model Two

This section is relevant to the three degree-of-freedom non-linear ARB vehicle model. Assuming pure vertical and lateral movement of the suspension and taking in account the static deflection of the suspension due to the weight of the vehicle body

$$F_z = F_{zL} + F_{zR} + \frac{mg}{2} \quad (\text{D.8})$$

or

$$F_z = \underbrace{-k_{az}\delta_{za_i}}_{F_{zL}} \overbrace{-k_{sz}\delta_{zs_i}}^{F_{zR}} + \frac{mg}{2} \quad (\text{D.9})$$

where δ_{za_i} = (“vert. displ. @ deflected posn.” - “vert. displ. @ static posn.”) which is

$$\delta_{za_i} = z_v + d_1\theta_v - (z_o + d_1\theta_o) \quad (\text{D.10})$$

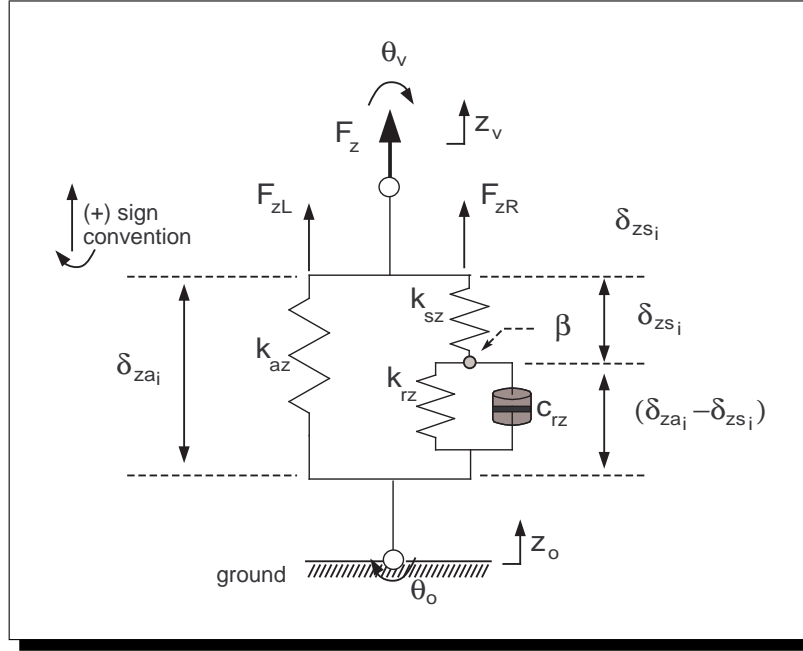


Figure D.2: Airspring Model 2

Moreover δ_{zs_i} is the deflection across the left series stiffness k_{sz} , and it is given by the following transfer function at point β (Figure D.2)

$$k_{sz}\delta_{zs_i} = k_{rz}(\delta_{za_i} - \delta_{zs_i}) + sc_{rz}(\delta_{za_i} - \delta_{zs_i}) \quad (D.11)$$

Re-arranging gives

$$\delta_{zs_i} \left(\frac{k_{rz} + k_{sz}}{c_{rz}} + s \right) = \delta_{za_i} \left(\frac{k_{rz}}{c_{rz}} + s \right) \quad (D.12)$$

$$\therefore \frac{\delta_{zs_i}}{\delta_{za_i}}(s) = \frac{\frac{k_{rz}}{c_{rz}} + s}{\frac{k_{rz} + k_{sz}}{c_{rz}} + s} \quad (D.13)$$

Due to the two airsprings the associated forces will be

$$F_{z_1} = -k_{az}\delta_{za_1} - k_{sz}\delta_{zs_1} + \frac{mg}{2} \quad (D.14)$$

$$F_{z_2} = -k_{az}\delta_{za_2} - k_{sz}\delta_{zs_2} + \frac{mg}{2} \quad (D.15)$$

where

$$\delta_{za_1} = z_v + d\theta_v - (z_o + d\theta_o) \quad (D.16)$$

$$\delta_{za_2} = z_v - d\theta_v - (z_o - d\theta_o) \quad (D.17)$$

and

$$\frac{\delta_{zs1}}{\delta_{za1}}(s) = \frac{\delta_{zs2}}{\delta_{za2}}(s) = \frac{\frac{k_{rz}}{c_{rz}} + s}{\frac{k_{rz} + k_{sz}}{c_{rz}} + s} \quad (\text{D.18})$$

D.1.3 Model Three

This airspring model can be incorporated in both 4 D-o-F vehicle (ARB) and tilting mechanism models.

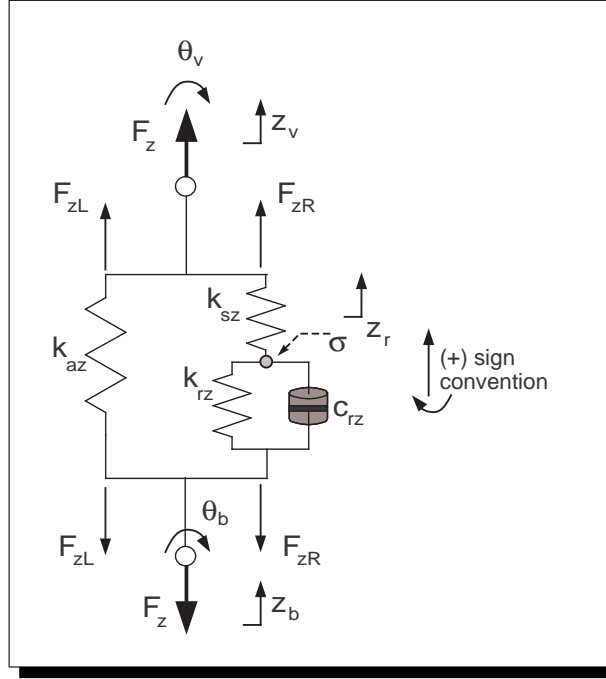


Figure D.3: Airspring Model 3

This section incorporates motion from the vehicle bogie (subscript ‘b’) as seen from Figure D.3 and it is an extended form of Section D.1.1. The total airspring force is given again by

$$F_z = F_{zL} + F_{zR} \quad (\text{D.19})$$

where now

$$F_{zL} = -k_{az}(z_v + d_1\theta_v - z_b - d_1\theta_b) \quad (\text{D.20})$$

$$F_{zR} = -k_{sz}(z_v + d_1\theta_v - z_r) \quad (\text{D.21})$$

F_{zR} is also given by

$$F_{zR} = -k_{rz}(z_r - z_b - d_1\theta_b) - c_{rz}(\dot{z}_r - \dot{z}_b - d_1\dot{\theta}_b) \quad (\text{D.22})$$

Thus \dot{z}_r can be easily obtained from (D.21) and (D.22)

$$\dot{z}_r = c_{rz}^{-1} \{-z_r(k_{sz} + k_{rz}) + k_{sz}(z_v + d_1\dot{\theta}_v) + k_{rz}(z_b + d_1\dot{\theta}_b) + c_{rz}(\dot{z}_b + d_1\dot{\theta}_b)\} \quad (D.23)$$

Vertical degrees of freedom are not considered in the modelling procedure and also z_r is replaced by the equivalent roll contribution $d_1\theta_r$. Thus (D.23) becomes

$$\dot{\theta}_r = c_{rz}^{-1} \{-\theta_r(k_{sz} + k_{rz}) + k_{sz}\theta_v + k_{rz}\theta_b + c_{rz}\dot{\theta}_b\} \quad (D.24)$$

Hence the airspring force is

$$F_z = -k_{az}d_1(\theta_v - \theta_b) - k_{sz}d_1(\theta_v - \theta_r) \quad (D.25)$$

Remark D.1.1. In the case of the tilt mechanism model, the requirement is to replace $\theta_b, \dot{\theta}_b$ with $(\theta_b + \theta_m), (\dot{\theta}_b + \dot{\theta}_m)$. This is due to both bogie and mechanism movements in the base of the airspring.

D.2 Suspension having Dampers with End-Stiffness

This damper with end-stiffness model is used in conjunction with the tilting mechanism model.

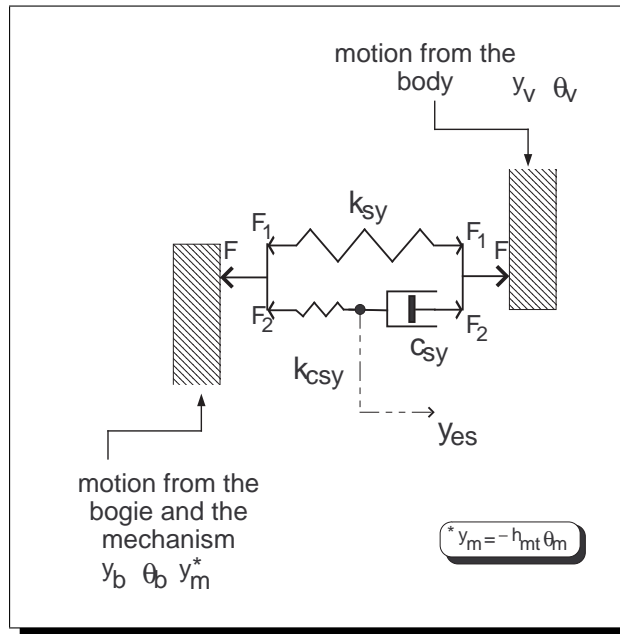


Figure D.4: Damper with end-stiffness

The overall force $F = F_1 + F_2$ where

$$F_1 = k_{sy}(-y_v + h_1\theta_v + y_b + h_2\theta_b + y_m) \quad (\text{D.26})$$

$$F_2 = c_{sy}(-\dot{y}_v + h_1\dot{\theta}_v + \dot{y}_{es}), \quad \text{or} \quad (\text{D.27})$$

$$F_2 = k_{csy}(-y_{es} + y_b + h_2\theta_b + y_m) \quad (\text{D.28})$$

From (D.27) and (D.28)

$$c_{sy}(-\dot{y}_v + h_1\dot{\theta}_v + \dot{y}_{es}) = k_{csy}(-y_{es} + y_b + h_2\theta_b + y_m) \quad (\text{D.29})$$

thus,

$$\dot{y}_{es} = c_{sy}^{-1} \left[c_{sy}\dot{y}_v - c_{sy}h_1\dot{\theta}_v + k_{csy}y_b + k_{csy}h_2\theta_b + k_{csy}y_m - k_{csy}y_{es} \right] \quad (\text{D.30})$$

where $y_m = -h_{mt}\theta_m$.

Appendix E

Model State Space Matrices

E.1 Anti-Roll Bar Model (4 DoF Linear) A, B

$$\mathbf{A}_v = \begin{array}{c} \left(\begin{array}{cccccc} (y_v) & (\theta_v) & (y_b) & (\theta_b) & (\dot{y}_v) & (\dot{\theta}_v) & (\dot{y}_b) \\ 0 & 0 & 0 & 0 & 1 & 0 & 0 \dots \\ 0 & 0 & 0 & 0 & 0 & 1 & 0 \dots \\ 0 & 0 & 0 & 0 & 0 & 0 & 1 \dots \\ 0 & 0 & 0 & 0 & 0 & 0 & 0 \dots \\ -\frac{2k_{sy}}{m_v} & \frac{2k_{sy}h_1}{m_v} & \frac{2k_{sy}}{m_v} & \frac{2k_{sy}h_2}{m_v} & -\frac{2c_{sy}}{m_v} & \frac{2h_1c_{sy}}{m_v} & \frac{2c_{sy}}{m_v} \dots \\ (2h_1k_{sy}+m_vg) & -(k_{vr}+2h_1^2k_{sy}+2d_1^2(k_{az}+k_{sz})) & -(2h_1k_{sy}+m_vg) & (2d_1^2k_{az}-2h_1h_2k_{sy}+k_{vr}) & \frac{2h_1c_{sy}}{m_v} & -\frac{2h_1^2c_{sy}}{m_v} & \frac{2h_1c_{sy}}{m_v} \dots \\ \frac{i_{vr}}{m_b} & -\frac{2h_1k_{sy}}{m_b} & -\frac{2(k_{sy}+k_{py})}{m_b} & -\frac{2(h_2k_{sy}-h_3k_{py})}{m_b} & \frac{2c_{sy}}{m_b} & -\frac{2h_1c_{sy}}{m_b} & -\frac{2h_1c_{sy}}{m_b} \dots \\ \frac{2h_2k_{sy}}{i_{br}} & (k_{vr}-2h_2h_1k_{sy}+2d_1^2(k_{az}+k_{sz})) & -\frac{2(h_2k_{sy}-h_3k_{py})}{i_{br}} & -(k_{vr}+2h_2^2k_{sy}+2h_2^2k_{py}+2d_2^2k_{pz}+2d_1^2k_{az}) & \frac{2h_2c_{sy}}{i_{br}} & -\frac{2h_2h_1c_{sy}}{i_{br}} & -\frac{2(h_2c_{sy}-h_3c_{py})}{i_{br}} \dots \\ 0 & \frac{i_{br}}{k_{sz}} & 0 & \frac{i_{br}}{k_{rz}} & 0 & 0 & 0 \dots \\ 0 & 0 & 0 & 0 & 0 & 0 & 0 \dots \\ 0 & 0 & 0 & 0 & 0 & 0 & 0 \dots \\ 0 & 0 & 0 & 0 & 0 & 0 & 0 \dots \end{array} \right) \end{array}$$

$$\mathbf{B}_v = \begin{array}{c} \left(\begin{array}{cccc} (\dot{\theta}_b) & (\theta_r) & (\theta_o) & (\dot{\theta}_o) & (y_o) \\ \dots 0 & 0 & 0 & 0 & 0 \\ \dots 0 & 0 & 0 & 0 & 0 \\ \dots 0 & 0 & 0 & 0 & 0 \\ \dots 1 & 0 & 0 & 0 & 0 \\ \dots \frac{2h_2c_{sy}}{m_v} & 0 & g & 0 & 0 \\ \dots -\frac{2h_1h_2c_{sy}}{i_{vr}} & \frac{2k_{sz}d_1^2}{i_{vr}} & 0 & 0 & 0 \\ \dots -\frac{2(h_2c_{sy}-h_3c_{py})}{m_b} & 0 & g & 0 & \frac{2k_{py}}{m_b} \\ \dots 1 & -\frac{(k_{sz}+k_{rz})}{c_{rz}} & 0 & 0 & 0 \\ \dots 0 & 0 & 0 & 1 & 0 \\ \dots 0 & 0 & 0 & 0 & 0 \\ \dots 0 & 0 & 0 & 0 & 0 \end{array} \right) , \quad \left(\begin{array}{cccc} (\delta_a) & (R^{-1}) & (\ddot{\theta}_o) & (\dot{y}_o) \\ 0 & 0 & 0 & 0 \\ 0 & 0 & 0 & 0 \\ 0 & 0 & 0 & 0 \\ 0 & 0 & 0 & 0 \\ 0 & -v^2 & -h_{g1} & 0 \\ \frac{k_{vr}}{i_{vr}} & 0 & -1 & 0 \\ 0 & -v^2 & -h_{g2} & \frac{2c_{py}}{m_b} \\ -\frac{k_{vr}}{i_{br}} & 0 & -1 & -\frac{2h_3c_{py}}{i_{br}} \\ 0 & 0 & 0 & 0 \\ 0 & 0 & 0 & 0 \\ 0 & 0 & 1 & 0 \\ 0 & 0 & 0 & 1 \end{array} \right)$$

Tilt Mechanism Model A continues

$(\dot{\theta}_b)$	(θ_r)	(y_{es})	(y_w)	(\dot{y}_w)	(θ_m)	$(\dot{\theta}_m)$	(θ_o)	$(\dot{\theta}_o)$	(R^{-1})	(y_o)
...0	0	0	0	0	0	0	0	0	0	0
...0	0	0	0	0	0	0	0	0	0	0
...0	0	0	0	0	0	0	0	0	0	0
...1	0	0	0	0	0	0	0	0	0	0
...0	0	$-\frac{2k_{csy}}{m_v}$	0	0	$-\frac{2h_{mt}(k_{sy}+k_{csy})+m_v g}{m_v}$	0	g	0	$-v^2$	0
... $\frac{c_{vr}}{i_{vr}}$	$\frac{2k_{sz}d_1^2}{i_{vr}}$	$\frac{2h_1k_{csy}}{i_{vr}}$	0	0	$\frac{(k_{vr}+2d_1^2k_{az}+2(k_{sy}+k_{csy})h_1h_{mt})}{i_{vr}}$	$\frac{c_{vr}}{i_{vr}}$	0	0	0	0
... $\frac{2h_3c_{py}}{m_b}$	0	$\frac{2k_{csy}}{m_b}$	$\frac{2k_{py}}{m_b}$	$\frac{2c_{py}}{m_b}$	$\frac{2h_{mt}(k_{sy}+k_{csy})}{m_b}$	0	g	0	$-v^2$	0
... $-\frac{(2d_2^2c_{pz}+2h_3^2c_{py}+c_{vr})}{i_{br}}$	$-\frac{2k_{sz}d_1^2}{i_{br}}$	$\frac{2h_2k_{csy}}{i_{br}}$	$-\frac{2h_3k_{py}}{i_{br}}$	$-\frac{2h_3c_{py}}{i_{br}}$	$\frac{(-k_{vr}-2d_1^2k_{az}+2(k_{sy}+k_{csy})h_2h_{mt})}{i_{br}}$	$-c_{vr}i_{br}$	0	0	0	0
...1	$-\frac{(k_{sz}+k_{rz})}{c_{rz}}$	0	0	0	$\frac{k_{rz}}{c_{rz}}$	1	0	0	0	0
...0	0	$-\frac{k_{csy}}{c_{sy}}$	0	0	$-\frac{h_{mt}*k_{csy}}{c_{sy}}$	0	0	0	0	0
...0	0	0	0	1	0	0	0	0	0	0
...0	0	0	$-\omega_{cm0}^2$	$-2\zeta_{m01}\omega_{cm0}$	0	0	0	0	0	ω_{cm0}^2
...0	0	0	0	0	0	1	0	0	0	0
...0	0	0	0	0	ω_{cm1}^2	$-2\zeta_{m1}\omega_{cm1}$	0	0	0	0
...0	0	0	0	0	0	0	0	1	0	0
...0	0	0	0	0	0	0	0	0	0	0
...0	0	0	0	0	0	0	0	0	0	0
...0	0	0	0	0	0	0	0	0	0	0

Tilt Mechanism Model B

$$\mathbf{B}_v = \begin{array}{c} \left(\begin{array}{cccc} (\theta_{m_i}) & (\dot{R}^{-1}) & (\ddot{\theta}_o) & (\dot{y}_o) \\ 0 & 0 & 0 & 0 \\ 0 & 0 & 0 & 0 \\ 0 & 0 & 0 & 0 \\ 0 & 0 & 0 & 0 \\ 0 & 0 & -h_{g1} & 0 \\ 0 & 0 & -1 & 0 \\ 0 & 0 & -h_{g2} & 0 \\ 0 & 0 & -1 & 0 \\ 0 & 0 & 0 & 0 \\ 0 & 0 & 0 & 0 \\ 0 & 0 & 0 & 0 \\ 0 & 0 & 0 & 0 \\ 0 & 0 & 0 & 0 \\ 0 & 0 & 0 & 0 \\ \omega_{cm1}^2 & 0 & 0 & 0 \\ 0 & 0 & 0 & 0 \\ 0 & 0 & 1 & 0 \\ 0 & 1 & 0 & 0 \\ 0 & 0 & 0 & 1 \end{array} \right) \end{array}$$

Appendix F

\mathcal{H}_∞ -based Controller Structures

The controllers listed in this appendix refer to full order controller size.

F.1 Mixed Sensitivity for ARB model

The \mathcal{H}_∞ controllers designed for the mixed sensitivity formulation in Chapter 7, section 7.4.3 are represented in the following transfer function form

$$K(s) = \frac{num(s)}{den(s)}$$

and the coefficients of the numerator and denominator for each case with their eigenvalues are listed in the following sections.

F.1.1 $K(s)$ for weightings set 1

The poles and zeros of the controller are:

poles	zeros
-6.2136e+002	-3.0000e+002
-1.9814e+001 ±1.3152e+002j	-2.0867e+001 ±1.6734e+002j
-3.9320e+001 ±5.1565e+001j	-1.4574e+001 ±6.8381e+001j
-4.2488e+001	-3.0000e+001
-2.3218e+001	-2.3215e+001
-6.1938 ±8.9729j	-2.5558 ±9.0273j
-2.4277 ±3.3371j	-6.8778e-001 ±4.1196j
-1.0000e-004	-

Table F.1: Controller TF coefficients for mixed sensitivity set 1

	num(s)	den(s)
s^{12}	0	1
s^{11}	1	822.57
s^{10}	431.3	1.62e+5
s^9	7.92e+4	2.7e+7
s^8	15.20e+6	2.7e+9
s^7	1.2e+9	1.75e+11
s^6	8.2e+10	6.8e+12
s^5	3.1e+12	1.43e+14
s^4	5.4e+13	1.7e+15
s^3	49.1e+13	1.24e+16
s^2	3.9e+15	4.42e+16
s^1	1.e+16	9.23e+16
s^0	4.47e+16	9.23e+12

F.1.2 $K(s)$ for weightings set 2

The poles and zeros of the controller are:

poles	zeros
-6.3849e+002	-3.0000e+002
-3.4555e+002	-2.0867e+001 ± 1.6734e+002j
-1.9459e+001 ± 1.3343e+002j	-1.4574e+001 ± 6.8381e+001j
-3.1794e+001 ± 4.9865e+001j	-3.0000e+001
-2.3428e+001	-2.3215e+001
-9.6822 ± 1.4755e+001j	-2.5558 ± 9.0273j
-3.6241 ± 3.0871j	-6.8778e-001 ± 4.1196j
-1.0000e-004	-

Table F.2: Controller TF coefficients for mixed sensitivity set 2

	num(s)	den(s)
s^{12}	0	1
s^{11}	1.43e+2	1.14e+3
s^{10}	6.17e+4	4.0e+5
s^9	1.13e+7	6.62e+7
s^8	2.17e+9	9.4e+9
s^7	1.72e+11	7.38e+11
s^6	1.2e+13	3.94e+13
s^5	4.5e+14	1.18e+15
s^4	7.7e+15	2.07e+16
s^3	7.0e+16	2.2e+17
s^2	5.6e+17	1.04e+18
s^1	1.43e+18	2.32e+18
s^0	6.4e+18	2.32e+14

F.2 Multi-Objective $\mathcal{H}_\infty/\mathcal{H}_2$ for ARB Model

State space continuous-time Matlab format A_k, B_k, C_k, D_k

A_k =

	x1	x2	x3	x4	x5	x6	x7	x8	x9	x10
x1	-60.72	-16.92	-5.139	45.29	-6.434	69.97	-401.8	43.05	9.321	2647
x2	-0.6867	0.7032	-2.738	-8.276	3.551	-10.74	40.91	4.741	-8.975	-310
x3	-40.32	-11.78	-13.99	35.89	-18.85	49.85	-306.2	3.836	40.43	2136
x4	-536.4	-170.5	12.02	589.7	-136.3	868	-4540	288.7	285.2	3.08e+004
x5	-556.8	-180.8	-7.856	646.2	-150.8	936.2	-4876	337.3	273.2	3.299e+004
x6	814	259.3	-3.092	-900.1	204.6	-1323	6937	-467.5	-410.1	-4.695e+004
x7	-612.7	-182.4	46.35	565.9	-147.2	867.2	-4667	188.9	427.7	3.202e+004
x8	-528.3	-180.1	-12.03	687.3	-161.2	984.1	-5045	348.7	268.8	3.415e+004
x9	68.29	14.17	-10.16	-9.749	5.512	-23.52	216.4	-0.00608	-37.77	-1495
x10	-280.4	-126.7	-49.7	639.2	-136.2	870.7	-4147	359.1	104.2	2.787e+004
x11	2.259e+005	7.169e+004	-776.8	-2.474e+005	5.637e+004	-3.607e+005	1.906e+006	-1.284e+005	-1.136e+005	-1.29e+007
x12	4553	1445	-15.76	-4984	1136	-7268	3.841e+004	-2587	-2289	-2.6e+005
x13	-1067	-338.4	3.692	1168	-266.1	1702	-8999	606	536.3	6.091e+004

	x11	x12	x13
x1	2.902e+004	8473	1.088e+005
x2	-3279	4559	5.857e+004
x3	2.311e+004	7487	9.615e+004
x4	3.35e+005	-1.308e+004	-1.684e+005
x5	3.593e+005	2162	2.736e+004
x6	-5.111e+005	-7419	-9.471e+004
x7	3.467e+005	-5.217e+004	-6.706e+005
x8	3.722e+005	1.568e+004	2.009e+005
x9	-1.615e+004	-4240	-5.444e+004
x10	3.047e+005	-1.47e+004	-1.892e+005
x11	-1.405e+008	-1.644e+004	-4.857e+004
x12	-2.83e+006	-416.7	-1548
x13	6.63e+005	89.42	246

B_k =

	u1	u2
x1	3	-19.39
x2	-0.3749	-7.949
x3	2.434	-12.39
x4	35.43	-3.705
x5	37.97	30.75
x6	-53.74	0.7161
x7	36.38	-117.2
x8	38.94	100.7
x9	-1.738	72.29
x10	31.63	338.4
x11	-1.467e+004	6572
x12	-295.6	133.2
x13	69.24	-31.18

C_k =

	x1	x2	x3	x4	x5	x6	x7	x8	x9	x10	x11	x12	x13
y1	-0.6711	-0.0713	-0.08947	-0.5179	0.1186	-0.4317	-0.3876	0.04353	0.2626	1.8	21.58	531.4	6827

D_k =

	u1	u2
y1	0.00285	-4.981e-006

(continues in the next page...)

Controller_poles =

```
-140427607.250319
-91.3446261264934
-42.5627952703617 + 50.6245843212897i
-42.5627952703617 - 50.6245843212897i
-11.3318349929862 + 30.8019859941792i
-11.3318349929862 - 30.8019859941792i
-11.9844265559739 + 8.83656137739561i
-11.9844265559739 - 8.83656137739561i
-11.7140384056253
-4.88118335331778
-3.40343575033742
-0.0803788208499184
-0.0378971322263747
```

F.3 \mathcal{H}_∞ Coprime Factorisation for Tilt Mechanism Model

State space continuous-time Matlab format A_k, B_k, C_k, D_k

A_k =

	x1	x2	x3	x4	x5	x6	x7	x8	x9	x10
x1	-53.7	-5.339	1.289	-0.07628	-104.4	-26.3	0	1	0	0
x2	3.897	-15.98	2.891	-0.1711	-234.1	-59	0	0	0	0
x3	-1.092	215.6	-52.03	3.08	4214	1062	1	0	0	0
x4	-108.8	312.8	-75.49	4.469	6115	1541	0	1	0	0
x5	5.628	20.09	-4.849	0.2871	392.8	98.97	0	0	1	0
x6	26.27	102.1	-24.64	1.459	1996	503	0	0	0	1
x7	-112.9	1055	-267.1	25.62	2.163e+004	5452	0	0	0	0
x8	-829.8	-601.8	161.5	-125.7	-1.246e+004	-3048	0	-0.91	0	0.91
x9	30.61	210.6	3.526	-42.86	-1.039e+004	1889	0	0	-10.87	2.109
x10	-69.81	669	-141.3	872.3	1.433e+004	331.6	0	7.28	3.104	-23.88
x11	-117.2	235.5	-56.83	18.36	4603	1170	0	0	0	1
x12	112.9	11.54	-2.785	0.1649	670	168.8	1	-0.844	0	0
x13	9.623e-013	5.515e-013	-1.331e-013	7.879e-015	1.078e-011	2.717e-012	0	0	0	0
x14	9.034e-011	-4.487e-011	1.083e-011	-6.41e-013	-8.771e-010	-2.21e-010	0	0	0	0
x15	-165.5	59.7	-14.41	0.853	1167	294.1	0	0	0	0
x16	-45.53	1806	-460.3	287	-1.153e+004	-1825	-341.7	-206.2	26.98	10.06
x17	0	0	0	0	0	0	0	0	0	0
x18	0	0	0	0	0	0	0	0	0	0

	x11	x12	x13	x14	x15	x16	x17	x18
x1	0	103.1	0	0	61.94	0	-23.7	-5.339
x2	0	231.3	0	0	138.9	0	3.897	-15.98
x3	0	-4162	0	0	-2501	0	-1.092	215.6
x4	0	-6039	0	0	-3629	0	-108.8	312.8
x5	0	-387.9	0	0	-233.1	0	5.628	20.09
x6	0	-1971	0	0	-1184	0	26.27	102.1
x7	0	-2.137e+004	0	0	-1.283e+004	0	-112.9	1055
x8	20.92	1.229e+004	0	0	7481	0.91	-829.8	-601.8
x9	0	282.1	1.011e+004	10.87	198.5	0	30.61	210.6

x10	-167.3	-1.13e+004	-2887	-3.104	-7493	-7.28	-69.81	669
x11	-25.05	-4546	0	0	-2721	1	-117.2	235.5
x12	0	-667.2	0	0	-400.5	0	112.9	11.54
x13	0	-1.065e-011	0	1	-6.397e-012	0	9.623e-013	5.515e-013
x14	0	8.662e-010	-987	-12.57	5.205e-010	0	9.034e-011	-4.487e-011
x15	0	-1153	0	0	-692.6	1	-165.5	59.7
x16	-133.3	9342	3500	47.14	3894	-81.97	154.1	-612.2
x17	0	0	0	0	0	0	-30	0
x18	0	0	0	0	0	0	0	0

B_k =

	u1	u2
x1	0	-1.335
x2	0	-3.994
x3	0	53.9
x4	0	78.2
x5	0	5.023
x6	0	25.53
x7	0	263.7
x8	0	-150.5
x9	0	52.65
x10	0	167.2
x11	0	58.87
x12	0	2.885
x13	0	1.379e-013
x14	0	-1.122e-011
x15	0	14.93
x16	0	-153
x17	1	0
x18	0	1

C_k =

x1	x2	x3	x4	x5	x6	x7	x8	x9	x10	x11	x12	x13
----	----	----	----	----	----	----	----	----	-----	-----	-----	-----

y1 0.4127 -5 1.257 -0.6116 -0.9015 -2.462 0.7066 0.4263 -0.05579 -0.0208 0.2756 5.122 -7.237

	x14	x15	x16	x17	x18
y1	-0.09747	5.632	0.124	0	0

D_k =

	u1	u2
y1	0	0

Controller poles =

-361.813295265681	
-240.871071875492	
-7.0032467864159	+ 104.038049766736i
-7.0032467864159	- 104.038049766736i
-14.1195265627634	+ 49.5983224916336i
-14.1195265627634	- 49.5983224916336i
-4.25363768561572	+ 34.313249130666i
-4.25363768561572	- 34.313249130666i
-29.9343265868606	
-23.8050891812024	
-8.80994469622064	
-2.49215127206927	+ 3.80207914136297i
-2.49215127206927	- 3.80207914136297i
-3.01487757288307	
-6.28318530717995	+ 30.7811959238846i
-6.28318530717995	- 30.7811959238846i
-30	
0	